JP0350052

JAERI-Review
2002-042

ANNUAL REPORT OF KANSAI RESEARCH ESTABLISHMENT 2001
APRIL 1, 2001 – MARCH 31, 2002

February 2003

Kansai Research Establishment

日本原子力研究所
Japan Atomic Energy Research Institute

本レポートは、日本原子力研究所が不定期に公刊している研究報告書です。
入手の問合わせは、日本原子力研究所研究情報部研究情報課（〒319-1195　茨城県那珂郡東海村）あて、お申し越しください。なお、このほかに財団法人原子力弘済会資料センター（〒319-1195　茨城県那珂郡東海村日本原子力研究所内）で複写による実費頒布をおこなっております。

This report is issued irregularly.
Inquiries about availability of the reports should be addressed to Research Information Division, Department of Intellectual Resources, Japan Atomic Energy Research Institute, Tokai-mura, Naka-gun, Ibaraki-ken 319-1195, Japan.

© Japan Atomic Energy Research Institute, 2003

編集兼発行　日本原子力研究所

JAERI-Review 2002-042

Annual Report of Kansai Research Establishment 2001
April 1, 2001 − March 31, 2002

Kansai Research Establishment

Japan Atomic Energy Research Institute
Kizu-cho, Souraku-gun, Kyoto-fu

(Received December 13, 2002)

This report is the third issue of the annual report of Kansai Research Establishment, Japan Atomic Energy Research Institute. It covers status reports of R&D and results of experiments conducted at the Advanced Photon Research Center and the Synchrotron Radiation Research Center during the period from April 1, 2001 to March 31, 2002.

Keywords: Annual Report, Kansai Research Establishment, JAERI, R&D, Advanced Photon Research Center, Synchrotron Radiation Research Center

---

Board of Editors for Annual Report
Editors: Toshiki TAJIMA(Editor-in-chief), Taikan HARAMI, Shun-ichi KAWANISHI , Keisuke NAGASHIMA, Hiroyuki DAIDO, Masato KOIKE, Eisuke MINEHARA, Kouichi YAMAKAWA, Yuichi SHIMIZU, Mitsuru YAMAGIWA, Nozomu HAMAYA, Jun-ichiro MIZUKI, Yuji BABA, Yoichi MURAKAMI, Atsushi FUJIMORI, Jun-ichi IGARASHI
Editorial assistants: Hiroshi YOSHIDA, Noboru TSUCHIDA

関西研究所年報 2001
2001 年 4 月 1 日－2002 年 3 月 31 日

日本原子力研究所
関西研究所

（2002 年 12 月 13 日受理）

本報告書は、日本原子力研究所関西研究所の第 3 号の年報であり、2001 年 4 月 1 日から 2002 年 3 月 31 日までの期間（平成 13 年度）に行われた光量子科学研究センター及び放射光科学研究センターの研究活動をまとめたものである。

関西研究所：〒619-0215　京都府相楽郡木津町梅美台８－１
年報編集委員会
（編集委員）田島俊樹（委員長）、原見太幹、河西俊一、永島圭介、大道博行、小池雅人、峰原英介、
山川考一、清水雄一、山極満、浜谷望、水木純一郎、馬場祐治、村上洋一、藤森淳、五十嵐潤一
（事務局）　吉田宏、土田昇

Contents

Foreword

This is the third Annual Report of Kansai Research Establishment covering the activities in the Fiscal Year 2001. Kansai Research Establishment consists of Advanced Photon Research Center (APRC) in Kyoto Prefecture and Synchrotron Radiation Research Center (SRRC) in Hyogo Prefecture. The FY 2001 has been the important year for us to move into the advanced research phase from the facility-development phase in previous years.

At APRC, very precise systematic data have been obtained on ionization of rare gas atoms at relativistic intensities with the 100-TW Ti:sapphire laser. Preparations for high-field experiments are in progress, with the expected government approval for the laser-based x-ray source in FY 2002. Compact, high-flux, short duration x-ray lasers have been demonstrated, and it has been applied to observe the domain structures of ferro-electric crystals near the critical point. With the super-conducting linac free electron laser, full energy recovery of the electron beam has been demonstrated, contributing to development of the next generation energy-recovery type synchrotron radiation facility.

SRRC is focused on material science research using the JAERI beamlines which have experimental hutches equipped with advanced facilities to determine atomic structures and electronic properties in-situ under various conditions. We have completed construction of the 4-th JAERI beamline BL22XU, which has a hutch in the RI Laboratory where we are planning to clarify the electronic properties of actinide compound crystals. A new research group on simulation in material science has been started in FY 2001 to help and guide the experimental research at SRRC.

As a part of Kansai Lab activities, Kid's Science Museum of Photons has been opened adjacent to APRC in July 1991. Various hands-on exhibits together with live demonstrations with light are regularly displayed to public so that children have easy access to basic science and technology without prior knowledge.

We would like to thank all who have helped in developing scientific and administrative activities at the Kansai Research Establishment during 2001. We are looking forward to further collaboration for creation of original concepts and results.

Yoshiaki KATO
Executive Director
Director General, Kansai Research Establishment
JAERI

Dedication

Dr. Toshizo Shirai, Principal Research Physicist at the Advanced Photon Research Center, passed away on September 3, 2002. This volume is dedicated to his memory. He is a well-known atomic physicist and has contributed immensely to the development of atomic database. His life work is condensed in his authoritative book (as co-author) "Spectral Data for Highly Ionized Atoms, Ti, V, Cr, Mn, Fe, Co, Ni, Cu, Kr, and Mo" (AIP, NY, 2000) in this field.

This is a blank page.

1. Summary

JAERI(Japan Atomic Energy Research Institute) is the research institute complex of nuclear science and technology where broad-ranged top-of-the-line energy research facilities can be synthetically utilized that encompass from synchrotron radiation, X-ray laser, to high-intensity proton accelerator(under construction), accelerators of electron beam and ion beam, nuclear research reactors and advanced computer system. Kansai Research Establishment was established six years ago to promote the research of laser and synchrotron radiation with the integrated theme of bright 'light'.

A new Long-Term Program for research, development and utilization of nuclear energy was drawn up in The Atomic Energy Commission of Japan in November 2000. This Program summarizes that nuclear science and technology has achieved remarkable developments in the 20th century and brought about substantial changes in lives and lifestyles. In the 21st century, the advance of nuclear science and technology is expected not only to form the basis for development of new energy technologies but also to serve to explore new frontiers. High brilliant synchrotron radiation and X-ray laser can contribute to the advance of life science and materials science related to nano-structure, environment and information technology. As JAERI is expected to join with JNC(Japan Nuclear Cycle Development Institute) in 2005 to become an integrated independent agency responsible for the over all atomic energy researcher in Japan our research will be pivotal in promoting the new direction in atomic energy research in Japan.

This Annual Report summarizes the research activities at both Synchrotron Radiation Research Center and Advanced Photon Research Center in the period from April 1, 2001 until March 31, 2002. Two previous Annual Reports were published as JAERI-Review 2001-003 in March 2001 and JAERI-Review 2001-046 in February 2002.

2. Facilities of the Advanced Photon Research Center

The core competence of the Advanced Photon Research Center (APRC) is advanced lasers with high brilliance and high fluence. These lasers include a compact ultra short pulse peta watt laser, a fully spetially coherent X-ray laser, and high-power extremely efficient free-electron laser. These lasers are tools for the exploration of new nuclear energy science and technology and the development of novel radiation sources of X-rays, γ-rays, electrons and ions. In order to support this development, simulation research using supercomputers (Super Simulation Center for Photon-SSCP) and development of fundamental technologies of optical elements and devices like laser crystals, mirrors, gratings, etc. are also implemented in the APRC.

The APRC has engaged in the research and development of advanced lasers such as compact high power lasers with a peak power of petawatts (10^{15} watts), X-ray lasers with soft X-ray, and free electron lasers with high average power and high efficiency. Utilizing these lasers, the APRC also challenges generation and application of high-energy ion and X-ray, development of new particle sources, X-ray microscopes, etc.

These advanced lasers and their producing highly energetic ions and X-rays have distinctive characteristics such as high intensity, high coherency, or short pulse, which are different from conventional radiations. The APRC develops various techniques for utilizing these high quality radiations to various fields of science and technologies, along with JAERI's own knowledge of neutrons, synchrotron radiation, and ion beams research. The APRC also collaborates with industries and universities in research and development activities.

A bird's-eye view of the Advanced Photon Research Center is shown in Fig. 1. Research activities are mainly performed in the laboratory building where four big laboratories for development and applications of high power lasers are provided and the researchers' building where a super computer is equipped. There are the conference hall where we can hold symposiums and meetings to introduce research results of Kansai Research Establishment, and the guesthouse for accommodation.

The buildings with a dome at the right foot in the photograph is the "Kids' Science Museum of Photons", which was opened in July 2001, contributing to science educations for the younger generation in Keihanna Science City. The IT-based laboratory (ITBL) building shown at the left top was opened in March 2002.

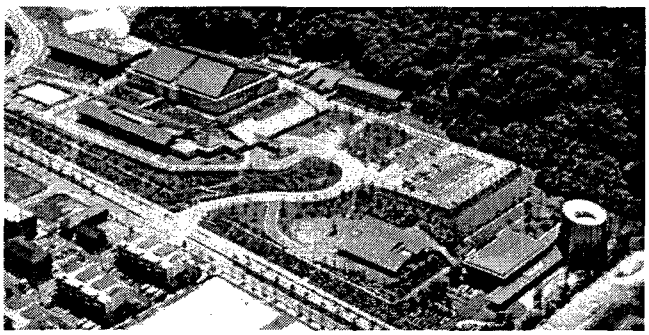

Fig. 1 The Advanced Photon Research Center

All-solid state, high average power laser laboratory

Ultrashort pulse, high peak power laser laboratory

Laser acceleration and high field science laboratory

X-ray laser laboratory

Fig. 2 Four main laboratories of the Advanced Photon Research Center

3. Facilities of the Synchrotron Radiation Research Center

SPring-8 is a synchrotron radiation light source the highest and brightest third generation light source in the world, culminating in the guest for bright light sources in the world's energy research. Such a bright light source can be employed to advance the energy research such as nuclear materials research, the materials science research, environmental research and nanoscience and biological research. SRRC of JAERI has contributed crucially to take a leadership in applications of this facility, in particular to material science in XXX nuclear materials.

SPring-8 was operated in 2001 as scheduled. Three JAERI beamlines were operated as well as a new fourth line has come into operation. In the beamline BL23SU, the vacuum chamber was replaced with a thinner chamber to get lower energy of photon with the first harmonic. Surface chemistry, radiation effect on DNA and electronic structure of electronic materials were studied. In the beamline BL14B1, structure analysis under high pressure, correlation between structure and function of materials were investigated. In the beamline BL11XU, nuclear resonant scattering of materials, resonant inelastic scattering of colossal magnetoresistance manganites and surface structure during molecular beam epitaxy growth. A new JAERI beamline, named quantum structure physics beamline BL22XU (Fig. 1), was constructed in SPring-8. All equipments and components of the beamline, an undulator, a frontend, shielding hutches, beamline control&interlock systems were completed by March 2002. The beamline has the experimental equipments for high pressure studies and resonant X-ray diffraction (Fig. 2).

JAERI and DOE of USA have entered into an agreement to cooperate in the field of synchrotron radiation research using the APS at Argonne National Laboratory and the SPring-8 under a Specific Memorandum of Agreement in May 2001.

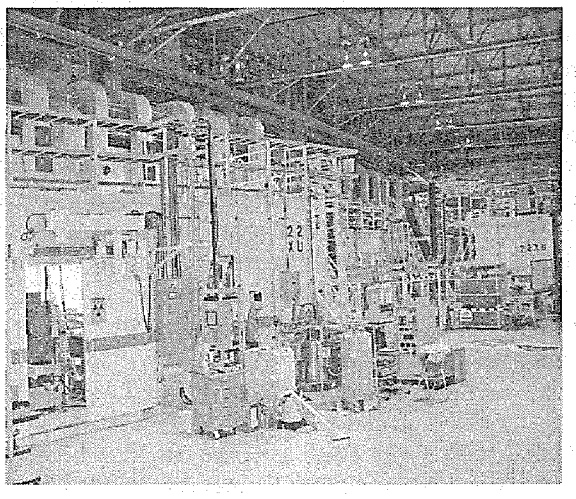

Fig. 1 Beamline BL22XU
Utilizing X-ray whose energy band is 3~70keV, it is possible to research into heavy atom and experiment in high pressure

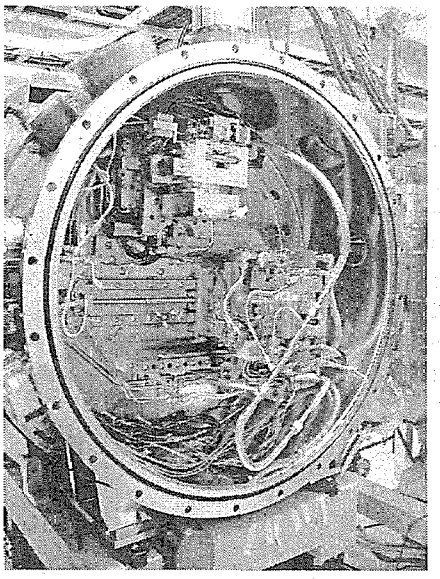

Fig. 2 A Double Crystal Monochromator of BL22XU
Silicon plane crystals are cooled by using a liquid nitrogen circulation system.

4. Advanced Photon Science

Toyoaki KIMURA
Advanced Photon Research Center

In FY2001, much progress has been made of research and development in the Advanced Photon Research Center (APRC). APRC has solidified its core competence of advanced lasers, the compact high-power multi tera (sub-peta) watt laser, the spatially·fully coherent X-ray laser, and high-power highly efficient energy-recovery free electron laser. In each of these and in their combination APPC has exercised its leadership in the world's community. These capabilities bring in new potentials in atomic energy research as well as a wood range of new high field science and other applications.

Two remarkable advances have been made in the development of the advanced photon sources. One is a success of an X-ray laser with short wavelength of 8.8 nm using lanthanum as target material of a compact driving laser with energy of 10J. This accomplishment leads to further progress in the development of an X-ray laser with wavelength of a "water window" which is an essential for developing an X-ray holographic microscope for observing dynamic behavior of living materials. The other is a success in demonstrating the perfect recovery of residual energy that electrons still hold after emitting photons using superconducting acceleration cavities in the development of a free electron laser (FEL). This achievement, first in the world, makes it possible to realize FELs with high output power and efficiency and contributes to extending their applications to industry and medical technology.

The full-scale preparation including installation of a laser transmission system has been made for utilizing a compact, ultra-short pulse, high-peak power laser (100 W T-cube laser) in experiments of high field science and laser acceleration. The laser intensity of 10^{19} W/cm^2 was obtained by focusing the T-cube laser and production of fast electrons with relativistic energy and ions with energy of 0.1 MeV was observed. Magnetic bacteria have been successfully observed with a precision of 0.1 μm using X-rays emitting from laser-induced plasmas. In the research of laser acceleration, a wake field of 20 GeV/m with a cycle of 130 fs was successfully observed using a frequency interferometer. This result gives promise of electron acceleration up to energy of 1 GeV with the 100 TW T-cube laser.

In the development of optical elements and devices, heat-resistance property in a Mo/Si multi-layered mirror has greatly improved by optimizing thickness of SiO_2 layer for preventing the decrease in reflection due to absorption by oxide. About 200 °C increase in the heat-resistance of the Mo/Si mirror was obtained as its reflection rate for soft X-rays was kept about 90 %. In the computer simulation research, efforts have been made focusing on studies about the interaction of lasers with plasmas for searching optimal conditions where highly energetic ions are produced efficiently and for analyzing experimental results. In APRC the super computer and its accessories form the basis for the SSCP (Super Simulation Center for Photon) that serves super computing community (as well as APRC) in photon simulation.

OECD Global Science Forum Workshop on Compact High-Intensity Short Pulse Lasers: Future Directions and Applications was held in APRC, May 28-31, 2001, planed and chaired by Dr. Yoshiaki Kato, Director General of Kansai Research Establishment, and with Prof. Daniele Hulin as Vice-Chair. The workshop was attended by 56 government-appointed delegates from 10 OECD member countries and 4 non-member countries, and approximately 30 observers from Japanese laboratories and institutions. Outstanding reports were new developments of atom and molecule science with attosecond ultrashort pulse lasers, applications of X-ray lasers like protein structure analysis, nuclear and high energy science, and applications in medicine and technology. It was proposed international coordination, collaboration, trans-national access to facilities, education, training, and public outreach, etc.

4.1 High Peak Power Laser Development

Laser System Development Group

Koichi YAMAKAWA

The research activities of the Laser System Development Group are focused on the following topics:

- Development of a petawatt Ti:sapphire laser system.
- Optical filed ionization of rare gas atoms in a relativistic intensity regime.
- Explosion dynamics of atomic clusters heated by the 100 TW, 20 fs laser.
- Development of a compact diode pumped solid-state laser with Yb-doped gain media.
- Quantum control of chemical reactions.
- Generation and applications of laser produced plasma x-ray sources.

Over the past decade, there has been rapid progress in generating high peak power, ultrashort laser pulses by incorporating the technique of chirped pulse amplification (CPA). In this year, we have successfully produced laser pulses with peak power of 0.34 PW and pulse duration of 52 fs (see Fig. 1). To our knowledge, this result represents the highest peak power pulses yet produced used in any Ti:sapphire CPA system. Also, a construction of a diode-pumped Yb:YLF regenerative amplifier system has been completed. A 24.3-mJ laser pulse was generated after regenerative amplification. To our knowledge, this is the highest energy chirped pulse regenerative amplifier based on Yb:YLF.

High field physics experiments are also carried out with the 100 TW, 10 Hz Ti:sapphire laser facility describe in more detail below address fundamental aspects of relativistic light-matter interaction for future studies. We find, in case of optical field ionization of xenon, krypton, and argon atoms, that such ionization produces charge-states as high as Xe^{26+}, Kr^{19+}, and Ar^{16+}, respectively, in the fully relativistic intensity regime. We have also observed the energy spectra of ions (the mean ion energy up to ~ 100 keV) resulting from the interaction of Xe clusters with the high intensity laser light. These studies should lead to better understanding of relativistic plasmas of atoms, molecules and clusters in all of their complex interactions. In finally, the adaptive pulse compression and shaping of the ultrashort laser pulses was demonstrated for the study of quantum control towards the isotope separation and selective formation of chemical products.

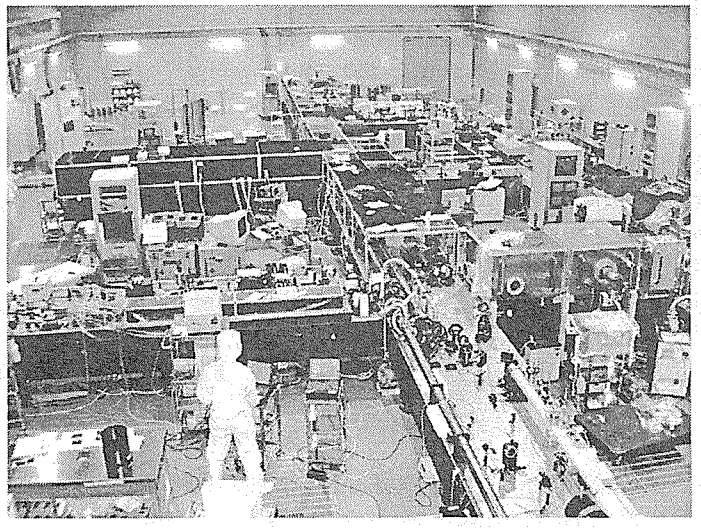

Fig. 1 Petawatt Ti:Sapphire Laser System

4.1.1 Development of a petawatt Ti:sapphire laser system

Makoto AOYAMA, Jinglong MA, Yutaka AKAHANE, Norihiro INOUE, Hideki UEDA, Hiromitsu KIRIYAMA and Koichi YAMAKAWA

1. Introduction

Since the development of the technique of chirped pulse amplification (CPA), there has been rapid progress in generating high peak power, ultrashort laser pulses. To date, pulses as short as 450-fs with over a petawatt peak power have been generated by using a large scale, inertial-confinement-fusion, Nd:glass laser[1]. Such lasers can realize a focused peak intensity of over10^{21} W/cm^2. These laser systems are useful for a variety of high-field applications such as electron and ion acceleration, laser induced nuclear photophysics, laboratory-based astrophysics and fast ignitor fusion[2]. We report on a laboratory-scaled Ti:sapphire CPA laser system which is capable of producing sub-30 fs pulses with peak power of 1 PW.

2. Petawatt laser system

In order to amplify the laser pulses up to petawatt power level, a 3-pass booster amplifier with a 80 mm diameter, 33-mm-long Ti:sapphire crystal (Crystal Systems Inc.) is added to our Ti:sapphire CPA laser chain that produces 100 TW, sub-20 fs laser pulses at 10 Hz [3]. The booster amplifier has been designed to achieve efficient energy extraction, and the amplified energy has been expected to be as much as ~40-J for a ~70-J green pump.

The pulse stretcher and compressor for the petawatt laser system are also considered to produce sub-30 fs laser pulses. These components are the Offner triplet stretcher and the Tracy type compressor based on the mixed grating scheme. In order to compensate for the phase distortion of the materials up to fourth order in the laser chain, we have chosen a 1,200 groove/mm ruled grating in the stretcher and 1,480 groove/mm holographic gratings in the compressor. The residual high-order dispersion will be controlled with an acoustic-optic programmable dispersive filter(AOPDF) [4]. The dispersion of this laser system should be considered up to fifth-order dispersion.

3. Experimental results

In a preliminary experiment, we have produced laser pulses with energies of 23.8 J for 51 J pump laser and conversion efficiency of 48.3 %. A measured autocorrelation trace of the laser pulse is shown in Fig.1. The FWHM of the measured pulse duration was 52.3 fs. Therefore the peak power of the laser pulse was 0.34 PW. We also confirmed that the laser pulses had a large cubic dispersion and other higher order dispersion with a FROG technique. These dispersions can be controlled with angles of the stretcher and the compressor and with the AOPDF. Therefore we can expect sub 30 fs pulse duration. This result indicates this laboratory-scaled Ti:sapphire laser system has the capability to deliver 1 PW laser pulses.

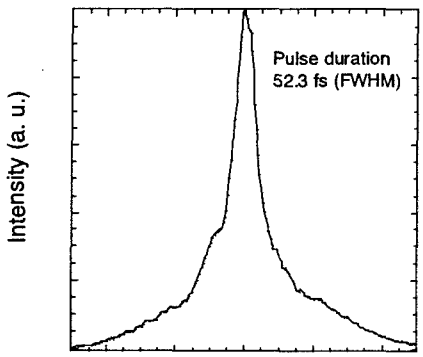

Fig. 1 Measured autocorrelation trace

References

1) M. D. Perry, D. Pennington, B. C. Stuart, G. Tietbohl, J. A. Britten, C. Brown, S. Herman, B. Golick, M. Kartz, J. Miller, H. T. Powell, M. Vergino, and V. Yanovsky, Opt. Lett. **24**, 160, 1999.
2) G. Mourou, C. P. J. Barty, and M. D. Perry, Phys. Today, **51**, 22, 1998.
3) K. Yamakawa, M. Aoyama, S. Matsuoka, T. Kase, Y. Akahane, and H.Takuma, Opt. Lett. **23**, 1468, 1998.
4) F. Verluise, V. Laude, Z. Cheng, C. Spielmann, and P. Tournois Opt. Lett. **25**, 575, 2000.

4.1.2 High-energy green beam generation using large aperture $CsLiB_6O_{10}$ crystlas

Hiromitsu KIRIYAMA, Norihiro INOUE and Koichi YAMAKAWA

1. Introduction

A high energy green laser radiation through second-harmonic generation (SHG) in near-infrared solid-state lasers such as the popular neodymium-doped laser system is of particular interest as a pumping source of high peak power Ti:sapphire chirped-pulse-amplification (CPA) lasers. Many nonlinear crystals have been used for SHG. Since the green pulse energy depends on the crystal size, the KH_2PO_4 (KDP), which can be grown to large size, therefore, still widely used in most high energy laser systems with a sacrifice of lower conversion efficiency mainly because of its small effective nonlinear coefficient. In order to obtain the modest conversion efficiency of 50 % using KDP crystal, the high input laser intensity level of several GW/cm^2 is required and thus close to the damage to threshold of optical materials[1]. The $CsLiB_6O_{10}$ (CLBO) crystal is recently developed borate crystal which can be easily grown to large size[2] and has a larger effective nonlinear coefficient compared with KDP crystal[3]. In order to achieve high conversion efficiency with low input intensity, large aperture CLBO frequency doubler has been developed.

2. Results and conclusion

The SHG experiment was carried out using a custom-built high power flash-lamp pumped Nd:silicate glass laser system. A two-stage CLBO crystal architecture was used to achieve high conversion efficiency and to minimize back-conversion. The first and second CLBO crystals each had a cross-section of 30 mm × 30 mm and their lengths were 11.5 mm and 15.5 mm.

Figure 1 shows the total 532-nm second-harmonic output pulse energy from two crystals as a function of the input 1064-nm fundamental laser pulse energy. A maximum total second-harmonic output pulse energy of 25 J was obtained with 34 J of input 1064-nm fundamental laser pulse energy. Figure 2 shows the 532-nm second-harmonic energy conversion efficiency plotted as a function of the input 1064-nm laser intensity. A maximum conversion efficiency of 74 % was achieved with an input laser intensity of only 370 MW/cm^2. The results clearly demonstrated the fact that CLBO crystal is suitable for efficient SHG of high power neodymium-doped lasers at low input intensities.

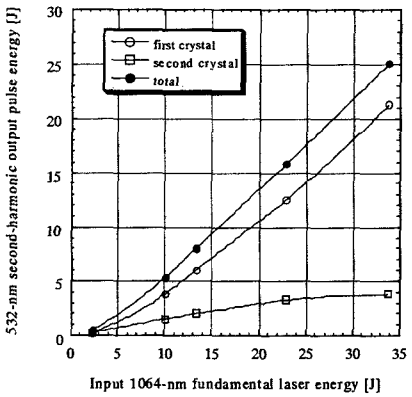

Fig. 1 Second-harmonic energy versus fundamental energy

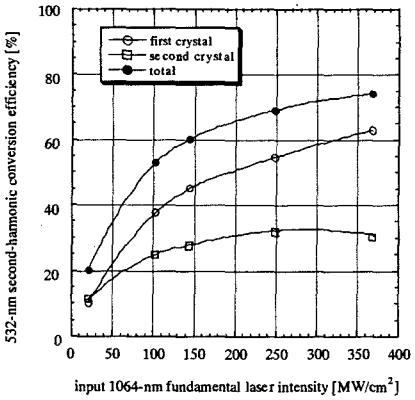

Fig. 2 Second-harmonic conversion efficiency versus fundamental intensity

References

1) G. J. Lindford et al., *Appl. Opt.*, **21**, 3633-3643, 1982.
2) Y. Mori et al., *Appl. Phys.Lett.*, **67**, 1818-1820, 1995.
3) H. Kiriyama et al., *J. Opt. Soc. Am. B*, **19** 1857-1864, 2002.

4.1.3 24-mJ, diode-pumped, chirped-pulse regenerative amplifier with a cooled Yb:$LiYF_4$

Junji KAWANAKA, Koichi YAMAKAWA, Hajime NISHIOKA[a)] and Ken-ichi UEDA[a)]
[a)]Institute for Laser Science, University of Electro-Communications

1. Introduction

Diode-pumped ultrahigh-peak-power lasers with a compact size and easy operation are in high demands for high-field science, such as field ionization, laser acceleration and novel x-ray generation. Ytterbium-doped materials are available for diode-pumped laser materials due to its long lifetime and absorption wavelength that overlapped with the emission wavelength of commercially obtainable high power laser diodes. The high quantum efficiency of > 90% leads to low thermal effects, which enable high average power operation. Yb:$LiYF_4$(Yb:YLF) crystal is one of the most promised laser materials in the next generation of the diode-pumped high-field lasers due to its wide spectral emission range, high thermal conductivity and low thermal lens effect. In our previous work, the laser gain and the spectral gain width of a diode-pumped Yb:YLF were dramatically improved at low temperature.[1] Then a diode-pumped, Kerr-lens mode-locked oscillator has been developed at liquid nitrogen temperature.[2] In the present work, a diode-pumped regenerative amplifier with a cooled Yb:YLF crystal has been demonstrated as a booster amplifier in our all solid-state ultrahigh-peak-power laser system.

2. Experimental setup

A schematic diagram of our diode-pumped regenerative amplifier was shown in Fig. 1. The x-type cavity is consisted of two high reflectors and two dichroic mirrors. A combination of a pre-bias-Pockels cell and a thin film polarizer was prepared for a seed pulse injection and a cavity damp. The 2 mm-thick, 20 at. % Yb:YLF crystal is cooled by a liquid nitrogen cryostat. A 600-μm-core fiber-coupled laser diode is used as a pump source in a quasi-continuous-wave operation mode with a typical repetition rate of 10 Hz. The emission duration was changed below 4 ms. The pump beam is focused on the crystal with a circular spatial profile at about 600 μm-diameter and the pump intensity was 25 kW/cm^2 at maximum on the crystal surface. The 85-fs pulses from a mode-locked Ti:sapphire laser oscillator were stretched in time with 1.2-ns by using a 1.2-km polarization-maintained single-mode fiber. The chirped pulse energy was about 20-pJ and the center wavelength was 1020- nm with 15-nm FWHM spectral width. The cavity Q was changed from low to high by applying zero-voltage to the Pockels cell in 40 μs after the pumping, and one in chirped pulse trains was synchronously trapped in the cavity. The cavity damp was executed after several ten round trips. The series of a Faraday rotator, half-wavelength plate and a polarizing beam splitter is use as an optical isolator. The regeneratively amplified pulse in the cavity was monitored with a PIN photo diode behind the high reflector.

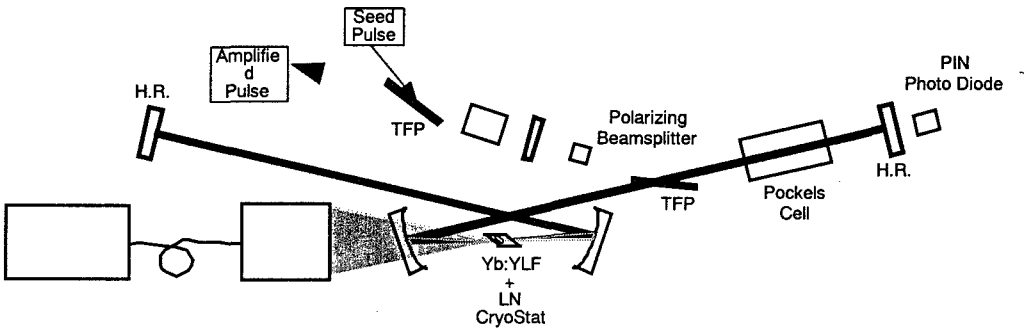

Fig. 1 Schematic diagram of a diode-pumped regenerative amplifier with a cooled Yb:YLF crystal

3. Results

Figure 2 showed the amplified output pulse energy as a function of peak pump power for different pump duration. The output pulse energy of 24.3-mJ was obtained at the 55th round trip at 92-W, 4-ms pump. The amplification factor was ~10^9. The optical-to-optical efficiency was 6.6% . The initial small signal gain was estimated to be 1.7 by fitting our numerical calculation to the experimental data of temporal growing of the trapped pulse in the cavity. The energy extraction efficiency was, therefore, calculated to be 45%. The spectral width was reduced to 5-nm due to spectral gain narrowing in Fig. 3. The output chirped pulse was compressed with a grating pair. The pulse energy and the pulse duration after compression were 10.2-mJ and 990-fs(Gauss) / 660-fs(sech^2), respectively. It should be noted that sub-100 fs pulse duration after compression could be obtained due to a 35-nm wide spectral gain width of a cooled Yb:YLF crystal by replacing the fiber stretcher to an antiparallel grating pair pulse stretcher and reshaping a gain spectrum with a pellicle etalon.

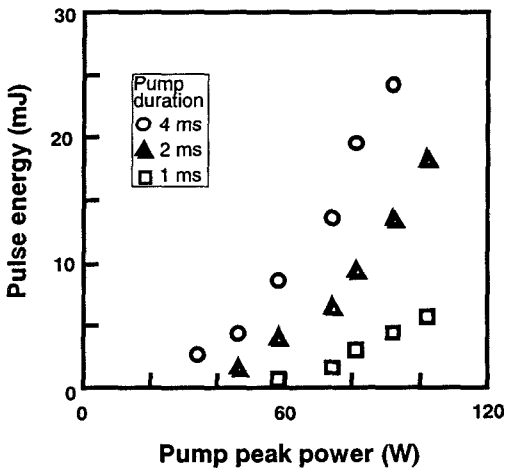

Fig. 2 Output pulse energy as a function of a peak pump power

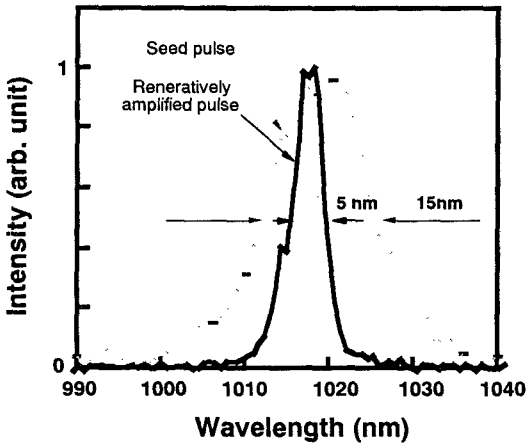

Fig. 3 Spectral profiles of a seed pulse and a regeneratively amplified output pulse

3. Summery

In summery, a diode-pumped regenerative amplifier has been demonstrated with a cooled-Yb:YLF. The 24.3-mJ pulse was generated after amplification at the repetition rate of 10-Hz. The optical-to-optical efficiency and the energy extraction efficiency were 6.6% and 45%, respectively. A 10-mJ pulse energy with sub-ps pulse duration was obtained after compression. To our knowledge, this is the highest energy chirped pulse regenerative amplifier based on Yb:YLF.

References

1) J. Kawanaka, H. Nishioka, N. Inoue, and K. Ueda, Appl. Opt. **40**, 3542-3546 (2001).
2) Extended Abstracts in the 48th Spring Meeting of the Japan Society of Applied Physics and Related Societies **3**,1092 (2001) (in Japanese).

4.1.4 Optical field ionization of rare gas atoms by high-intensity, ultrashort laser pulses

Yutaka AKAHANE, Yuji FUKUDA, Keiko SUTO, Makoto AOYAMA, Norihiro INOUE, Hideki UEDA, Takayuki UTSUMI and Koichi YAMAKAWA

1. Introduction

Ultrahigh-peak power CPA laser system are now capable of producing fully relativistic intensity regime over 10^{19}W/cm^2. In such a high intensity, the laser electric field becomes 20 times larger than the Coulomb field in hydrogen atom, and inner shell electrons for many atoms are fully ionized. There are various applications in these relativistic ultrahigh-intense laser field , such as Larmor radiation, generation of high energy electrons and X-rays. In order to these applications, understanding the ionization process of atoms in the relativistic regime is fundamentally important. So, in this study, we have investigated the optical field ionization processes by measuring the ionization of rare gas atoms (Ar, Kr, Xe) and evaluating the ion yield up to the relativistic intensity regime (>10^{19} W/cm^2).

2. Experiment

The high-peak power, ultrashort laser pulses from the 100 TW, 20 fs Ti:sapphire laser system in JAERI[1] were used in this high-field photoionization experiment. By means of the time-of-flight (TOF) mass spectrometer, multiply-charged ions of the rare gas atoms can be detected differentially in this study. In order to restrict the detection volume of the spectrometer only to the high-intensity laser focal region, an adjustable slit with a width of 300 μm is placed on the central axis of the drift tube. This slit eliminates the noise signals produced by ionizing contaminants at the large-volume, low-intensity region, and enables us to detect the feeble signals from multiply charged ions with a high signal-to-noise ratio.

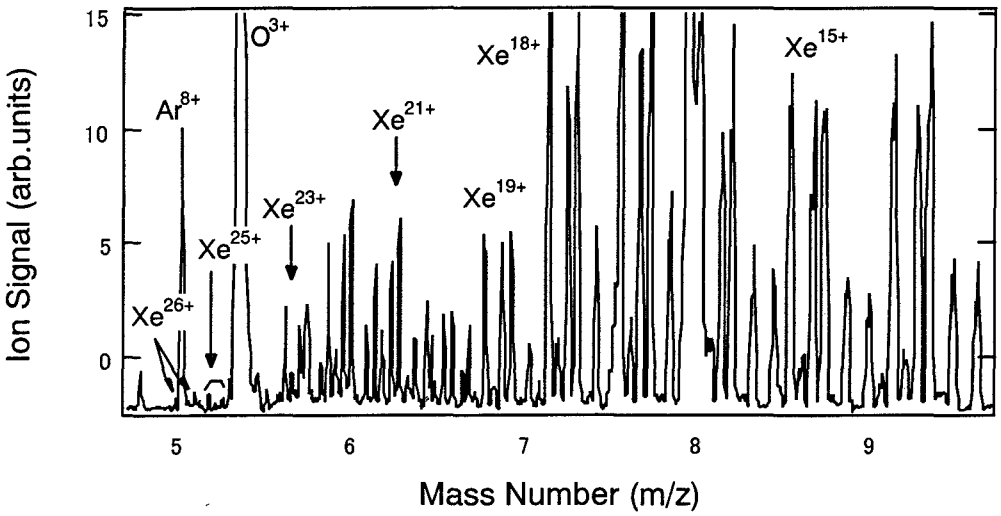

Fig. 1 Time-of-flight mass spectrum for Xe atom at an intensity of 2.6×10^{19} W/cm^2

The typical TOF mass spectrum of Xe ions is presented in Fig.1. From measured optical parameters of the laser pulse, such as pulse energy (530 mJ), pulse duration (25 fs at FWHM), and spot size (11 μm at 1/e^2), the laser peak intensity was estimated to be 2.6×10^{19} W/cm^2 As shown in Fig. 1, the isotopes of Xe are clearly resolved for each charge-state. The sudden decrease in ion intensity is observed between the charge-states 18 and 19 due to the electronic shell closing. The highest charge-state observed in this spectrum is 26, which corresponds to Ni-like Xe. The maximum ion charge states of Ar, Kr that were observed in the experiment were up to 16, 19, respectively.

3. Discussion

In order to investigate the ionization processes of rare gas atoms, the relative yields of multiply charged ions as a function of laser peak intensity are evaluated by integrating peak area of the TOF mass spectra. Fig.2 shows the typical peak intensity dependence of Kr ion yields. The solid lines in this figure are theoretically calculated yields by using the ADK tunneling ionization formula [2]. In the lower charge states

of Kr ions, such as Kr^{+}~Kr^{3+}, experimental yields are in good agreement with the ADK calculated results. But in the middle charge states of outer-shell, such as Kr^{4+},Kr^{5+},there are slight differences between experiment and the ADK curve. And there are some inflection points on the experimental yields of highly-charged Kr ions over Kr^{9+}. As the same case as Kr, whether the experimental ion yield of all charge states of rare gas atoms are generally following the ADK calculation curves, there are some differences between the ADK curve and the experimental data of highly-charged ions, that is, the difference of saturation intensity, and the existence of inflection points. The saturation intensities are mainly depends on the ionization potential (I_p) of each charge state of ions. So the difference of the saturation intensity implies that the conventional I_p are not applicable as they are in this high intensity region over $10^{16}W/cm^2$ on account of the electronic correlations in the ionizing atoms. And the existence of inflection points implies the presence of the simultaneous ionization process, such as electronic "rescattering" process[3]. We are trying to interpret the experimental results based on the non-sequential tunneling ionization model using the ADK formula.

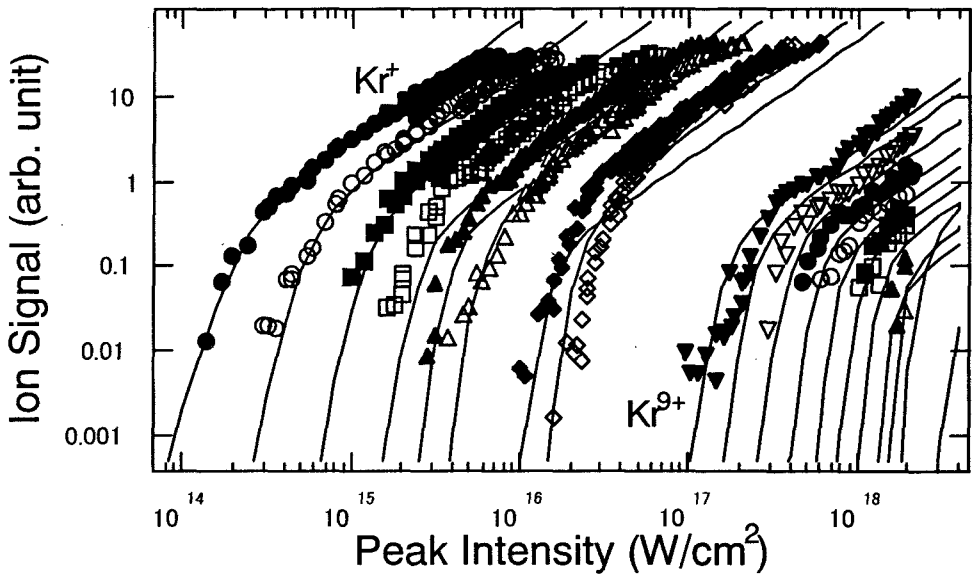

Fig. 2 Laser peak intensity dependence of Kr ions

4. Conclusion

In order to clarify the ionization process of atoms in the high intense laser fields, we have measured the ionization of rare gas atoms and evaluated the ion yields up to the relativistic intensity regime. In the experiment, highly-charged ions of which inner-shell elections were ionized have been systematically observed for the first time. Comparison between the experiment and ADK theory implies that some modifications on the ADK calculation are needed to describe ionization process more exactly in this high-intensity regime. We are currently working on the non-sequential tunneling ionization model to explain our experimental data more qualititabrly. These attempts will definitely contribute to the progress of the relativistic high-field science.

References

1) K. Yamakawa et al., Opt. Lett. **23**, 1468 (1998).
2) N. B. Delone et al., Phys. Usp. **41**, 469 (1998).
3) B. Sheehy et.al., Phys. Rev. A**58**, 3942 (1998)

4.1.5 Explosion of noble-gas clusters heated by the ultrafast, ultrahigh-intensity Ti:sapphire laser

Yuji FUKUDA, Yutaka AKAHANE, Makoto AOYAMA, Norihiro INOUE, Hideki UEDA, Yasuaki KISHIMOTO[a)] and Koichi YAMAKAWA

a) Naka Fusion Research Establishment, Japan Atomic Energy Research Institute

We have probed the interaction of intense laser fields with Xe clusters (~1,5000 atoms/cluster) by measuring the energy and charge-state distributions of emitted particles, i.e. ions and electrons, using the 100 TW, 20 fs, Ti:sapphire laser system developed at JAERI [1]. This work demonstrates that the energetic particle emission from the laser-cluster interaction can be optimized by seeing into explosion dynamics of the clusters using the ultrafast laser pulse and manipulating the characters of the laser pulse.

Figure 1 shows the typical energy distributions of the emitted multiply-charged ions, Xe^{n+}, obtained when the Xe clusters were irradiated by the various pulse durations under the fixed laser peak intensity of 2×10^{17} W/cm^2. The resulting energy distributions are found changed significantly with the pulse duration: When the Xe clusters were irradiated by the 20-fs pulse with the laser energy of 2.6 mJ, the energy distribution with the bulk component less than ~1 keV was obtained. As the pulse duration became longer, the energy distributions shifted to higher energies, and almost flat distribution was established for the 500-fs pulse with the laser energy of 66 mJ. The optimal pulse duration giving the maximum ion energy is achieved when the Xe clusters are irradiated by the 500-fs pulse. Similar trend was also observed for the energy distributions of the emitted electrons.

From the analysis of charge-state, n, distributions of the emitted multiply-charged ions, Xe^{n+}, when the Xe clusters were irradiated by the 500-fs pulses, it is revealed that for ions with the kinetic energy of 100 keV the peak charge-state was ~20 with some ions having charge-state as high as ~30. This is much higher than ~14 expected from the tunnel ionization of single Xe atoms at this laser intensity. On the other hand, when the Xe clusters were irradiated by the 20-fs pulse, the peak charge-state for ions with the kinetic energy of 8 keV was found ~10 with some ions as high as ~18. These results indicate that the strong collisional ionization by hot electrons created through the resonant absorption would play a crucial role to strip the ions to higher charge-states in the case of the 500-fs pulses, while the field ionization would be a dominant process in the case of the 20-fs pulse. Theoretical simulations based on three-dimensional (3D) particle-in-cell (PIC) code also predict the importance of the collisional ionization to produce the ions with higher charge-states.

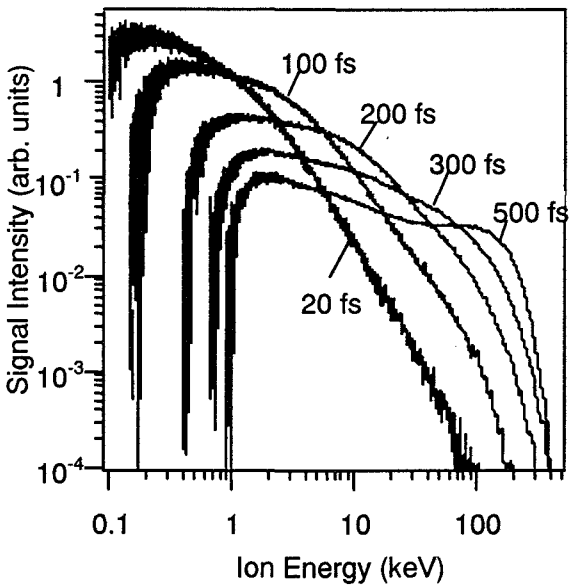

Fig.1 Energy distributions of the emitted ions

Reference

1) K. Yamakawa *et al. Opt. Lett.* **23**, 1468 (1998).

4.1.6 Study of coherent quantum control in APR

Keiichi YOKOYAMA, Junkei KOU, Yuji FUKUDA, Makoto AOYAMA, Yutaka AKAHANE, Norihiro INOUE, Hideki UEDA and Koichi YAMAKAWA

1. Introduction

Control of quantum systems like atoms and molecules is one of the important challenging applications for the current laser technologies. In particular, pulse-shaping techniques and generation of transform-limited pulses are indispensable for the precise coherent quantum control[1] as well as for the development of high peak-power lasers. So far, several methods have been examined to modulate the spectral phase and/or amplitude, for example, with a spatial light modulator using a liquid crystal array or a deformable mirror which was placed on the Fourier plane in the dispersion-free 4*f* configuration of a grating pair.

The goal of the pulse shaping is to obtain an electric field optimal for a specific quantum control. In general, such an electric field should be highly complicated and no explicit guideline has been established to search the optimal solution. Instead, the goal may be achieved by a learning system in which certain properties (*e.g.* reaction yield) affected by a modulation are monitored and feedbacked to generate the next modulation. In other words, the quantum system can teach lasers to control quantum system itself. Some prototypes of the learning system were demonstrated for quantum controls using evolutionary algorithms. Development of general pulse-shaping system and understanding of the control mechanism are really exciting issues and key technologies to facilitate the invention of new materials.

We have developed a new type of learning pulse-shaping system using an acousto-optic programmable dispersive filter (AOPDF) combined with the evolutional strategy for optimization algorithm. Its performance is examined in the adaptive temporal compression of femtosecond pulses.

2. Temporal compression of optical pulses

Femotosecond pulses from a Ti:Sapphire mode-locked oscillator (Spectra-Physics, Tsunami) was delivered to the 25-mm-thick TeO_2 crystal in the AOPDF (FASTLITE, Dazzler) with a repetition rate of 80 MHz and a spectral band width of 22 nm centered at 800 nm. The duration of the output pulse from the AOPDF was measured with an autocorrelator (Spectra-Physics, 409).

With an appropiate parameterization of electric field, the adaptive compression yielded 65-fs pulse duration. Figure 1 shows the auto correlation signal of the compressed pulses together with that of unmodulated pulses from the TeO_2 crystal. The unmodulated pulse is stretched to 714 fs due to the group velocity dispersion (GVD) of the crystal. A compensation of the GVD by the AOPDF gives 49-fs pulses as denoted by "manual compression". Considering the effective band width of 17 nm for the modulated pulses, the obtained pulse duration (65 fs) indicates a success of the present adaptive compression close to the transform limit.

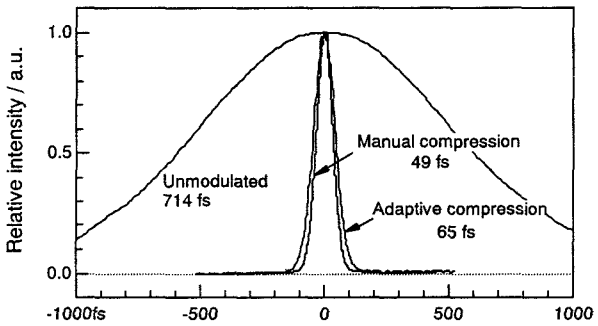

Fig. 1 Autocorrelation signal of the pulses passed through the AOPDF

Also, we presented, in this study, a new method to parameterize the electric field, in which optical field is defined by the superposition of linearly chirped pulses. Because many schemes proposed theoretically for various quantum controls use a series of linearly chirped pulses, this new parameterization should reduce the number of meaningless steps in the blind search and make the evolution more efficient. In fact, the above adaptive pulse compression used only four parameters.

3. Conclusion

The success of adaptive compression and implementation of the new parameterization enable us to study a number of new schemes in quantum control here in APR, for example, selective complete excitation of atoms and molecules or vibrational ladder climbing. These are of fundamental importance towards the isotope separation and selective formation of chemical products.

Reference

1) H. Rabitz, R.de Vivie-Riedle, M. Motzkus, K. Kompa, Science **288**, 824, 2000.

4.1.7 Short pulse keV X-ray generation by fs laser pulse irradiation

Fumiaki MATSUOKA, Ingo USCHMANN[a)], Etsuya YANASE, Masayuki SUZUKI, Takatsugu OKETA, Keiko SUTO, Mamiko NISHIUCHI, Hiroyuki DAIDO
a) Institut für Optik Quantenelektronik, Friedrichi-Schiller-Universität Jena

1. Introduction

Recently, time-resolved crystal structure analysis with short pulse keV X-ray from laser plasma is reported[1)]. Not only inorganic but also organic crystals can be observed by this technique. Observation of structure dynamics of intricate materials like protein or DNA is expected to make clear the interrelation between the function and the structure of these materials. In the first stage, we generated keV order X-ray by irradiating short pulse laser to a solid target.

2. Experimental

Figure 1 shows experimental setup of X-ray generation. Short pulse Ti:sapphire laser (25mJ, 120fs, 0.21TW) was focused by a lens (f=130mm) and irradiated to an aluminum moving wire target. The generated X-ray was focused onto a CCD camera or an imaging plate (IP) by a bent crystal. The bent crystal works as an X-ray focusing mirror and a spectrometer[2)].

3. Results

Figure 2 shows observed X-ray spectra near Al Heα line, and inset shows wide range spectra around the line. Atomic spectrum, Al Kα line, Heα line, Lyα line, etc. were observed[3),4)]. Some satellite peaks could be observed near main Heα line. The satellite peaks cannot be explained by atomic spectra. The origin of these peaks is not clear.

We are preparing an X-ray diffraction system used by the Al kα line with time resolve X-ray pump-probe technique to observe crystal dynamics. We are also preparing a higher peak power laser system, which provide higher energy X-ray, such as Cu Kα or Zn Kα lines.

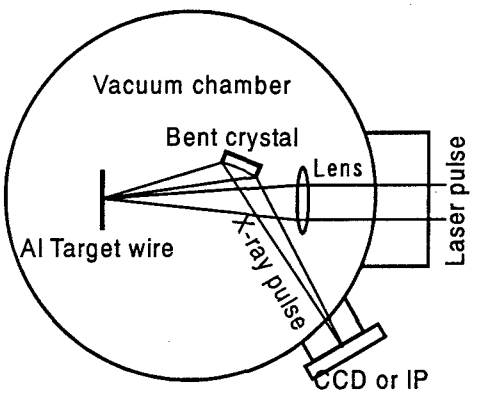

Fig. 1 Experimental setup of X-ray generation

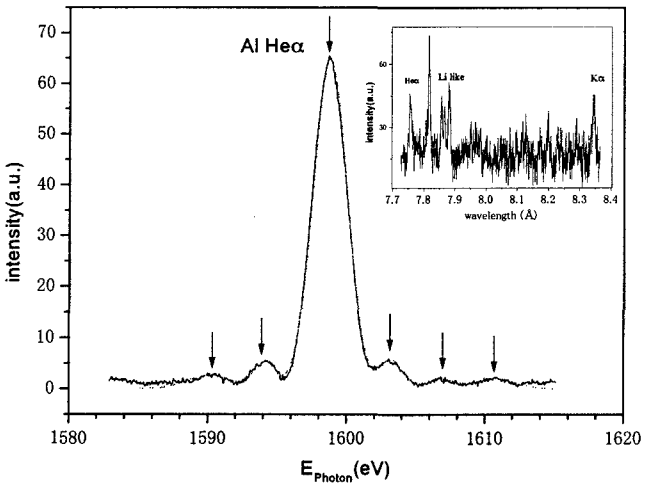

Fig. 2 X-ray spectrum near Al Heα line Inset shows wide range spectra.

References

1) Rousse, C. Rischel, J.Gautheir, Rev. of Mod. Phys., **73**, 17, 2001
2) E.F ster, I. Uschmann, P. Gibbon and T. Feurer, Proc. of SPIE, **3451**, 32,1998
3) U. Andiel, K. Eidmann, K. Witte, I. Uschmann and E. F rster, Appl. Phys. Lett., **80**, 198, 2002
4) H. Nakano, T. Nishikawa and N. Uesugi, Appl. Phys. Lett., **79**, 24, 2001

4.2 X-ray Laser Development

Keisuke NAGASHIMA, Maki KISHIMOTO, Masataka KADO, Tetsuya KAWACHI, Noboru HASEGAWA, Momoko TANAKA, Kouta SUKEGAWA, Renzhong TAI, Peixiang LU, Huajing TANG[1], Hiroyuki DAIDO
1 Institute of Laser Engineering, Suita, Osaka, 575-0001, Japan

Outline of x-ray laser research

The x-ray laser research at Advanced Photon Research Center has started on April 1998. The main purpose is to develop compact high performance x-ray laser system. In 1999, the experimental system, of which main device is a CPA (chirped pulse amplification) laser using Ti:sapphire and Nd:glass, was installed in a new laboratory at the KIZU site. We achieved the first x-ray lasing at 32.6 nm (Ti target) by transient collisional excitation scheme (Fig.1). In 2000, we succeeded in generating x-ray lasing at shorter wavelengths of 11.9 nm (Sn target) and 13.9 nm (Ag target). The saturated amplification was achieved by using traveling wave pumping.

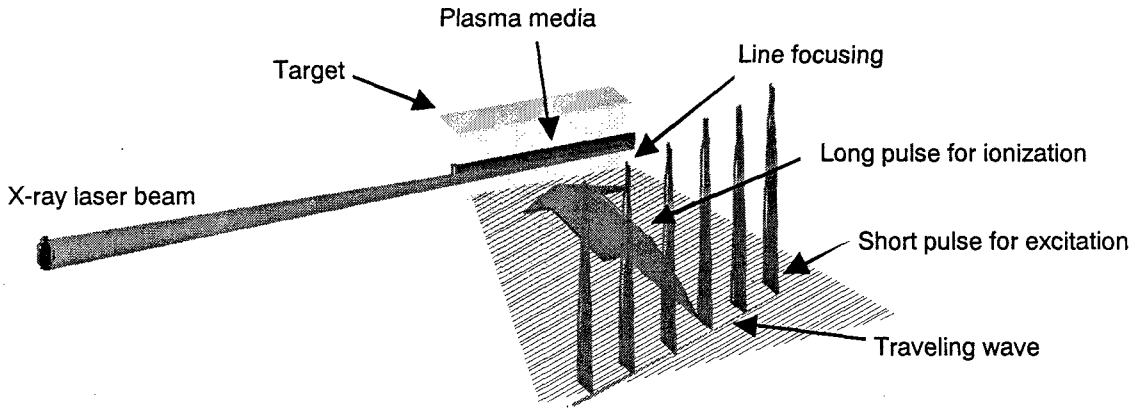

Fig.1 Transient Collisional Excitation(TCE) Scheme

In 2001, we have pushed on the shortening of the wavelength up to 8.8 nm using La target (**4.2.1**). This is the shortest wavelength achieved by use of compact pumping laser systems. The detail of plasma gain media examined from the measurement of near-field x-ray intensity profiles (**4.2.2**). We have succeeded in generating x-ray lasers using gaseous materials, Ar and Xe, of which wavelengths are 46.9 nm and 10.0 nm, respectively (**4.2.3**). For advancing the quality of the x-ray laser beam, we are planning the amplification of coherent seeding light by the x-ray laser media (**4.2.4**). The several applications have been started using these x-ray lasers. The surface microstructure of BaTiO3 crystal was examined from a speckle pattern of coherent x-ray beam (**4.2.5**) and the x-ray microscope was developed using a schwarzschild optics and a zone-plate with a spatial resolution of 200 μm (**4.2.6**).

4.2.1 Observation of strong soft x-ray amplification at 8.8 nm

Tetsuya KAWACHI, Akira SASAKI, Momoko TANAKA, Maki KISHIMOTO, Noboru HASEGAWA, Keisuke NAGASHIMA, Masato KOIKE, Hiroyuki DAIDO and Yoshiaki KATO

1. Introduction

Development of intense and efficient x-ray lasers in a shorter wavelength region is one of the most important objectives of x-ray laser research. Recent progress in the transient collisional excitation (TCE) scheme allows us to achieve the gain-saturation in a wavelength region up to 12 nm with a pumping energy of ~ 10 J [1], and demonstration of strong lasing in shorter wavelength region than 10 nm is an urgent subject.

In shorter wavelength x-ray lasers, the optimum gain condition is expected in high temperature and dense region. For an example, the optimum plasma parameters for the Ni-like La (z =57) laser at 8.8 nm are estimated to be T_e ~ 900 eV and n_e ~ 8×10^{21} cm^{-3}, which is higher than the critical density of a pumping laser pulse at a wavelength of 1 μm.

In order to provide the pumping energy to high density region, frequency conversion of the pumping laser has been used. However, the frequency conversion of a pulse with ps-duration and ~ 15 J requires a large non-linear medium, and its low conversion efficiency (~50%) requires a large amount of energy, which is not practical and contradicts the concept of table-top x-ray lasers. Rather, it is realistic to optimize the pre-formed plasma condition to achieve effective heating of the dense region by the fundamental laser light. Although the fundamental laser light can not penetrate into the over-dense region, the laser energy absorbed near the critical density can be delivered to the dense region by the electron thermal conduction. In this report, we show that substantial gain can be obtained at a wavelength of 8.8 nm in the TCE scheme by reducing the pre-pulse intensity, where the scale-length of the pre-formed plasma becomes short enough to obtain the plasma temperature of KeV in the over-dense region.

2. Experiment and discussion

The details of our pumping laser and experimental setup have been described in elsewhere [2]. A 2 μm-thick La slab target coated on a 1 mm-thick glass substrate was irradiated by a line-focused compact CPA Nd:glass laser at a wavelength of 1.053 μm. The laser pulses consisted of a pre-pulse and a main pulse with a duration of 200 ps and 7 ps, separated by 250 ps. The intensity on the target was 3.0×10^{12} W/cm^2 for the pre-pulse and 1.4×10^{15} W/cm^2 for the main pulse. We employed a quasi-traveling wave pumping. The emission from the La plasma was observed using a grazing incidence spectrograph, GIS1, and a KAP crystal spectrograph (KAPCS). The GIS1, which covered spectral range of 6 ~ 40 nm and was set in the propagation direction of x-ray laser beam. The KAPCS covered 0.8 ~1.0 nm and the n = 3 - 5 transitions of the Ni-, Co- and Fe-like La ions were observed. The detectors were back-illuminated CCD.

Figure 1 (a) and (b) show the spectra taken by GIS1 for the target lengths of 5.3mm and 2.6mm, and the spectrum taken by KAPCS, respectively. The lasing line and the resonance lines of the Ni-, Co- and Fe-like ions are marked by arrows. Substantial amplification of the 8.8 nm line of the Ni-like La ions is obvious. In this target shot, the energy of the pre-pulse and main pulse was 1 J and 17 J, respectively. The gain coefficient, g, and gain-length product, gL, were derived to be 14.5 ± 1.5 cm^{-1} and gL = 7.7 ± 0.8, respectively.

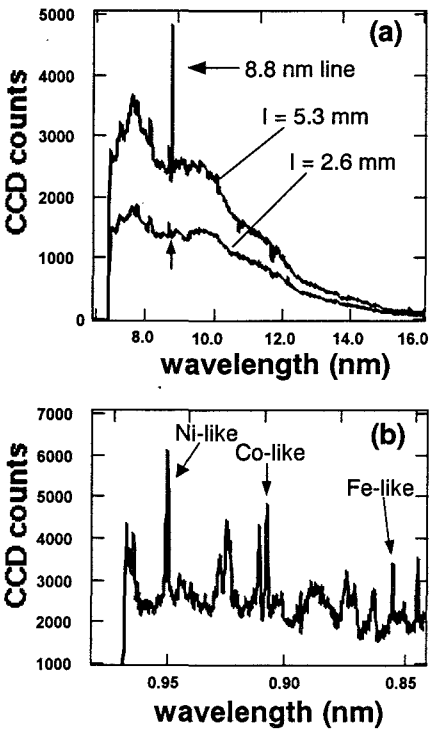

Fig. 1 Typical spectrum of La ions taken by GIS1 and KAPCS

We observed the dependence of the 8.8 nm line output on the pre-pulse intensity. The main-pulse energy was fixed, and the pre-pulse intensity was changed from 5×10^{11} through 1.2×10^{13} W/cm^2. Figure 2 shows the result. The abscissa is the intensity of the pre-pulse, and the closed circles represent the output of the 8.8 nm line. The 8.8 nm output has a peak at around pre-pulse intensity of 3×10^{12} W/cm^2. The open triangles and open diamonds

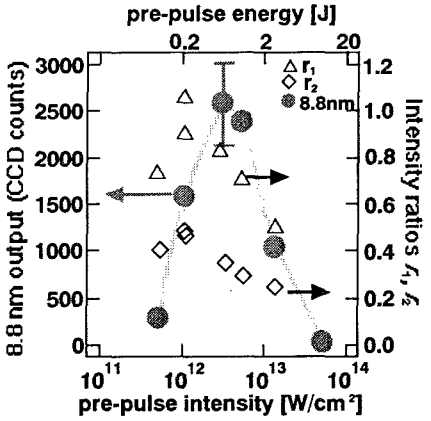

Fig.2 The 8.8 nm output (Solid circle) for various prepulse intensities The open triangle and diamond are intensity ratios of the Ni-, Co- and Fe-like ions.

represent the line intensity ratios, r_1 and r_2, of the $3d$-$5f$ lines of the Ni-like (0.95 nm), Co-like (0.91 nm) and Fe-like ions (0.86 nm), *i.e.*, r_1 = I(Co-like)/I(Ni-like) and r_2 = I(Fe-like)/I(Ni-like), respectively. The increase of these intensity ratios corresponds to the increase of the electron temperature.

In the pre-pulse intensity region of 1×10^{12} ~ 1.2×10^{13} W/cm^2, the r_1 and r_2 increase with decrease of the pre-pulse intensity. This indicates that by reducing the pre-pulse intensity, the volume of the pre-formed plasma is reduced, and the main pulse energy is absorbed in a localized area. This tendency is reproduced by a 1-D hydrodynamics code HYADES: As the pre-pulse intensity increases, the calculated result shows that the spatial profile of the electron temperature becomes broader, and the peak value becomes lower.

At the pre-pulse intensity of 1×10^{12} W/cm^2, Fig. 2 shows that the r_1 and r_2 values increase, whereas the x-ray laser output becomes small compared with the peak value. This may be due to the refraction of the amplified x-ray in the gain medium. This implies the x-ray beam propagation is sensitive to the pre-pulse intensity in the present case, and in order to achieve more efficient lasing at this wavelength we have to compensate the refraction by use of additional means such as curved targets.

In summary, we have demonstrated substantial amplification of 8.8 nm line in the TCE scheme with a pumping energy of 18 J. This is the first demonstration of strong amplification by use of a compact pumping system.

References

1) T. Kawachi *et al.*, Phys. Rev. A. (in press)
2) T. Kawachi *et al.*, Appl. Optics. (in press)

4.2.2 Ray trace of the x-ray laser with two peaks in the gain profile

Momoko TANAKA

1. Introduction

We have been generated the TCE x-ray laser in saturation regime [1] and observed the near field pattern of intensity profile of Ni-like silver x-ray laser [2, 3]. The observed spatial pattern shows two peaks in the parallel direction to the target surface. The origin of the two peaks is assumed to be due to two peaks in the gain profile. In order to derive the spatial gain profile, we performed a two-dimensional ray tracing calculation, in which the amplification of the x-ray and the effect of the refraction were included. Here, we will report a model and result of the calculation.

2. Calculation

We considered 6.0 mm long gain medium plasma, which is uniform in gain coefficient and electron density along propagation direction of the x-ray laser. The electron density gradient of the plasma was calculated using one dimensional hydrodynamics simulation code, the HYADES, under an assumption of cylindrical symmetry for simplicity. We divided the gain medium in the section plane into 43 x 51 cells with a size of 2 μm x 2 μm and assumed that the gain coefficient and the density were uniform inside each cell. As a spontaneous emission of the x-ray lasing line, 400 rays from each cell in cone angle of 20 mrad are taken into account. Initial intensity of the spontaneous emission was assumed to be proportional to the gain coefficient, which is roughly proportional to the population of the upper lasing level. The ray emitted from each cell was firstly amplified by the gain at this position. The propagation direction of the ray was changed due to the refraction at a boundary between the initial cell and next cell. This procedure was iterated until the amplified photons reached at the end of plasma.

The spatial profiles of the output x-ray laser light were calculated for various spatial gain profiles. Two peaks were not produced when any gain profiles with single peak were used. Shown in Fig. 1 (b) is the calculated spatial profile of the x-ray laser using the gain profile shown in Fig. 1 (a). The gain region was assumed to be 50 μm distant from the target surface and had two peaks separated by 50 μm in vertical direction. Since the gain medium plasma had steep density gradient, some of x-rays are escaped from the gain region with refraction. However, after propagation of 6.0 mm in the gain medium, the two peaks were still remaining in the spatial profile and the x-ray laser did not much leave from the target surface, since the escaped rays from the gain region were much weaker than the gain guided x-rays. It is consistent with our experimental results.

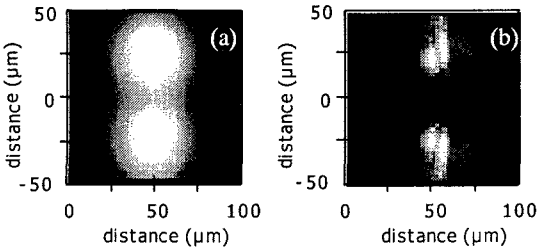

Fig. 1 The result of ray traces. (a); The spatial gain profile with two peaks used in calculation, (b); calculated spatial profile of the x-ray laser after 6 mm propagation.

References

1) T. Kawachi, et al. Phys. Rev. A to be published.
2) M. Tanaka et al. JAERI-Review 2001-046, 18, 2002
3) M. Tanaka et al. Surface Review and Letters 9, 641, 2002

4.2.3 Demonstartion of transient collisional excitation x-ray lasers in gases

Peixiang LU, Tetsuya KAWACHI, Maki KISHIMOTO, Kouta SUKEGAWA, Momoko TANAKA, Noboru HASEGAWA, Masayuki SUZUKI, Renzhong TAI, Masataka KADO, Keisuke NAGASHIMA, Hiroyuki DAIDO, Yoshiaki KATO, Henry FIEDOROWICZ[a)] and Andrzej BARTNIK[a)]
a) Institute of Optoelectronics, MUT, Poland

1. Introduction

One of the most promising ways of developing table-top x-ray lasers for applications is a scheme based on transient collisional excitation (TCE). In this report, we present results on TCE x-ray lasers using a gas puff target. The use of a gas puff instead of a solid target may bring us a high repetition rate x-ray laser without production of target debris, which is very favorable for practical applications.

2. Experimental

The experiment was performed on a CPA laser at JAERI.[1)] This laser provides up to 20 J of light at 1053 nm with the shortest pulse duration of 400 fs. In the experiment, the driving laser pulse for the soft x-ray lasing experiment consisted of a prepulse and a main pulse both with a ps duration, separated by 1.2 ns. The line focus is with a length of 0.55 cm and a width of 20 μm.[1)] Traveling wave geometry with a traveling velocity of 0.98c was used to irradiate the target by using a stepped mirror technique.[1)] The gas puff target was equipped with a nozzle in a form of a 0.6-cm-long and 500-μm-wide slit. Argon and xenon gases were used to form gas puff targets. The laser beam illuminated the gas puff target in the transverse direction with respect to the flow of gas. The valve time delay between the opening of the valve and the laser pulse was set to be 410 μs. The maximum gas density in the interaction region was roughly estimated to be ~5×10^{19} cm^{-3} for a backing pressure of 10 bars in the valve.

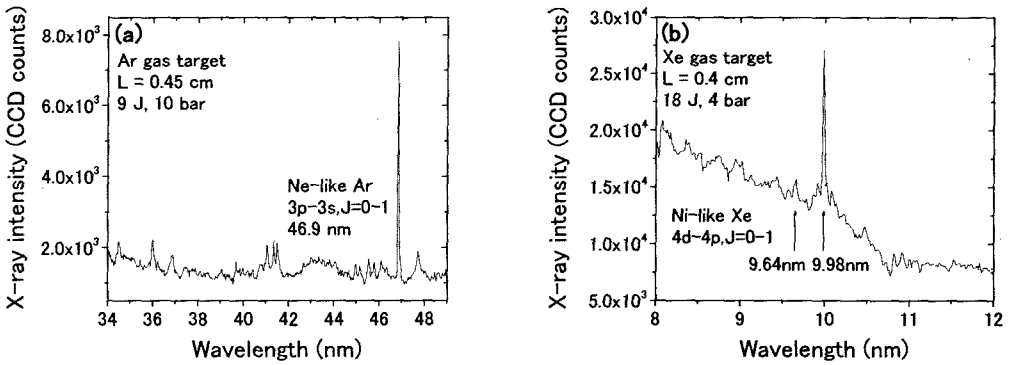

Fig. 1 On-axis x-ray spectra for (a) a 0.45-cm-long argon and (b) a 0.40-cm-long xenon gas puff targets.

3. Results

In the experiment, strong soft x-ray lasing on the transient collisionally excited $3p\ ^1S_0$ - $3s\ ^1P_1$ transition for neon-like argon at 46.9 nm was observed by irradiation of a gas puff target with two 1.5 ps driving laser pulses with ~9 J total energy, with a high gain of 18.7±1.0 cm^{-1} and a narrow beam divergence of less than 3.7 mrad.[2)] To extend it to the shorter wavelength region, we also performed an experiment for nickel-like xenon x-ray lasers by irradiation of an elongated gas puff target with two 3.0 ps driving laser pulses with ~18 J total energy. Soft x-ray lasing on the transient collisionally excited $(3d_{3/2}, 4d_{3/2})_0$ - $(3d_{5/2}, 4p_{3/2})_1$ transition at 9.98 nm and $(3d_{3/2}, 4d_{3/2})_0$ - $(3d_{3/2}, 4p_{1/2})_1$ transition at 9.64 nm for nickel-like xenon ions was observed for the first time, gains of 17.4 ± 2.7 cm^{-1} and 5.9 ± 1.8 cm^{-1} were measured on these laser transitions for target lengths up to 0.45 cm.[3)]

References

1) T. Kawachi *et al.*, Phys. Rev. A (to be published)
2) Peixiang Lu *et al.*, Jpn. J. Appl. Phys. **41**, L133, 1990
3) Peixiang Lu *et al.*, Opt. Lett.(to be published)

4.2.4. High order harmonic generation as the seed light of 14nm x-ray laser

Noboru HASEGAWA, Tetsuya KAWACHI, Maki KISHIMOTO, Kouta SUKEGAWA
and Keisuke NAGASHIMA

1. Introduction

Transient collisional excitation (TCE) x-ray laser, which has monochromatic and short pulse duration, is one of the short wavelength light sources and has been intensively studied in order to achieve high peak brightness with small pumping energy. Especially, the nickel-like silver x-ray laser (λ=13.9nm) has several advantages. Firstly, strong amplification has been achieved in our previous work, in which the output intensity is order of 10^{10} W/cm^2 [1]. Secondly this wavelength region is very important in the application experiment because high reflectivity Mo/Si multi-layer mirror is available. However the spatial coherence is not satisfactory for the applications. We proposed a method to generate highly spatial coherent x-ray laser, in which high order harmonics was used as a seed light of a laser-produced x-ray amplifier. The high-order harmonic is very suitable for this purpose because it has high spatial coherence[2].

The x-ray lasers in the case of TCE scheme have a very narrow bandwidth ($\Delta\lambda/\lambda \sim 10^{-4}$)[3] and have a few picosecond pulse duration[4]. In this scheme, the intensity of the output x-ray strongly depends on the beam divergence of the seed light and the spectral coupling efficiency between the x-ray laser medium and the harmonics ($=\Delta\lambda_{\text{x-ray laser}} / \Delta\lambda_{\text{harmonic}}$). In this report, we conducted a preliminary experiment for generating the high order harmonic as the seed light for the 14nm x-ray laser using Ti;Sapphire laser.

2. Experiment and results

The quite high order(57th) harmonic is required for the seed light for Ni-like silver x-ray laser with the wavelength of 13.9 nm. It was generated by irradiating Ti;Sapphire laser on Ne gas jet target under the conditions that central wavelength of fundamental light was 790 nm, spectrum band width was 20nm, pulse duration was 60 fs, incident laser intensity was 8.3×10^{14} W/cm^2, neutral gas density was 3×10^{18} cm^{-3}, laser interaction length was about 3mm, focal F-number was 53 and focal spot size was 60μm. Fundamental laser light was cut with 0.5μm thickness Zr filter and the generated harmonics were detected by grazing incidence spectrometer. Figure 1 is the spectrum of high-order harmonics controlled for 57th harmonic intensity will be maximum. The spectrum was integrated over 1800 shots. The wavelength of 57th was 13.7nm and a bandwidth ($d\lambda/\lambda$) was 10^{-2}. The beam divergence was very small (1.8 mrad) compared with typical TCE x-ray laser (~10 mrad) and the conversion efficiency was 3×10^{-8}.

3. Summary and future plan

We obtained the 57th-order harmonic for the purpose of high spatial coherent 14nm x-ray laser. The conversion efficiency and beam divergence were good enough for the seed light of TCE x-ray laser. The wavelength and bandwidth was not satisfactory in this experiment because the fundamental laser parameter was not optimized. We are planing the high precision experiment using the central wavelength and the spectral bandwidth tunable Ti;Sapphire laser which was constructed for this purpose in previous works[5].

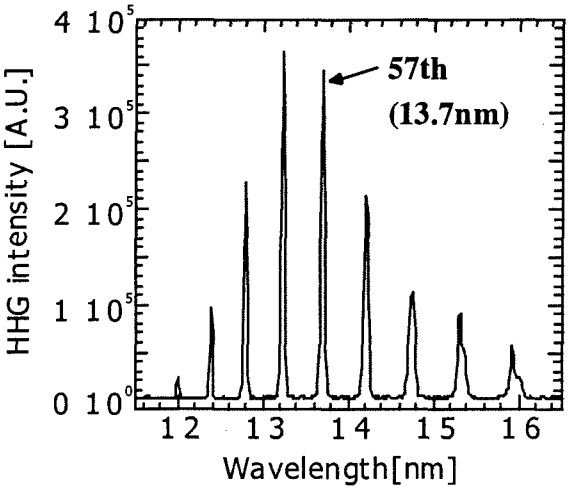

Fig. 1 A typical spectrum of high-order harmonics The spectrum was integrated over 1800 shots.

References

1) T. Kawachi *et al.*, Phy. Rev. A to be published.
2) T. Ditmire *et al.*, Phys. Rev. Lett. 77, 4756 ,1996
3) Jeffrey A. Koch *et al.*, Phy. Rev. A 50, 1877, 1994
4) A. Klisnick *et al.*, SPIE Proceedings 4505, 75, 2001
5) N. Hasegawa *et al.*, SPIE Proceedings 4505, 204, 2001

4.2.5 Study of Ferroelectric Domain Correlations in $BaTiO_3$ with Soft X-ray Laser Speckles

Renzhong TAI, Kazumichi NAMIKAWA[a)], Maki KISHIMOTO, Momoko TANAKA, Kouta SUKEGAWA, Noboru HASEGAWA, Tetsuya KAWACHI, Peixiang LU, Keisuke NAGASHIMA, Hiroyuki DAIDO, Akikatsu SAWADA[b)] and Yoshiaki KATO

a) The department of physics, Tokyo Gakugei University

b) The department of physics, Okayama Univeristy

1. Introduction

The reason why no clear soft phonon in BaTiO3 has been observed to date has been considered to be ascribable to the existence of the dipole clusters at above the Cuie point. However, no other efficient methods up to now can be used to verify this cluster model due to the small size (down to nm) and the short life time (down to ps). In this study, we try to use powerful x-ray laser to experimentally observe this phenomenon of the clusters and more to study the ferroelectric origin for this famous material.

2. Experimental

In Fig. 1, a 80μm (Horizontal)×200μm (Vertical) slit placed at 1.9 *m* from the silver slab target was used to produce a fully spatially coherent x-ray beam. The sample is flux-grown ferroelectrics BaTiO3 single crystal with its alternative a/c domains aligned in parallel. The Curie temperature is 122℃. The sample was located close to the slit with its domain boundaries (walls) set in the vertical direction. The temperature of the sample was controlled within a precision of ±0.5℃. The grazing angle was 10 degrees.

3. Results

Figure 2a shows a pattern of the probing beam measured in a direction of free propagation of the x-ray beam via the slit. Figure 2(b) ~ (h) show a series of the speckles diffracted from a region of multiple *a/c* domains when heating the sample from 24℃ to 130℃.

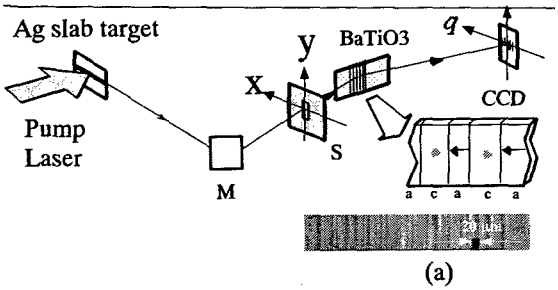

Fig. 1 Experiment setup

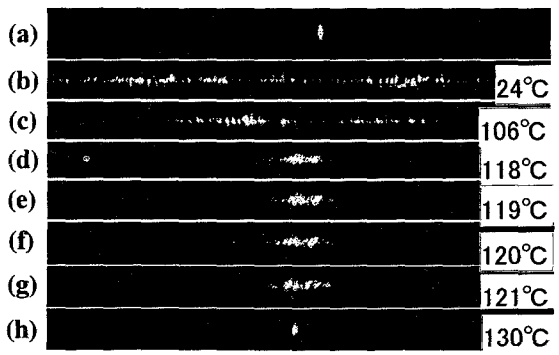

Fig. 2 Speckles at various tempertures

The correlation functions and the spatial power spectra of these domains on BaTiO3 have been calculated from the data shown in Fig .2. We conclude the results as follows. First the transient surface structures induced by ferroelectric domains decrease as temperature increases towards the Curie temperature (T_c) and completely disappear above the T_c; Second, the dramatic change of the spatial configuration of the *a/c* domains was observed to occur from a temperature 2℃ below the T_c, near which the transient surface domain density at equilibrium diverges via $[(T_c\text{-}T)/T]^{-\eta}$, with $\eta = 0.38\pm0.02$. These results yield a positive prospect for the further observation of the domain-like clusters in the future.

4.2.6 Development of Soft X-ray Microscopy System Using X-ray Laser

Maki KISHIMOTO, Momoko TANAKA, Renzhong TAI, Kouta SUKEGAWA,
Masataka KADO, Noboru HASEGAWA, Huajing TANG, Tetsuya KAWACHI,
Peixiang LU, Keisuke NAGASHIMA, Hiroyuki DAIDO, Yoshiaki KATO,
Koumei NAGAI[a)] and Hisataka TAKENAKA[a)]
a) NTT Advanced Technology Corporation

In Japan Atomic Energy Research Institute (JAERI) Kansai, we are developing a soft X-ray microscopy system using an X-ray laser. Figure 1 and Figure 2 show a schematic diagram of the X-ray microscopy system and a view of optical layout of X-ray microscope, respectively. This X-ray microscopy system consists of a Schwarzschild optics and a zone plate. The 13.9nm X-ray laser pulse is generated by irradiating a silver slab target with an intense pump laser light using the TCE (transient collisional excitation) scheme [1]. The generated X-ray laser pulse is sent to the Schwarzschild optics and is condensed onto the sample through a pin hole. The X-ray image of the sample is magnified with the objective zone plate and is projected onto a soft X-ray CCD. The diameters of convex and concave Mo/Si multi-layer mirrors used in the Schwarzschild optics, fabricated by NTT-AT, are 4.9mm and 25.4mm, respectively. The pin hole is used to eliminate the back-ground X-ray and the visible light which directly propagate from the plasma formed by the pump laser pulse on the slab target to the CCD through the gap between concave and convex mirrors in the Schwarzschild optics. The diameter and the focal length of the zone plate are 275μm and 2mm, respectively. The width of the outermost zone plate line is 100nm and the theoretically expected spatial resolution of this X-ray microscopy system is 122nm. Figure 3 shows a Cu mesh image taken by this X-ray microscopy system. The magnification is 140x. The black lines in the image are the Cu mesh shadows and the distance between the mesh shadows is 25μm. The evaluated spatial resolution of this microscopy system from the obtained X-ray images was about 200nm.

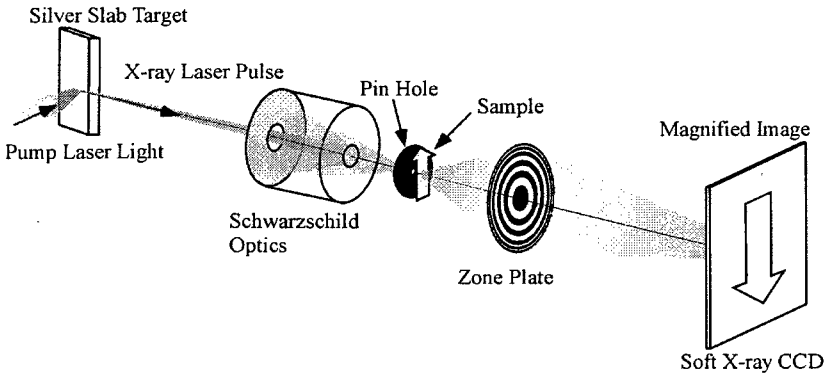

Fig. 1 Schematic diagram of X-ray microscopy system

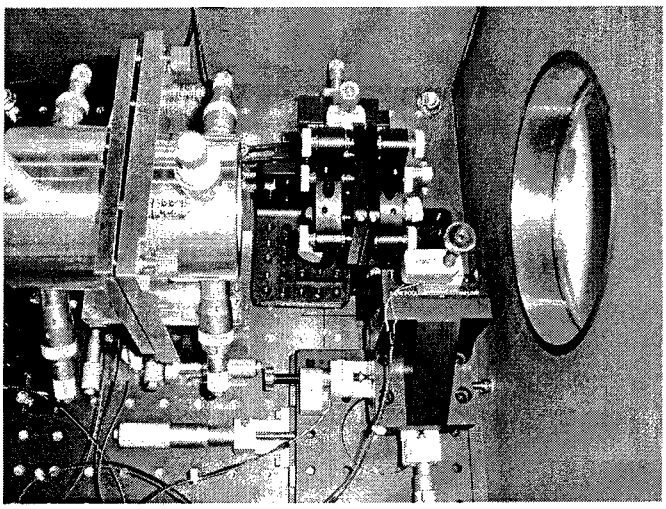

Fig. 2 View of X-ray microscope

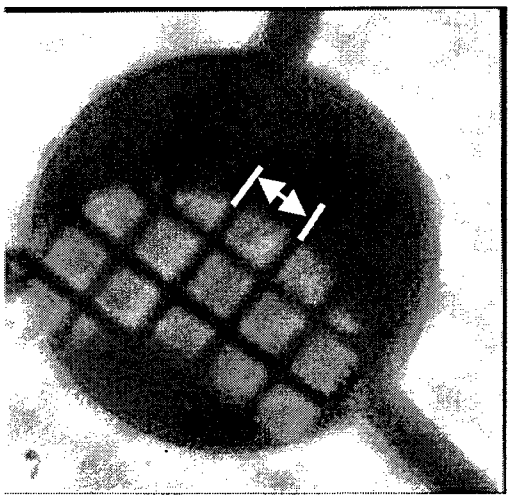

Fig. 3 Cu #1000 mesh image

Reference

1) T. Kawachi et al., CLEO-Pacific Rim 2001, Technical digest Vol.1, 66, 2001

4.3 Free-Electron Laser Development

Eisuke J. MINEHARA

1. Brief Description of FEL Group Activities

There have been long requested a compact, ultra-fast, powerful and efficient free-electron laser (FEL) for industrial uses, for examples, pharmacy, medical, civil engineering, shipbuilding, semiconductor industry, chemical industries, environmental sciences, space-debris orbit control, power beaming and so on[1]. In order to realize such a tunable, highly-efficient, high average power, high peak power and ultra-fast FEL, the JAERI FEL group have successfully demonstrated the efficient and powerful FEL driven by a compact, stand-alone and zero-boil off super-conducting rf linac with and without an energy-recovery geometry[2]. Because the JAERI FEL has successfully produced the world-shortest FEL pulse length of 255 fs, the highest efficiency of 6-9%, the highest peak power of 1 GW and the highest average power of >2 kW, we have first opened and tired to apply the newly-discovered lasing FEL mode[3] with the novel researches and applications itemized above.

Our reports and discussions on the FELs in the subsections will cover the industrial high power FELs, the JAERI compact, stand-alone and zero-boil off cryostat and operational experiences over these 11 years[4], our discovery of the new, highly-efficient, high-power, and ultra-short pulse lasing mode, some preliminary works of the first energy-recovery experiments and so on. Applications of the IRFEL and nuclear isomer studies will be included as a possible and future extension in the JAERI FEL research activities. As a routine operation, we kept the whole cryogenic system running without any trouble, any stop, and warming up for about 280 days from May 2001 to March 2002 including the scheduled power failure at Tokai site utilizing a rental emergency power generator. We plan to continue the "no-warm-up" cryogenic operation for 10 to 20 years because we succeeded to show virtually no decaying performance and no bad indication of the system with no liquid evaporation after 5 accelerated aging tests to simulate volatile gaseous materials, intended air leaks and dirt accumulation in the coldest parts of the cooling engine being expected during any future cold maintenance.

2. Energy Recovery FELs at JAERI

Energy recovery concept had been discussed and tried at Stanford University, Jefferson laboratory and others since 1965[5]. First demonstration of the same-cell energy recovery of the superconducting rf linac (ERL) has been successfully done in 1999 at Jefferson laboratory to cut 75% of the needed rf power. Only a few % or slightly larger rf power of the non-energy recovering FEL is needed to run the ERL-FEL, and wall thickness of an ordinary building may be enough to shield very weak and low energy X rays level. Therefore, we can easily cut most of the budgets of rf power amplifiers and heavy shielding walls of the buildings to construct the ERL-FEL facilities. A 360-degree circular ERLs are planned here to apply for academic facilities like an X-ray FEL and a light source to produce soft and hard X-rays ranging from 10 to 0.01nm.

Another ERL geometry with a 180-degree isochronous reflextron bending magnet[6] has been considered to decelerate the electron beam anti-parallel with the acceleration direction.

In the reflextron ERL, average or centroid velocities of the electron pulses in both the acceleration and deceleration are nearly the same along the accelerator cavity on the contrary to the circular ERL, which has the largest velocity difference around the entrance and exit of the accelerator. The reflextron ERL has needed a small number of beam optical components, and small building space required to install anywhere. The reflextron ERL can accept and recover the lower energy electron beam than a few MeV because nearly no velocity difference can be between the deceleration and acceleration. The JAERI plans to make a prototype for the industrial FELs using the reflextron to realize an ideal ERL-FELs.

3. Industrial FELs near Future

Four industrial models of the reflextron ERL-FEL have been under consideration. Three of them are IR FELs, and the fourth UV FEL. The FIR FEL ranging from 200 to 50 micron wavelengths uses the 500MHz UHF band cavity of 5-10MeV electron energy. The smallest model of the industrial FIR FEL will be the best to perform an FEL higher power demonstration than 10kW or 100kW, to produce an intense Compton-backscattering gamma-ray flux of about 10MeV in synchrotron light sources, to image foreign materials inside foods, grain, fruits and powder as nondestructive inspection, custom inspection, and so on. A MIR FEL ranging from 50 to 8micron wavelengths will use the 500MHz UHF band cavity of

12-24MeV electron energy. Possible and typical applications are expected to be large-scaled photochemical processing, medical, pharmacy, rare-material separation and so on. A NIR FEL ranging from 12 to 2micron uses the same cavity of 24-48MeV electron beam energy. A 10kW or higher industrial FEL which can lase at around a fiber-transmittable wavelength of 1.3micron will be very useful to transmit their power to a pin-pointed position in a distant area from the FEL. These ERL-FEL will be popular, and widely used in the many factories like a shipyard, nuclear fuel reprocessing and partitioning, nuclear power plant decommissioning, an automobile factory, civil engineering plant and so on. An UV FEL ranging from 0.3 to 0.1 micron wavelengths will be planned to use a S or L band cavity of 200-300MeV electron energy with the reflextron geometry. The FEL will be applied to ERL light source development, lithography, photochemical processing, polymer surface modification, optical mass spectrometer, and so on.

References

1) J. Hecht and D. Teresi, Laser, Supertool of the 1980s, Ticker & Fields, 383 Orange Street, New Heaven, Connecticut 06511, U.S.A., 1982
2) E.J.Minehara *et al.*, Nucl. Instrum. Methods Phys. Res. Sect.A**445**, 183, 2000
3) N.Nishimori *et al.*, Phys.Rev. Lett. **86**, 5707, 2001
4) E.J.Minehara *et al.*, pp159-161, in the proceedings of Particle Accelerator Conference, Dallas, 1995
E.J.Minehara *et al.*, Free Electron Laser Challenge 2(SPIE), **3614**, 62-71, 1999
5) G. R. Neil *et al.*, Phys. Rev. Lett. **84**, 662, 2000
6) E.A.Heighway, "Magnetic Beam Defection System". Canadan Patent 993124, issued 1976.

4.3.1 Chirp Estimation of Ultrashort FIR-FEL Pulse

Ryoji NAGAI, Ryoichi HAJIMA, Masaru SAWAMURA, Nobuyuki NISHIMORI,
Nobuhiro KIKUZAWA and Eisuke MINEHARA

1. Introduction

A few cycle optical pulse was generated in far-infrared region at the so-called synchronism of the optical resonator by a superconducting RF linac based FEL at Japan Atomic Energy Research Institute (JAERI-FEL)[1]. The frequency chirp is one of the significant parameter of the ultrashort pulse. We can estimate the chirp from fringe-resolved SHG autocorrelation (FRSHG) signal assuming that the electric field of the pulse is $\mathrm{sech}^{1+jA}(t)$ shape, where A is a chirp parameter. The FRSHG signal is obtained by using a second-harmonic generation in Te crystal[2,3]. The chirp parameter is estimated by the fitting of the FRSHG signal to analytical FRSHG form of the pulse.

2. Experiment and estimation

The FEL radiation is coupled out through a 4 mm diameter center-hole in one of the mirros and extracted to the air through a KRS5 window. The radiation is guided via transport system in the air to the autocorrelator, which is installed near the output window in accelerator room. Residual fundamental component after the Te crystal is blocked by ZnSe filtter. The Te crystal has a length of 2 mm. Since the Te crystal is birefringent, phase-matching is possible by fitting orientation of the crystal to phase-matching angle. Since second-harmonic conversion efficiency of the Te crystal is sufficiently high[3,4], higher harmonic signals of the FEL radiation are negligible.

As shown in Fig. 1, the observed autocorrelation signal and fitting result are denoted dots and solid line, respectively. In the result of the fitting, the chirp parameter, pulse width and wavelength are 1.47, 318.5fs and 23.34 μm, respectively. The chirp parameter and pulse width correspond to the transform-limited pulse width of 1.55 cycles.

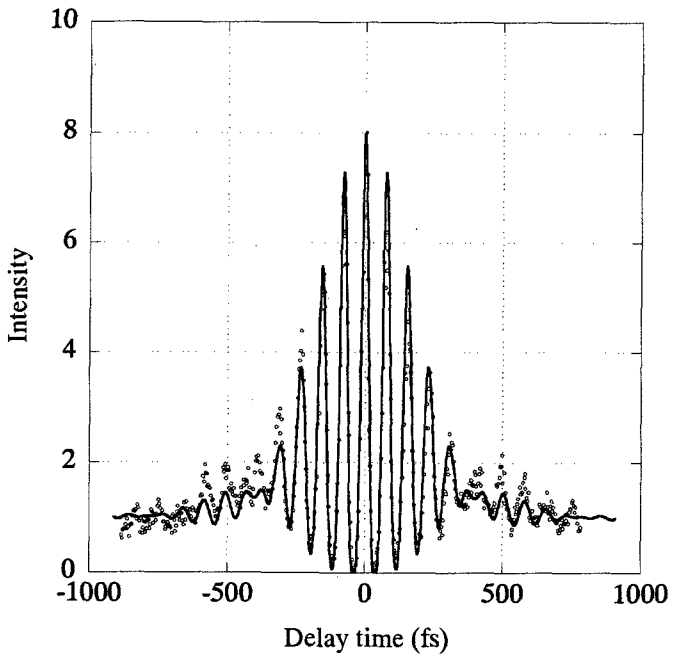

Fig. 1 Observed FRSHG and fitting result

In numerical simulation of the FEL, the frequency chirp is calculated with the chirp parameter of 1.99. The simulation result corresponds to the pulse width of 1.24 cycles for transform-limited pulse. The frequency of tailing part of the pulse is down due to the electron energy chirping, because the FEL light is amplified during the overtaking the electron beam.

3. Conclusion

The frequency chirp of the ultrashort FIR-FEL pulse is estimated that the chirp parameter is 1.47 with assumption of the $\mathrm{sech}^{1+jA}(t)$ pulse shape. The chirp parameter corresponds to 14.3 % frequency sweep on the pulse. The estimation is good agreement with the numerical simulation.

For temporal characterization technique of the ultrashort pulse, FROG[4] is well known, we will try to characterize the ultrashort FIR-FEL pulse using such kind of the measurement technique.

References

1) R. Nagai et al., Nucl. Instr. and Meth. **A483** (2002) 129-133.
2) C. K. N. Patel, Phys. Rev. Lett. **15** (1965) 1027-1030.
3) G. H. Sherman and P. Coleman, IEEE J. Quantum Electron. **QE-7** 11971) 403-409.
4) B. A. Richman, et al., Nucl. Instr. and Meth. **A358** (1995) 268-271.

4.3.2 Quantum tunneling in high-K isomeric decays

Toshiyuki SHIZUMA, Yoshifumi R. Shimizu[a)] and Takehito HAYAKAWA
a) Department of Physics, Kyushu University, Fukuoka 812-8581, Japan

1. Introduction

Nuclear isomers have been attracted in part due to their potential usage as a storage medium of nuclear energies, as reviewed in Ref. 1. Much of the interest has centered on the ^{178}Hf, $T_{1/2}$=31-yr, $I^{\pi}=K^{\pi}=16^{+}$ long-lived high-spin isomer of which energies may be prompt-released by irradiation of synchrotron radiations [2),3)]. Existence of other long-lived isomers would give further opportunities to explore the stimulated decays of the isomers.

In the Hf-W-Os nuclei around A$\sim$180, many high-j and high-Ω Nilsson orbitals are close to the Fermi surface for both the proton and neutron single-particle levels. High-K($=\Sigma\,\Omega$) intrinsic states, therefore, lie at low-lying, competing with collective states to form a yrast line [1)]. Since the K quantum number is approximately conserved in axial symmetric nuclei, transitions requiring large K changes are forbidden or retarded by the K-selection rule. Consequently, high-K states are often isomeric. High-K isomeric transitions can proceed by admixture of K values. The Coriolis interaction changes the spin orientation which leads to a ΔK=1 mixing, while shape fluctuations towards γ deformation can couple states with K quantum numbers differing by two units (ΔK=2 mixing). In high-K isomeric decays, surprisingly low hindrance factors have been observed in spite of the very large K changes of the transitions [4)]. So far, different mechanisms including Fermi-aligned Coriolis K mixing [5)], γ-tunneling through the potential barrier [6)], and the statistical K mixing due to high level density [7)] have been proposed.

2. Calculations

In the ε_2-γ deformation plane, low-K and high-K states are identified at $\gamma\sim0^{\circ}$ and $\gamma\sim-120^{\circ}$, respectively, with a similar ε_2 value. These states can, therefore, be connected by the γ deformation variable. When a potential energy is plotted against a path of the γ-deformation variable, one can find that low-K and high-K states are separated by a potential barrier. In the γ-tunneling model, it is assumed that no direct transition between low-K and high-K states exists, but the wave functions of the states penetrate to each other by quantum tunneling. Details of the model are described in Refs. 6,8.

3. Results and Discussion

In Fig. 1, the experimental and calculated hindrance factors are compared. Considering that the accuracy of the calculation is within an order of magnitude due to the uncertainties of the spin interpolation in the cranking calculation as well as the simple assumption of the leading order formula for the transition rates, the observed and calculated hindrance factors are in good agreement. Thus, for the highly K-forbidden transitions (Δ K $\geqq$ 10), the γ-tunneling plays an important role in the high-K isomeric decays. We have also investigated γ-tunneling probabilities for the A=170$\sim$180 neutron-rich nuclei, and have found the largest action at spin 16 for the doubly mid-shell nucleus ^{170}Dy. The result indicates that long-lived high-K isomer which may be used as an irradiation target would exist in this nucleus.

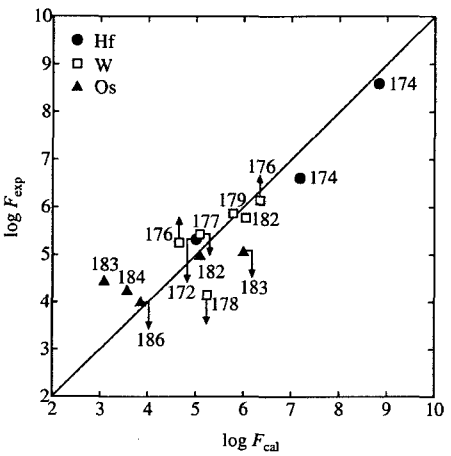

Fig. 1 Comparison between the calculated and experimental hindrance factors for the stretched E2 transitions with ΔK$\geqq$10 in the Hf, W, Os nuclei

References

1) P.M. Walker and G.D. Dracoulis, Nature **399**, 35, 1999
2) C.B. Colins *et al.*, Phys. Rev. Lett. **82**, 695, 1999
3) I. Ahmad *et al.*, Phys. Rev. Lett. **87**, 072503, 2001
4) P. Chowdhury *et al.*, Nucl. Phys. **A485**, 136, 1988
5) P.M. Walker *et al.*, Phys. Rev. Lett. **67**, 433, 1991
6) K. Narimatsu, Y.R. Shimizu and T. Shizuma, Nucl. Phys. **A601**, 69, 1996
7) P.M. Walker *et al.*, Phys. Lett. B **408**, 42, 1997
8)T. Shizuma *et al.*, J. of Nuclear Science and Technology **39**, 2002, in press

4.3.3 Systematic study on maximum efficiencies at JAERI-FEL

Nobuyuki NISHIMORI, Ryoichi HAJIMA, Ryoji NAGAI and Eisuke J. MINEHARA

1. Introduction

Recently, high efficiency operation was realized at an FEL oscillator in JAERI. A unique feature of the efficiency curve as a function of detuning length of an optical cavity, dL, is a sharp peak near dL = 0[1]. A numerical simulation with a shot-noise included in every fresh electron bunch succeeded in reproducing the efficiency curve including the sharp peak, while the simulation without shot-noise could not reproduce the peak[2]. An interesting result of the simulation with shot-noise is that the sharp peak is obtained at dL = 0 despite the lethargy (see Ref. 3)). In order to verify the numerical result, we measured the absolute detuning length around dL = 0 by using a pulse-stacking method, using an external laser, which was originally developed in the Stanford FEL center[4]. We obtained experimental confirmation of sustained lasing at dL = 0[5]. We also found that the efficiency became highest at dL = 0 in the high gain regime only, while the highest efficiency was obtained at the detuning length shorter than dL = 0 in the low gain regime[5]. This indicates that there is some threshold for lasing at dL = 0. We made a systematic measurement of maximum efficiencies (η_{max}) with several gain and loss parameters to search the threshold condition.

2. Experiments and results

The experimental details are described in Ref. 5). The detuning length and FEL power were measured simultaneously and independently by coupling out the FEL light with a scraper mirror. The efficiency was calibrated with an energy analyzer placed after the undulator. The maximum efficiency is shown in Fig. 1 as a function of $1/\sqrt{\alpha}$. Here $\alpha=2\alpha_0/j_0$ is normalized loss, where j_0 is dimensionless beam current, α_0 optical cavity loss. The solid circles and the crosses are experimental data for the j_0 and α_0 measurements, respectively. In the range $1/\sqrt{\alpha}<13$, the experimental η_{max} is slightly smaller than the theoretical value in the superradiant regime. It seems, however, that the extrapolation of the experimental data crosses the origin. This is consistent with the theoretical prediction that the efficiency is proportional to $1/\sqrt{\alpha}$ in the superradiant regime except for the factor of 1.43. In the region $1/\sqrt{\alpha}>13$, η_{max} shows a different dependence on $1/\sqrt{\alpha}$ from the conventional superradiant theory. In the range $1/\sqrt{\alpha}>23$, the normalized efficiency $4\pi N_w\eta_{max}$ saturates at a value of 60. For more information, see Ref. 7).

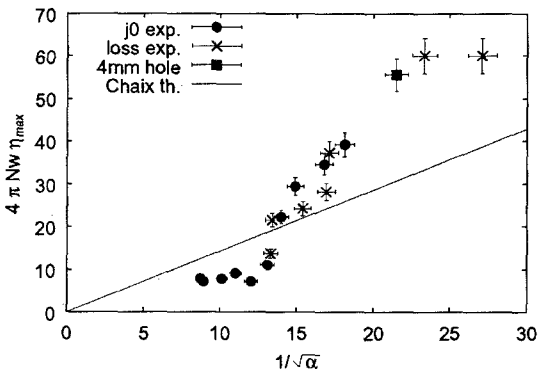

Fig. 1 Maximum efficiency as a function of $1/\sqrt{\alpha}$
The solid circles and crosses are experimental data obtained at several j_0 with a fixed scraper mirror, and several losses with fixed j_0 of 50, respectively. The solid square denotes the maximum efficiency obtained in another experiment with a hole coupling. The solid line represents the theoretical maximum efficiency in the superradiant regime[6].

References

1) N. Nishimori, R. Hajima, R. Nagai, and E. J. Minehara, Nucl. Instrum. Meth. Phys. Res. A **475**, 266 (2001).
2) R. Hajima, N. Nishimori, R. Hajima, R. Nagai, and E. J. Minehara, Nucl. Instrum. Meth. Phys. Res. A **475**, 270 (2001).
3) G. Dattoli and A. Renieri, *Laser Handbook* (North Holland, Amsterdam, 1985), Vol. 4, p.75.
4) K.W. Berryman et al., Nucl. Instrum. Meth. Phys. Res. A **358**, 260 (1995).
5) N. Nishimori, R. Hajima, R. Nagai, and E. J. Minehara, Phys. Rev. Lett. **86**, 5707 (2001).
6) P. Chaix, N. Piovella, and G. Gregoire, Phys. Rev. E **59**, 1136 (1999).
7) N. Nishimori, R. Hajima, R. Nagai, and E. J. Minehara, Nucl. Instrum. Meth. Phys. Res. A **483**, 134 (2002).

4.4 Optics Research and Development

The Novel Optics Research Group

Masato KOIKE, Osamu YODA, Akira SUGIYAMA, Masahiko ISHINO, Hiroyasu FUKUYAMA and Kazuo SANO[a)]

a) Shimadzu Scientific Research Inc.

1. Introduction

Development of advanced lasers such as the T-cube laser and soft X-ray laser requires novel optics including laser crystals, multilayer mirrors, and diffraction gratings in addition to development of laser oscillation technology. The efforts of the Novel optics research group are devoted to the research and development on optical components, optical systems, and basic technologies for development and application of the advanced lasers and other soft X-ray state-of-arts light sources.

2. Achievements

Nd:YAG laser crystal, having less than 0.1 at-% uniformity of doped concentration was successfully grown by improvements of a continuous charge double crucible Czochralski method with a RF induction heater. (Fig. 1) The optimization of vertical temperature distribution at the crystal growth part, the prevention of asymmetric crystal growth, stable supplement of material powders and the fast rotation of a seed crystal brought about Nd:YAG crystal of 185 mm length.

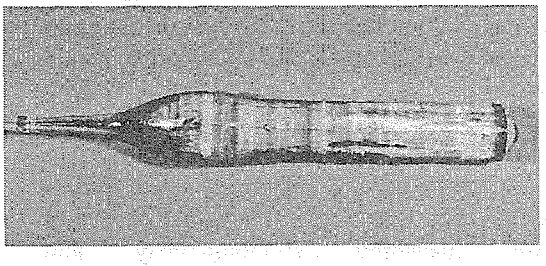

Fig. 1 Nd:YAG crystal grown by a double crucible CZ method

The Mo/Si multilayer has a high soft X-ray reflectivity around 13 nm even at near normal incidence angles. However, the Mo/Si multilayer is known to be unstable at temperatures over 300°C. This is because Mo and Si atoms at the interfaces mix together and form Mo-silicides through inter-diffusion. To improve the heat stability of the Mo/Si multilayer, we have introduced silicon oxide (SiO_2) layer to the Mo/Si multilayer as a barrier layer. We have found that the Mo/SiO_2/Si/SiO_2 multilayer having unequal SiO_2 layer thicknesses of 0.5 nm at the Si-on-Mo interface and 1.5 nm at the Mo-on-Si interface has thermally the most stable structure and maintains a high soft X-ray reflectivity after annealing at 400°C (Fig. 2).

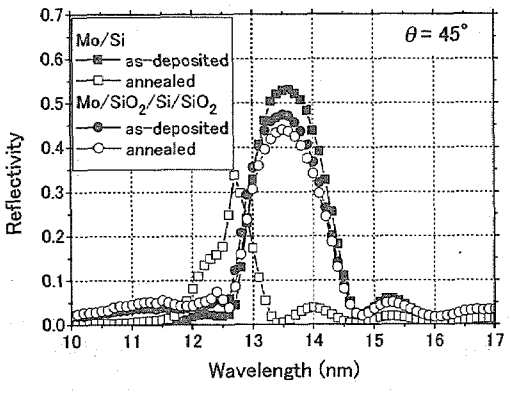

Fig. 2 Measured soft X-ray reflectivities of the multilayer samples

For the purpose of characterizing soft X-ray optical elements in the wavelength range of 0.7-2 nm, so called the boundary region of crystal and grating monochromators, we have completed a new monochromator employing a scanning mechanism based on Surface Normal Rotation (SNR). The SNR scheme provides high throughput at short wavelengths and simple scanning mechanism by means of a grating rotation about its normal. We confirmed the performance of the monochromator by measuring various samples including an Al filter, Pt/C multilayered mirrors, and a MgO powder.

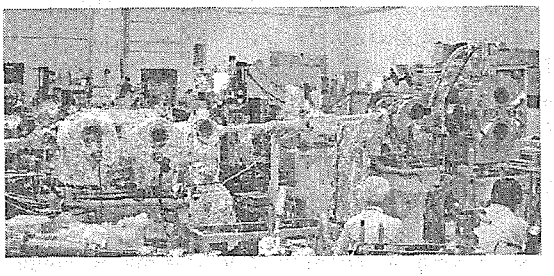

Fig. 3 Soft X-ray optical evaluation system featuring the new SNR monochromator

4.4.1 Nd:YAG laser crystal growth by a double crucible method

Akira SUGIYAMA

1. Introduction

In the enlargement of laser crystals, the deterioration of optical quality is inevitable problem that causes output power loss and laser beam distortion. The quality of laser crystals has strong influence on laser performance. To get the high power of T-cube Ti:sapphire laser system, powerful light source composed of Nd doped $Y_3Al_5O_{12}$ (Nd:YAG) laser crystals are essential. Unfortunately, Nd:YAG crystal has intrinsic problems[1], such as low segregation factor of 0.17 and high melting point of 2203 K. Therefore, we have studied the growth technique of Nd:YAG crystals using a continuous charge double crucible Czochralski method with a RF induction heater, shown in Fig. 1, to realize high optical quality large crystals.

2. Experimental results

The crystal growth system is composed of Ir double crucible, growth furnace, a PID controller for growing boule diameter and an additional powder supply unit. The Ir crucible has an inner cylinder of ϕ50 mm and outer of ϕ80 mm. The height of the inner was 10 mm longer than outer one to prevent directly dropping of supplying powder inside. The inner wall has four square holes of 20 x 10 mm at the bottom to transfer the material from outer strip in order to keep material solution level constant. The powder supply unit consists of an electric balance and a screw motor which are connected with PC to control feeding rate. The powder is made of bulk Nd:YAG crystals. The size of the grounded powder is 100~200 μm in diameter. In our study, feed rate of powder supply was 1 g/h.

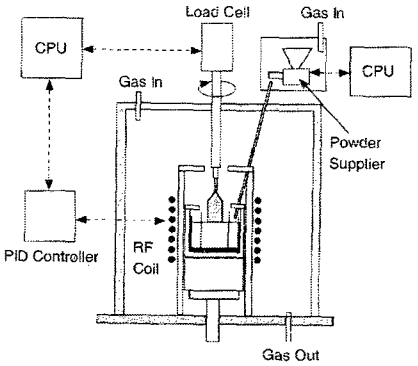

Fig. 1 Apparatus of our crystal growth system

In this crystal growth system, we optimized insulator configuration to make large vertical and radial temperature gradients at the crystal growth part for prevention of asymmetric growth. The asymmetric growth easily occurred when the growth axis did not locate on the crucible center in small temperature gradients.

Figure 2 shows the variation of Nd concentration analyzed by ICP along the growth direction, and the fluctuation of doped concentration was less than 0.1 at-%. Grown crystal was cut into {211} and {111} plates to measure scattering center by a laser tomography method[2]. An arrow shows the growth direction of the crystal. In the regions A and C, the scattering center appeared. On the other hand, there is no scattering in region B. The A and C correspond to the duration of powder supply. From the result, it seems that scattering center is caused by small bubbles and Ir particles which are formed in the Ir feeding pipe for powder supply[3]. To reduce the scattering center, now we are modifying the through holes of crucible inner wall for securing the impurity decomposition.

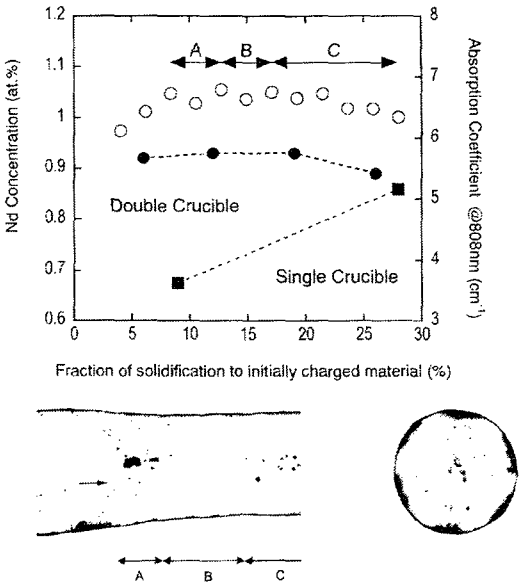

Fig. 2 Distribution of Nd concentration and scattering center inside crystal

References

1) A. Sugiyama, Y. Anzai, M. Katsurayama, T. Yamaguchi, K. Yamagishi, T. Sasuga, T. Arisawa and H. Takuma, JAERI-Tech. **97-049**, 1997
2) A. Sugiyama and H. Fukuyama, JAERI-conf. **2002-008**, 174, 2002
3) M. Katurayama, Y. Anzai, A. Sugiyama, M. Koike and Y. Kato, J of Crystal Growth, **229**, 193, 2001

4.4.2 Development of Mo/Si multilayer mirror with high heat stability

Masahiko ISHINO and Osamu YODA

The Mo/Si multilayer has a high soft X-ray reflectivity around 13 nm even at near normal incidence angles and has been successfully applied to optical system such as extreme ultraviolet lithography (EUVL)[1]. However, it is known that the Mo/Si multilayer is structurally unstable over 300°C. This is because Mo and Si atoms at the interfaces mix together and form mixed layers of Mo-silicides through inter-diffusion. The mixed layers as well as roughness at the interfaces reduce the soft X-ray reflectivity of the Mo/Si multilayer mirror. Silicon oxide (SiO_2) is known to be chemically and thermally stable. Therefore, we tried to introduce the SiO_2 layer in the Mo/Si multilayer as a barrier layer and evaluated the heat stability of the fabricated multilayer samples.

The Mo/Si multilayers inserted with the SiO_2 barrier layers having various thicknesses were fabricated by the ion beam sputtering method. To evaluate the heat stability of the multilayer sample, the fabricated multilayers were annealed successively at temperatures up to 600°C in a vacuum furnace for one hour. To characterize the multilayer structure, the small angle X-ray scattering measurement was carried out with CuK α_1 X-rays using a standard θ–2θ scan. Figures 1(a) and 1(b) show changes in the first-order Bragg-peak reflectivity and the periodic length of the multilayer samples, respectively, derived from the small angle X-ray scattering measurements as a function of annealing temperature. The X-ray reflectivity and the periodic length of the conventional Mo(4.0)/Si(6.0) multilayer decrease after annealing over 300°C. The X-ray reflectivity of the Mo(4.0)/Si(4.0)/SiO_2(2.0) multilayer inserted with 2.0 nm thick SiO_2 layers at the Mo-on-Si interfaces does not change up to 400°C, and the periodic length decrease gradually over 300°C. The Mo(4.0)/SiO_2(0.5)/Si(4.0)/SiO_2(1.5) multilayer, which has the SiO_2 layers with 0.5 nm at the Si-on-Mo interface and with 1.5 nm at the Mo-on-Si interface, keeps almost the same X-ray reflectivity and the periodic length up to 500°C. The Mo(4.0)/SiO_2(2.0)/Si(2.0)/SiO_2(2.0) multilayer is not affected by annealing up to 600°C. We also measured the soft X-ray reflectivity of the as-deposited and the 400°C annealed samples in the wavelength region of 13 nm at an incidence angle of 45° using synchrotron radiation[2]. The soft X-ray reflectivity of the multilayer samples inserted with SiO_2 layers decreases because of the absorption of X-rays by oxygen. Nevertheless the Mo(4.0)/Si(4.0)/SiO_2(2.0) multilayer and the Mo(4.0)/SiO_2(0.5)/Si(4.0)/SiO_2(1.5) multilayer have relatively high soft X-ray reflectivities and keep almost the same soft X-ray reflectivities with little shift in the peak position after annealing.

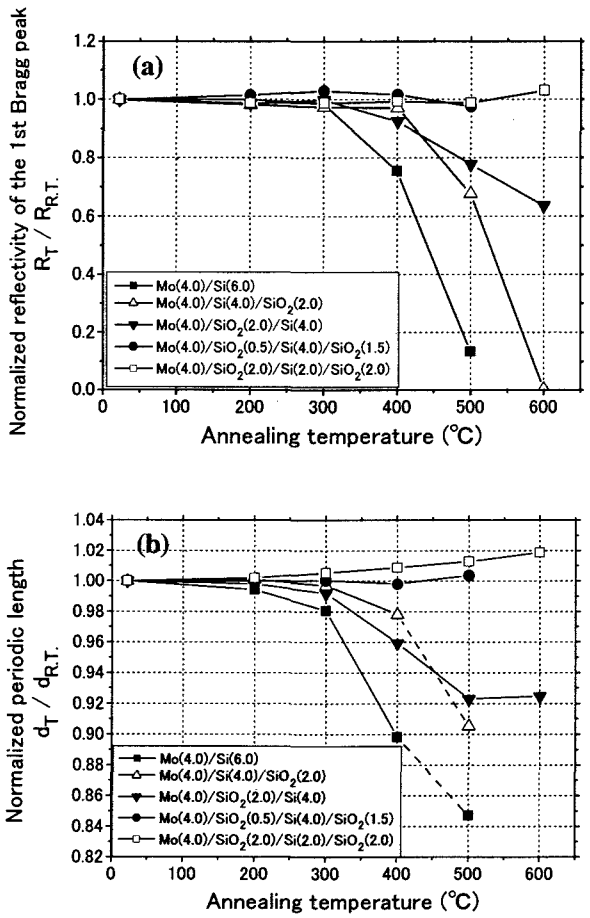

Fig. 1 Changes in the first-order Bragg-peak reflectivity and the periodic length of the multilayer samples. The X-ray reflectivities and the periodic lengths of the samples were normalized by those of the respective as-deposited ones.

References

1) C. W. Gwyn, R. Stulen, D. Sweeney, D. Atteood, J. Vac. Sci. Technol. B **16**, 3142, 1998.
2) M. Koike, K. Sano, O. Yoda, Y. Harada, M. Ishino, M. Moriya, H. Sasai, H. Takenaka, E. Gullikson, S. Mrowka, M. Jinno, Y. Ueno, J. H. Underwood, T. Namioka, Rev. Sci. Instrum. **73**, 1541, 2002.

4.4.3 New type of Monk-Gillieson monochromator capable of covering a 0.7-25 nm range

Masato KOIKE, Kazuo SANO[a)], Osamu YODA, Yoshihisa HARADA[b)], Masahiko ISHINO, Masafumi JINNO[b)] and Takeshi NAMIOKA[c)]
a) Shimadzu Scientific Research Inc., b) Shimadzu Corp., c) Tohoku University

1. Introduction

For the purpose of realizing an evaluation beamline for characterizing soft X-ray optical elements in a wide wavelength range of 0.7-25 nm, we have designed and constructed a new type of monochromator that combined two types of Monk-Gillieson monochromators. One is a conventional type equipped with three varied-line-spacing plane gratings, allowing a choice of two included angles. The other is a new type that employs a scanning mechanism based on Surface Normal Rotation (SNR). The SNR scheme provides high throughput at short wavelengths taking advantage of conical diffraction configuration and simple scanning mechanism by means of a grating rotation about its normal. The monochromator is operated in the SNR and conventional modes over the ranges of 0.7-2.0 nm and 2.0-25 nm, respectively. We describe the wavelength scanning system of the monochromator and preliminary experimental data, such as the total yield photoelectron measurement on a MgO powder, the transmittance of an Al filter, and the wavelength and angular characteristics of a Pt/C multilayer mirror.

2. Instrumentation

The monochromator system is basically a Monk-Gillieson (M-G) type monochromator which consists of a concave mirror and plane grating. In a M-G type monochromator, a plane grating is illuminated by the convergent beam reflected from a concave mirror. Wavelength scanning is done by a simple rotation of the grating at the grating center about the axis parallel to the grooves. The conventional M-G monochromator is equipped with three laminar-type VLS holographic gratings G1 (300 lines/mm), G2 (600 lines/mm), and G3 (1200 lines/mm).[1,2] These gratings are used interchangeably at an inclusion angle of either 176° or 172°, depending on the required scanning range. One particular inclusion angle is easily selected by only inserting vertical focusing spherical mirror M3 having an angle of incidence of 88° into the beam or retracting M3 and M4 from the beam to choose M5 having an angle of incidence of 86° (See Fig.1) .

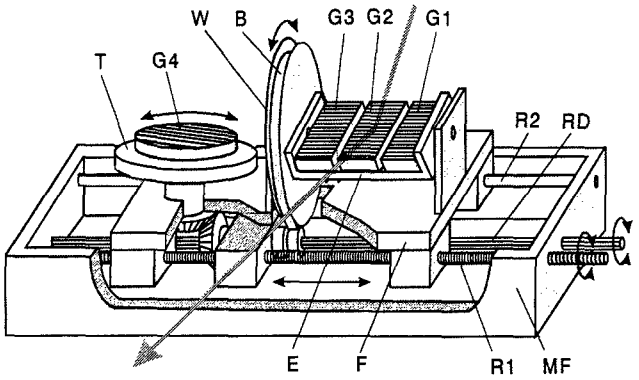

Fig. 1 Schematic diagram of the mechanical system for the selection of one particular grating

When the convertible monochromator works in the SNR mode the vertical focusing spherical mirror M4 is inserted into the beam at an angle of incidence of 88°. The convergent beam reflected from M4 illuminates a CLS plane grating G4 (1200 lines/mm), which is used at an inclusion angle of 176°. This SNR Monk-Gillieson monochromator covers a wavelength range of about 0.7~2 nm. The detail of the design of this monochromator and a method of the wavelength calibration are described in Refs. 3 and 4, respectively.

3. Performance

Figure 2 shows the total yield photoelectron spectra for the MgO powder detected by a channeltron in the wavelength range of 0.3-3 nm. The solid and point-dotted curves indicate the intensities for the M-G SNR monochromator (MG-SNR) and conventional M-G monochromator (MG-VLS), respectively. The gray-colored curve shows a 40× enlargement of that for the conventional M-G monochromator. This measurement gives a rough estimate of the difference in the flux obtained by the two monochromators as well as a low stray light feature of the M-G SNR monochromator in the wavelength range of < 0.7 nm.

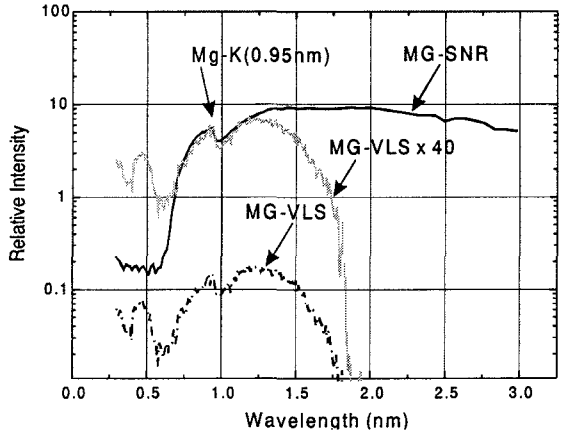

Fig. 2 Total yield photoelectron spectra for the MgO powder detected by a channeltron

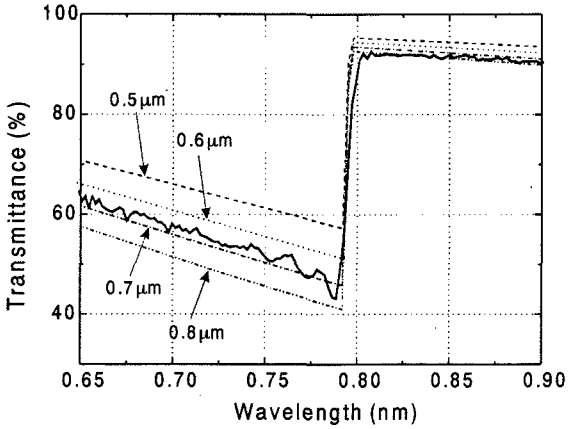

Fig. 3 The transmittance curve reduced from the measured data shown in Fig. 4 (solid line) and those calculated from Ref. 17 assuming films of thickness 0.5, 0.6, 0.7, 0.8-μm (dotted line).

The transmittance curve of an Al filter is shown in Fig. 3. The measured curve (solid line) is compared with those of calculated transmission curves. Those calculated for films of thickness 0.5, 0.6, 0.7, and 0.8-μm are indicated by dotted lines. The measured curve agrees well with the calculated curve for a film of thickness 0.7-μm.

The wavelength and angular characteristics of a Pt/C multilayer mirror were measured by use of the M-G SNR monochromator in the 0.7-1.5 nm region. The reflectance measured at angles of incidence of 80°, 81°, 82°, 83°, 84°, and 85° are shown in Fig. 4, where the open circles and the solid curves indicate the data of the measured and theoretical reflectance assuming a surface roughness of 0.43 nmRMS, respectively. The mulitlayer used for the evaluation was deposited by Dr. Tamura at Graduate School of Science, Nagoya Univ. and has a period of 1.78 nm, a value of 0.37 for Pt-layer thickness/period, and 30 layer pairs. It is clearly seen in the figure that the peak wavelengths depending on the angle of incidence agree with those are expected by the simulation. All the data presented above support the versatility and effectiveness of the convertible M-G monochromator when it is applied to an evaluation system for characterizing soft X-ray optical elements.

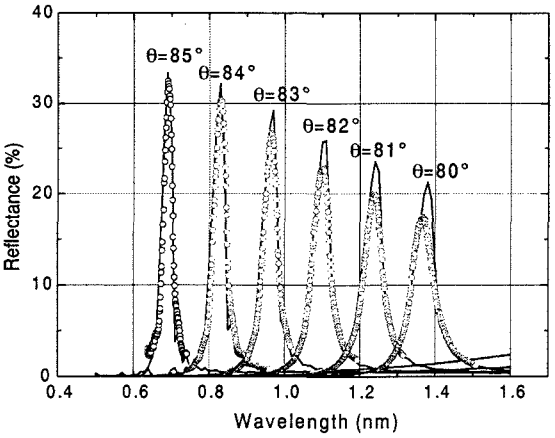

Fig. 4 Reflectance of a Pt/C multilayer at angles of incidence of θ = 80°, 81°, 82°, 83°, 84°, and 85°. The open circles and the solid curves indicate the data of the measured and theoretical reflectance assuming a surface roughness of 0.43 nmRMS, respectively.

References

1) M. Koike, T. Namioka, Appl. Opt. **36**, 6308, 1997.
2) M. Koike, T. Namioka, J. Electron Spectroscopy and Related Phenomena, **80**, 303, 1996.
3) M. Koike, T. Namioka, Appl.Opt.**41**, 245, 2002.
4) M. Koike et al. to be published in Proc. SPIE, **4782**.

4.5 Research on Laser Particle Acceleration

Laser Acceleration Research Group

Kazuhisa NAKAJIMA

A number of concepts of particle acceleration by laser fields have been proposed almost since the beginning of the laser evolution. Recently great advances of ultraintense ultrashort pulse lasers have brought about tremendous experimental and theoretical progress in maturity of laser-driven particle accelerator concepts. In particular, relativistic electron acceleration mechanism due to ultraintense laser-plasma interaction can be expected to make a compact high energy accelerator. In this context there is growing a great interest in the world-wide community of laser, plasma and accelerator physics.

A novel particle acceleration concept was proposed by Tajima and Dawson [1], which utilizes plasma waves excited by intense laser beam interactions with plasmas for particle acceleration, known as laser-plasma accelerators. Recently there has been a great experimental advance on the laser wakefield acceleration (LWFA) of electrons since the first ultrahigh gradient acceleration experiment made by Nakajima et al. [2]. Although recent world-wide experiments have successfully demonstrated that the self-modulated LWFA mechanism is capable of generating ultrahigh accelerating gradient of the order of 100 GeV/m, the maximum energy gain is limited at most to 100 MeV with energy spread of 100 % because of dephasing and wavebreaking effects in plasmas. In the meantime the first high energy gain acceleration attaining 300 MeV has been observed with the injection of an electron beam at an energy matched to a wakefield phase velocity in a fairly underdense plasma by our Group[3].

Since several effects limit the energy gain in a single-stage of laser-plasma accelerators; laser diffraction, electron dephasing, pump depletion and laser-plasma instabilities, it is essential to extend the acceleration length to a cm-scale length or to invent a novel acceleration concept free of such restrictions in order to achieve GeV energy gains. In addition, it is important to generate a high quality beam with a narrow energy spread and a small emittance for practical applications. Our activities on laser acceleration research have focused on the laser wakefield accelerator developments for high energy electron acceleration achieving > 1 GeV, and on high quality beam generation with both conventional and advanced technologies, and on theoretical studies of new laser acceleration concepts as summarized below.

The main task has been devoted to completion of the Laser Acceleration Test Facility (LATF) consisting of the photocathode RF gun, the 150 MeV microtron accelerator and the test beam line as well as the estimation of radiation doses produced by LATF for the radiation safety clearance. With the use of LATF, we plan to demonstrate the channel-guided LWFA in which both the driving laser pulses and particle beams can be guided through the capillary discharge plasmas with a cm-scale length. The development of the plasma waveguide is underway after the first demonstration of propagating a 2 TW, 90 fs laser pulse through a stable 2 cm plasma channel produced by an imploding phase of fast Z-pinch discharge in a gas-filled capillary without wall ablation[4]. We have initiated to construct the Z-pinch capillary discharge system assembled from a Marx generator and a water capacitor with four laser trigger spark gaps for the prototype of the channel-guided LWFA. This system can generate a 10 cm long capillary discharge in a diameter of 1 mm driven by 100 kA current without time jitter.

In order to produce a high quality electron beam with low momentum spread and small pulse-to-pulse energy stability, it is required that femtosecond electron bunches should be injected with the energy higher than trapping threshold and femtosecond synchronization with respect to a wakefield accelerating phase space, typically less than 100 fs in a longitudinal scale and 10 μm in a transverse size. There are proposed several schemes capable of generating a fs electron bunch injected into a correct wakefield phase within a few fs jitter. The promising method we conceive is based on slicing a bunch through a process of energy modulation due to the inverse free electron laser mechanism created in the interaction of electrons with a fs laser pulse split from a main pump pulse, referred to as a bunch slicing scheme. The bunch slicing scheme will be composed of an undulator magnet and a beam splitting chicane in the test beam line[5].

Recently novel schemes which use laser triggered injection of plasma electrons into the wakefield have been proposed as a plasma cathode. Although there are three major schemes which may be named as a transverse optical injection[6], a colliding pulse optical injection[7], and a nonlinear wavebreaking injection scheme[8]. The proof-of-principle experiments for these schemes have not been demonstrated so far. The most promising scheme we conceive is the colliding pulse optical injection that uses three short

transverse optical injection[6], a colliding pulse optical injection[7], and a nonlinear wavebreaking injection scheme[8]. The proof-of-principle experiments for these schemes have not been demonstrated so far. The most promising scheme we conceive is the colliding pulse optical injection that uses three short laser pulses, one high-intensity pump pulse and two counterpropagating injection pulses with different frequencies generating a laser beat wave with a slow phase velocity to pump background plasma electrons into a fast wakefield. As a first step of this plasma cathode development, we present the first direct observation of 20 GeV/m of coherent ultrahigh gradient wakefields excited by a 2 TW, 50 fs laser pulse in a gas jet as well as precise measurements of its time-resolved gas density distribution[9]. In the PIC simulations of the colliding pulse injection[10], a remarkable beam quality is verified with ultrahigh peak brightness and ultrashort pulse required of next generation particle accelerators and free electron lasers.

A novel concept of laser ponderomotive acceleration named as "Dirac accelerator" is presented[11]. Particles are accelerated due to direct strong field interactions with laser pulses of which a group velocity is less than the vacuum speed of light in plasma. We first illuminates its acceleration mechanism with relativistic quantum mechanics. In this mechanism the energy gain increases in proportion to the laser intensity rather than the laser field. Therefore a "Dirac accelerator" concept may allow us to construct superhigh energy particle accelerators achieving GeV to TeV energies by the use of Petawatt lasers.

References

1) T. Tajima and J. M. Dawson, Phy. Rev. Lett. **43**, 267 (1979).
2) K. Nakajima et al., Rhy. Rev. Lett. **74**, 4428 (1995).
3) H.Dewa et al., Nucl. Instr. and Meth. in Phys. Res. **A410**, 357 (1998); M. Kando et al., Jpn. J. Appl. Phys. **38**, L967 (1999)
4) T. Hosokai et al., Optics Letters, **25**,10-12 (2000).
5) K. Nakajima et al., AIP conference proceedings **569**, 112 (2001).
6) D. Umstadter et al., Phy. Rev. Lett. **76**, 2073 (1996).
7) E. Esarey et al., Phy. Rev. Lett. **79**, 2682 (1997).
8) S. Bulanov et al., Phys. Rev. **E58**, R5257 (1998).
9) H. Kotaki et al., Phys. Plasamas **9**, 1392 (2002).
10) S. Masuda et al., Nucl. Inst. and Meth. **A455**, 172 (2000)
11) K. Nakajima, AIP conference proceedings **611**, 447 (2002).

4.5.1 Measurement of ultra-high gradient wakefield excitation by intense ultrashort laser pulses in plasma

Hideyuki KOTAKI, Masaki KANDO, Takatsugu OKETA, Shin-ichi MASUDA, Shuji KONDO, Shuhei KANAZAWA, Takashi YOKOYAMA, Toru MATOBA and Kazuhisa NAKAJIMA

1. Introduction

Laser-driven plasma accelerators have been conceived to be the next-generation particle accelerators, promising ultrahigh field particle acceleration and compact size compared with conventional accelerators[1,2]. A direct measurement of the plasma density oscillation can be done by means of ultrafast time-resolved frequency domain interferometry (FDI)[3]. Several measurements have been made with FDI to demonstrate wakefield excitation by ultrashort laser pulses in an underdense plasma[4-7]. These measurements have been done for a relatively low density plasma in a gas filled chamber using laser pulse durations around 100 fs and pump peak powers less than 1 TW. In these measurements the pump pulses were tightly focused to enhance the plasma wave excitation due to 2D effects. In a 2D dominant regime, where the pulse width is longer than a spot size, the radial wakefield is higher than the longitudinal one. Therefore a shorter pulse is preferable to generate a more 1D coherent planar wakefield in the higher resonant plasma density. We have developed a pump-probe frequency domain interferometer consisting of a 2 TW pump laser pulse with a duration of 50 fs at a wavelength of 800 nm and two frequency doubled probe pulses split from the pump pulse with a variable delay. The measurement of laser wakefields has been made in a less 2D dominated regime to suppress radial effects[8].

2. Measurement of laser wakefields

An intense ultrashort laser pulse produces a fully ionized plasma through optical field ionization on ultrafast time scales of the order of femtoseconds and excites electron density oscillations in the plasma behind the laser pulse. This plasma density oscillation can be measured by the FDI technique[3,8].

The experimental setup of the FDI is shown in Fig. 1. The 2.6 TW 10 Hz Ti:sapphire laser pulse at a wavelength of 800 nm with a maximum energy of 135 mJ and a duration of 52 fs (FWHM) is split into two beams. The reflected beam (80%) is used as the pump pulse and the transmitted beam as the probe beam. The pump and probe pulses are focused by an off-axis parabolic mirror with a focal length of 15 cm. The focal spot images taken with a CCD camera show that the pump focused intensity profile is approximately a Gaussian distribution with a rms radius (at 1/e) σ_r = 8.9 μm, while the probe beam radius is σ_{rp} = 3 μm and centered on the pump beam. The peak pump intensity is 8.4×10^{17} W/cm^2 (a_0 0.6), producing fully ionized He gas in the focal region. The probe beam is separated from the pump beam with a dichroic beam splitter after passing through the plasma and guided through an optical fiber into the spectrometer to

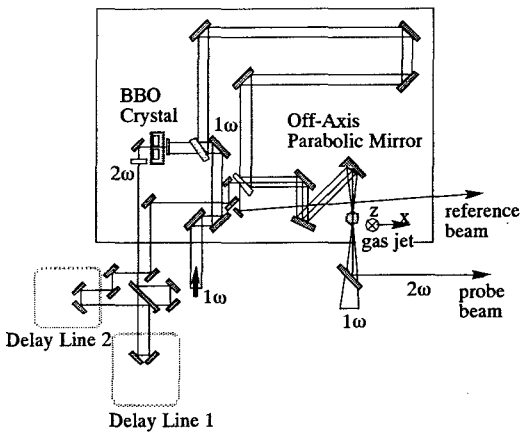

Fig. 1 Experimental setup of the frequency domain interferometry

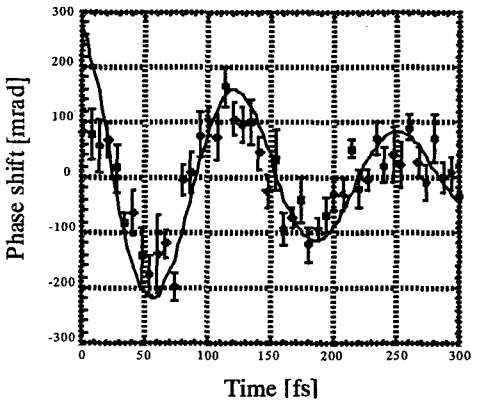

Fig. 2 The relative phase shift as a function of the time delay for the measurement of the plasma density oscillation in the gas-jet operated at a backing pressure of 10atm

analyze the interferograms. A part of the probe beam is sent directly to the spectrometer to make the reference fringes. The spectrometer is a Czerny-Turner type with a focal length of 1.33 m and a grating of 1800 gr/mm. The spectral resolution is 0.06 Å. The phase shift at each position was obtained by averaging 50 shots of the phase shift data to reduce pulse-to-pulse fluctuations. The gas jet was operated at a backing pressure of 10 atm for He gas. The pump pulse was focused 1.5 mm below the end of the nozzle where a fully ionized plasma was expected with an electron density of 7.2×10^{17} cm^{-3} from the neutral gas density measurements[8,9].

Figure 2 shows the results of the wakefield measurement. In the region where the probe pulse was delayed after the pump pulse, a large amplitude density perturbation excited by the pump pulse was detected as indicated by the phase shifts. From the phase shift data, the period and the amplitude of the electron density oscillation and the amplitude of the longitudinal wakefield are obtained as a function of time delay between the pump and the probe pulses. The oscillation period of the electron plasma wave is 130 ± 3.4 fs behind the pump. This plasma wave period corresponds to the electron density of $7\times10^{17}\pm 8.5\times10^{15}$ cm^{-3} in linear wakefield theory, which is in good agreement with the electron density for the fully ionized He gas expected from the neutral gas density measurements[8,9]. The measured density perturbation before damping is $(\delta n/n_e)_m$ 0.74 with the plasma length $L_p = 1$ mm. The maximum longitudinal wakefield of 20 GV/m is deduced. These estimates are in good agreement with the density perturbation $(\delta n/n_e)_{th}=$ 0.75 and the longitudinal wakefield of 21 GV/m calculated by linear wakefield theory.

3. Conclusion

In order to investigate the laser-wakefield excited by an intense laser pulse in plasma, we study the measurement of the laser wakefield. We made the first direct observation of coherent ultrahigh gradient wakefields excited by an intense ultrashort laser pulse in a gas-jet plasma with a density around 7×10^{17} cm^{-3}. The wakefield with the oscillation period of 130 fs and maximum longitudinal amplitude of 20 GV/m was observed, showing fast damping in time from a few oscillation periods to ten periods. These measured wakefield parameters are quite consistent with the neutral gas density measurements and wakefield theory.

References

1) T. Tajima and J. M. Dawson, Phy. Rev. Lett. **43**, 267 (1979).
2) K. Nakajima, D. Fisher, T. Kawakubo, H. Nakanishi, A. Ogata, Y. Kato, Y. Kitagawa, R. Kodama, K. Mima, H. Shiraga, K. Suzuki, K. Yamakawa, T. Zhang, Y. Sakawa, T. Shoji, Y. Nishida, N. Yugami, M. Downer, and T. Tajima, Phy. Rev. Lett. **74**, 4428 (1995).
3) E. Tokunaga, A. Terasaki, and T. Kobayashi, Opt. Lett. **17**, 1131 (1992).
4) K. Nakajima, Nucl. Instr. and Meth. in Phys. Res. A **455**, 140 (2000); H. Dewa, H. Ahn, H. Harano, M. Kando, K. Kinoshita, S. Kondoh, H. Kotaki, K. Nakajima, H. Nakanishi, A. Ogata, H. Sakai, M. Uesaka, T. Ueda, T. Watanabe, K. Yoshii, Nucl. Instr. and Meth. in Phys. Res. A **410**, 357 (1998); M. Kando, H. Ahn, H. Dewa, H. Kotaki, T. Ueda, M. Uesaka, T. Watanabe, H. Nakanishi, A. Ogata and K. Nakajima, Jpn. J. Appl. Phys. **38**, 967 (1999).
5) C. W. Siders, S. P. Le Blanc, D. Fisher, T. Tajima, and M. C. Downer, Phys. Rev. Lett. **76**,3570 (1996); C. W. Siders, S. P. Le Blanc, A. Babine, A. Stepanov, A. Sergeev, T. Tajima, and M. C. Downer, IEEE Trans. Plasma Sci. **24**, 301 (1996).
6) J. R. Marquès, J. P. Geindre, F. Amiranoff, P. Audebert, J. C. Gauthier, A. Antonetti, and G. Grillon, Phys. Rev. Lett. **76**, 3566 (1996); J. R. Marquès, F. Dorchies, P. Audebert, J. P. Geindre, F. Amiranoff, J. C. Gauthier, G. Hammoniaux, A. Antonetti, P. Chessa, P. Mori, and T. M. Antonsen Jr., Phys. Rev. Lett. **78**, 3463 (1997); J. R. Marquès, F. Dorchies, F. Amiranoff, P. Audebert, J. C. Gauthier, J. P. Geindre, A. Antonetti, T. M. Antonsen Jr., P. Chessa, and P. Mori, Phys. Plasmas **5**, 1162 (1998).
7) E. Takahashi, H. Honda, E. Miura, N. Yugami, Y. Nishida, and K. Kondo, J. Phys. Soc. Jpn. **69**, 3266 (2000); E. Takahashi, H. Honda, E. Miura, N. Yugami, Y. Nishida, K. Katsura, and K. Kondo, Phys. Rev. E **62**, 7247 (2000).
8) H. Kotaki, M. Kando, T. Oketa, S. Masuda, J. K. Koga, S. Kondo, S. Kanazawa, T. Yokoyama, T. Matoba, and K. Nakajima, Phys. Plasmas **9**, 1392 (2002).
9) H. Kotaki, S. Masuda, M. Kando, S. Kondo, S. Kanazawa, T. Yokoyama, T. Matoba, and K. Nakajima, JAERI-Review "Annual Report of KANSAI Research Establishment 2000", 40 (2001).

4.5.2 Design and construction of electron beam line for laser wakefield acceleration experiments

Masaki KANDO, Hideyuki KOTAKI, Shuji KONDO, Shin-ichi MASUDA, Takashi YOKOYAMA[1], Shuhei KANAZAWA, Takayuki HOMMA, Toru MATOBA and Kazuhisa NAKAJIMA[a)]
a) JAERI Kansai and High Energy Accelerator Research Organization (KEK)

1. Introduction

The second generation laser wakefield electron acceleration (LWFA)[1)], which will achieve an improved energy spectrum of accelerated electrons and high energy gain such as 1 GeV over diffraction length, is planned at JAERI-Kansai. One of the key technologies to achieve this is high quality test electron source[2)]. We developed a photocathode RF gun based racetrack microtron accelerator (phtocathode microtron) and verified the beam quality[3)]. Since the beam tests were done with a short beam line, the electron beam line should be extended to an interaction point where both the electron and laser beams are focused to tens of micrometers. The extending beam line equipped with focusing magnets are designed and constructed. A bunch slicing technique, which extracts a femtosecond electron slice from a picosecond electron beam, is also considered.

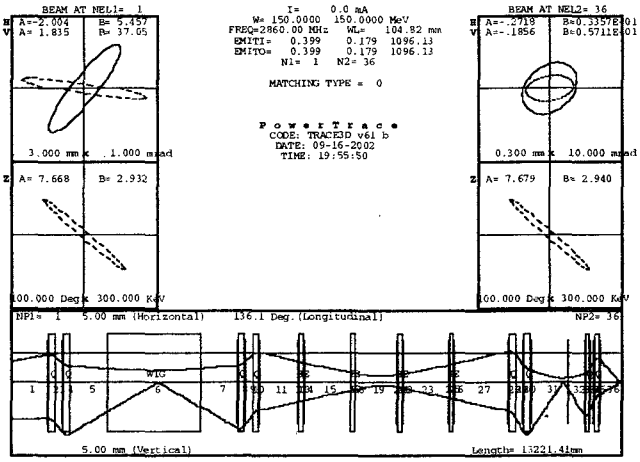

Fig. 1 Electron beam envelopes calculated by TRACE-3D

2. Design of electron beam line

Electron beam line has been designed with the use of the TRACE-3D[4)] code which calculates beam envelopes and Twiss parameters at each beam optics. The doublet of quadrupole magnets with field gradients of 20 T/m is used to focus the electron beam. The designed optics and the beam envelopes are shown in Fig. 1. Expected beam size is 40 μm in radius, which is same as that of the laser beam in the LWFA experiments. In this calculation, we used the measured emittances and Twiss parameters as the initial condition. The future plan for bunch slicing is also included. The bunch slicing requires an undulator where the electron beam is modulated through inverse free-electron laser (IFEL) mechanism, dipole magnets and beam stopper that extracts a modulated femtosecond electron bunch. The resonance condition for the IFEL is written as $\lambda_u = 2\gamma^2\lambda_L/(1+K^2/2)$, where λ_u is the undulator period, γ is the Lorentz factor of the electron beam, λ_L is the laser wavelength, and K is the K-parameter of the undulator. The energy modulation is given by[5)]

$$(\Delta E)^2 = 4\pi\alpha A_L \hbar\omega_L \frac{K^2/2}{1+K^2/2}\frac{M_u}{M_L},$$

where $\alpha(=1/137)$ is fine structure constant, A_L is the laser pulse energy, $\hbar\omega_L$ is the photon energy of the laser, M_u and M_L are the number of optical cycles in the undulator period and the laser wavelength, respectively. Using typical parameter of A_L = 100 μJ, λ_L = 0.8 μm, K = 2.2, M_L = M_L =19, the energy modulation of 9 MeV is expected.

3. Construction and beam transport tests

The overview of the experimental system is shown in Fig. 2. The extending beam line consists of eight quadrupole magnets, four dipole magnets and eight steering magnets. The quadrupole and dipole magnets were settled with an accuracy of 0.3 mm by transits. Vacuum chambers and ducts were also placed care-

[1] Present address: Sumitomo Heavy Industries. Ltd.

fully by transits. Four turbo-molecular pumps are employed to pump down to 10^{-9} Pa which is same order of vacuum pressure in the Microtron. Two amorphous core monitors are placed in the beam line to measure the beam current. Four phosphor screen profile monitors with a random shutter trigger CCD camera are equipped. The magnets are controlled by a VME based control system. Preliminary beam tests have been made and a charge of 30 pC was successively transported to the beam dump.

4. Achievements

We have designed electron beam line for the laser wakefield acceleration experiments. The beam line has a bunch slicing option to produce tens of femtosecond short electron bunch. A spot radius of 40 μm electron beam will be obtained. The electron beam line was constructed and evacuated to 10^{-9} Pa. The electron beam test was conducted. A charge of 30 pC was transported to the beam dump.

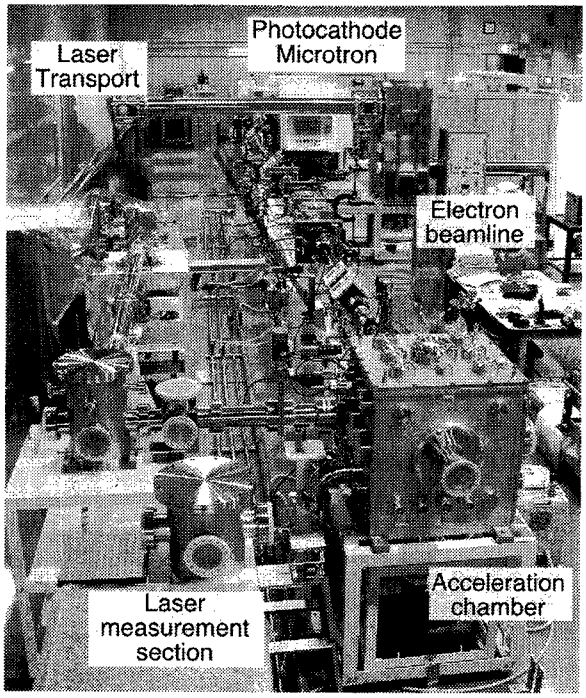

Fig. 2 An overview of the laser wakefield acceleration test facility

References

1) K. Nakajima et al. : Proceedings of the 9th Advanced Accelerator Concepts, Santa Fe, 2000 (in print)
2) X. J. Wang et al. : Nuclear Instruments and Methods **A 375**, p.82, 1996
3) M. Kando et al. : Proceedings of the 26th Linear Accelerator Meeting in Japan, pp. 132-134, 2001
4) K. R. Crandall (Revised by D. P. Rusthoi) : TRACE-3D Documentation, Second Edition, LA-UR-90-4146, Los Alamos National Laboratory, 1990
5) A. A. Zholents and M. S. Zolotorev : Phys. Rev. Lett., **76**, 6, pp. 912-915, 1996

4.5.3 1D PIC Simulation of Plasma Cathode

Shinichi MASUDA, Hideyuki KOTAKI, Masaki KANDO, Shuji KONDO,
Shuhei KANAZAWA, Takayuki HONMA and Kazuhisa NAKAJIMA[a)]
a) JAERI Kansai and High Energy Accelerator Research Organization (KEK)

1. Introduction

Interactions of high-intensity laser pulses with plasmas crucial for laser plasma acceleration [1,2]. In past few years, progress of ultrashort high-intensity laser system realizes the laser-plasma interaction in relativistic regime. Generations of high energy electrons are observed experimentally by high power laser pulse injection into the plasma [3,4,5,6,7].

A plasma cathode using such optical injection scheme is expected as a high quality electron source. 100TW laser system at JAERI Kansai [8] reaches intensity up to $I=10^{20}$ W/cm^2, when focused. We are planning plasma cathode experiment in new parameter regime with this laser system.

We conducted simulation study using 1D PIC code before the experiment. Next section explains 1D PIC simulation code and results of simulation of the plasma cathode. Section 3 summarizes this report.

2. Simulation Results

We developed a particle-in-cell (PIC) [9] code to simulate laser plasma interaction. Trajectories of each electrons and ions in an electromagnetic field are tracked by solving Lorentz force equation. These differential-equations are translated to space- and time-centered finite-difference equations. Temporal evolution of the electromagnetic field is solved by Maxwell equations. The magnetic field **B** and the particle velocity $\mathbf{u}=\gamma\boldsymbol{\beta}$ are updated by leap-frog method over the electric field **E** and the particle position **r**. Field quantities, **E** and **B**, are staggered in space grid. This guarantees second order accuracy and space-time reversibility. In order to push the particles, the field quantities at the particle positions are determined by linear interpolation. Current density, **j**, on each grid point is calculated from the particle position and velocity with the volume weighting scheme. Lindman algorithm [10] is adopted to implement an open boundary condition for the outgoing electromagnetic waves.

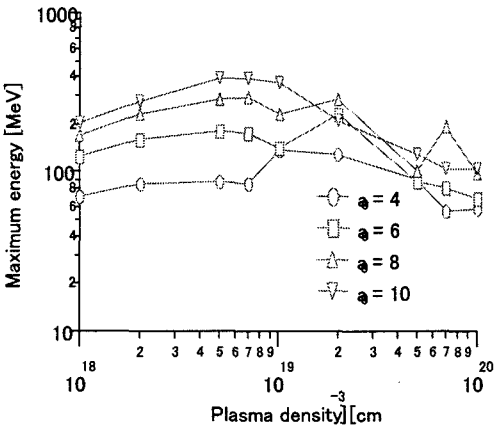

Fig. 1 Maximum energy of electrons as a function of the plasma density

Figure 1 shows maximum energy of electrons ejected from plasma. The simulations are conducted for the plasma density from 10^{18} to 10^{20} cm^{-3}. The plasma length is 500 μm. 20 fs laser pulse is injected into the plasma. Multi-hundred MeV electrons are generated around 10^{19}cm^{-3} plasma.

3. Summary

We have constructed 1D PIC simulation of the plasma cathode experiment. 300 MeV electrons are generated when the 10^{20} W/cm^2 laser pulse focused on the plasma. It is noted that 1D PIC cannot treat self-focusing of laser pulse. Higher energy is expected if the self-focusing occurs.

References

1) T. Tajima and J. M. Dawson, Phys. Rev. Lett., 43, 267 (1979
2) E. Esarey, et. al., IEEE Trans. Plasma Sci., 24, 252 (1996)
3) D. Gordon, et. al.,Phys. Rev. Lett., 80, 2133 (1998)
4) C. Gahn, et. al., Phys. Rev. Lett., 83, 4722 (1999)
5) X. Wang, Phys. Rev. Lett., 84, 5324 (2000)
6) V. Malka, et. al., Phys. Plasmas, 8, 2605 (2001)
7) M. Santala, et. al., Phys. Rev. Lett., 86, 5324 (2001)
8) K. Yamakawa, et. al., Opt. Lett., 23, 1468 (1998)
9) C. K. Birdsal and A. B. Langdon, Plasma Physics via Computer Simulation, McGrow-Hill, 1985
10) E. Lindman, J. Comput. Phys., 18, 66 (1975)

4.5.4 High-energy ponderomotive acceleration in super-strong laser-particle interaction

Igor V. SMETANIN and Kazuhisa NAKAJIMA[a)]
a) JAERI Kansai and High Energy Accelerator Research Organization (KEK)

1. Introduction

Ponderomotive motion of charged particles in the field of a non-uniform electromagnetic wave has been under investigation for a long time, being initiated by P. L. Kapitza and P. A. M. Dirac[1)]. The slow averaged motion of particles in the field of a traveling wave is determined by the ponderomotive potential force, which can be used for the acceleration of particles[2)]. Recent advances in high-intensity laser systems have renewed interest in the development of technology for the next generation of high-gradient laser-driven accelerators[3)].

We investigate a new regime of high-energy ponderomotive acceleration of particles in the laser field of relativistic intensity which occurs when the group velocity of the high-power laser pulse is less than the vacuum speed of light. The group velocity of the laser pulse in vacuum is determined by the characteristic transverse size of the pulse and the focusing conditions, and, in the case of laser-plasma interaction, by the plasma density. The physical mechanism of acceleration is the elastic scattering of particles by the ponderomotive potential in the reference frame moving at the laser pulse group velocity.

2. Dispersion of a focused femtosecond laser pulse in vacuum

Diffraction of the spatially bounded laser pulse can be treated as the limiting case of the propagation in a waveguide. For the circular waveguide and σ the transverse size of the laser pulse, we have in the limit of the infinite waveguide radius that, although both the phase and group velocities of a given (TM_{0n}) mode tends to the vacuum speed of light $\omega_0 / k_n \to c$, $k_n c^2 / \omega_0 \to c$ (ω_0 is the frequency and k_n is the mode longitudinal wavenumber), the mode with maximal amplitude has the group velocity which tends to the value $\sim c(1-(2\omega_0\sigma/c)^{-2}) < c$, less than the vacuum speed of light. Laser pulse has to propagate in the manner close to that of the transverse mode of the maximal amplitude, rather than that of the plane wave in the conventional approach.

We have studied the propagation of a focused ultrashort Gaussian laser pulse in vacuum, taking into account the difference between the pulse group velocity and the speed of light. It is developed the corresponding slow varying amplitude and phase (SVAP) approximation which is based on the transverse Hankel mode of the maximum amplitude. We have shown that the difference between the laser pulse group velocity and the speed of light leads to the dispersion of the ultrashort laser pulse, whith the characteristic dispersion length is $L_0 = k_0 v_g^2 \gamma_g^2 \tau_p^2$, where $v_g = k_0 c^2 / \omega_0$ is the pulse group velocity, γ_g is the corresponding Lorentz factor, τ_p is the pulse duration, and k_0 is the longitudinal wavenumber for the transverse mode of the maximal amplitude. For the focused Gaussian pulse we find

$$L_0 = \frac{L_d}{1+(L_d/f)^2}(k_0 c\tau_p)^2,$$

where $L_d = k_0\sigma^2$ is the characteristic diffraction length and f is the focal length.

The dispersion-dominated propagation regime emerges when the characteristic dispersion length becomes less than the diffraction length $L_0 < L_d$ and the focal length $L_0 < f$, i. e. , for the ultrashort laser pulse with the sufficiently small number of optical oscillations $N_{osc}\ f < L_d/(k_0 c\tau_p)^2 \sim L_d / N_{osc}^2$. In this dispersion-dominated focusing regime, the pulse duration grows rapidly with the propagation distance $\tau_p(z) = \tau_p\sqrt{1+z^2/L_0^2}$ accompanying the corresponding decrease in laser field peak amplitude $\sim (1+z^2/L_0^2)^{-1/4}$. Taking for as an estimate an ultrashort Gaussian laser pulse of wavelength 0.8 μm, initial duration τ_p = 15 fsec, and initial radius σ = 1 cm, we have that dispersion-dominated propagation is at the focal length f<60cm and can be realized in the experiment. The dependence of the laser field amplitude on the focal spot size for different pulse durations is shown in the Fig. 1.

3. High-energy laser ponderomotive acceleration of electrons

We have studied the ponderomotive acceleration of particles in the field of the laser pulse propagating at

the group velocity which is less than the vacuum speed of light. The physical mechanism of acceleration is the elastic scattering of particles by the ponderomotive potential in the reference frame moving at the laser pulse group velocity. We have shown that the energy gain for the scheme proposed is determined by the initial energy of the particle and pulse group velocity only, and does not depend on the laser peak intensity. For the particle initially at rest $\gamma_0 = 1$, the gain in energy is $\gamma \approx 2\gamma_g^2$, and for the acceleration of relativistic electrons at $\gamma_0 >> 1$ co-propagating with the laser pulse, we have $\gamma \approx \gamma_g^2 / \gamma_0$. The energy gain scales thus as the square of the group velocity Lorentz factor γ_g, which is determined by the relation $\gamma_g \approx f / \sigma \approx 2\pi w_0 / \lambda$ in the case of tight focusing, w_0 is the focal spot radius, and is inversly proportional to the plasma density, $n_e[cm^{-3}] \approx 1.115 \cdot 10^{21} \gamma_g^{-2} \lambda^{-2}[\mu m]$ for the plasma-dominated dispersion regime. Geometrical restrictions on the laser pulse group velocity due to the focusing conditions lead to the limit for the energy gain of accelerated particle at given laser power $\gamma < 1.35 \cdot 10^3 P^{1/2}[PW]$. The dependence of the energy gain on the laser pulse power and intensity for the acceleration of electrons of 15 MeV the initial energy is shown in the Fig. 2.

Laser intensity determines the threshold condition for the acceleration: the particle is scattered if its energy in the moving frame is less than the laser ponderomotive potential $\gamma' < (1 + a_0^2/2)^{1/2}$, a_0 is the normalized laser amplitude $a_0 = 0.85 \cdot 10^{-9} \lambda[\mu m](I[W/cm^2])^{1/2}$. In the quantum feature, laser intensity determines the probability for the particle to be reflected from the leading edge of the pulse and, thus, the number of accelerated particles. To estimate this probability, we have solved the Klein-Gordon equation. The acceleration thus can be considered as the scattering of de Broglie wave by the "photon plasma" in analogy with the scattering of electromagnetic wave by the plasma boundary[4].

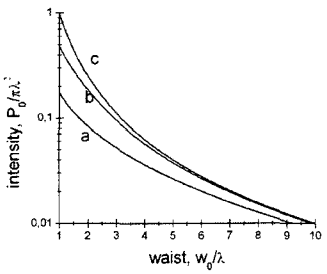

Fig. 1 The dependence of the normalized intensity on the focal spot radius at different pulse durations 1- 20fsec, 2- 35fsec, 3 100fsec.

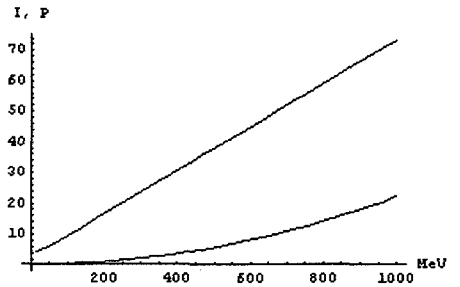

Fig. 2 Laser pulse intensity I (10^{18} W/cm^2) and power P (PW) vs the limiting energy gain for the acceleration of 15 MeV electrons in vacuum.

References

1) P. L. Kapitza and P. A. M. Dirac, Proc. Cambridge Philos. Soc. **29**, 297 (1933)
2) A. V. Gaponov and M. A. Miller, Sov. Phys. JETP **7**, 168 (1958)
3) T. Tajima and J. M. Dawson, Phys. Rev. Lett. **43**, 267 (1979); E. Esarey, P. Sprangle, J. Krall, A. Ting, IEEE Trans. Plasma Sci. **24**, 252 (1996); B. Rau, T. Tajima, H. Hojo, Phys. Rev. Lett., **78**, 3310 (1997); B. Quesnel, P. Mora, Phys. Rev. E, **58**, 3719 (1998); Y. I. Salamin, C. H. Keitel, Phys. Rev. Lett, **88**, 095005 (2002); B. Hafizi, E. Esarey, P. Sprangle, Phys. Rev. E, **55**, 3539 (1997); P. X. Wang, Y. K. Ho, X. Q. Yuan et al., Appl. Phys. Lett., **78**, 2553 (2001); C. J. McInstrie and E. A. Startsev, Phys. Rev. E, **54**, R1070 (1996).
4) I. V. Smetanin, C. Barnes, K. Nakajima, Proc. Int. Conf. HEACC'2001(Tsukuba, Japan, March 2001); I. V. Smetanin, K. Nakajima, Proc. Int. Symp. Sci. Super-Strong Field Interactions (Soken-dai, Japan,

4.6 Advanced Photon Simulation Research

The simulation group for advanced photon science
Toshiki TAJIMA, Toshizo SHIRAI†, Mitsuru YAMAGIWA, Akira SASAKI, James KOGA, Kengo MORIBAYASHI, Yutaka UESHIMA, Takayuki UTSUMI, Takao KONDOU, Takuya ARAKAWA, Ichirou FUKUMOTO, Keiko SUTO, Yasuaki KISHIMOTO, Shingo SUZUKI[a)], Hiroo TOTSUJI[b)]
a) Japan Science for Promotion of Science
b) Okayama Univ.

This Section is dedicated to the late Dr. Toshizo Shirai of our Group who led the pioneering research in atomic physics in photon research and the associated database development. His work has scientifically advanced our research and spiritually encouraged our endeavor. His work and person are etched deeply in our Group.

The Simulation Group is charged to carry out spear-heading research that explores future exploratory frontier issues associated with the application of intense laser irradiation and one that interprets ongoing laser experiments at the APRC. The Group mission also includes the development of large-scale and high performance computational physics and science that are driven by the above photon research. Through this activity the Group has managed to promote the computational nexus of excellence that serves not only the computational need of our Group described above, but also the computational community at large in Kansai and Japan. The Group is also helping the newly starting ITBL (Information Technology-Based Laboratory) at Kansai.

The following are some of our recent activities.

A two-dimensional particle-in-cell (PIC) code and visualization system supporting large simulations have been tuned for the massively parallel computer. They have been applied to simulations of acceleration of proton beams by relativistically self-focused intense laser pulses, of interaction between intense short-pulse laser and a thin and dense hydrogen plasma, and of high energy ion generation and nuclear fusion in laser-cluster interaction.

An efficient emission of picosecond bunches of energetic protons and carbon ions from a thin layer spalled from a organic solid by a laser prepulse has been demonstrated numerically by combining the molecular dynamics technique and multi-component collisional particle-in-cell method with plasma ionization. The energy distribution of hot electrons produced by a very short, intense laser pulse has also been investigated theoretically via particle simulation and compared with the experimental measurements.

Computerized prediction of the effect of laser irradiation impact has been done by classical molecular dynamics simulation and the density functional molecular dynamics method has also been applied to the hydrogen plasma in the domain of liquid metallic hydrogen.

We have developed a new numerical method based on the constrained interpolation profile (CIP) method to solve the Multiconfiguration Dirac-Fock (MCDF) equations, from which the relativistic atomic states are constructed.

Mechanism of producing soft x-ray gain in short intense laser irradiated plasma has been investigated. The processes of ionization of the plasma and successive excitation of the upper laser level have been analyzed using the collisional radiative (CR) model coupled with plasma hydrodynamics. The present model is being integrated with the massive database of atomic energy levels and ionization and excitation rates, which appears to be useful studying the atomic spectra observed in laboratory and astrophysical plasmas.

We have studied the x-ray spectra emitted from the inner-shell excited states of highly charged ions in high-density hot plasmas generated by high intensity laser irradiation on Xe clusters. At the electron density of 3×10^{23} cm^{-3} and the temperature of more than 5 keV, a great deal of x-rays are emitted from the highly charged ions of Xe^{35+} as seen in the actual x-ray spectra.

Laser field effects of electron capture processes in collisions between O5+ and C6+ ions have been calculated by using a close-coupling treatment with molecular-orbital expansion. In this calculation, laser intensity and collision energy are about 7x10^12 W/cm^2 and 1 keV/amu, respectively. Strong enhancement of the electron capture cross section has been found when thephoton energies are equal to the excitation energies of O5+ ions.

†: deceased Sept. 3, 2002

4.6.1 Computational science for advanced photon simulation

Yutaka UESHIMA, Takuya ARAKAWA, Akira SASAKI, Takayuki UTSUMI, James KOGA, Mitsuru YAMAGIWA, Takao KONDOU, Daisuke WAKABAYASHI[a)] and Toshiki TAJIMA
a) Research Organization for Information Science and Technology

1. Graphics computing ability of Super Simulation Center for Photon

1.1 Introduction

In 2001, A lot of computer systems were introduced as a part of the Super Simulation Center for Photons (SSCP) in JAERI Kansai Research Establishment at the Kizu site. The SSCP consists of a ES40-4/227 system, a vector parallel system VPP300/16(Fujitsu), a wide screen virtual reality system ONYX3400(Silicon Graphics), a High resolution liquid crystal display system SHD(NTT east), high performance graphics computers Professional Workstation SP750/2(Compaq), Nonlinear editing computers Professional Workstation SP750/2(Compaq), a Data base server GP4000(fujitsu), and a high end computing server RS6000(IBM). Recently, advanced simulation has become large-scale and multi-dimensional. In the data of the simulation, the size and number of data files and number of species is very large. Graphics performance is most important to analyze such a data as fast as possible. In other words, the most advanced simulation is supported by graphics technology. We test graphical performance of the SSCP computers.

1.2 Catalogue Specification of Graphics Computers in SSCP

The catalogue specification of graphics computers used in the test is shown in Table 1.

Table 1 Specification of graphics computers in SSCP

Computer	Compaq Professional Workstation SP750	Compaq Professional Workstation SP750	AlphaServer ES40-4
OS	Windows-NT4.0	Windows-NT4.0	Tru64 UNIX 5.1 AlphaServerSCv2.5
CPU	Pentium III Xeon 866MHz	Pentium III Xeon 866MHz	Alpha21264 833MHzX4
Memory	2GB	2GB	32GB
Extension bus PCI	64bit/66MHz PCIx2, 33MHz PCIx10	64bit/66MHz PCIx2, 33MHz PCIx10	64bit/66MHz PCI x 10
Extension bus AGP	AGP Pro (AGP 4X) x1	AGP Pro (AGP 4X) x1	
Display	1280x1024(24bit TrueColor) 72Hz	1280x1024(24bit TrueColor) 72Hz	1280x1024(24bit TrueColor) 72Hz
Graphics Card	Volume-ro500 ELSA GloriaIII (64MB)	Spectra7400 (32MB)	PowerStorm350

Computer	SUN Ultra10	ONYX3400
OS	Solaris8	IRIX6.5
CPU	Ultra SPARC II i 440MHz	MIPS R12000 400MHzX12
Memory	256MB	3GB
Extension bus PCI	32bit/33MHz PCI x 4	I-Brick 8GB/s
Extension bus AGP		
Display	Display mode 1280x1024(24bit TrueColor) 72Hz	Display mode 1256x1004(60Hz)
Graphics Card	ELSA Gloria Synergy creator3D	Inifinite Reakity 3 x 2P

1.3 Measurement of the Graphics Performance

We measured the graphics performance of the computers in Table 1. The first measurement was performed with ProCDRS-03 in ViewPerf6.1.2 of the benchmark programs which adopted OPC, which can be downloaded at http://www.specbench.org/gpc/opc.static/opcview.htm. The second measurement was performed with AVS/Express, because its visualization software is used by a lot of scientific researchers on thermo-fluid and electro-magnetic dynamics and so on.

The first measurement consists of 10 tests, test1 wireframe - Weight 25%, test2 wireframe, walk

through - Weight 25%, test3 shaded - Weight 10%, test4 shaded, walk through - Weight 10%, test5 shaded with texture - Weight 5%, test6 shaded with texture, walk through - Weight 5%, test7 shaded with texgen eye linear - Weight 3%, test8 shaded with texgen eye linear, walk through - Weight 3%, test9 shaded with color per vertex - Weight 7%, and test10 shaded with color per vertex, walk through - Weight 7%. The results are shown in Fig.1.

In the Onyx, all tests would not work except for test1. The results indicate that the system consisting of the PC and high-end graphics card (GloriaIII) has the highest performance.

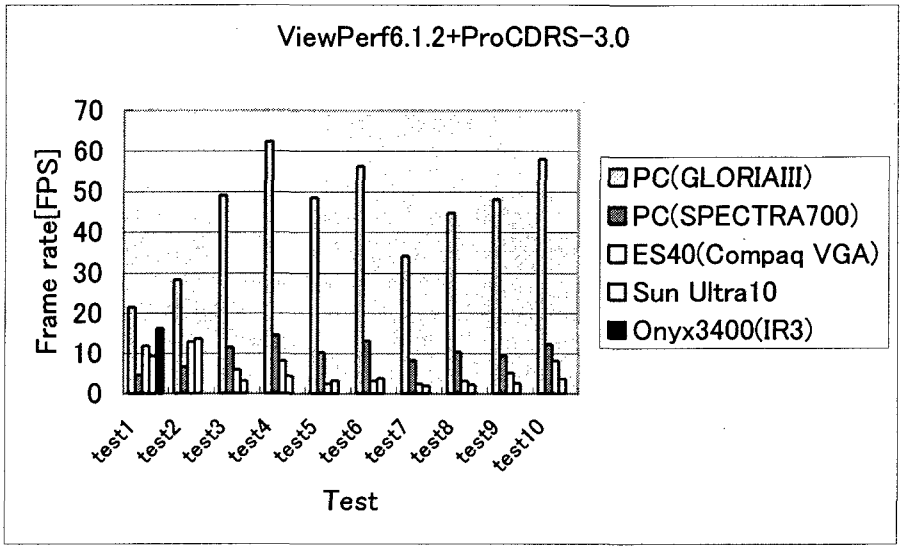

Fig. 1 Results of ProCDRS-03 in ViewPerf6.1.2

The second measurement consists of 2 tests, test1 surface rendering of triangle polygons; (carib.geo=26,529, kenki.geo=37,315, lobster.fld127=87,278, lobster.fld1=146,778), test2 volume rendering of lobster.dat which is a sample dataset attached to AVS/Express. The results of surface rendering tests are shown in Fig.2 and 3.

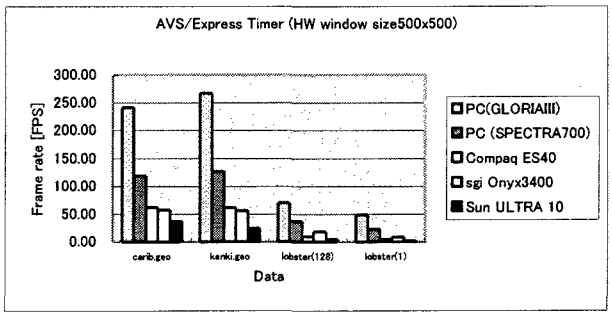

Fig. 2 Results of graphic card acceleration mode

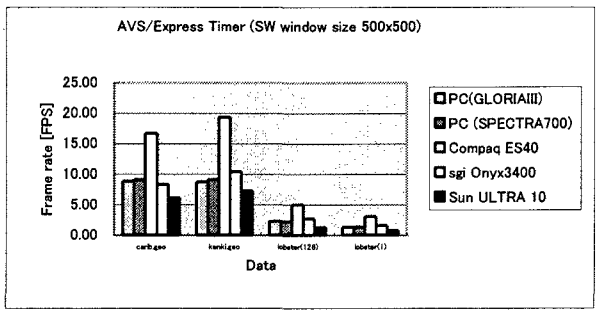

Fig. 3 Results of CPU SW emulation mode

In the case of HW acceleration mode, the system consisting of the GloriaIII PC has the highest performance. In the case of SW emulation mode the higher the ability of the CPU (FLOPS) the higher the graphics performance becomes.

The results of volume rendering tests with the modes of BTFtextur, RayTrace, and FatRay are shown in Fig.4. In the case of using a hardware volume-rendering card (VolumePro500) the FPS is 51.9. The high-end workstations, ONYX and ES40, have comparatively high performance. However, Ultra10 has quite low performance.

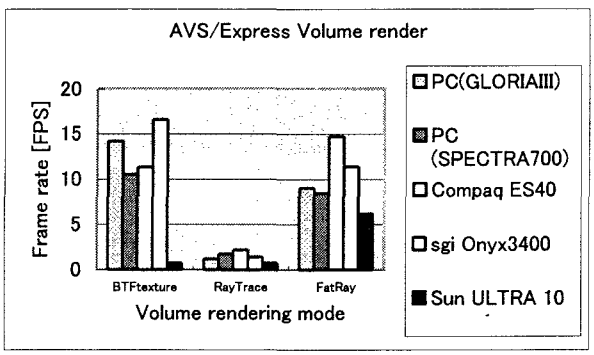

Fig. 4 Results of volume rendering test

1.4 Results

We test graphical performance in a PC, ES40, ONYX3400, and ULTRA10. The results indicate that the PC system has high performance. The better system to analyze large simulation data is that of a client of a PC with a high-performance graphic card and servers handling data with high-performance CPUs.

2. Visualization program development using Java

Method of visualization programs using Java for the PC with the graphical user interface (GUI) is discussed, and applied to the visualization and analysis of 1D and 2D data from experiments and numerical simulations. Based on an investigation of programming techniques such as drawing graphics and event driven program, example codes are provided in which GUI is implemented using the Abstract Window Toolkit (AWT). The marked advantage of Java comes from the inclusion of library routines for graphics and networking as its language specification, which enables ordinary scientific programmers to make interactive visualization a part of their simulation codes. Moreover, the Java programs are machine independent at the source level. Object oriented programming (OOP) methods used in Java programming will be useful for developing large scientific codes which includes number of modules with better maintenance ability.

3. The Constrained interpolation profile method for multiphase analysis

We have reviewed the CIP method that is known as a general numerical solver for solid, liquid , gas and plasmas. This method is a kind of semi-Lagrangean scheme and has been extended to treat incompressible flow in the framework of compressible fluid. Since it uses primitive Euler representation, it suits for multi-phase analysis. The recent version of this method guarantees the exact mass conservation even in the framework of semi-Lagrangean scheme. Comprehensive review is given for the strategy of the CIP method that has a compact support and subcell resolution including front capturing algorithm with functional transformation, a pressure-based algoritthm, and other miscellaneous physics such as the elastic-plastic effect and surface tension. Some practical applications are also reviewed such as milk crown or coronet, laser-induced melting, and turbulent mixing layer of liquid-gas interface.

4. New numerical method for the solutions of the MCDF equations based on the CIP method

4.1 Introduction

In the 1960's, Grant derived the MCDF equations as simple closed formulae by methods involving the use of Racah algebra. Since then various numerical procedures and computer programs has been developed, and a number of calculations for the relativistic atomic structure have been reported. As a result, demands to obtain higher precision estimates of the properties of atomic systems are increasing. That is to say, there is continuing interest in developing more confident and accurate methods to solve the MCDF equations.

4.2 Method of solution

We have developed a new numerical method [1] based on the constrained interpolation profile (CIP) method [2] to solve the Multiconfiguration Dirac-Fock (MCDF) equations. The radial wave functions are represented by the values and the spatial derivatives on an arbitrary grid system, and approximated by cubic polynomials. Owing to this representation, the values and the spatial derivatives of the effective charge distribution and inhomogeneous term are calculated using the previous cycle's wave functions. Then the homogeneous MCDF equations are integrated to obtain two linearly independent solutions, which are used to construct the Green function, by the adaptive stepsize controlled Runge-Kutta method controlling the truncation errors within a prescribed accuracy. The radial wave function is improved by taking the convolution of the Green function and the inhomogeneous term. The effectiveness of this numerical procedure is investigated after implementing it into the relativistic atomic structure code GRASP92.

4.3 Results

For the verification of the proposed algorithm, we have implemented the numerical procedure into the relativistic atomic structure code GRASP92 [3], replacing routines related to solve the MCDF equations. Table1 shows the results of the extended average level (EAL) calculation for the upper *4d* level ($(3d_{3/2}4d_{3/2})_{J=0}$ in the *jj*-coupling scheme) in Ni-like Eu(Z=63), which is used as a lasing medium in the first demonstration of x-ray lasers using Ni-like ions. The error of the norm in our calculation is within 10^{-10} for all the orbitals. We can see that acceptable orbitals are obtained and the energy parameters show good agreement with those calculated by GRASP92. It is noted that GRASP92 judged the inhomogeneous terms for the $4f, 4f$ orbitals to be too small to solve correctly and changed the integration method to one prepared for the case when the energy parameter is near an eigenvalue.

We can see all the orbitals are calculated with sufficient accuracy with our new method.

Orbital	Đε	Đε^H	norm	nodes	sign	Đε (GRASP92)	norm (GRASP92)
1s	1851.1450710	1846.1871220	1.0	0	+	1851.1450890	0.9999990
2s	354.4090967	345.3738693	1.0	1	+	354.4090984	1.0000000
2p	338.7349502	332.0572852	1.0	0	+	338.7349558	0.9999998
2p	314.7018670	308.9725940	1.0	0	+	314.7018715	0.9999999
3s	118.4372132	113.7053725	1.0	2	+	118.4372061	0.9999999
3p	111.8757876	107.5882572	1.0	1	+	111.8757822	0.9999998
3p	106.5867523	102.8150376	1.0	1	+	106.5867461	1.0000001
3d	95.7591468	92.8396384	1.0	0	+	95.7591442	0.9999999
3d	94.5955895	91.8856138	1.0	0	+	94.5955866	1.0000000
4s	56.0560622	55.1555357	1.0	3	+	56.0560560	0.9999972
4p	53.4610588	52.5693620	1.0	2	+	53.4610530	0.9999969
4p	51.7175455	50.9496777	1.0	2	+	51.7175403	0.9999985
4d	47.6143752	46.8714124	1.0	1	+	47.6143696	0.9999984
4d	47.1824751	46.5071115	1.0	1	+	47.1824699	0.9999996
4f	42.8724599	42.1584131	1.0	0	+	42.8724550*	1.0000000*
4f	42.6796002	42.0556836	1.0	0	+	42.6795933*	1.0000000*

Table 2
Calculated orbital parameters. The ε, ε^H, *node* and *sign* column show the binding energy (a.u.), eigenvalue of the homogeneous equation, the sign of the first extremum of *P* and number of nodes in *P*, respectively. (* indicates that the orbital is integrated by the method 2 in GRASP92.)

5. Collaboration with NTT in large data transfer using GEMnet

We began collaboration with NTT regarding methods of holding visualized and numerical data in common under protection of copy rights, bearing in mind applications to remote analysis and use of large simulation data from a TFLOP-class massively parallel computer. In FY2001, we transferred the visualized data of electromagnetic fields and plasma density profiles from a simulation of the interaction of an intense laser with an underdense plasma to NTT-Musashino. These data were transferred to Stanford University through the NTT-GEMnet for demonstartion of stable data transmission and sharing among remote sites. Monitoring the transferred visualized data with a super high definition image display was successful in the U.S. and the high quality of the image was confirmed, leading to the start of this collaborative work between the remote facilities. Electric water marking for a part of the image data from the scientific research, which is in the testing stage, was also done and no significant deterioration of the image quality was found.

References

1) T. Utsumi and J. Koga, Computer Phys. Comm., in print.
2) T. Yabe and T. Aoki, Computer Phys. Comm., **66**, 219, 1991.
3) F.A. Parpia, C.F. Fischer, and I.P. Grant, Computer Phys. Comm., **94**, 249, 1994.

4.6.2 Advanved photon simulation with particle-in-cell (PIC) codes

James KOGA, Mitsuru YAMAGIWA, Yasuaki KISHIMOTO, Yutaka UESHIMA, Akira SASAKI, Takao KONDOU, Alexi ZHIDKOV[a)], Daisuke WAKABAYASHI[b)], Tomohiro MASAKI[b)], Toshihiro OYAMADA[c)] and Toshiki TAJIMA
a) University of Tokyo
b) Research Organization for Information Science and Technology
c) Compaq Computer K. K.

1. Acceleration of proton beams by relativsitically self-focused intense laser pulses

1.1 Introduction

Ultraintense laser interactions with matter can generate enormous numbers of highly energetic electrons, photons, and ions. Recent laser-matter interaction experiments have revealed acceleration of 10^{10} electrons with the maximum energy up to 100 MeV and production of 10^{12} ions up to several tens of MeV[1)]. In two-dimensional PIC simulations for propagation of ultraintense laser pulses of the order of 10^{20}W/cm^2 in underdense plasmas of 10^{20}cm^{-3}, we have found that large amplitude positive electrostatic fields of the order of a few TV/m are generated over a 1 mm scale in the front of a relativistically self-focused laser pulse[2)]. These enormous fields imply the capability of accelerating protons. The solitary structure of the electrostatic field with a spatial and temporal size of the order of μm can produce a femtosecond ion pulse. We propose a new acceleration mechanism for ions due to enormous accelerating fields generated by relativistically self-focused laser pulses in plasmas. This mechanism may open up a new regime of ultraintense laser-matter interactions and new fields of high energy particle physics.

1.2 Simulation parameters

To study the self-focusing of a high intensity short pulse laser in a plasma we use the code P^3 (Progressive Parallel Plasma Code) which is a 2 dimensional fully relativistic particle-in-cell(PIC) code[3)] running on the Compaq ES40/227 node parallel computer. The simulation box is 672 mm (23000 cells) by 37.4 mm (1280 cells) in the x and y directions respectively. The boundary conditions are periodic in the y direction and outgoing in the x direction. There is a vacuum region at one end of the simulation box of length 21.9 mm. The plasma density is chosen to be 5.3x10^{19}cm^{-3} which corresponds roughly to doubly ionized Helium gas at atmospheric pressure. There are 8 electrons and 8 ions in each simulation cell with an ion to electron mass ratio of 1836. The linearly s polarized laser pulse starts in the vacuum region and propagates into the plasma. The parameters of the laser are of the 100 TW Ti:sapphire laser at the Japan Atomic Energy Research Institute [4)]. The pulse length is 19 fs with a spot size of 10 μm. The wavelength is 0.8 μm. The corresponding unitless laser strength parameter a_0=7.4 where $a_0=eE_0/(m_0\ \omega_0 c)$, E_0 is the peak electric field, m_0 is the electron mass, and ω_0 is the laser frequency. The critical power P_{cr} for the relativistic self-focusing of a Gaussian laser pulse is given by [5)], $P_{cr}(GW)=17(\omega_0/\omega_p)^2$, where ω_0 is the laser frequency and ω_p is the plasma frequency. With the current density P/P_{cr}~179, where P is the laser power. Thus, the laser pulse should relativistically self-focus in the plasma. With the given density and laser pulse length a large wake field behind the pulse should not occur.

1.3 Results

Figure 1(a) shows the laser pulse after it has propagated 256 mm ($340c/\omega_p$). The laser pulse has relativistically self-focused, has filamented, and the central portion has narrowed. The amplitude is approximately a factor of 2 higher than the initial laser pulse amplitude. Due to a large buildup of electrons at the front of the pulse, there is a large positive electrostatic field in the propagation direction of the laser pulse created there. Figure 1(b) shows the structure of the electric field after the same propagation distance. The electric field rises rapidly to a maximum of 6.5 TeV/m and gradually drops off until it becomes negative behind the laser pulse. As the laser pulse propagates in the plasma it depletes. In conjunction with the laser pulse depletion the electrostatic field also decreases. We propose to use the large field created at the front of the pulse to accelerate injected protons to higher energies[2)]. In order to determine the minimum energy of injection of the protons we can use

the theory developed for determining the minimum energy of injection for electrons in a wakefield[6]. From the given parameters if we inject protons at the minimum injection energy, we can get an increase of up to 0.8 GeV. We measured the velocity of the pulse from the simulations giving a minimum injection energy of 2.06GeV. In order to insure that some protons are injected in front of the electrostatic field a proton beam with an initial energy spread was input into the simulation. The beam was uniformly distributed in the y direction and placed in the same initial position as the laser pulse with a length of 29.2 mm. In Figure 2 is shown the energy distribution of the injected proton beam. In Figure 2(a) one can see that the final distribution (solid line) is shifted from the initial distribution (dotted line). In a close-up of the peak in Figure 2(a)(inset) the shift corresponds to an equivalent acceleration of 90 MeV. In a log plot of the distribution in Figure 2(b) one can see that there is an increase in the high energy tail of the proton beam. One can see that this increase corresponds to an equivalent acceleration of 450 MeV. The 90 MeV and 450 MeV increases in energy correspond to average acceleration gradients of 0.14 and 0.7 TeV/m, respectively. These gradients are reasonable in comparison to the maximum electrostatic field gradient of 6.5 TeV/m. The optimal energy and position of the injected protons still need to be determined. For this paper the main point was to show the possibility of acceleration of protons by the large electrostatic field generated at the front of the laser pulse. There are several factors which affect or limit the acceleration of ions. One is the depletion of the laser pulse. With the depletion of the laser pulse the acceleration efficiency also drops. Another factor affecting the acceleration is the "snaking" instability which causes the laser pulse to deviate from it's original propagation direction[7]. All these factors need to be considered for the optimal acceleration of protons.

2. High energy ions and nuclear fusion in laser-cluster interaction [8]

Highly efficient energy conversion of laser to high-energy components of ions and resulting rapid expansion take place upon the laser irradiation of clusters.

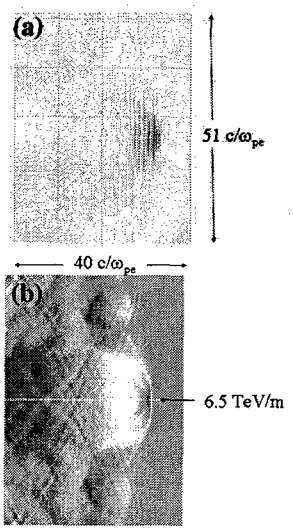

Fig. 1 (a) Laser Field E_z and (b) E_x Field

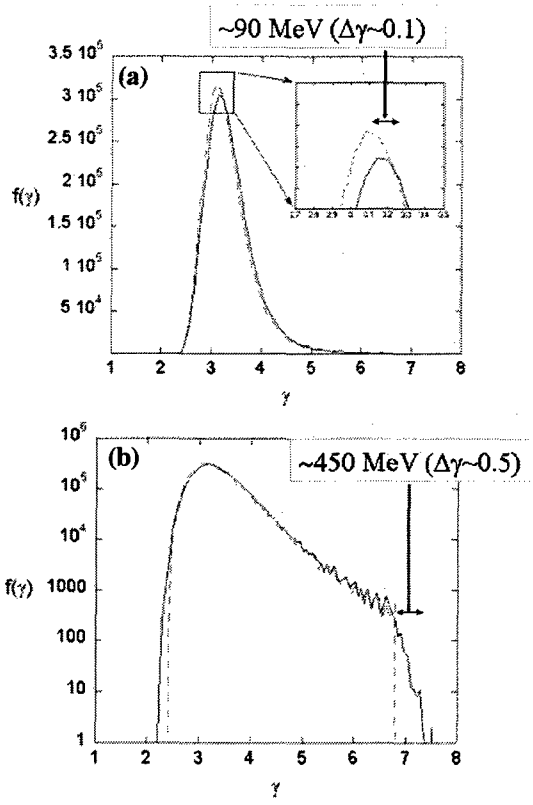

Fig. 2 Energy Distribution of Protons (a) linear and (b) log scale

Depending on the interrelationship between cluster size a and the electron excursion length ζ e (which is related to the laser field amplitude), the expansion characteristics is categorized into the Coulomb explosion ($a << \zeta$ e) and alternative hydrodynamic ambipolar expansion ($a >> \zeta$ e), revealing different features in the ion energy distribution. In the Coulomb explosion regime, a flat and/or slightly inverted ion energy distribution effective for enhanced fusion reactivity is generated. The critical cluster size and laser field amplitude which demarcate the expansion characteristics is investigated and the optimal fusion cross section is found in the domain of Coulomb explosion. A high fusion neutron yield is expected in the Coulomb explosion regime with greater cluster size and higher packing fraction.

3. Short-laser-pulse-driven emission of energetic ions into a solid target from a surface layer spalled by a laser prepulse [9)]

An efficient emission of picosecond bunches of energetic protons and carbon ions from a thin layer spalled from a organic solid by a laser prepulse is demonstrated numerically. We combine the molecular dynamics technique and multi-component collisional particle-in-cell method with plasma ionization to simulate the laser spallation and ejection of a thin (~20-30 nm) solid layer from an organic target and its further interaction with an intense femtosecond laser pulse. In spite of its small thickness, a layer produced by laser spallation efficiently absorbs ultrashort laser pulses with the generation of hot electrons that convert their energy to ion energy. The efficiency of the conversion of the laser energy to ions can be as high as 20%, and 10% to MeV ions. A transient electrostatic field created between the layer and surface of the target is up to 10 GV/cm.

4. Pulse duration effect on the distribution of energetic particles produced by intense femtosecond laser pulses irradiating solids [10)]

The energy distribution of hot electrons produced by a very short, intense laser pulse (I = 2-4$\times 10^{18}$ W/cm^2, 60 fs, = 800 nm, obliquely incident p polarized) is investigated theoretically via particle simulation and experimentally via measurements of the electron distribution in the MeV region and the Doppler-shifted emission spectrum of fast ions. This energy distribution is shown to be greatly different from the known two-temperature distribution. The hot electrons with energies near the maximal (~2 MeV) constitute the distribution with an effective temperature Th considerably higher than that of lower-energy electrons, which dominate the emission of energetic ions. The temperature scaling with the laser intensity differs from the known Th~$I^{1/2}$.

5. PIC simulation of interaction between intense short-pulse laser and a thin and dense hydrogen plasma layer

Massively parallel large PIC (particle-in-cell) simulation of high energy ion generation in the interaction of a relativistically intense (> 10^{20} W/cm^2) short-pulse (~ 20 fs) laser with a thin (< 1 ì m) and dense (~ 5×10^{22} cm^{-3}) hydrogen plasma layer is reported. Ion and electron dynamics and the electromagnetic fields structures are studied in the two-dimensional geometry.

We use 2D PIC simulations with a system size of 80 λ in the x (laser) direction and 40 λ in the y (transverse) direction, where λ is the incident laser wave length. We assume initially Gaussian pulses with a full width at half maximum of 7.5 λ (6.3 λ) in the x (y) direction. The linearly polarized laser pulse is normally incident to the target. The laser intensity expressed as a normalized electric field a_0 is ~ 14. The plasma layer width is 0.5 λ . There exists a vacuum region on both sides of the thin plasma layer. There are 10 particles per cell for the electrons with the same number for ions in the plasma layer. The initial temperatures are $T_e = T_i$ = 10 keV. The plasma density is $n_e = n_i$ = 5×10^{22} cm^{-3}. A real proton to electron mass ratio of m_i / m_e = 1836 is adopted.

When the main part of the incident laser reaches the target, a strong electrostatic field E_x in the x-direction is induced near the surface. The magnitude of E_x is comparable to that of the laser field. The sign changes negative (left-side of the surface) to positive (right-side of the surface). Some ions are accelerated by this strong electrostatic field. The laser field is mostly reflected at the target surface. As shown in Fig. 3, although by when the reflected field reaches the left boundary, the clear negative-to-positive shape of E_x is smeared out, the positive part works for accelerating ions in the +x-direction. We can also see the B_z field near the target (Fig. 4). This magnetic field is considered to

come from the electric current component in the same direction as E_x. Ion and electron density profiles indicate that particles near the region of laser focusing are pushed forward and that values of the particle densities there reduce significantly (Fig. 5). The maximum ion (electron) energy reaches over 40 MeV (100 MeV). It has also been found that over one-fourth of the laser energy is converted to kinetic energy and that the total energy of ions can be about three times larger than that of electrons.

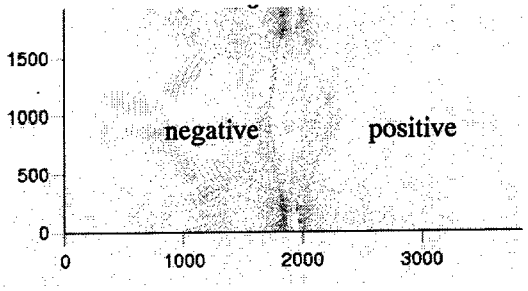

Fig. 3 Image of Ex field

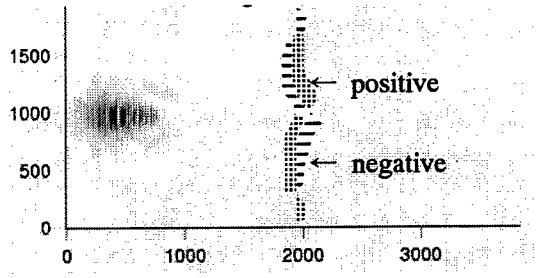

Fig. 4 Image of Bz field

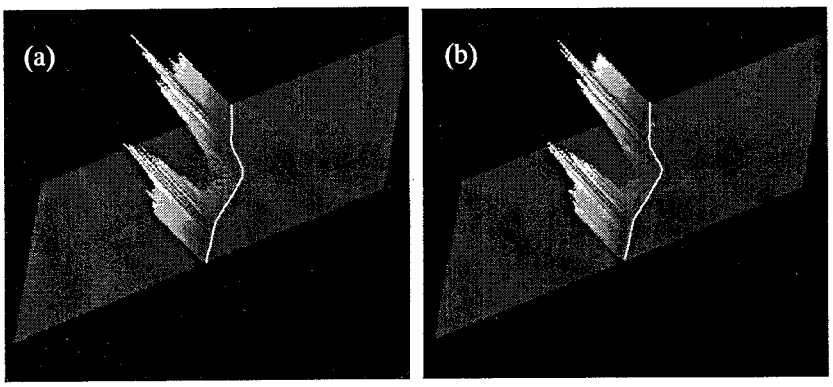

Fig. 5 Bird's-eye view plots of (a) ion and (b) electron density profiles

References

1) T.E. Cowan, et. al., Nucl. Instr. Meth. Phys. Res. A, 445, 130, 2000.
2) J. Koga, K. Nakajima, K. Nakagawa, AIP Conference Proceedings, 611, 126, 2002.
3) Y. Ueshima, Y. Sentoku, and Y. Kishimoto, Nucl. Instr. Meth. Phys. Res. A, 455, 181, 2000.
4) K. Yamakawa, M. Aoyama, S. Matsuoka, T. Kase, Y. Akahane, and H. Takuma, Opt. Lett., 23, 1468, 1998.
5) G. Z. Sun, E. Ott, Y. C. Lee, and P. Guzdar, Phys. Fluids, 30, 526, 1987.
6) E. Esarey and M. Pilloff, Physics of Plasmas, 2, 1432, 1995.
7) N. M. Naumova, Physics of Plasmas, 8, 4149, 2001.
8) Y. Kishimoto, T. Masaki, T. Tajima, Phys. Plasmas, 9, 589, 2002
9) A.G. Zhidkov, L.V. Zhigilei, A. Sasaki, T. Tajima, Appl. Phys. A, 73, 741, 2001.
10) A.G. Zhidkov, A. Sasaki, I. Fukumoto, T. Tajima, T. Auguste, P. D'Oliveira, S. Hulin, P. Monot, A.Ya. Faenov, T.A. Pikuz, I.Yu. Skobelev, Phys. Plasmas, **8**, 3718, 2001.

4.6.3 Advanced photon simulation with molecular dynamics codes

Ichirou FUKUMOTO, Hiroo TOTSUJI[a)] and Junzo CHIHARA[b)]
a) Okayama University
b) Research Organization for Information Science and Technology

1. Computerized prediction of the effect of laser irradiation impact

"High-power, short-pulse!" That's a virtual laser battle cry today since it brings high accuracy in precision micro-fabrication as a by product in the high power laser progress. High-power, short-pulse laser instantly evaporates the irradiated material. This process can be well utilized for microfabrication due to its high level of control over other methods. Powerful shock waves are induced toward material interiors from the evaporated area. This is the laser impact phenomenon characteristic of the ultra short –pulse laser. Its application are not limited to precision micro-fabrication. The phenomenon can induce dislocations such as atom hopping in the crystal lattice of the material during the process of shock wave propagation. Material distortion from lattice dislocations adversely affects fabrication accuracy. Thus it is necessary to clarify the mechanism of lattice dislocation generation, which is believed important in the laser application to precision fabrication in the future.

JAERI has studied the laser impact on the material crystal structure via molecular dynamic method, which treats materials as an assembly of atoms to calculate and predict atomic behavior (atomic force) through a computer simulation.

Early in the research program few examples existed application of the molecular dynamic method to the laser shock phenomenon. Most studies analyzed the phenomenon by assuming material as a continuum. On the other hand, the molecular dynamic method treats the material structure from the atomic unit for detailed analysis of crystal structure changes. For some materials, such as metals wherein free electrons greatly affect thermal conduction, a new method to meet thermal conduction bas been introduced by free electrons in practical simulation of realistic physical properties.

Compression and tension of atoms in the material irradiated by 200GW/cm^2 (gigawatt) for one pico second (10^{12} seconds) show that in the stressed region, atoms under stronger compression are reddened. Circular shock waves are generated within the material as a reaction of explosive surface evaporation from laser irradiation. Line traces within the material show misaligned crystal caused by the propagation of lattice dislocations inwardly generated by the shock wave.

In this state no change of atomic force in the evaporated area is considered, thus the analysis was limited to the solid area of the material. A new calculation model for further analysis with atomic forces in the evaporated region will be introduced in the near future.

The molecular dynamic method demands a large amount of computing time constaning the number of computed atoms and simulation analysis. An masterly parallel processing computer has been employed to enable such large calculations. In the near future much faster simulation with a greater number of atoms will become a reality.

2. Quantum simulation of hot dense plasmas

Density functional molecular dynamics method is applied to the hydrogen plasma in the domain of liquid metallic hydrogen. The effects of the density gradient are taken into account in both the electronic kinetic energy and the exchange energy and it is shown that they almost cancel with each other, extending the applicability of the Thomas-Fermi-Dirac approximation to the cases where the density gradient is not negligible. It is also shown that this method, treating the electron density as a dynamical variable instead of wave functions, is a candidate for feasible simulations of large systems.

4.6.4 Atomic process simulation

Akira SASAKI, Kengo MORIBAYASHI, Toshizo SHIRAI, Shingo SUZUKI[a)],
Noriyuki SHIMAKURA[b)], Hiroki NAKAMURA[c)], Keiichi YOKOYAMA,
Yuzuru KUROSAKI and Yoshiaki TERANISHI[d)]

a) Japan Society for Promotion of Science
b) Niigata University
c) Institute for Molecular Science
d) RIKEN

1. Analysis of x-ray lasers with the hierarchical atomic model

1.1 Introduction

Mechanism of producing soft x-ray gain in short intense laser irradiated plasma is investigated. The processes of ionization of the plasma and successive excitation of the upper laser level are analyzed using the collisional radiative (CR) model coupled with plasma hydrodynamics. The present model is being integrated with the massive database of atomic energy levels and ionization and excitation rates, which appears to be useful studying the atomic spectra observed in laboratory and astrophysical plasmas.

1.2 Model

Given the target material, intensity and temporal profile of the pumping laser, the one dimensional hydrodynamics calculation is performed to provide the temporal evolution of the plasma to be used to calculate atomic level population with the CR code. The present CR code is designed to reproduce hierarchical structure of the atomic level, following the standard definition of atomic level in the spectroscopy as from its root to leaf as the charge state, shell, configuration, relativestic subconfiguration, to fine structure level. In the case of calculating soft x-ray gain of the transient collisional excited (TCE) Ni-like laser, a set of rate equation is solved including charge states typically from Kr-like through Ar-like ions. All major atomic processes in high temperature such as electron collisional excitation and ionization, radiative recombination, spontaneous emission and their reverse processes[1] are considered. For the Ni-like ion, the detailed energy levels and rates are calculated by the HULLAC[2], otherwise the level energies are calculated by the screened hydrogenic model, and the rates are estimated from empirical formulas.

1.3 Results and discussion

Figure 1 shows the gain at 13.9nm of Ni-like Ag laser for a plasma irradiated by two ps laser pulses. The calculation shows the importance of the pedestal level of the laser between pre- and main-pulse to keep sufficiently high temperature of the plasma to maintain the Ni-like population. The calculated gain is consistent with experimental value of 35/cm from the spatially and temporally averaged measurement[3]. La laser at λ=8.8nm is also investigated. It is found that the gain is produced in the overcritical density plasma heated by the electron thermal conduction. The experiment also suggests the gain region is very close to the target surface as predicted by the calculation.

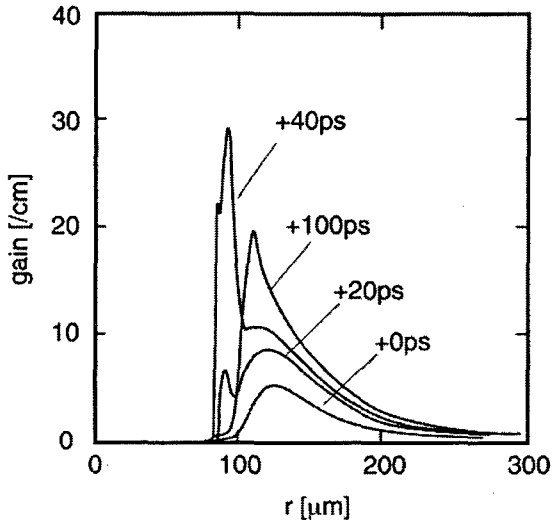

Fig. 1 Calculated temporal spatial evolution of the gain of Ni-like Ag laser

The plasma hydrodynamics is calculated for the intensity of pre- and main- pulse of 1.6 and 8×10^{14}W/cm^2, with a duration of 1.5 ps, separation of 1.2 ns, and the pedestal level of 10^{12} W/cm^2 is assumed.

1.4 Integration with database

Application of the present CR code to predict the emission spectrum of multiple charged ions is also investigated. A database of numerical atomic data including approximately 500 ionic species is developed. Integration of the database and CR code is realized with based on web technology. Complete Whiam (Web oriented HIerarchical Atomic Model) is being developed. Using this software system, a user on the internet submits a request by choosing elements, plasma temperature and density, which invokes a sequence of inquiries to the database and calculation of the CR code, and eventually the spectrum is visualized on user's web browser.

2. Theoretical study on dielectric recombination of O^{6+} ions in metastable states [4]

A computational scheme, based on the theory of the continuum-bound transitions of Bell and Seaton [J. Phys. B 18, 1589 (1985)] and the close-coupling *R*-matrix approach, has been developed to treat dielectronic recombination (DR) in high-lying resonance-energy regions. This scheme and our presented numerical method to compute DR in low-lying resonance-energy regions [Phys. Rev. A 62, 022706 (2000)] have been applied together to elucidate the experimental spectra of the DR of O^{6+} ions in the metastable $1s2s^3S$ and $1s2s^1S$ states. For comparison, a perturbative theoretical calculation of DR for O^{6+} has also been accompanied. The reasonable representation of the general dielectronic spectral shape is yielded by both our close-coupling and perturbative calculations. However, both the methods do not reproduce the experimental double-peak structure at ~6-8 eV. This shows that the further investigation on DR of this kind of ions is required both experimentally and theoretically.

3. Extended description for electron capture in ion-atom collisions: Application of model potentials within the framework of the continuum-distorted-wave theory [5]

We perform an extension of the continuum-distorted-wave (CDW) approximation for single electron capture by introducing model potentials to describe the interaction of the active electron with the residual-target and projectile ions. The cross sections for electron transfer in collisions of bare and dressed projectile ions with H and He atoms are calculated and compared with experimental data and previous CDW calculations that make use of approximate analytical wave functions to represent the active electron initial and final states. For electron capture in proton-He collisions into definite final states the present calculations are in better agreement with experiments. We trace the differences in the results from both models to a different behavior at projectile scattering angles close to the Thomas peak. In the case of dressed projectiles with different charge states impinging on H and He the present version of CDW gives a better representation of the filling of the unoccupied orbitals of the dressed ion and, therefore, of the cross section as a function of the impinging ion charge state.

4. Electron capture processes in a strong laser field

4.1 Introduction

Control of molecular dynamics by laser has been the recent interesting subject in relation to the applications of intense pulse lasers. Especially for electron capture processes in ion-atom and ion-ion collisions, it is considered to control the production of state-selective excited ions in X-ray laser sources which require the production of population inversion. In this study we calculated the cross section for an electron capture process, $O^{5+}(1s^22s) + C^{6+} \rightarrow O^{6+}(1s^2) + C^{5+}(n=2,3)$ in a strong laser field.

4.2 Calculation

We used a semi-classical close-coupling method expanded by molecular-orbitals with electron translation factor. The close-coupling equation expressed in the atomic unit is,

$$i\frac{dc_m}{dt} = \left[c_m + \vec{E}(t)\cdot\left\langle\phi_m\middle|\vec{r}\middle|\phi_m\right\rangle\right]c_m + \sum_{n\neq m}\left[\vec{E}(t)\cdot\left\langle\phi_m\middle|\vec{r}\middle|\phi_n\right\rangle + \vec{v}\cdot(\vec{P}_{mn} + \vec{A}_{mn})\right]c_n$$

where, r is the electronic coordinate, v the impact velocity of the ion, E(t) the laser field, c the transition amplitude, ϕ the molecular orbital, (P+A) the non-adiabatic coupling with the correction of the electron translation factor[6,7]. The laser field is set to the circularly polarized light. The cross section is averaged over the six laser injection angles and over the four phases of the oscillating electric field. The laser field exists during the internuclear distance below 30 a.u.; pulse duration is about 7 fs.

4.3 Results

Figure 2 shows the electron capture cross section as a function of the photon energy ω. There are two sharp peaks at ω=0.44 and 3.02. These energies are equal to the excitation energies from the ground state, $O^{5+}(1s^2 2s) + C^{6+}$, to the excited states, $O^{5+}(1s^2 2p) + C^{6+}$ and $O^{5+}(1s^2 3p) + C^{6+}$. To clarify this reason, we checked the time dependence of the transition probabilities at ω=0.44. The transition probabilities for the ground state and the excited states, $O^{5+}(1s^2 2p) + C^{6+}$, oscillate strongly and the oscillation is out of phase. This means that the strong coupling of the laser field between both the states causes this phenomenon, *i.e.*, the formation of the dressed states. The excited states have the close energy levels to the electron-captured states. Therefore the enhancement of the electron capture cross section is brought about by the transition from the excited states to the electron-captured states by the non-adiabatic coupling. The direct transition from the ground state to the electron-captured states is not clearly found at the ω for the resonant condition because of the relatively smaller coupling by the laser field.

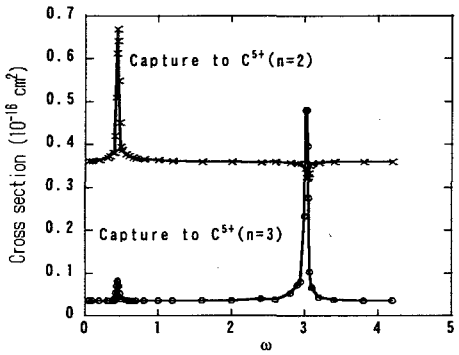

Fig. 2 Electron capture cross sections as a function of the photon energy, ω
The collision energy is 1 keV/amu and the electric field strength is 0.01 a.u. (7.02×10^{12} W/cm^2).

5. Short wavelength x-ray emission generated by high intensity laser irradiation on Xe clusters

5.1 Introduction

Recent progress in intense pulsed lasers allows us some sources of high brightness x-rays[8,9]. fast electrons[10], and multiply charged ions[11] used for the production of inner-shell excited states and hollow atoms.

The interaction of high intensity laser with clusters may yield high density hot plasmas only for sub-pico seconds[12]. For Xe or Kr clusters, there are several measurements of short wavelength x-rays from the inner-shell excited states[13]. The inner-shell excited states are generated by the fast electron impact. The x-rays may become a short-pulse x-ray source because the inner-shell excited states decay around 1fs and are produced only when the high-density hot plasma exists.

We have researched the x-ray spectra emitted from the inner-shell excited states of the highly charged ions in the high density hot plasmas generated by high intensity laser irradiation on Xe clusters. We employ the ground state of Ni-like Xe ions as an initial state and the electron densities (n_e) of 10^{22} to 5×10^{23} cm^{-3} and the electron temperature (T_e) of 1 to 40 keV, respectively. We assume that the plasmas continue for about 100 fs[12]. We consider the electron impact ionization, the autoionization, and the radiative transition processes.

5.2 Results and discussions

Figure 3(a) shows x-ray intensities vs. wavelengths (λ) emitted from the inner-shell excited at T_e=20 keV for various values of n_e. When $n_e < 10^{22}$ cm^{-3}, a great deal of the x-rays are emitted from

the inner-shell excited states of Xe^{27+}. The x-ray intensities from the highly charged ion of Xe^{35+} increase as n_e becomes larger. The x-ray emission from Xe^{35+} is the largest when $n_e \geq 3\times10^{23}$ cm^{-3}, as seen in the x-ray spectra of Ref.[13] though this density is much larger than that estimated in Ref.[12]. The temperature dependence is shown in Fig. 3(b) where $n_e=5\times10^{23}$ cm^{-3}. The shape of the spectra is independent of T_e for $T_e \geq 5$ keV, that is, the x-ray intensity increases as the wavelengths become shorter.

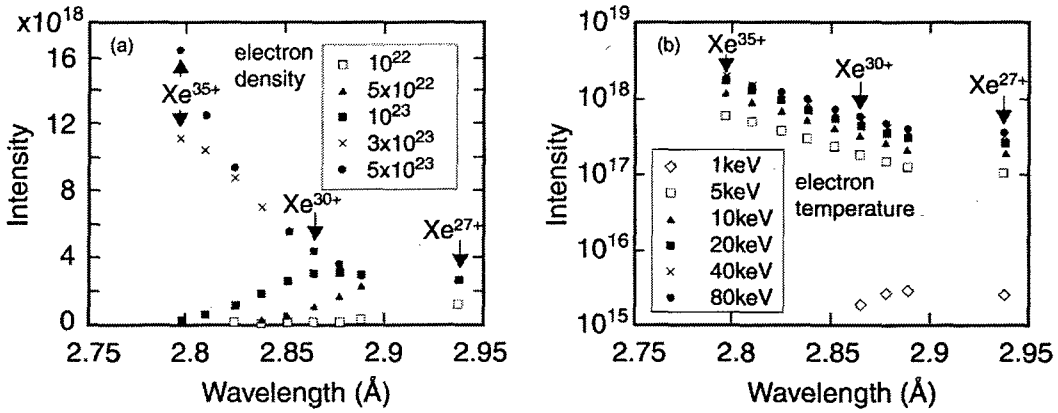

Fig. 3 X-ray intensities vs. averaged wavelengths (Å) emitted from the inner-shell excited states for (a)various electron densities at T_e=20 keV and (b)various electron temperatures at $n_e=5\times10^{23}$ cm^{-3}, respectively

The correspondence between (a) the densities ((b)temperatures) and symbols is shown in the box.

6. Theoretical study of laser control of molecular dynamics processes

A new experimental method of quantum laser control of atoms and molecules has been considered. Instead of classical resonance, in quantum control one can design the laser pulse in such a way to exactly cancel the electronic wavefunction by quantum interference (or exactly add up). This way we can selectively control chemical reactions with short chirped pulses of laser. This idea includes: (i)The selective and complete excitation to 7d states of Cs atoms; the same idea may be applied to isotope separation, (ii)The complete electronic excitation of diatomic molecule of Cs_2 by a linear chirp pulse laser; We confirm that a pulse-laser with the wavelength of 800 nm can be employed. (iii)The control of photo-dissociation of diatomic molecules by using complete reflection; We calculated the photo-dissociation of HI and Cl_2.

References

1) A.Sasaki, T.Utsumi, K.Moribayashi, M.Kado, M.Tanaka, N.Hasegawa, T.Kawachi, H.Daido, J. Quant. Spectrosc. Radiat. Transf. **71**, 665, 2001.
2) M.Klapisch and A.Bar-Shalom, J. Quant. Spectrosc. Radiat. Transf. **58**, 687, 1997.
3) T. Kawachi, *et al.* accepted for publication, Phys. Rev. A.
4) Li-Bo Zhao, T. Shirai, Phys. Rev. A, **64**, 052704, 2001.
5) L.Gulyas, P.D. Fainstein, T. Shirai, Phys.Rev. A, **65**, 052720, 2002.
6) S. Suzuki, N. Shimakura, and M. Kimura, J. Phys. B**29**, 1063, 1996.
7) S. Suzuki *et al*, proceedings of XXII International Conference on Photonic, Electronic and Atomic Collisions, 2001.
8) K.Moribayashi, A.Sasaki, and T.Tajima, Phys.Rev.A, **58**, 2007, 1998.
9) K.Moribayashi, A.Sasaki, and T.Tajima, Phys.Rev.A, **59**, 2732, 1999.
10) K.Moribayashi, A.Sasaki, and A.Zhidkov, Physica Scripta, **T92**, 185, 2001
11) K.Moribayashi, K. Suto, A. Zhidkov, A. Sasaki, and T. Kagawa, Laser and Particle Beams, **19**, 643, 2001.
12) T. Ditmire T. Donnelly, A.M. Rubenchik, R.W. Falcone, and M.D. Perry, Phys.Rev.A, **53**, 3379, 1996.
13) W.A. Schroeder, *et al,* J. Phys.B, **34**, 297, 2001.

4.7 High Power Laser Applications

Hiroyuki DAIDO

Recently, ultra-high intensity short pulse lasers have been applied to the fields of hard x-ray generation and high energy particle generation. The essence of the laser-produced plasma is that a laser can feed its ultra-high energy density into the matter via the ponderomotive heating of electrons. Then the electron energy is transferred into the atoms and ions which include excitation, ionization by collisions and ion acceleration by electro-static potential driven by electron ejection from a plasma. Subsequently, high flux few tens of MeV x-ray can drive nuclear reactions, which open up the new fields of plasma physics and applications. The ultra-high intensity short pulse lasers also contribute to the various fields such as pump probe measurement for ultra-fast phenomena in crystalline materials and coherent control of chemical reactions and so on. In this section, we will introduce the present status of the projects on the high intensity physics applications of the ultra-short high intensity lasers. The basic laser-plasma interaction study with a practical point of view opens up the new attractive fields not only the practical applications but also the new aspects of the basic sciences such as control of high temperature and high density relativistic plasma. The high intensity physics experiments of this project is schematically shown in Fig. 1.

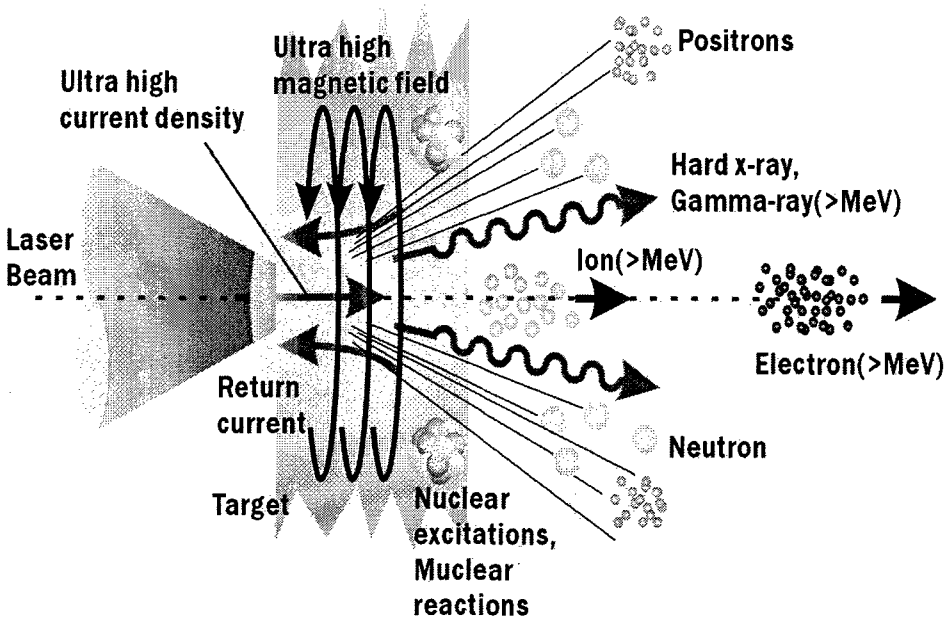

Fig. 1 The high intensity physics experiments of the project

4.7.1 Laser driven high energy ion generation for development of a compact cancer therapy accelerator

Koji MATSUKADO[a)], Hiroyuki DAIDO, Yukio HAYASHI, Satoshi ORIMO, Ken-ichi KINOSHITA[a)], Zhong LI[a)], Kenjiro TAKAHASHI[a)], Alexei ZHIDKOV[a)], Mitsuru UESAKA[b)], Koji YOSHII[b)], Takahiro WATANABE[b)], Tomonao HOSOKAI[b)], Akira NODA[c)], Yoshihisa IWASHITA[c)], Toshiyuki SHIRAI[c)], Shu NAKAMURA[c)], Atsushi YAMAZAKI[c)], Akio MORITA[c)], Atsushi OGATA[d)], Yoshio WADA[d)] and Tetsuo KUBOTA[d)]

a) National Institute of Radiological Sciences
b) Nuclear Engineering Research Laboratory School of Engineering, University of Tokyo
c) Institute for Chemical Research, Kyoto University
d) Graduate School of Advanced Sciences of Matter, Hiroshima University

1. Introduction

We started a project in which a very compact accelerator whose size would be 3m x 10m x 10m for cancer therapy would be developed. It is well known that high-energy ions of about a few MeV per nucleon are emitted from the plasma irradiated by an ultra-intense laser pulse[1) 2)]. To reduce the size of the system, we adopted a laser plasma ion source using a compact ultra-high intensity laser with a few tens of fs pulse duration. We encounter two issues to be solved. One of them is concerned about the pulse duration of the driver laser. A lot of papers have been published on the laser driven ion sources including theoretical interpretations. However the physics of the ion generation by the much shorter pulse width; fs-laser-pulse is not well known. We must investigate and confirm the physics of the interaction between a plasma and the fs-laser-pulse. The other is technical issue. The energy spread of the ions is too broad to be injected into the accelerator. If we can reduce the energy spread keeping the particle number with a proper method, that is a phase rotation method[3)], the laser plasma ion source can be used as an injector system of the heavy ion synchrotron. We have performed ion generation experiments at the University of Tokyo. In the present report, the results of the experiments are shown and discussed.

2. Experimental setup

Figure 1 shows the experimental setup. We used an ultra-high intensity table-top laser system. In the experiment, the wave length and the pulse duration were 800 nm and 50 fs, respectively. Peak power was 4-5 TW. The laser pulse with normal incidence angle to the target was focused onto the target with 15 μm diameter, giving irradiance of 3-4x1018 W/cm^2. We found a pre-pulse. Although we did not precisely characterize the pre-pulse, the time interval between the pre-pulse and the main-pulse was approximately 5 ns, and the intensity ratio was 10^{-5}. Target foils were metals (Ti, Al) and plastics (polypropylene, polyethylene) with the thicknesses of 4-100 μm. We used CR39 track detectors which were made of placed at ~70 mm away from the laser-target interaction-point to observe the angular distribution of ions. Energy of ions was measured with the range filter of 0.8 μm Al foil. During the measurements, the degree of vacuum was kept around 10^{-4} Torr .

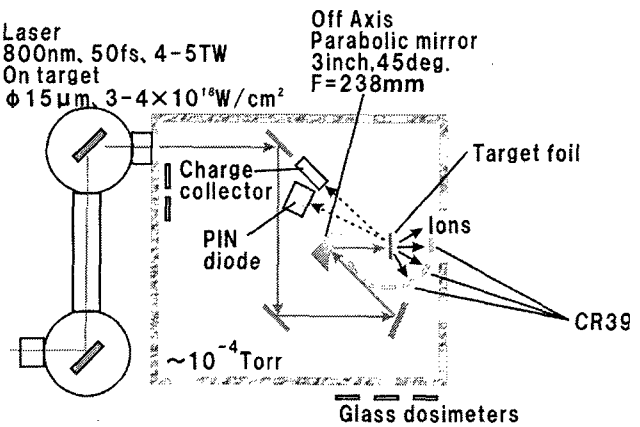

Fig. 1 Experimental setup

3. Results and Discussion

The angular distribution of ion emission is shown in Fig. 2. In the figure, we defined a direction of the laser propagation as 0 degree and represented it as "forward". The targets were Ti and polyethylene with 20 μm and 100 μm thickness, respectively. The Ti ion emission had peaks in both the forward and the backward directions. The peak at backward direction was larger than that of the forward direction. The results of the analysis of trucks with range filters showed that the maximum energy of ions was up to 100 keV if the ions were supposed to be protons.

According to the scaling law which associates with the maximum energy of ion as a function of laser intensity, generation of ions with energy of a few MeV per nucleon is expected[1][2]. Because of the much shorter laser pulse width of 50 fs than a sub-pico-second duration, the acceleration field for ions lasts much shorter. The optimum target thickness for ion acceleration is much more crucial and critical. In this experimental condition, optimistic thickness is 0.1 μm predicted by PIC simulation. We should also point out an effect of the pre-pulse. The intensity of the pre-pulse was about 10^{13} W/cm^2 which is high enough to generate a pre-formed plasma. The main-pulse interacts with the pre-formed plasma after 5 ns expansion. As a result, interaction of the main-pulse with the pre-formed plasma may occur before the focusing position, resulting in reducing the laser intensity on the plasma surface. If the resonance absorption occurs, the ions are mainly emitted backward[4]. While, it was also suggested that the JxB-heating mechanism[5] or not-so-resonance absorption[6] began to be significant, because the peak in the ion emission distribution is clearly visible in the forward direction for the Ti-target. The experimental result suggests that the high energy collimated ions can be generated in the forward direction in the proper experimental condition.

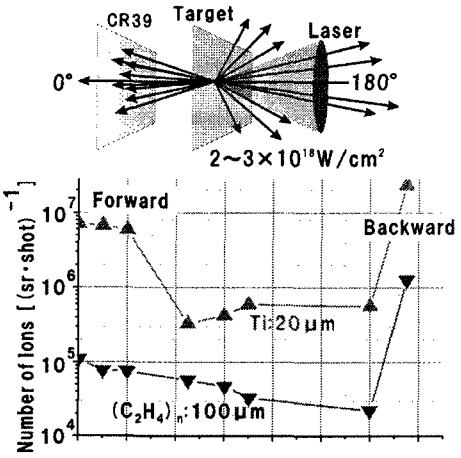

Fig. 2 Angular distribution of ion emission

Acknowledgements

The authors must thank Dr. F. Nishiyama of Hiroshima University, Prof. N. Sakamoto and Dr. J. Karimata of Nara women's University, Dr. S. Nakamura of Kyoto University, Prof. S. Okuda of Osaka Prefecture University for their corporation and useful discussion on the calibration of detectors. We also thank TORAY Industries Inc. for providing us a polypropylene foil as a target. These works ware supported by the fund of Advanced Compact Accelerator Development Project from the Ministry of Education, culture, sports, science and technology of Japan.

References

1) E. L. Clark et.al.,Phys. Rev. Lett. **85**, 1654, 2000.
2) A. Maksimchuk *et al.*, Phys. Rev. Lett. **84**, 4108, 2000
3) A. Noda *et al.*, Beam Science and Technology **6**, 21, 2001
4) J. P. Friedberg *et al.*, Phys. Lett. **28**, 795, 1972
5) W.L. Kruer , Kent Estabrook, Phys. Fluids. **28**, 430, 1985
6) F. Burunel, Phys. Rev. Lett., **59**, 52, 1987

4.7.2 Phase rotation scheme of the ions accelerated by an intense femtosecond laser

Shu NAKAMURA[a)], Yoshihisa IWASHITA[a)], Toshiyuki SHIRAI[a)], Akira NODA[a)],
Koji MATSUKADO[b)] and Hiroyuki DAIDO
a) Nuclear Science Research Facility, Institute for Chemical Research, Kyoto University
b) National Institute of Radiological Science

1.Introduction

Studies on interactions between short-pulse intense laser and solid or dense plasma began to be reported[1-5] recently. Several these reports indicate emission of high energy ions whose kinetic energy reaches some MeV/u[3-5]. While its high energy is a great advantage as an ion source, the number of ions decreases exponentially with its energy[3]. In order to make better use of such high energy ions, we plan to gather ions around an energy about 2 MeV/u and produce a mono-energetic distribution: ions with excessive energy are decelerated and those with less energy are accelerated by RF voltage synchronized with the laser.

2. Phase rotation (Energy compression) Scheme

A phase rotation scheme is investigated for the ion beam that is emitted from foil target irradiated by a high power(~100 TW) short-pulse(~20 fs) laser. By application of an RF electric field synchronized with the laser pulse, the ion beams in the energy range of ±5 % is expected to be compressed into the range within ±1 % of our goal.

The initial time spread of ions is thought to be of the order of the laser pulse duration(~20 fsec). The longitudinal emittance is estimated about 3×10^{-9} eV•sec/u for beams within ±5 % energy spread at a center energy K_0 of 2 MeV/u. This value is also very small compared with that of conventional linac(4×10^{-5} eV•sec/u)[6]. However, the energy spread of ±5 % is too large for a synchrotron. This energy spread can be compressed with the phase rotation scheme. The ion bunch with the energy spread is lengthened during its flight(see Fig. 1). At the distance s_1 from the target, faster ions come earlier than slower ones. Applying decelerating electric field for the earlier arrived ions and accelerating one for the later arrived ions, we can compress the energy spread(see Fig. 2).

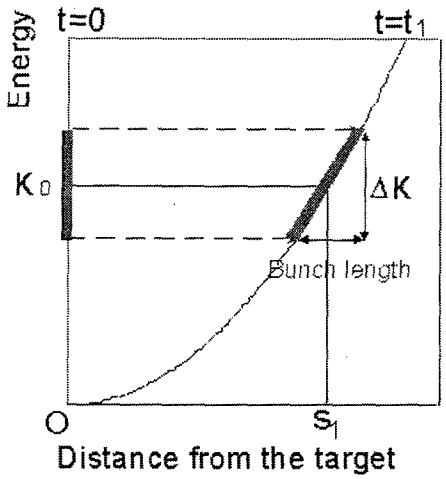

Fig. 1 Ion distribution at t=0 and $t=t_1$ Ions with central energy K_0 arrive at s_1 when $t=t_1$.

For the energy spread of ±5 %, the drift time difference for an ion to reach an acceleration gap is almost proportional to its energy difference from central energy. This scheme requires almost linearly changing voltage, which can be provided by an RF-cavity as a part of a sinusoidal waveform. To make use of the linear part of such sinusoidal wave, we would restrict the width of phase angle less than ±π/4 in order to reduce the ±5 % energy spread within ±1 % considering no space charge effects, where a linearity error ΔV_{error} is given by

$$\Delta V_{error} = \frac{\sin\theta - \theta}{\sin\theta}.$$

The time spread Δt of the ion bunch with full energy spread ΔK at the location s_1 is given by

$$\Delta t = \left(\sqrt{\frac{m_i}{2K_0 - \Delta K}} - \sqrt{\frac{m_i}{2K_0 + \Delta K}} \right) s_1,$$

where m_i is the ion mass. Thus the frequency f of the RF-cavity is given by $f = 1/(4\Delta t)$. The distance between the target and the

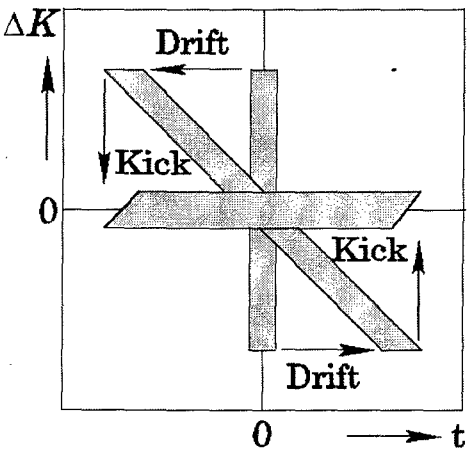

Fig. 2 Phase rotation scheme
ΔK and Δt are differences of energy and time from central values, respectively.

RF-cavity becomes 1.2 m at the frequency f of 80 MHz. The bunch length is 6.1 cm at the cavity location. The required RF-amplitude is 280 kV for C^{6+}. Assuming that the electric field distribution is constant E_0 in the gap and zero elsewhere, the electric field is expressed as

$$E(z,t) = \begin{cases} E_0 \cos(2\pi ft) & -g/2 < z < g/2 \\ 0 & z < -g/2 \text{ or } z > g/2 \end{cases}$$

Then a voltage gain ΔV for an ion at a distance Δz from the bunch center is expressed by

$$\Delta V = V_0 T \sin 2\pi \frac{\Delta z}{\beta\lambda},$$

where V_0 is gap voltage(gE_0) and T is the transit time factor:

$$T = \frac{\beta\lambda}{g\pi} \sin\left(\pi \frac{g}{\beta\lambda}\right),$$

where $c\beta$ is velocity of ion as c is light velocity, λ is wavelength of the RF. Transit Time Factor, T is larger than 0.9 between g = 0 cm and 3 cm(see Fig. 3). A quarter wave resonator is a good candidate for the RF-cavity(see Fig.4). For such a double-gap cavity with gap length of 2 cm, the average electric field gradient in the gap becomes 280 kV / (2 × 2 cm) = 7 MV/m. The maximum surface electric field would be 14 MV/m at the edge of the electrode, which is about 40 % higher than the Kilpatrick criterion[7] of 10.5 MV/m at 80 MHz. In general, it is known that the maximum surface electric field has been achieved up to 1.4 times as large as the Kilpatrick criterion. A preliminary designed cavity with the diameter of 20 cm has shunt impedance of 1.5 MΩ, where 15 kW RF power can generate 150 kV on a gap.

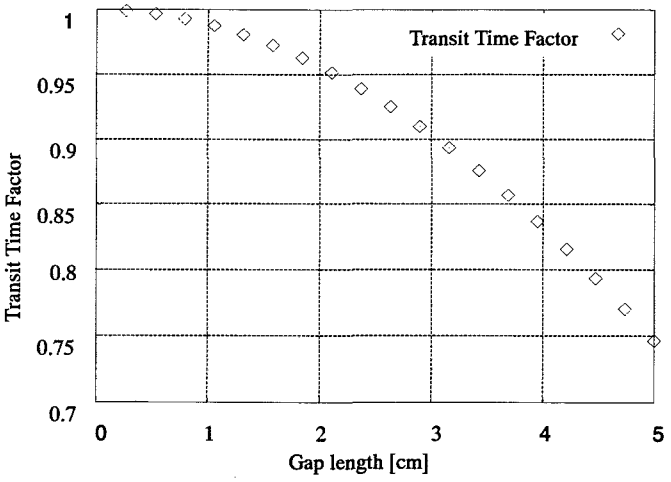

Fig. 3 Transit Time Factor
A central energy of ions K_0 is 2 MeV/u.

3. Conclusion

A scheme of phase rotation of laser produced ion(C^{6+}) beam is proposed. The energy spread of ±5 % around the central value of 2 MeV/u is expected to be reduced to less than ±1 % in order to match the requirement from the next step of electron beam cooling[8]. Although some assumptions are used in the present scheme, they will be experimentally studied in their feasibility from now on.

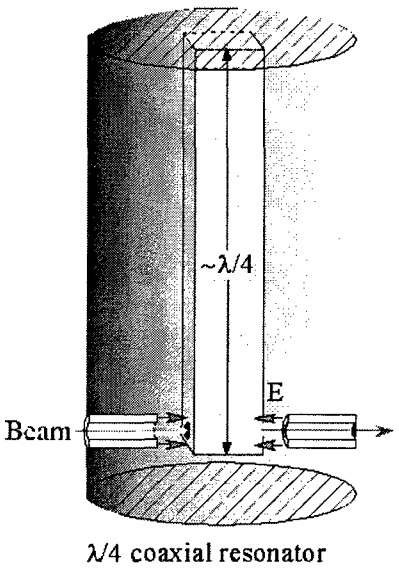

Fig. 4 A quarter wave resonator with double gap

Reference

1) M.Yamagiwa *et al.*, Phys. Rev. E. **60**, 5987, 1999
2) M. Shnürer *et al.*, Phys. Rev. E. **61**, 4394, 2000.
3) E. L. Clark *et al.*, Phys. Rev. Lett. **85**, 1654, 2000
4) K. Krushelnick *et al.*, Phys. Plasmas. **7**, 2055, 2000
5) E. L. Clark *et al.*, Phys.Rev.Lett. **84**, 670, 2000
6) H.Dewa *et al.*, Bull. Inst. Chem. Res. Kyoto Univ. **70**, 89, 1992
7) W.D.Kilpatrick, The Review of Scientific Instruments. 28, 824, 1957
8) H. Fadil et al., JASEM Studies in Applied Electromaginetics and Mechanics. 9, 381, 2001

4.7.3 Calibration of an electron spectrometer for a laser-driven ion source

Zhong LI[a)], Koji MATSUKADO[a)], Kenjiro TAKAHASHI[a)], Yukio HAYASHI[b)], Satoshi ORIMO[b)], Hiroyuki DAIDO[b)], Shu NAKAMURA[c)], Toshiyuki SHIRAI[c)], Yoshihisa IWASHITA[c)] and Akira NODA[c)]

a) National Institute of Radiological Sciences, Chiba, Japan

b) Advanced Photon Research Center, Kansai Research Establishment,Japan Atomic Energy Research Institute, Kyoto, Japan

c) Institute for Chemical Research, Kyoto University, Kyoto, Japan

Electron spectrometer (ESM) is an important instrument to determine the energy spectrum of electrons produced in a laser produce plasma experiment. The kernel of the electron spectrometer we used includes a collimator, a magnetic field induced by a pair of magnets, and an imaging plate (IP). The electrons will be aligned firstly and enter the magnetic field, go along a circle path whose radius depends on the energy according to the Lorentz law, and then be recorded by the IP.

The calibration included the distribution of the magnetic filed strength, parameters determination of the IP and the energy spectrum of the ESM correspondingly. The profile of the magnetic field strength allows to determine the motion of an electron in the ESM. It is the fundamental parameter for making simulation of an electron motion. It was determined with a Gauss meter typed THM7025, a 3-axis Hall Magnetometer produced by Metrolab Instrument SA with an interval of 5 mm around the entrance axis.

The IP used to record the electron is not a real time detector. It cannot be read immediately after exposure because of necessary operations. The luminescence in IP caused by electrons will decay with time after exposure. It should be taken into account for the data analysis. The imaging plates which were exposed by a 362 KBq ^{137}Cs γ source at a distance of 20 cm time were read out at 0.5 to 100 hours after the same time exposure. A calibration curve was obtained for normalizing the read out luminescence.

A 3.04 MBq ^{90}Sr-^{90}Y β source was used to calibrate the ESM. The β source was fixed before the collimator. The electron flux entering into the ESM was 94 electrons per second. The ESM was exposed for 5 hours and 1 hour with magnets marked 1200 Gauss and 70 Gauss separately. The electron signals (the dark regions) images were shown in Fig. 1. The scale at the right side is the energy in keV.

There are two energy-edges in electron energy spectrum of the ^{90}Sr-^{90}Y β source because of its link β decays. They were used to calibrate the energy scale and the energy spectrum of the ESM.

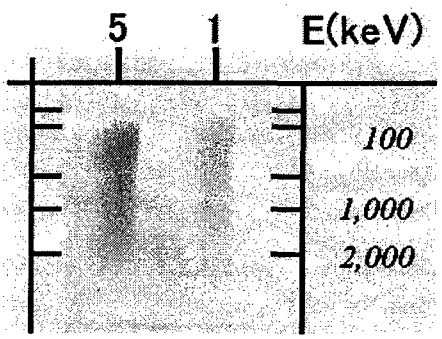

(a) B=1200 Gauss

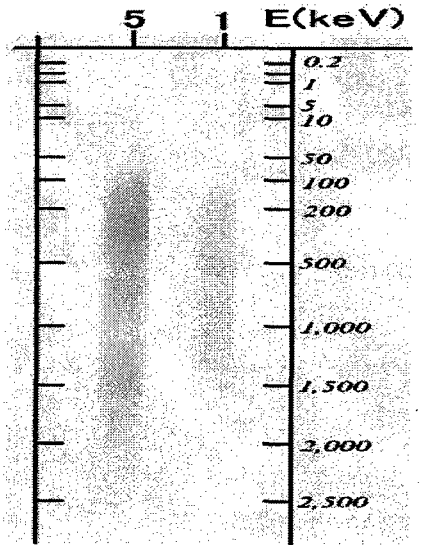

(b) B=70 Gauss

Fig. 1 Electron traces exposed for 5 and 1 hour(s)

Acknowledgement

Kenjiro TAKAHASHI acknowledges good discussion with Prof. K.A.Tanaka of Osaka University during early phase of this development.

4.7.4 Fe spectroscopy; Search the possibility for "Laboratory Astrophysics"

Mamiko NISHIUCHI, Tetsuya KAWACHI, Momoko TANAKA, Kazuhito YASUIKE and Hiroyuki DAIDO

1. Introduction

During the last few years, considerable progresses have been made in simulating astrophysical phenomena on laboratory experiments using lasers. For example, hydrodynamics, hydrodynamical instability, shocks, relativistic plasmas, atomic physics, and x-ray transport of various astronomical object.

We investigated one of the possiblity for contributing to the field "Laboratory Astrophysics" with the JAERI lasers, related to the atomic physics. For the first step, we aimed at one of the unresolved problems of the spectral analyses in the X-ray astronomy; the discrepancy between predictions from the ionization codes in the existing literatures (e.g. [1-3]) and the observed spectra from typical astronomical objects, such as Supernova Remnants (SNRs), Black Hole binary, and so on. The discrepancy is especially prominent in the energy region around 1 keV, where most of the L-shell emission lines from iron (Fe) fall between. Among the various ionization stages of Fe, Fe_{XVII} (neon-like iron) is the dominant ion over the broad temperature range and the L-shell lines from this ionization stage have been observed in many astrophysical objects, such as SNRs, solar coronae, and coronae of binary stars [4]. Fe_{XVII} is particularly a useful diagnostic for measuring density [5,6], temperature [7] and ionic fractional abundances [5]. However, the accuracy of atomic models used to interpret the spectra is hardly perfect, which severely influence on the accuracy of plasma diagnostics.

Many theoretical works on the atomic data have been extensively performed. In order to properly predict the X-ray line emission, many complex and uncertain processes must be involved in the calculation. However, most of the current calculations can practically cover only a fraction of the entire processes and also rely on various approximations and assumptions.

The laboratory measurement is, therefore, required to determine the accurate atomic data. The Electron Beam Ion Trap (EBIT), in particular, has recently provided excellent atomic data as well as ionization and recombination crosssections within the energy region of this interest [8-14]. However, it should be noticeable that the electron density in EBIT, mostly distributes between $10^{10}\sim10^{13}$ cm^{-3}, quite rarefied, where the coronal approximation is valid. On the other hand, the laboratory measurements with the high density plasma conditions have not been extensively done yet, compared from those with the low density plasma conditions, although many astronomical objects provides high density plasma conditions (e.x. around black hole). We, therefore, carried out the spectral measurement of iron with slightly higher density region ($\sim10^{20}$ cm^{-3}) using plasma produced with the CPA glass laser at JAERI.

2. Experimental results

Our final goal for this study is to establish the "useful diagnostic tool" for density measurement at the high density plasma conditions. We should make clear the relation between the plasma density and the line intensities of Fe_{XVII} lines to check which line intensities are sensitive to the density.

2.1 Laser parameters

Double pulses of the CPA glass laser (λ=1053 μm) irradiated the Fe solid target. This laser can irradiate double pulses on the target. Each pulse has a line focus of approximately 6 μm length with 50 μm width. Therefore, the resultant plasma is in the shape of plane-like geometry, meaning that we can assume the two-dimensional flow for the growing plasma. The laser parameters are determined from the hydrodynamical simulation using the HYADES code to satisfy the condition that the major ionic stage of the resultant plasma is Fe_{XVII} and the density of the plasma is less than the critical density for the second harmonic light. We planned to use the second harmonic light for the probe light for interferometry at the next step of this experiment. The suitable laser parameters are as follows; the first (second) pulse duration and energy are 250 ps and 10 J (2.5 ps and 10 J), respectively, which corresponds to the intensity of 4×10^{12} Wcm^{-2} (4×10^{14} Wcm^{-2}). The separation between two pulses is 500 ps.

2.2 Diagnostic tools

We used grating spectrometers (1200 grooves/mm and 2400 grooves/mm) coupled with the soft-X-ray

CCD camera for the spectroscopy. These spectrometers view the plasma from side as is shown in Fig.1. For the 2400 grooves/mm spectrometer, we used a toroidal mirror. Therefore, we can obtain the spatially resolved spectra in the direction of plasma flow. One of the examples of the spatially resolved spectra obtained with 2400 grooves/mm is shown in Fig.2. Each spectrum was integrated over 170μm in the direction of plasma expansion. The spectrum at the bottom is nearest to the target position and that shown at the top is farthest. It clearly shows that the dominant ionization stage changes as the position goes far away from the target; the F-like plasma expands to 700μm scale, while the Ne-like iron plasma expands over 1mm scale. The 1200 grooves/mm spectrometer is used for detecting the X-ray laser from the plasma. Because X-ray laser can be emitted from the plasma which satisfies the conditions for lasing, we can roughly restrict the plasma condition by detecting the lasing line. At the same time, the KAP crystal spectrometer (KAP) coupled with the X-ray CCD camera or X-ray pinhole camera (XPC), by turns, views the plasma from the top side (see Fig.1). As for the XPC, the pinhole used was in the size of 50μm in diameter and the X-ray image was taken with a front illumination type X-ray CCD. We used 0.8μm Al and 10μm Be filters, therefore, the rough energy distribution of the X-ray emission in the direction of the plasma flow is observable. The scale length of the plasma whose electron temperature is around 1keV is ~900μm from the target surface. If we assume that the plasma expands with the sound velocity, the X-ray photons are emitted for about 1ns. The details of spectral analyses are now on the way, including the calibration of the detectors, with the combination of the spatial information from XPC.

3. Summary

In order to show the laser produced plasma to be one of the practical sites for "Laboratory Astrophysics", the first step of the experiments which is related to the long lasting puzzle of X-ray astrophysics was carried out. The objective of the experiment is to figure out the relationship between the line ratios of specific lines and the plasma density. The details of the data analyses are now on the way. As the second step of the experiments, we should carry out the density measurement by the interferometry using the second harmonic light and compare the line ratio of specific lines with that of the plasma density in order to know which lines can be useful diagnostic tools for density measurement.

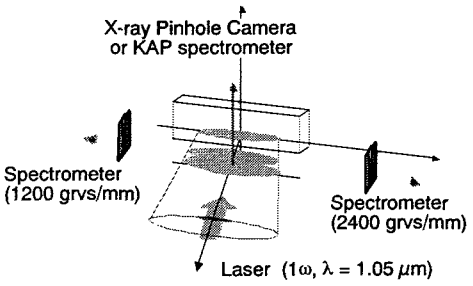

Fig. 1 Schematic figure of the experimental set-up

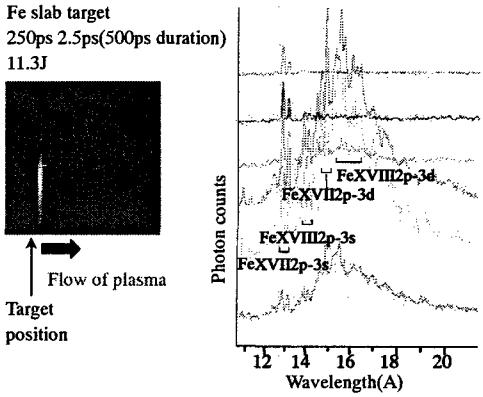

Fig. 2 Example of the spatially resolved spectra as well as the image taken with 2400 grooves/mm spectrometer

References

1) R. Mewe, E.H.B.M. Gronenschild and G.H.J. van den Oord, A&ASS, **62**, 197 (1985).
2) R. Mewe, J.R. Lemen and G.H.J. van den Oord, A&ASS, **65**, 511 (1986).
3) J.S. Kaastra, I. Asaoka, K. Koyama and S. Yamauchi, A&A, **264**, 654 (1992).
4) E. Behar, J. Cottan and S.M. Kahn, ApJ, **548**, 966 (2001).
5) K. Waljeski *et al.*, ApJ, **429**, 909 (1994).
6) K.J.H. Phillips, C.J. Greer, A.K. Bhatia and F.P. Keenan, ApJ, **469**, L57 (1996).
7) J.C. Raymond and B.W. Smith, ApJ, **306**, 762 (1986).
8) K.J. Phillips *et al.*, A&AS, **138**, 381 (1999).
9) G.V. Brown *et al.*, LLNL preprint UCRL-JC-136647 (2000).
10) G.V. Brown *et al.*, AJ, **502**, 1015 (1998).
11) M. Cornille *et al.*, A&AS, **105**, 77 (1994).
12) A.K. Bhatia and G.A. Doschek, At Data Nucl. Data Tables, **52**, 1 (1992).
13) P.L. Hagelstein and R.K. Jung, At Data Nucl. Data Tables, **37**, 121 (1987).
14) M. Loulergue and H. Nussbaumer, A&A, 24, 209 (1975).

4.7.5 Estimation of the radiation doses from ultra-high intensity laser-produced plasmas

Yukio HAYASHI, Shuji KONDO, Syuhei KANAZAWA and Hiroyuki DAIDO

1. Introduction

An ultra short-pulse high power laser (greater than 1TW) can produce large flux of MeV particles [1)-3)] (gamma ray photons, x-ray photons, neutrons, and ions). These particles are generated as follows. The laser-produced plasmas are generated by the interaction of the laser and the target. Then the electrons in the plasmas are accelerated by ponderomotive force, and the ambipolar field, which is caused by ejected electrons, accelerates the ions. Finally x-ray photons and neutrons are emitted via accelerated particles collisions.

No high-energy particle accelerators are required to make the radiation from the laser-produced plasmas. The mechanism of laser-produced radiation is similar to that of conventional high-energy radiation sources. However, because extremely high photon flux is converted into electrons, very high brightness radiation source cause produced at the laser-plasmas interaction region.

It is necessary to estimate the radiation doses from laser-produced plasmas because of the radiation safety. But the information of radiation from the laser-produced plasmas in the open literatures is quite poor at present as far as the authors know. We have calculated the radiation doses of the laser-produced plasmas for this reason.

2. Estimation method

2.1 The condition for generating the laser-produced plasmas

As the radiation doses increase with the laser power, we have chosen the maximum power laser [4)] from ultra-short high power laser for the maximum dose estimation.

The parameters of the radiation dose estimation are shown in Table 1.

Table 1

Laser power *Ib*	0.2J/shot
Width of laser pulse *Ir*	20fs
Repetition Rate *f*	1Hz
Laser wavelength ë	800nm
Laser intensity *I*	10^{20}W/cm^2
Operation time for a week	40hours
Target	Thick Pb target

2.2 The calculation of the radiation doses rate

The high-energy electron distribution from the laser-produced plasmas is described as a relativistic Maxwell-Boltzmann distribution function,

$$\frac{dN(E)}{dE} = E^2 \times \frac{\exp(-E/T_{hot})}{T_{hot}^3} \times \frac{Ib \times f \times K}{3T_{hot}}, \qquad (1)$$

where $N(E)$ is the energy distribution of electrons per second, E is the electron energy [MeV], K is the conversion efficiently from laser energy into electron energy, and T_{hot} is the hot electron temperature [MeV].

The parameter T_{hot} and the parameter K depend on $I\ddot{e}^2$ (W ì m^2/cm^2). When $I\ddot{e}^2$ exceeds 10^{18}(W ì m^2/cm^2), T_{hot} can be written as the next form[1), 2)],

$$T_{hot} = 0.511 \times \left(-1 + \sqrt{1 + \frac{I\lambda^2}{1.37 \times 10^{18}}} \right) . \quad (MeV) \qquad (2)$$

According to the measurements reported by S.P.Hatchett [5)], the parameter K is taken to 0.5.

The severe conditions are imposed to avoid the underestimation of the radiation doses. One is that all of the high-energy electrons are radiated to the normal direction of the target surface. Another is that the divergence of the high-energy electrons is neglected.

The Pb target is thick enough to stop the high-energy electrons, which are accelerated by ponderomotive force. The high-energy electrons are converted to the bremsstrahlung x-ray photons, and the neutrons are

generated by photonuclear reaction. The method to estimate radiation dose from the electron accelerator with a beam dump can apply to the radiation doses estimation for laser-produced plasmas, because this generation mechanism are exactly same as the case of the electron accelerator with the beam dump.

I have used the following formulae [6)-8)], which are often used in the doses estimation of the electron accelerator,

$$Hx = 1.443\times 3\times 10^{2}\times E\times\frac{P}{10^{3}}\times\frac{10^{-\Sigma(d/\tau)}}{r^{2}} \quad , \qquad (at \quad \theta = 0\,\mathrm{deg})$$

$$= 1.443\times 50\times\frac{P}{10^{3}}\times\frac{10^{-\Sigma(d/\tau)}}{r^{2}} \quad , \qquad (at \quad \theta = 90\,\mathrm{deg}) \qquad (3)$$

$$Hn = 282\times 3600\times 0.3\times E\times J\times 10^{-16}\times\frac{10^{-\Sigma(d/\varpi)}}{4\pi r^{2}} \quad . \qquad (isotopic) \qquad (4)$$

Here, Hx (H_n) is the dose rate of x-ray photons (neutrons) [Sv/h], P is the total energy of the electrons [W], $\hat{o}$ ($\hat{o}_n$) is the shielding material for x-ray photons (neutrons) [m] to 1/10 of the incident flux, J is the number of high-energy electrons generated per hour [s^{-1}], $\grave{e}$ is the angle between the target normal and the estimated electron, r is the distance from the source point [m], d is the thickness of the shielding material [m].

Moreover, I have calculated the radiation doses of the streaming component and the skyshine component [8), 9), 10)]. The calculation has been performed by use of the well-known formulae to estimate radiation doses of these components.

3. Results

Taking into account the shielding material (concrete wall, lead block, etc.) and the geometry of a laboratory, maximum value of the radiation doses rate is 0.308 (μSv/h), which is much smaller than the value authorized by ICRP.

We will systematically organize the experiments on radiation doses characterization from ultra-high intensity laser produced plasmas for safety and various applications.

Acknowledgements

The authors wish to thank Mr. Manabe and Mr. Ueno of JAERI for their encouragement and supports.

Reference

1) G. Malka et al. "Experimental Confirmation of Ponderomotive-force Electrons Produced by an Ultrarelativistic Laser Pulse on Solid Target," Physical Review Letters **77**, pp.75, 1996
2) Yuji Oishi et al. "Production of relativistic electrons by irradiation of 43-fs-laser pulses on copper film, " Applied Physics Letters **79**, pp.1234, 2001
3) E. L. Clark et al. "Energetic Heavy–Ion and Proton Generation from Ultraintense Laser-Plasma Interactions with Solids," Physical Review Letters **85**, pp.1654, 2000
4) Koichi Yamakawa et al. "Ultrafast, Ultra-high-Peak power Ti: Sapphire laser system," Jaeri-Research 2001-051, 2001
5) S.P.Hatchett at al. "Electron, photon, and ion beams from the relativistic interaction of Petawatt laser pulses with Solid targets, " Physics of Plasmas **7**, pp.2076, 2000
6) W.P.Swanson, Radiological Safety Aspects of the Operation of Electron Accelerators, IAEA Technical Reports Series No.188, 1979
7) Shoji Nakamura, "The radiation shielding design of high-energy Accelerator facility," Genshiryokukougyo 33,pp.27, 1978 (in Japanese)
8) Shuji Kondo et al. "Dose estimation of photocathode microtron," Jaeri-Review 2001-046, pp.42, 2001
9) K. Tesch et al.: "Attenuation of the Photon Dose in Labyrinths and Ducts at Accelerators", Radiation Protection Dosimetry, 20, 169, 1987
10) K. Tesch: Particle Accelerator, 12, p.169, 1982

4.7.6 X-ray generation from a laser produced double nozzle gas-puff plasma

Masayuki SUZUKI[a)], Rafal ROKOWSKI[b)], Andrj BARTNIK[b)],
Henrky FIEDOROWICZ[b)], Kunioki MIMA[a)] and Hiroyuki DAIDO
a) Institute of Laser Enegnieering Osaka University
b) Institute of Optoelectronics, Warsaw, Pland

1. Introduction

There have been many studied on the interaction of laser pulses with solid and gaseous targets for many years. Especially, x-ray generation from a laser produced plasma using solid and gaseous targets irradiated by a laser pulse has been reported in many areas of science, technology, and physics[1)]. The gas-puff target can avoid debris productions. Recently, strong x-ray emissions between 5-20 nm wavelength region have been reported by using a double nozzle gas-puff target irradiated by a laser pulse[2)]. In order to obtain the strong x-ray emission in keV region, we have measured the x-ray spectra from double nozzle gas-puff target irradiated by a laser pulse. Using Argon gas, we could obtain strong x-ray emission in the wavelength range of 0.3-0.4 nm.

2. Experimental setup

An Nd: glass laser that delivered laser energy of 5 J in 1 ns at 1053 nm was used. The laser beam was focused with a plano-convex lens with a 100 mm focal length, giving the total intensity of about 10^{13}W/cm^2. A double nozzle consists of two combined solenoid valve[3)]. Figure 1 shows the schematic view of the double nozzle gas-puff target. The detail was described in Ref 2 and 3. The laser irradiated the double nozzle gas-puff target perpendicularly with respect to the flow of the gas. The focused position was about 1 mm from the nozzle exit. The valve was backed with a gas having a pressure of 10 atm. We have used Argon as a target gas, and Helium as a guide gas. The x-ray spectra were observed by using an ADP crystal with a one dimensional CCD camera.

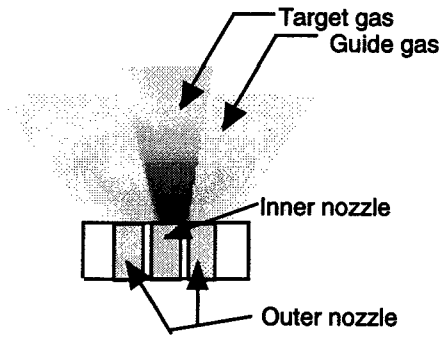

Fig. 1 Schematic of the double nozzle gas-puff target. The inner nozzle was surroung by outer nozzle.

3.Experimental results

Figure 2 shows the x-ray spectra from the double nozzle Argon gas-puff plasma. Using the double nozzle gas-puff target, x-ray emission from He-α, He-β, and Li-like lines are observed around the 0.4 nm wavelength region. On the other hands, we could not observe the x-ray spectra without Helium gas[4)]. This is considered that the gas density is too low to couple efficiently between a laser pulse and a plasma. Using the double nozzle, the gas density was about 10^{20}cm^{-3}. Futher intepretation of the experimental results is now going on.

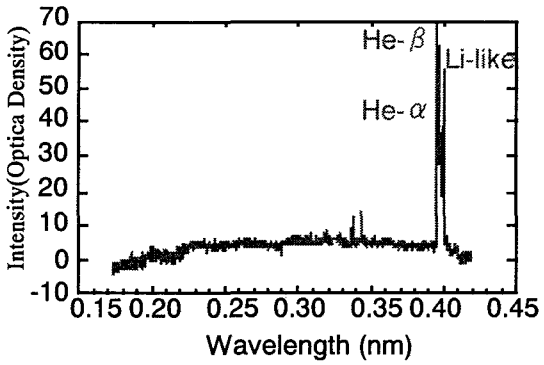

Fig. 2 The x-ray spectra from the double nozzle Argon gas-puff target irradiated by Nd: glass laser

Reference

1) M. Suzuki et al., *2nd International Conference on Inertial Fusion Science an Application (IFSA 2001) Kyoto Internatonal Conference Hall, Kyoto, Japan, Sep. 9-14, 2001,* 1252, and references therein.
2) H. Fiedorowicz et al., Opt. Commum. **184**, 161, 2000.
3) H. Fiedorowicz et al., Appl. Phys. B**70**, 305, 2000.
4) H. Fiedorowicz et al., Opt. Commum. **163**, 103, 1999.

4.7.7 The electrical probe measurement of the late stage of the plasma produced by laser irradiation in an argon gas-puff target

Koichi OGURA

1. Introduction

When a high-power pulsed laser is focused on to a target, a plasma is generated. It is interesting as a source of extreme ultraviolet radiation, X-rays and ions, because the plasma emits photons in a broad spectrum from visible rays to X-rays and includes high density ions. The laser plasma X-ray sources are an almost ideal X-ray probe for the study of time-dependent processes and an X-ray source for lithography. The high density ions can be used for ion etching or atomic physics experiments. Generally, such a plasma is produced by high-power laser irradiation of a solid target. When the solid target is irradiated, the debris is generated. The debris causes the degradation of the reflectivity of the X-ray optical elements and the reduction of the efficiency of focusing optics. Therefore it is necessary to develop a target which will not generate any debris. In order to develop a gas puff target without debris as a X-ray source or an ion source, we should characterize the plasma especially for the temperature, the density, the atomic process, and the plasma expansion.

Here, the electron temperature as a characteristics of the late stage of the expanding plasma, generated by focusing the laser beam into a gas target, is measured with a Langmuir probe to characterize the plasma expansion.

2. Experimental

The gas puff target was made by gas expanding through a nozzle, which was installed in a vacuum chamber. The throat of the nozzle was 800 μm in diameter, and the jet expansion half-angle was 45°. Gas flow through the nozzle was initiated by a fast solenoid valve. The backing pressure of the valve was 2 MPa. The pressure in the vacuum chamber was maintained at 10^{-3} Pa before opening the valve. The laser plasma was produced by focusing the laser beam (λ=532 nm) produced with an Nd:YAG laser system. The laser beam irradiated the gas jet transversely with respect to the flow of the gas and the laser focus was placed 1.0 mm above the nozzle tip causing plasma. The laser pulse energy was 460 mJ. The electron temperature of expanding plasma was measured by the Langmuir probe which was installed at distance of 100 mm from the nozzle tip. The probe was made of tungsten wire with a diameter of 0.7 mm and a length of 3 mm. The potential was applied to the probe externally.

3. Results

Figure 1 shows the typical electron current vs. voltage characteristics at 80μs after laser irradiation. The electron temperature is obtained to be 0.4 eV from Fig.1. It was found that the electron temperature of the gas puff plasma at the late stage (40 ~ 160 μs after laser irradiation) was 0. 1~1.0 eV. The electron temperature decreased by the plasma expansion in the gas-target. These data are used to give an analysis of the laser plasma behavior that includes the plasma-expansion in the gas-target.

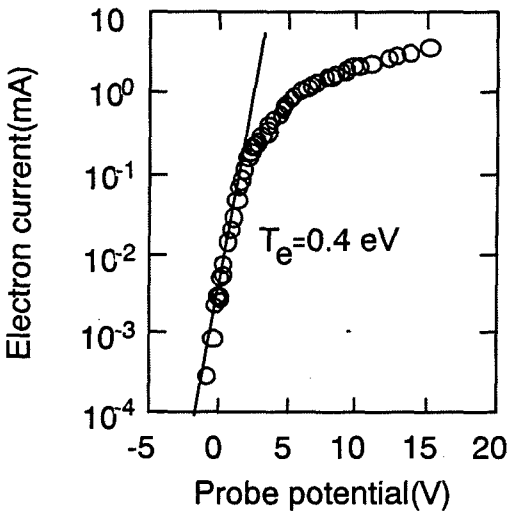

Fig. 1 The electron current voltage characteristics curve at the backing pressure of 2 MPa and 80 μs after laser irradiation

4.7.8 X-ray contact microscopy using Laser-Produced Plasma X-rays

Etsuya YANASE, Masayuki SUZUKI, Takatsugu OKETA, Hiroyuki DAIDO
Yasuhito KINJO[a)], Eiji SATO[b)], Sadao FUJII[b)], Takeyoshi NAKAYAMA[c)]
a) Tokyo Metropolitan Industrial Technology Research Institute
b) Kawasaki Heavy Industries, Ltd.
c) University of Kinki

1. Introduction

Soft X-ray microscope has been expected to be a useful analytical tool to study biological specimens in a natural state. Several approaches to realize a high-resolution soft X-ray microscope have been demonstrated. One of the most popular methods is to use a zone plate objective coupled with a synchrotron radiation source[1)]. Although synchrotron radiation sources are powerful, it is not so convenient for a biologist because the machine time is severely limited. Another approach to obtain a high-resolution soft X-ray microscope on a laboratory scale compact plasma sources. A relatively small pulsed laser produces a bright soft X-ray source. This X-ray source has not only high enough brightness but also has short enough for observation of living biological specimens in the water. The combination of a laser-produced plasma X-ray source and contact microscopy technique has realized a compact soft X-ray microscope on a laboratory scale. As was expected, X-ray microscopy makes it possible to observe various biological specimens without thin sectioning or staining with a better resolution than that of optical microscopy. One of the most interesting biological materials for observation by an X-ray microscope is the chromosome of higher organisms because of their characteristic hierarchical structures with sizes ranging from the nanometer to the microns. We present here the system of compact soft X-ray microscopy with a laser-produced plasma and show X-ray images of chromosome obtained with only one shot using a 0.5J/8ns Q-switched Nd: YAG laser.

2. Experimental

Unstained human chromosomes with no fixative in either a dry or hydrated state were duplicated by X-ray contact microscopy with laser-produced plasma X-rays and recorded on a PMMA photoresist (polymethylmethacrylate; PMMA) which were observed by an atomic force microscope (AFM). Chromosomes from a human lymphocyte cell line (RPMI1788) were prepared by the surface spreading technique[2) 3)]. A photoresist with either dry or hydrated chromosomes from human lymphocytes were exposed by X-rays from a plasma created by focusing a laser beam on a gold foil target using a compact Nd: YAG laser system. The schematic view is shown in Fig. 1. An environmental specimen chamber which consisted of two silicon wafers having 0.1 μm thick Si_3N_4 windows was used to observe hydrated specimens. The parameters used for the exposure are shown in Table 1. The exposed resist was developed with the mixture of methylisobutylketone and isopropanol after removing all cell-derived materials including chromosomes with 0.5% sodium hypochlorite solution. An X-ray image on the resist after development was observed by an AFM (SPI 3700, SEIKO Instruments Inc. Chiba, Japan) in a cyclic contact mode (tapping mode) using a cantilever with the spring constant of 20N/m.

Table 1 Parameters for X-ray exposure

Laser wavelength	1.06 μm
Laser energy	0.5 - 0.7 J
Diameter of focused laser beam	100 μm
Specimen-target distance	9 - 10 mm
Estimated photon flux[4)]	1.2 - 30x10^{11} photons/cm^2/shot

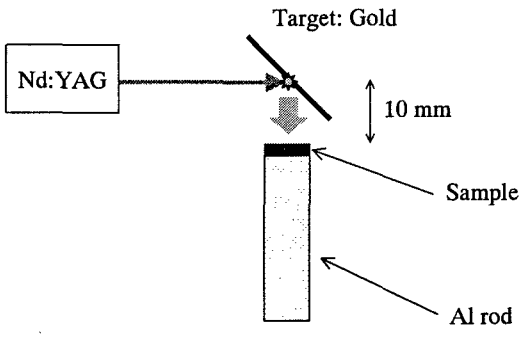

Fig.1 Schematic view of X-ray exposure

3. Results

Figure 2(a) shows a typical image of mitotic chromosomes in a dry state. The region indicated by the arrow was magnified and is shown in Fig. 2(b), in which tightly packed chromatin fiber appears knobby. Figure 3

shows X-ray image of a hydrated specimen. In Fig. 3(b), a magnified view of the part of the chromosome indicated by the arrow in (a) is shown. Clear images of mitotic chromosomes and their hierarchical fine structure, including chromatin fibers and also beads with diameters ranging from ca. 30 to 100 nm, were obtained. These data were compared to the previous data[5) 6)], which were obtained by the "replica method"[7)] in combination with transmission electron microscopy (TEM). The data clearly show that X-ray contact microscopy has the capability of revealing the fine structure of biological specimens in a hydrated state with a resolution at least 10 times higher than that of optical microscopy.

X-ray images of chromosomes as biological specimens were clearly observed with a resolution down to 50nm by only one shot X-ray exposure, which were produced by a commercial table top Nd: YAG laser. We plan to use an electronic imaging devise instead of a PMMA photoresist in future for microscopy. The electronic imaging devise makes it possible to realize almost real time observation. The eventual goal of this work is to produce a relatively low-cost commercial laboratory instrument for general purposes in the fields of biology and medicine.

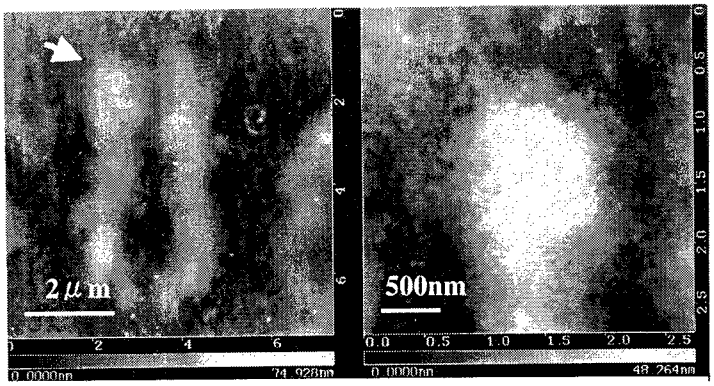

(a) (b)

Fig. 2 (a) Multiple mitotic chromosomes in a dry state, and (b) a magnified view of the part of the chromosome indicated by the arrow in (a)

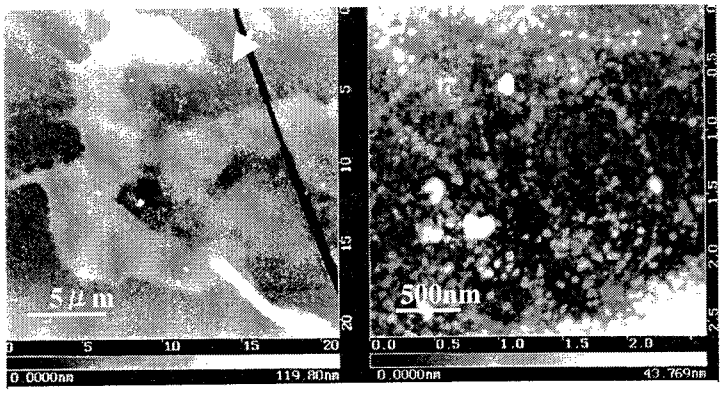

(a) (b)

Fig. 3 (a) Multiple hydrated chromosomes
(b) a magnified view of the area indicated by the arrow in (a)

References

1) C. Jacobsen *et al.*, Opt. Commun. **86**, 351, 1991
2) J. Gall, Science, **139**,120, 1963
3) Y. Kinjo *et al.*, Cytologia, **61**,327, 1996
4) G.M.Zeng *et al.* J. Appl. Phys., **72**, 3355, 1992
5) K. Shinohara *et al.*, Proc. SPIE, **1741**, 386, 1992
6) Y. Kinjo *et al.*, J. Microsc., **176**, 63, 1994
7) A. Tanaka, Seikagaku (in Japanese), **55**, 1212, 1983

4.7.9 Qualitative and quantitative analysis of hormarably active agent for the study on the chemical reactions using soft x-rays

Yuichi SHIMIZU

1. Introduction

In our research center, an active development of x-ray laser which mainly emits lights of soft x-ray regions is being carried out. Soft x-ray is expected to be utilized in many applications through the observation of the interaction between the ray with materials. One particularly exciting application of soft x-ray on the chemistry field, especially chemical reaction, is the environmental science. For this purpose, we had manufactured the experimental apparatus previously[1]. In this report, detailed descriptions are given about qualitative and quantitative analysis of hormarably active agent. A brief discussion of a study on the chemical reactions using soft x-rays is also given.

2. Experimental

Phenol compound was selected as a model material of hormarably active agent for the study on the chemical reactions using soft x-ray. That of guaranteed reagent grade used in this study was obtained from Tokyo Kasei. The analysis of phenol was carried out with both high-performance liquid chromatography (HPLC) and ultraviolet spectrophotometer (UV). HPLC analysis was performed using a Shimadzu LC-6A instrument [column: HYPERSIL ODS-5, column size: 4.6 × 250 mm, mobile phase: $H_2O/MeOH/CH_3COOH$ (65/33/2)[2], flow rate: 0.5 ml min^{-1}, column temp.: 30℃, detector: UV 280 nm]. UV spectra were recorded on a Shimadzu UV-3101 spectrophotometer.

3. Results

Figure 1 shows a typical HPLC chromatogram of phenol compound. As shown, the sharp peak was detected at elution time of ca. 25.7 min. Similar peaks were also observed in various concentrations of phenol, showing an excellent linear relationship between the peak areas and the concentrations. Thus, it was clearly demonstrated that the phenol is satisfactorily separated with this method.

Figure 2 shows a typical UV spectrum. As shown, this compound exhibits its absorption maxima at 313 nm[3]. Also, a result similar to HPLC analyses was obtained concerning the relation between the absorbances and the concentrations.

From these results, it was evidently proved that this phenol compound can be analyzed with HPLC and UV methods in both qualitative and quantitative determinations under these analytical conditions. One application on the environmental science such as the conversion into nontoxic material of hormarably active agent, for example, phenol compound is currently under way.

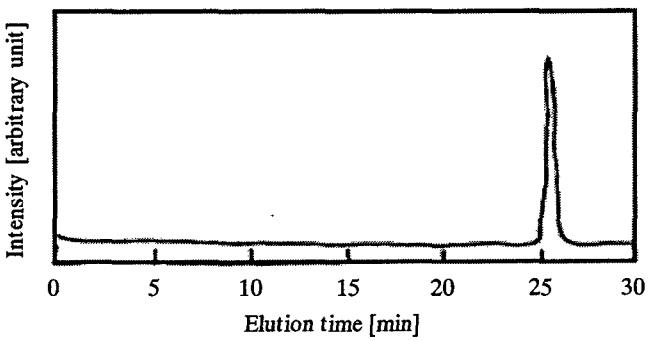

Fig. 1 HPLC chromatogram (1.25×10^{-4} % aq.)

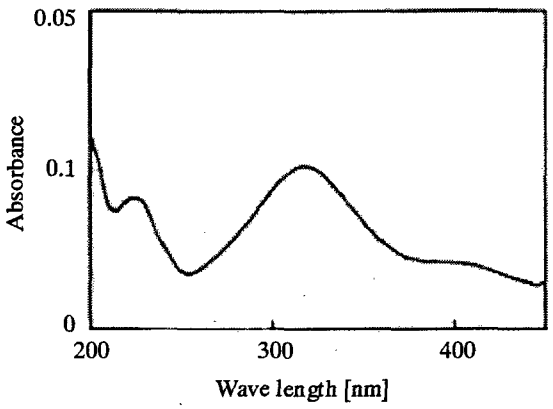

Fig. 2 UV spectrum (6.25×10^{-5} % aq.)

References

1) Y. Shimizu, JAERI-Review **2001-046**, 63 (2002).
2) M. A. Otuban et al., Environ. Sci. Technol., **34**, 3474 (2000).
3) D. S. Baldwin et al., Environ. Sci. Technol., **35**, 713 (2001).

4.7.10 Direct Ab Initio Molecular Dynamics Study of Photodissociation of Acetaldehyde

Yuzuru KUROSAKI and Keiichi YOKOYAMA

1. Introduction

A lot of experimental and theoretical work has been done for photodissociation of acetaldehyde, since this has been considered a key molecule in understanding the photochemistry of larger carbonyl compounds. It was observed that at a low vibrational level acetaldehyde in the S_1 state mainly decays to a highly vibrationally excited level of S_0 via internal conversion (IC) between S_0 and S_1. For excitation wavelengths shorter than 317 nm, however, the dissociation channel to the CH_3 + HCO radicals via intersystem crossing (ISC) between S_1 and T_1 opens; this radical channel has been shown the major dissociation process of acetaldehyde photolysis in the UV region. A number of laser induced fluorescence (LIF) studies have strongly supported this radical decay channel; the fluorescence was found to disappear for excitation wavelengths shorter than 317 nm, indicating the opening of the radical channel through ISC.

At a sufficiently high energy the rates of IC and ISC become comparable because of the increase in density of states. Recently, Gherman et al.,[1] using the vacuum UV LIF method, have examined the molecular CH_4 + CO channel of acetaldehyde photodissociation at a wavelength of 248 nm. They have measured the vibrational and rotational state distributions of the product CO molecule; as a result, the CO was found to be highly rotationally excited, but no vibrationally excited CO was detected. They have also carried out ab initio calculations at the density functional theory level for the CH_3CHO CH_4 + CO reaction on the S_0 surface. It was predicted that the reaction is exoergic by 1.7 kcal mol^{-1} and the barrier height is 81.1 kcal mol^{-1}. The vector of the imaginary vibrational mode for the transition state (TS) strongly suggested that the rotationally hot and vibrationally cold CO is produced, which is consistent with their experimental observation.

In the present work we theoretically investigate the CH_4 + CO channel of acetaldehyde photodissociation using the ab initio direct molecular dynamics method.

2. Methods of calculation

Trajectories were started at the TS in the direction of the imaginary vibrational mode with the kinetic energy of 34.2 kcal mol^{-1}. This energy corresponds to the difference between the photolysis energy 248 nm[1] and the theoretical barrier height 81.1 kcal mol^{-1} that has most recently been calculated at the B3LYP/cc-pVTZ(-f) level.[1] Zero-point energies (ZPEs) were added to the remaining vibrational modes, the initial phases of which were selected randomly. The rotational temperature was set to 0 K. A total of 100 trajectories were integrated with the step size of 0.25 $amu^{1/2}$ bohr using the analytical Hessian at the RMP2(full)/cc-pVDZ level of theory. For each trajectory integration of 180 steps were done when the distance between the products CH_4 and CO was ~6 Å. The total energy was conserved to 10^{-5} hartree. The average time for the trajectories was ~80 fs. The trajectory calculations were carried out using the code implemented in the GAUSSIAN 98 program package.

3. Results and discussion

Figure 1 shows the distribution of the relative translational energy of the products CH_4 and CO for the calculated 100 trajectories. The population of the relative translational energy is seen to be the largest around 35 - 40 kcal mol^{-1} and its average is 36.9 kcal mol^{-1}. At the starting point of the trajectories, kinetic energy of ~35 kcal mol^{-1} was added to the reaction coordinate. Since the reverse barrier height with the ZPE correction was calculated to be ~95 kcal mol^{-1} at the RMP2(full)/cc-pVDZ level (see Table 3), the available energy for the total system at the exit region is ~130 kcal mol^{-1}. In short, one can state that 28 % of the available energy transfers to the relative translational energy and the rest to the internal energies of CH_4 and CO. Figure 2 displays the distribution of the product internal energy: (a) CO and (b) CH_4. The CO internal energy exhibits a sharp distribution and the population is the largest around 25 - 30 kcal mol^{-1}, while the CH_4 internal energy has a wide distribution and the population is large in the region 85 - 110 kcal mol^{-1}. The averages of the CO and CH_4 internal energies are 28.8 and 94.4 kcal mol^{-1}. Subtracting the ZPEs of CO and CH_4, one obtains the average energies to be 25.8 and 65.8 kcal mol^{-1}, which are 20 and 51 % of the available energy. The reason why CH_4 has larger internal energy and broader energy distribution than CO is that CH_4 has larger degrees of freedom and the vector of the reaction coordinate at the TS will cause a highly excited vibrational motion of a CH bond of the CH_4 product.

The distributions of the CO rotational and vibrational quantum numbers are shown in Figures 3a and 3b,

respectively. In obtaining the quantum numbers we assumed that the coupling between rotation and vibration is negligible. As expected from the vector of the imaginary mode at the TS and the analysis of the sample trajectory, the CO product is highly rotationally hot and vibrationally cold. The distribution of the CO rotational quantum number is seen to be the largest around 70 – 75 and its average is 68.2. It has been predicted that 85 % of the CO vibrational quantum number is 0. These computational results qualitatively agree with the observation of Gherman et al.[1] that no vibrationally excited CO was detected and the rotational temperature was 1300 ± 90 K. In the present work we have predicted that 15 % of the product CO is in the first vibrationally excited state and found that the rotational temperature could not be determined. This is probably because the chosen initial condition is somewhat artificial; the excess energy at the TS was given only to the reaction coordinate. Other reasons may be that the trajectories were run in a very short time, i.e., ~80 fs, and that the total number of the trajectories was not sufficient, i.e., 100.

It is of interest to compare with the computational results for the H_2CO H_2 + CO reaction obtained by other groups. The calculated product state distributions for this reaction and the CH_3CHO CH_4 + CO reaction are qualitatively quite similar. It was predicted that the product CO for the H_2CO photodissociation is vibrationally cold and rotationally hot; the average of the vibrational quantum number is ~0.1 and that of rotational quantum number is ~45. On the other hand the product H_2 was calculated to be vibrationally hot and rotationally cold; the average of the vibrational quantum number is ~1.2 and that of rotational quantum number is only ~3. These data are comparable with experiment. The H_2 vibrational excitation corresponds to the CH vibrational excitation in the product CH_4 in the CH_3CHO photodissociation. It seems that the calculated average CO rotational quantum number, 68.2, for the CH_3CHO photodissociation is about one and half times larger than that for H_2CO. Note that in the present calculations kinetic energy of ~35 kcal mol^{-1} was added to the reaction coordinate and the total available energy is ~130 kcal mol^{-1}, while in the H_2CO calculations kinetic energy of 5 kcal mol^{-1} was added to the reaction coordinate, thus the available energy being about 100 kcal mol^{-1}. It is obvious that the average CO rotational quantum number strongly depends on the total available energy. Assuming that the percentage of energy partitioning does not sensitively depend on the total available energy, we will predict the average CO rotational quantum number to be ~60 if we add kinetic energy of 5 kcal mol^{-1} instead of 35 kcal mol^{-1} to the reaction coordinate at the TS in the trajectory calculations. This means that the rotational state of the product CO from the CH_3CHO is more highly excited than that of the CO from the H_2CO photodissociation.

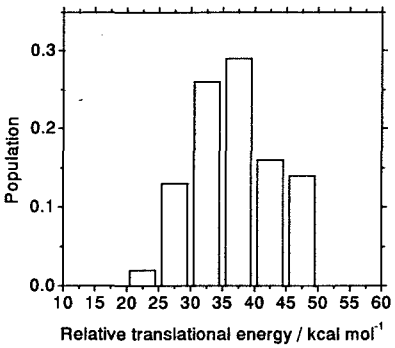

Fig. 1 Relative translational energy distribution of the products

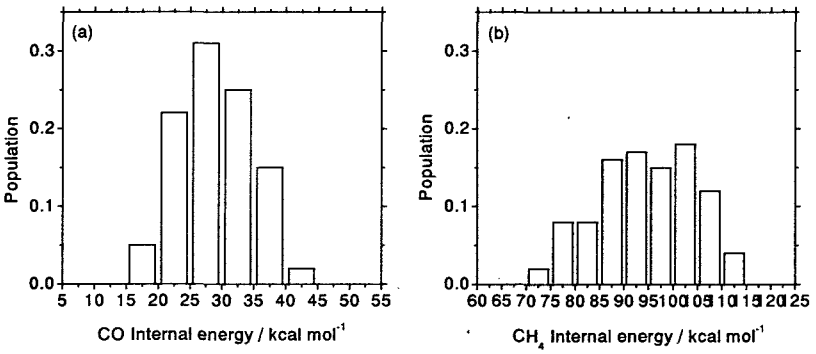

Fig. 2 Internal energy distributions for the products: (a) CO; (b) CH_4

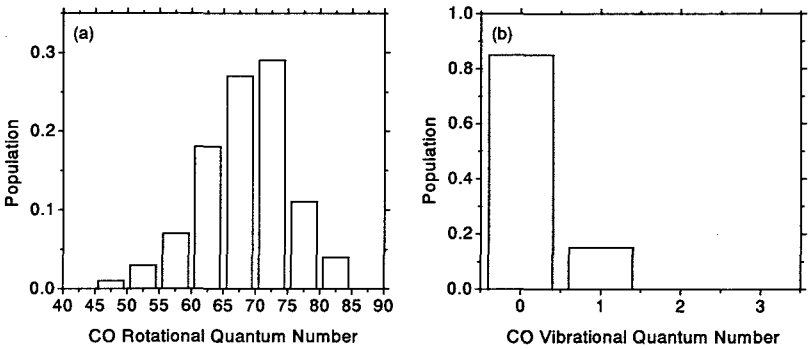

Fig. 3 Product state distributions: (a) CO rotational quantum number; (b) CO vibrational quantum number

References

1) B. F. Gherman, R. A. Friesner, T.-H. Wong, Z. Min, and R. Bersohn, J. Chem. Phys. **114**, 6128 , 2001.

4.7.11 Spectrum analysis of Al and C ions produced by high intensity laser irradiation

Keiko SUTO, Akira SASAKI, Kengo MORIBAYASHI, Kenjiro TAKAHASHI, Masayuki SUZUKI, Etsuya YANASE, Takatsugu OKETA, Hiroyuki DAIDO and Takashi KAGAWA[a)]
a) Nara Women's University

1. Introduction

Recently, through development of the production techniques of high intensity short pulse lasers[1)], the experimental and analytical study for interaction of high intensity short pulse lasers with solid has become possible. We investigate temparature and density profile of C and Al plasmas produced by the irradiation of a high intensity short pulse laser, by analyzing the soft x ray spectrum radiated from the plasmas. We will report only on the results from the last investigation of various fundamental properties.

2. Experiment

A laser pulse having a temporal duration of 1.5ps is focused on the solid targets of CH and Al giving an intensity of 10^{15}W/cm^2. We compare the x ray spectrum from the plasmas produced by the laser with and without the pre-pulse. The pre-pulse has duration of 600ps and it has a half of the main pulse energy. We analyze the L-shell-x ray spectrum from Al and the K-shell-x ray spectrum from C for wavelengths between 20Å and 80 Å.

3. Results

As basic research for the study of laser produced plasmas, we analyze the K-x ray spectrum from C, for the purpose of reconsidering the method, which has been used previously[2,3)]. We estimate the density from the Inglis-Teller-limit[4)] of the longer wavelength edge of the continuum radiation, and the temperature from the slope of a continuum spectrum as well as the intensity ratio between the H-like and He-like ions. As the measurement point becomes farther from the solid surface, the densities decrease rapidly. We investigate effect of the pre-pulse on the density profile by comparing the experimental results with the calculated results by original the HYADES[5)] fluid model code. These results suggest that higher-density plasma is produced by a shorter pulse laser irradiation. Special attention should be paid to the steep temperature slope near the surface of the solid. It is considered that the effect of ionizing plasmas appeared. Further, the satellite lines are observed only the steep temperature gradient region. These results indicate the possibility of production of hollow atoms by laser irradiation on solids. It is necessary to clarifying physical processes in the high intensity short pulse laser irradiated plasma. The time-dependent-CR-model, which is now constructed, will make direct information on these processes. The comparison between the experiment and the model prediction is now performed.

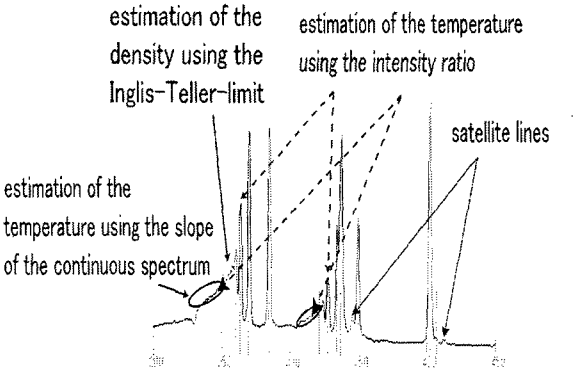

Fig. 1 analysis the spectrum by the methods, which have been used

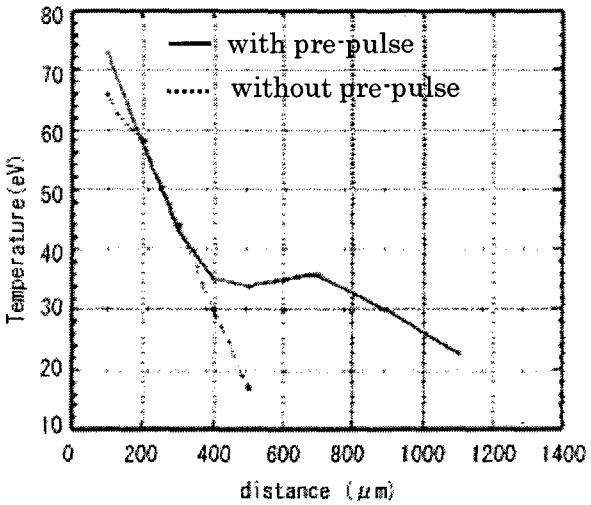

Fig. 2 the temperature of the plasmas

References

1) K. Yamakawa et al, JAERI-RESERCH 2000-051
2) T. Fujimoto and T. Kato, Phys. Rev. A, **32**,1663,1985
3) H. R. Griem, Principles of Plasma Spectroscopy,1997
4) D. R. Inglis et al, Astrophys. J.,**90**,439,1939
5) J. T. Larsen et al, J. Quant. Spectrosc. Radiat. Trandf.,**51**,179,1994

4.7.12 Temperature dependence of ultrafast energy relaxation of a dye molecule in complex systems -Expanding the time window of observation up to 10 ns-

Hiroshi MURAKAMI

The structural dynamics of complex systems, such as liquids, polymers and biomolecules have attracted much attention, because they play an important role in chemical or biological reactions, and are an issue of the condensed matter physics [1, 2]. Methods to measure the structural dynamics of such a system in the spatial scale of atom and in real time, e.g. time-resolved diffraction by a laser-produced plasma X-ray pulse, have recently been demonstrated, while the dynamics of electronic state due to the structural dynamics of the medium can be observed using various optical spectroscopic techniques. It is ideal that the two types of measurements are applied to the system simultaneously because information obtained from those measurements is complementary in order to understand the system. A signal/noise ratio is usually very small in the time-resolved X-ray measurements, and it is necessary to confirm whether the structural dynamics due to photoexcitation occurs or not. Hence, in practice, a time-resolved optical spectroscopy should be performed for the system before time-resolved X-ray measurements, because it can probe the structural dynamics responsible for the electronic state dynamics with high sensitivity.

In order to study the ultrafast energy relaxation in the electronic excited state of a dye molecule in complex systems, we have developed a temperature-dependence measurement system of femtosecond time-resolved fluorescence intensity and applied to a dye solution from 150 K to room temperature [3, 4]. In this system, the time window is at most up to a few ns because of using an optical delay line. On the other hand, the time profiles of the wavelength-resolved fluorescence intensity should be measured in the wavelength range of the fluorescence spectrum of the sample in order to obtain the time-resolved fluorescence spectra, which are direct measure to characterize the energy relaxation, using the reconstruction method [3]. At room temperature, the exponential decay component due to fluorescence lifetime of the order of nanosecond is dominant in the time profile of the fluorescence intensity after a few ns, and so the time profile after a few ns is well extrapolated using an exponential decay with a fluorescence lifetime. The time profile of the fluorescence intensity, however, has a component due to the diffusion-like motion of the medium comparable with or longer than the fluorescence lifetime at low temperatures, and so the extrapolation is not effective any longer. Hence we need the time profile of the fluorescence intensity from a few ns after photoexcitation also. Thus, in this study, we have accomplished the measurement of the time behavior of the fluorescence intensity on longer time scale in combination with a streak camera and a digital delay generator under the same condition as at the femtosecond time-resolved measurement, and measured time-resolve and wavelength-resolved fluorescence intensity of a dye solution in the temporal range from femtosecond to 10 ns, from room temperature up to 150 K.

The temperature-dependence measurement system of femtosecond time-resolved fluorescence spectroscopy is described in detail [3, 4]. We employed a coumarin dye dissolved in a mixture of ethanol and methanol with a voluminal ratio of 4:1 as a sample. The sample was excited by the second harmonic (410nm) of the mode-locked Ti:Sapphire laser pulse. The streak camera (Hamamatsu, C5680) was connected with a monochrometor (Spex) to obtain time-resolved and wavelength-resolved fluorescence intensity. The gate and trigger pulses for the streak camera were synthesized from a reference pulse synchronized with the laser pulse using a digital delay generator (Hewlett-Packard, DG535). The instrumental response function to the excitation pulse for this system was a few ten ps in the scan range of 0.5 ns and in the average mode. It has been found that the time behavior of the fluorescence intensity of the sample shows a decay and rise component in the short-wavelength and long-wavelength side, respectively on a time scale of ns at low temperatures, and the time scale of the decay and rise is longer with decreasing temperature. This is considered to be ascribed to the energy relaxation due to the diffusion-like motion of the surroundings of the dye molecule. In progress is the reconstruction of the time-resolved fluorescence spectra using the data thus obtained as well as the data from the femtosecond time-resolved measurement.

References

1) See for a review, The Glass Transition: Relaxation Dynamics in Liquids and Disordered Materials, ed. E. Donth (Springer, 2001).
2) H. Murakami, T. Kushida, H. Tashiro, J. Chem. Phys. 108 (1998) 10309.
3) H. Murakami, J. Mol. Liq. **89** (2000) 33.
4) H. Murakami, J. Lumin. (accepted).

5. Synchrotron Radiation Science

Osamu SHIMOMURA
Synchrotron Radiation Research Center

Synchrotron Radiation Research Center (SRRC), together with RIKEN, entrusted the operation and management of SPring-8 to JASRI. Thirty-eight beamlines including 24 public beam lines were operated in 2001 fiscal year. Total operation time in 2001 fiscal year was 5400 hrs, among which 4500 hrs were for user time. Accepted proposals are 971. More detail statictics and prominent scientific results are summarized in 'SPring-8 Annual Report' and 'Science Frontier' edited by JASRI, respectively.

The key words of SRRC for SR research is 'characterization', 'process' and 'prediction' using SR, and the mutual intimate relation among three is of important. With this concept, seven research groups including theory group are built up, which consist of about 60 staff including scientific staff, posdoc fellow, supporting staff and management staff. We have constructed 4 JAERI beamlines at SPring-8 and 1 beamline at Photon Factory in order to perform specified subject to our center.

Following are typical results obtained at each group in the last financial year. These results were reported and discussed at the SRRC symposia held at June and December.

A new JAERI beamline, named 'quantum structure physics beamline' BL22XU, was constructed in SPring-8 by instrument development group. This beamline has the experimental equipments for high pressure studies and resonant X-ray diffraction. The end station for the latter is set up at the RI hall where RI materials can be treated with unsealed condition. This is a complementary beamline to BL23U, where soft X-ray is use for unsealed RI materials. All the system has been completed by March 2002, and will be commissioned from financial year 2002. With these beamlines the SRRC materials science research has a strong core on heavy elements and their strong electron correlation effects.

An in-situ X-ray diffraction study was conducted on the graphite-diamond conversion with H_2O fluids as solvent-catalyst using SMAP2 cubic anvil press by high pressure group. Time dependencies of the conversion rate were observed. The result showed that it takes long time to form diamonds by the spontaneous nucleation in the aqueous fluid with dissolved MgO at 5-6 GPa and 900-1400℃ which is supposed to be the conditions where natural diamonds were formed.

An inelastic X-ray scattering measurements on a single crystal of $La_{0.85}Sr_{0.15}CuO_4$ was done in order to study dynamical fluctuations of wide(Q,ω)space. The inelastic peaks originated from optical phonon branches were observed. The highest optical branch was shown around 80 meV along <100>. The phonon softening is observed in many materials having perovskite structure of high temperature super conductors.

A different oxidation mechanisms for clean and H_2O-chemisorbed Si(001)surface were investigated on the experimental basis of the high-energy-resolution photoemission spectroscopy and the incident energy control of O_2 molecules. Potential energy barriers for O_2 chemisorption are found in the oxidation of Si(001) surface passivated by H_2O molecules. No potential energy barriers were not found for oxygen saturated surfaces. The oxidation of the topmost Si dimmer backbond sites increases of Si^{3+} and Si^{4+} components.

The resonant inelastic X-ray scattering spectra of $La_{1-x}Sr_xMnO_3$ (x=0(parent compound of colossal magnetoresistive manganites, Mott insulator), 0.2(ferromagnetic metal) and 0.4(metallic compound)) were measured by the spectrometer at BL11XU to investigate the hole-doping effect to $LaMnO_3$. Clear differences between those materials were found in excitation energy and scattering intensity with temperature.

The electronic structure of heavy-fermion Ce-based compounds $CeMIn_5$(M=Rh and Ir) were investigated by the resonant photoelectron spectroscopy. $CeRhIn_5$ displays antiferromagnetic with T_N=3.8K in ambient pressure, but it undergoes superconducting state under high pressure. $CeIrIn_5$ is a superconducting with Tc=0.4K in ambient pressure. The Ce 4f electrons in these compounds are found to be in the nearly localized regime. The hybridization between the conduction electrons and the Ce 4f electrons in $CeIrIn_5$ is slightly larger than that in $CeRhIn_5$.

The excitations in antiferro-quadrupole-ordered CeB_6 were studied theoretically to compare the neutron scattering intensities with Bouvet's experiments. CeB_6 is a typical dense Kondo system and exhibits at 3.3K a phase transition associated with antiferro-quadrupole order of 4f electrons of Ce ions. The antiferro-quadrupole order is difficult to be observed, but recently resonant X-ray scattering was detected due to a staggered quadrupole ordering. This study clarified the nature of excitations in CeB_6.

5.1 Beamline and Experimental Facilities Development

5.1.1 Construction of New JAERI Beamline in SPring-8

Hiroyuki KONISHI, Hideaki SHIWAKU, Kazukiyo TOZAWA and Takahisa SHOBU

The construction of a new JAERI beamline in SPring-8, a quantum structure physics beamline BL22XU, was authorized in a revised budget of FY 2000. All equipments and components were ordered till the end of FY 2000.[1)]

A frontend was installed during the machine-shutdown term in the summer of 2001. The fabrication of shielding hutches began in September. An undulator was installed in a storage-ring during the machine-shutdown term in the winter. Almost beamline components were completed till the end of January 2002. Installations and adjustments of them were carried out in February. The installation of beamline control and interlock systems were finished in March, so the construction of BL22XU was completed. We have made the examination of interlock system on March 31. A beamline commissioning started in the middle of May, 2002.

An overview of BL22XU in the experimental hall of the storage-ring facility is shown in Fig. 1. High-pressure studies by using a multi-anvil press or diamond anvil cells are carried out in experimental hutch 1. Experimental hutch 3 is in the RI (Radio Isotope) laboratory to investigate the orbital, charge or magnetic ordering of interesting materials such as actinide (uranium) compounds by using resonant X-ray diffraction methods.

A high energy X-ray is useful for the high-pressure studies, while a low energy X-ray is needful for the resonant methods, for example, the energy of the M-absorption edge of uranium is about 3.5keV. ID22, the in-vacuum type undulator with a magnet period of 38mm for BL22XU can provide 3keV photons as fundamental radiation. Higher harmonics are utilized to get the high energy X-ray below about 70keV. To take out the monochromatic X-ray from the broad energy range, we prepared two double crystal monochromators. One is a SPring-8 standard type and provides the monochromatic low energy X-ray of 3.1keV to 37keV. The other is a numerical coupling type. Each Bragg angle of two crystals of the monoshromator is controlled from a computer independently. It is able to cover the high energy range of 35keV to 70keV. Si(111) plane crystals cooled by liquid nitrogen are used at both monochromators.

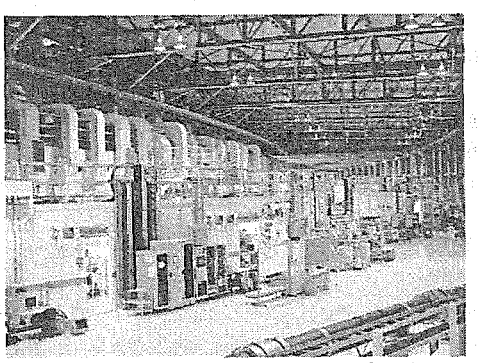

Fig. 1 Overview of BL22XU in the strage-ring facility

In order to avoid the large absorption of the low energy X-rays, all beryllium windows can be removed from an optical axis and the beamline can turn to be windowless type. Water-cooling system is not necessary for movable beryllium windows at the understream of the monochromators, so they are basically made of ordinary gate-valves with a window. We designed a new beamline component for a water-cooled movable beryllium window system at the upstream of the monochromators as shown in Fig. 2. A standard water-cooled beryllium window apparatus and a vacuum gate valve are attached to two vacuum tubes respectively. These tubes and branched bellows constitute partially branched vacuum paths. The beryllium window apparatus and the gate-valve can exchange the position on the optical axis each other by an air-driven slide unit. Windowless status can be achieved by putting the gate-valve on the optical axis and keeping it open using the interlock system.

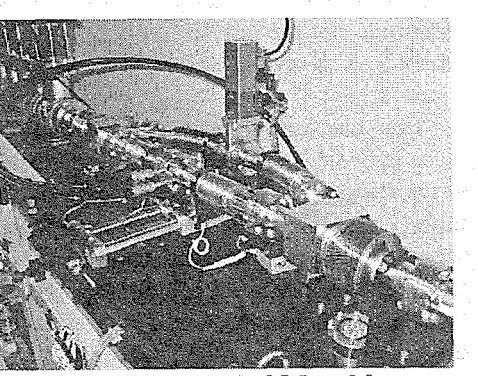

Fig. 2 Water-cooled Movable Beryllium Window

Reference

1) H.Konishi,H.Shiwaku,K.Tozawa,T.Shobu et al., SPring-8 Information, 6, 198, 2001

5.1.2 A Soft X-ray Beamline BL23SU

Akane AGUI, Akitaka YOSHIGOE and Takeshi NAKATANI

1. Introduction

BL23SU[1] is an only soft x-ray beamline along JAERI beamlines. This has a high energy-resolution monochromator[2]. At the beamline, soft x-ray spectroscopy studies in a wide variety of applications, such as surface chemistry and condensed matter physics are going.

Researches are performed not only by the JAERI beamline scientists but also by public users. During the 2001AB term, eleven experiments were offered for JASRI users. They had studied surface chemistry biology and solid state physics. The popularity was shown on TV program of Science & Technology of Japan. (see Fig. 1) Some parts of BL23SU have been improved and modified.[3,4] Short notes of the changes are in the following section.

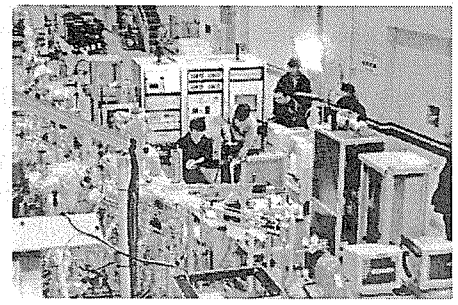

Fig. 1 Making TV program (2001 Feb. 13)

2. Improvements and modifications

Light source of BL23SU is an insertion device (ID23). The electron beam position correlation table of ID23 steering magnets has been improved with help from the accelerator division of SPring-8. The result is shown somewhere in this review.

To get lower energy with the first harmonic, we have replaced the vacuum chamber of ID23 with a thinner chamber. For the human and machine radiation safety, local radiation shield have been added to Mv and Mh chambers in the optical hutch. To make maintenance easy the shield system was built up on rails. Figure 2 shows the system at Mv chamber.

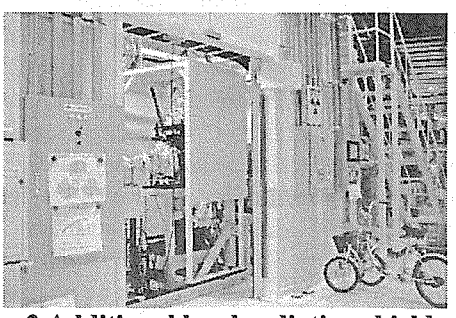

Fig. 2 Additional local radiation shield system at Mv chamber (2002. Jan 10)

The x-ray profile changes as the polarization of ID23 changes. To observe the profile, a wire type x-ray beam position monitor have been replaced by a four-blades type x-ray beam position monitor. Figure 3 shows the four-blades type monitor. The tuning will be done in the coming year.

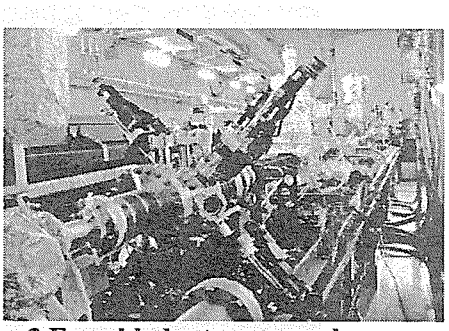

Fig. 3 Four-blades type x-ray beam position monitor (2002 Dec 18)

A synchrotron radiation performance monitor system has been installed downstream of the biology section of BL23SU. The main parts of the system are analysis and preparation chambers, an electron energy analyzer and manipulators. The energy position, intensity and resolving power of BL23SU will be investigated by using the system. Figure 4 shows the side view of the vacuum system.

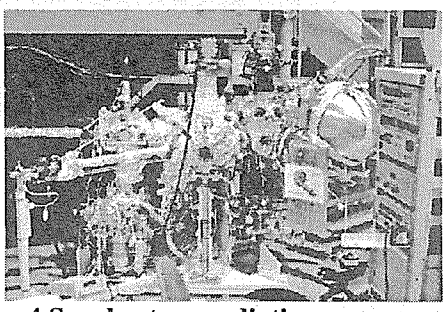

Fig. 4 Synchrotron radiation performance monitor system

References

1) A. Yokoya, *at al.*, J. Synchrotron Rad. 5, 10,1998
2) Y. Saitoh *et al.* Nucl. Instrum. Methods A474, 253, 2001
3) A. Agui *et al.* JAERI-Tech 2002-064, 2002
4) T. Nakatani *et al.* to be submitted to JAERI-Tech, 2002

5.1.3 Measurement of photoneutron spectrum due to gas bremsstrahlung in the forward direction of the SPring-8 beamline

Yoshihiro ASANO

1. Introduction

Photoneutron generated by the interaction of the gas bremsstrahlung with thick target such as shield material is one of the most important issues of the safety analysis of the synchrotron radiation beamline in the third generations, because the intensity of gas bremsstrahlung generated by the interaction of stored electrons with residual gas molecules in a storage ring vacuum chamber is seriously high to creep into the beamline. A combination of a long straight section and high energy of the stored electrons generates an extremely intense and highly collimated gas bremsstrahlung, and associated photoneutron are grown up. Therefore, the evaluations of photoneutron and gas bremsstrahlung are needed precisely for the shielding design of the synchrotron radiation beamlines and the experimental data for the benchmark are required seriously. Especially, few measurements of the photoneutron spectrum were performed until now in the forward direction.

2. Experiments and results

The photoneutron was measured by using the liquid scintillator, NE213, within the lead shield box of 1cm in thickness to reduce the back ground of gamma rays, which was installed into the beam axis of the BL40XU at Spring-8 with thick target of lead. The intensities of gas bremsstrahlung were measured by using PWO detector. The target with NE213 and the PWO detector were installed alternately on the photon beam axis upstream of the monochromator. The targets were employed for lead of 13 cm in thickness ($23.1X_0$, X_0: radiation length). High sensitive He-3 counters with polyethylene moderators were also set in the lateral direction outside the hutch wall. NE213 has high sensitivity for gamma rays as well as photoneutron so that we employed the method of pulse shape analysis to separate neutrons from gamma rays. **Figure 1** shows the measurement results of the pulse shape analysis of photoneutron due to gas bremsstrahlung. As shown in the figure, the neutrons can be separated from the gamma rays clearly. The neutron spectrum, therefore, can be obtained by using unfolding method.

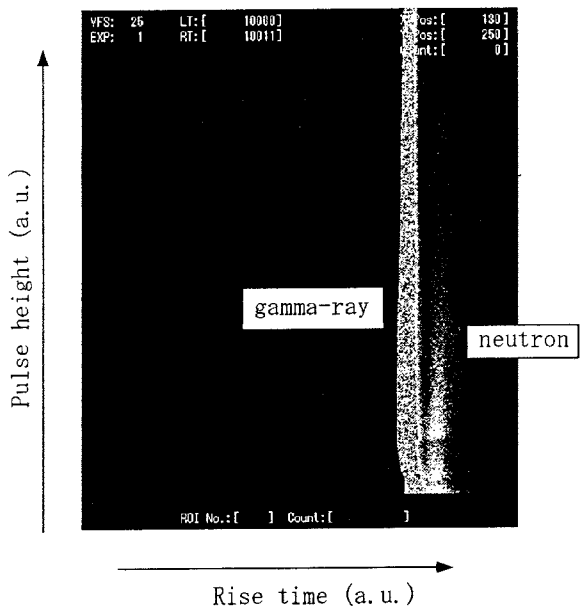

Fig. 1 The result of pulse shape analysis of NE213 for photoneutron due to gas bremsstrahlung
Horizontal axis shows the pulse rise time in arbitrary unit and vertical shows the pulse height. The intensities are showed by the contrast of the light.

Acknowledgement

This experiment was carried out in the collaboration with Professors Horoshi Yoshida and Yasuhisa Tajima of Yamagata university and their students, Masaki Moriya, Masakazu Yamamoto, Michitaka Itaya, Tomoo Hario.

5.2 High Pressure Science

5.2.1 The Temperature and Pressure dependence of the structure for Vitreous Silica

Yasuhiro INAMURA, Yoshinori KATAYAMA, Wataru UTSUMI and Ken-ichi FUNAKOSHI[a)]
a) Japan Synchrotron Radiation Research Institute

1. Introduction

Vitreous silica is permanently densified by high-pressure (HP) and high temperature (HT) treatments. The densified glass is widely studied to reveal relations between structure and properties of glass. However, how the densification occurs under HP and HT is not well understood yet: in-situ HP measurements are limited at room temperature [1,2]. The reported pressure-induced structural change at room temperature is gradual but a recent molecular dynamics calculation suggests a possibility of a pressure-induced first-order amorphous-amorphous transformation in vitreous silica under HT [3]. To study structural change of vitreous silica under HP and HT conditions, we performed in-situ x-ray diffraction experiments.

2. Experimental

Experiments were performed using large-volume multi-anvil presses; SPEED1500 installed at BL04B1 and SMAP2 at BL14B1 in the SPring-8. X-ray diffraction profiles were measured by the energy-dispersive method using the white synchrotron radiation beam from a bending magnet. Diffraction data were obtained in a pressure range from 3.6 GPa to 17 GPa and a temperature range from room temperature to 1450 K.

3. Results and discussion

Figure 1 shows temperature dependence of X-ray structure factor, $S(Q)$, as a function of momentum transfer, Q, of vitreous silica at 9.9 GPa. With increasing temperature, a first sharp diffraction peak (FSDP), associated with the intermediate range structure, shifts to higher Q and its shape becomes sharper. Since a linear relation between the position of FSDP and the density is reported for densified glass, the shit of FSDP to higher Q suggests that the densification undergoes with increasing temperature. The radial distribution function calculated from $S(Q)$ shows that the SiO_4 tetrahedron unit is stable whereas the average Si-O-Si bond-angle is increased by about 5 at 900℃. Therefore, we may say that the intermediate structure is relaxed or homogenized by increasing temperature under HP.

The shift and sharpening of the FSDP is observed at any other pressures, although in different manners. Figure 2 shows temperature dependence of FSDP position at different pressures. At 3.6 GPa, the FSDP shifts above 300℃. At 4.8 GPa and 5.5 GPa, it shifts gradually from room temperature to crystallization temperature. Above 9.9 GPa, the shift occurs only below 300-400℃. The temperature range where the shift of FSDP occurs becomes lower with increasing pressure. However, we have not observed a sudden structural change of vitreous silica in the present pressure and temperature range.

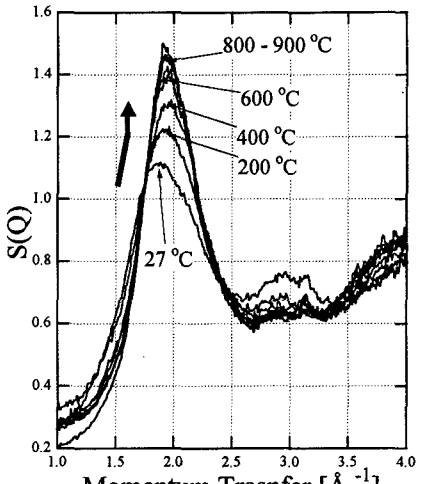

Fig. 1 Temperature dependence of observed S(Q) at 9.9 GPa

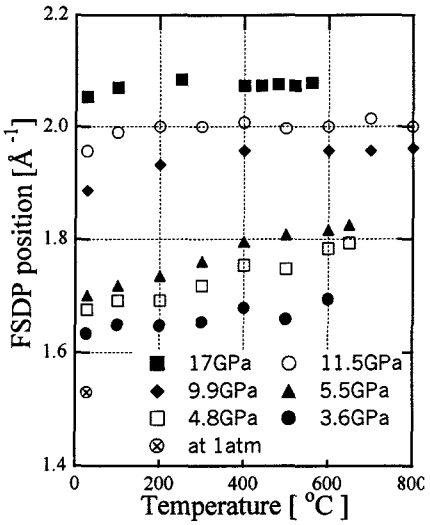

Fig. 2 Temperature dependence of FSDP position

References

1) R.J. Hemley, H.K. Mao, P.M. Bell and B.O. Mysen, Phys. Rev. Lett **57**,747,1986.
2) C. Meade, R.J. Hemley and H.K. Mao, Phys. Rev. Lett. **69**, 1387, 1992.
3) D.J. Lacks, Phys. Rev. Lett. **84**, 462, 2000.

5.2.2 Structural study of icosahedral Cd-Yb quasicrystal and its approximant under hydrostatic pressure up to 40 GPa

Tetsu WATANUKI, Taku J. SATO[a)], An Pang TSAI[a)] and Osamu SHIMOMURA
a) National Research Institute for Metal

1. Introduction

Very recently, Tsai et al. found binary quasicrystals in the Cd-M (M=Yb, Ca) alloy system, which is the first example of a two-component stable icosahedral quasicrystal. This system has additional characteristic features. One is no chemical disorder in the structure, while more than ternary quasicrystals generally have chemical disorder. In this sense, this system can be mentioned as one of ideal quasicrystals. Another is the existence of approximant crystal whose chemical composition is very close to the quasicrystals; Cd 85.1: Yb 14.9 for quasicrystal phase, and Cd 85.7: Yb 14.3 (Cd_6Yb_1) for cubic 1/1 approximant crystal phase. They have much similarity in the local structure, but have difference in the middle- or long-range structure. The aim of this work is 1) to reveal the structural stability of Cd-Yb quasicrystalline phase, and 2) to pick up the difference between quasicrystalline phase and its approximant with respect to the structural properties under high pressure, which should reflect the middle- or long-range arrangement of their lattice.

2. Experiments

In order to detect intrinsic characteristics under high pressure, to pick up any slight structural change, and to detect the large Q_{perp} reflections which are weak but have much information about the quasicrystalline lattice, good hydrostatic conditions must be requrered. So, we use He gas as a pressure medium in a diamond anvil cell which can generate quasi-hydrostatic condition up to 50 GPa. In addition to this, the powder sample was made into a pellet of 10 μm (t.), which is thin enough to avoid direct compression by anvils. And we performed powder X-ray diffraction experiments of Cd-Yb quasicrystalline phase and its approximant under pressure up to about 40 GPa at SPring-8 at BL10XU.

3. Results

As for the quasicrystalline phase, no significant change of the x-ray diffraction profiles up to 39 GPa were observed. However, Bragg peak broadening was observed in the pressure region above 15 GPa (Fig. 1a), where the line width is depends on Q_{par} in linear not on Q_{perp}. These results show that Cd-Yb quasicrystalline phase is compressed isotropically up to 15 GPa, and strain is induced with increasing pressure above about 15 GPa, but no phason strain is induced. The induced strain is large one estimated at 0.6%, and is reversible one. As for the approximant phase, distortion of the cubic lattice with increasing pressure was observed just above ambient pressure (Fig. 1b). This distortion is saturated around 20 GPa, and is suppressed in higher pressure region, and the lattice recovers cubic again at about 40 GPa. The results show that the cubic lattice of the approximant phase is unstable under pressure, but is stabilized again in high pressure region near 40 GPa. The difference of the structural stability of these two phase is considered to come from symmetry matching of local structure with their lattice.

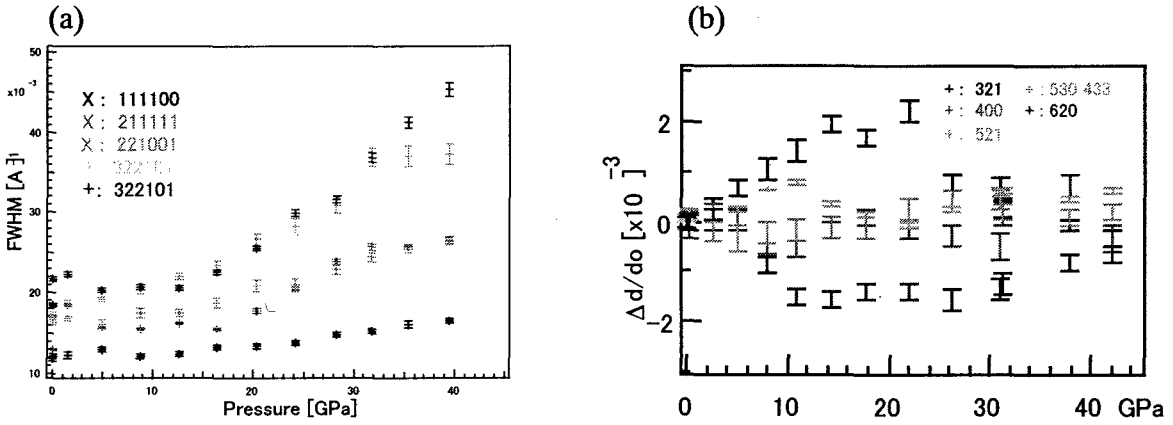

Fig. 1 Pressure dependence of Bragg peak widths of icosahedral Cd-Yb quasicrystal (a) and pressure dependence of d-value deviation from average in Cd-Yb approximant crystal(b)

5.2.3 Real time observation of the graphite-diamond transition with H_2O fluids

Wataru UTSUMI, Taku OKADA and Nozomu HAMAYA

1. Introduction

The formation mechanism of natural diamonds in the earth's mantle remains a debated topic. On the basis of diamond inclusion studies, a strong relationship between diamond formation and mantle fluids has been suggested. Although experimental simulations of high pressure diamond synthesis have brought us much information, most of the previous experiments have been based on the "quench method." Since fluids are unquenchable, direct observation of the phenomena under high-pressure and temperature, such as in situ x-ray diffraction, would be indispensable to clarify the role of catalysts in the natural diamond forming process. We have conducted an in situ x-ray diffraction study on the graphite-diamond conversion with H_2O fluids as a solvent-catalyst using SMAP2 cubic anvil press installed on the beamline BL14B1.

2. Experimental

A mixture of brucite ($Mg(OH)_2$) and graphite was packed in a molybdenum capsule that was embedded in a cubic-shaped high pressure cell assembly. In situ x-ray observations were performed by energy dispersive powder diffraction method using white x-rays and Ge solid state detector. Pressure was first increased at room temperature, and then the temperature was increased at a constant applied load. At certain high temperature (around 1100ºC), brucite dehydrated and supercritical aqueous fluid was formed, which acted as a solvent-catalyst for the graphite-diamond conversion. After we confirmed the dehydration of brucite, temperature was jumped to the target temperature. When the target condition was achieved, temperature was stabilized and diffraction profiles were recorded every 10 second to observe the time-dependence of transition. Experiments were carried out at six different P-T conditions (1700, 1835 °C at 7.7 GPa, and 1400, 1450, 1500, 1630 °C at 8.8 GPa).

3. Results

Figure 1 shows the variation of the diffraction profiles with time at 8.8 GPa and 1450 °C. The first plot in this figure was obtained at the instant the temperature was stabilized. It is clear that intensity of the graphite 002 peak was reduced while the diamond 111 peak became larger, reflecting the amount of diamond present. The first appearance of the diamond diffraction peaks was observed 440 seconds after the attainment of target temperature (incubation time), and the graphite peaks completely disappeared 920 seconds later, while three diamond peaks (111, 220, 311) were clearly observed. Owing to the use of the high-intensity synchrotron radiation and our technical developments on a high-pressure cell assembly, the time-dependent data could successfully be taken for a short exposure time no less than 10 seconds.

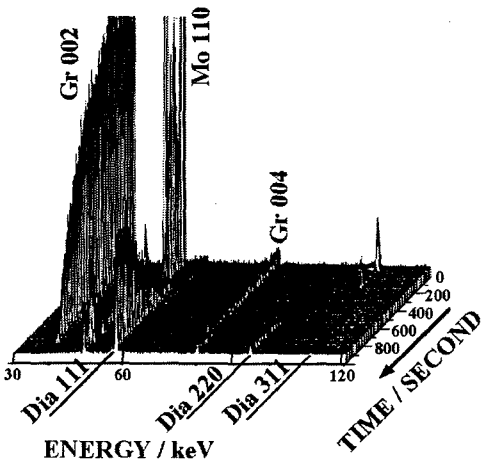

Fig. 1 Variation of diffraction profiles with time in the graphite-diamond transition at 8.8GPa and 1450 °C

Time dependences of the conversion rate were calculated from variation of the integrated peak intensities in graphite and diamond. As temperature and pressure became lower, longer incubation time for diamond spontaneous nucleation was needed and conversion speed became slower. The experimental data were analyzed by using the Avrami rate equation ($y=1\ k\cdot t\hat{}n$, y: conversion rate, k: a rate constant, t: time, n: a constant which depends on a mechanism controlling kinetics) and the following values were obtained: n=1.7 (1835 °C at 7.7 GPa), n=3.2 (1700 °C at 7.7 GPa), n=2.8 (1500 and 1630 °C at 8.8 GPa), n=5.2 (1450 °C at 8.8 GPa). Present results show that very long time is necessary to form diamonds by the spontaneous nucleation in the aqueous fluid with dissolved MgO at 5-6 GPa and 900-1400 °C, which is supposed to be the conditions where natural diamonds were formed.

5.3 Structural Physics Research

5.3.1 Crystal structure of Pd-perovskite catalyst in redox fluctuating atmosphere III

Yasuo NISHIHATA, Jun'ichiro MIZUKI, Hirohisa TANAKA[a], Mari UENISHI[a] and Noriaki HAMADA[b]
a) Materials R&D Div., Technical Center, Daihatsu Motor Co., Ltd.
b) Faculty of Science and Technology, Tokyo University of Science

1. Introduction

Catalytic converters are widely used to reduce the amount of NOx, CO and unburned hydrogen carbons in automotive emissions. In conventional catalysts, precious metals initially have nanometer-order dispersions, but the catalytic activity deteriorates through the particle growth of metals during the vehicle use. It is important to control the catalytic active site not only to maintain high efficiency, but also to economize on precious metals. Perovskite crystals including the precious metal such as palladium, $LaM_{1-x}Pd_xO_3$ (M = Fe, Co, $Fe_{0.6}Co_{0.4}$), retain its high metal dispersion owing to structural responses to the reduction-oxidation (redox) fluctuations in exhaust-gas composition that occur in state-of-the-art gasoline engines. The purpose of this study is to clarify the mechanism to maintain high catalytic activity and to suppress the particle growth of precious metals[1].

2. Experiments

Pd-containing perovskite catalysts were prepared by the alkoxide method. The powdered catalyst, $LaFe_{0.57}Co_{0.38}Pd_{0.05}O_3$, was subjected to thermal ageings under oxidation, reduction, re-oxidation atmospheres in due order at 800 °C for 1 hour on each ageing step. We employed the X-ray anomalous diffraction (XAD) and X-ray absorption fine structure (XAFS) techniques near the Pd K-edge (24.35 keV) in order to determine the distribution of Pd in the catalysts, using Si (311) double crystal monochromator and two mirrors for higher-order harmonics rejection at bending-magnet beamline BL14B1 of SPring-8.

3. Results

Since the energy dependence of x-ray intensity for (100) and (110) Bragg reflections from the oxidized catalyst showed the cusp at the Pd K-edge, we understood without any uncertainty that Pd occupied the B-site (6-fold coordination) in the perovskite lattice of the oxidized catalyst. On the other hand, the cusp of the intensity was not observed for the reduced catalyst, implying that Pd did not occupy any site in the perovskite lattice of the reduced catalyst. The results of XAFS analysis showed that trivalent Pd occupied the B-site in the oxidative atmosphere, and that Pd segregated out from the perovskite crystals and formed small metallic alloy particles with Co in the reductive atmosphere. The local structure of the re-oxidized sample was essentially the same as that of the oxidized, indicating that it could be changed in a completely reversible manner. The catalyst retained a predominantly perovskite structure throughout a redox cycle.

Figure 1 represents the reversible change of a Pd-perovskite particle under the redox fluctuation in exhaust-gas. A perovskite particle (~1μm) contains Pd at the B-site of the perovskite structure in an oxidative atmosphere, while metallic particles (1~3nm) segregate out and appear on the surface of the perovskite particle in a reductive atmosphere. The agglomeration and growth of the metal particles is suppressed as a result of the Pd movement between inside and outside the perovskite lattice. Therefore, this catalyst might refresh by itself during driving a car.

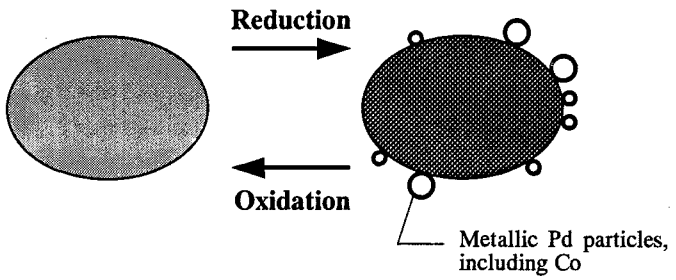

Fig. 1 Reversible change of a catalyst particle under the redox fluctuation in exhaust-gas

Reference

1) Nishihata, Y. *et al. Nature* **418**, 164-167 (2002).

5.3.2 Time-resolved X-ray diffraction study on surface structure and morphology during molecular beam epitaxy growth

Masamitu TAKAHASI, Yasuhiro YONEDA, Hirotane INOUE,
Naomasa YAMAMOTO and Jun'ichiro MIZUKI

The reflection high energy electron diffraction (RHEED) oscillation has been widely adopted for studies on growth kinetics and dynamics in molecular beam epitaxy (MBE). Recent development in brilliant X-ray source has enabled similar experiments with X-rays [1], which has great advantage in a straightforward interpretation of results and in a high angular resolution. In general, the diffracted intensity from surface is proportional to the surface structure factor associated with the surface reconstruction, F, multiplied by a damping factor associated with the surface roughness, m. We show that the two factors, F and m, can be obtained separately by measuring diffuse scattering around the two-dimensional Bragg peak during growth.

The experiments were performed with a six-axis surface diffractometer coupled to an MBE chamber at a synchrotron radiation facility, SPring-8. This apparatus allows the sample to be subjected to X-ray measurements at the same position as prepared. Diffracted intensity of X-rays was measured during the homoepitaxial growth of GaAs(001) at a substrate temperature of 700 K. Under the condition used, the RHEED pattern changed from the c(4x4) to the 2x1 symmetry at the start of growth.

The X-ray intensity distribution along $(1+\eta,1-\eta,0.05)$ consists of a spiky two-dimensional Bragg peak and a broad diffuse scattering. Figure 1 shows the peak intensity evolution during the growth as a function of time. In the peak intensity, both contributions from F and m are included. To decompose the two contributions, we measured the change in the intensity distribution profile by composing several cycles of growth at different values of η. By applying analysis based on the single-scattering theory, the temporal evolution of F and m was deduced as shown in Fig. 2 under a reasonable assumption that the surface structure is homogeneous.

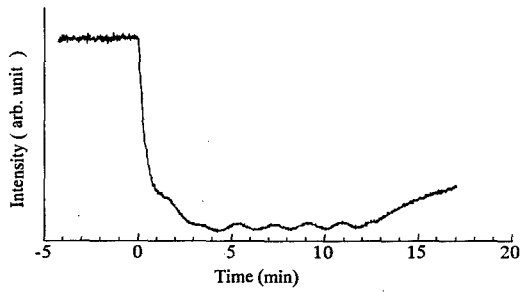

Fig. 1 The X-ray peak intensity evolution at (1,1,0.05) during growth

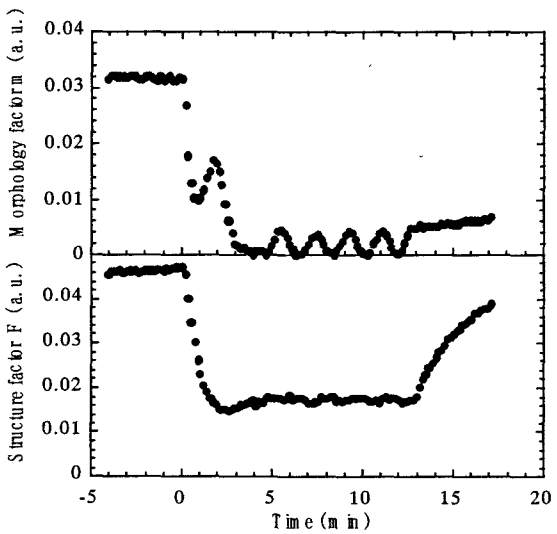

Fig. 2 The temporal evolution of the morphology factor and the structure factor during the homoepitaxial growth of GaAs(001) at 700 K

References

1) E. Vlieg, A. W. Denier van der Gon, J. F. van der Veen, J. E. Macdonald and C. Norris, Phys. Rev. Lett. 61 (1988) 2241.

5.3.3 Nickel Ionic Adsorption Induced by Amidosulfonic Acid Anions on an Au(111) substrate in a Nickel Amidosulfate Solution

Hiroyuki KAWAMURA, Masamitu TAKAHASI and Jun'ichiro MIZUKI

1.Introduction

A single atomic layer can be formed by the electrochemical process using underpotential deposition (UPD), which is a surface-limited reaction to a sub-monolayer or monolayer coverage. In UPD, the electrochemical deposition of foreign metals onto substrate is performed at a positive potential relative to the reversible Nernst potential for bulk deposition. The formation of Ni monolayer is important since Ni is the material used for industrial purposes such as electrocatalysis, magnetic devices, and battery electrodes. A nickel monolayer could be deposited on an Au(111) electrode at underpotential region in an amidosulfonic solution since the XPS spectrum for Ni 2p state was observed from the sample obtained at the UPD potential[1]. However, no scanning tunneling microscopy (STM) study is possible since the resolution of the STM image is lost[1]. In order to understand the mechanism of the Ni UPD and to obtain a well-defined Ni monolayer, it is necessary to verify the electrode surface in situ, by investigating the three-dimensional surface structure, such as the surface-normal structure of adsorbate layer consisting of more than one layer, and the buried interface structure between the adsorbate layer and the substrate. Then, the Ni UPD layer structure normal to the substrate surface has been investigated by in-situ specular X-ray reflectivity measurements.

2.Experimental

The in-situ specular X-ray reflectivity measurements were carried out using a k-type multi-axis diffractometer installed on beamline 14B1 at SPring-8, Japan. The Ni UPD layer was formed on a pre-treated Au(111) disk electrode in the electrolytic solution contained 40 mM $Ni(NH_2SO_3)_2$ and 100 mM H_2SO_4 as the supporting electrolyte. The Ni UPD potential was applied to the Au(111) electrode during the measurements. The theoretical specular reflectivity for the electrode surface is given by the kinematical approximation. In the quantitative determination of the structure of the near-surface layers that include the surface adsorbate layers and the underlying Au layer, the parameters representing the electron density profiles are optimized so as to adequately describe the observed reflectivity.

3.Results

Figure 1 shows the specular reflectivity for the Ni UPD layer (open circle). The line is the calculated reflectivity profile for the Ni UPD layer based on the model where a 0.54 ± 0.01 ML amidosulfonic acid anion layer is on the reconstructed Au(111) surface and a 0.28 ± 0.01 ML Ni layer is above the amidosulfonic acid anion layer.

The specular reflectivity measurement shows that the Ni UPD layer exists in the vicinity of the electrode surface. However, the electrochemical measurements shows that the charge corresponding the UPD current is consumed only by the desorption of the amidosulfonic acid anions. This leads to the conclusion that the Ni^{2+} ions are not reduced, i.e. Ni layer is probably Ni^{2+} ionic one. The adsorption of Ni^{2+} ions in the form of metal-ligand complex may be induced by the presence of the amidosulfonic acid anions adsorbed on the Au(111) substrate.

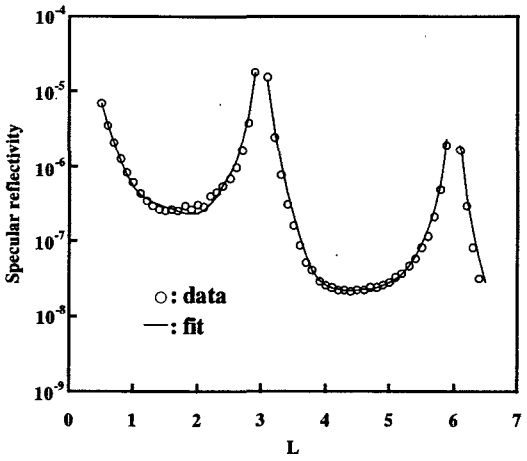

Fig. 1 Specular reflectivity for the Ni UPD layer on an Au(111) substrate in 40 mM $Ni(NH_2SO_3)_2$ + 100 mM H_2SO_4

References

1) J.L. Bubendorff, L. Cagnon, V. Costa-Kieling, J.P .Bucher, and P. Allongue, Surf. Sci., **384**, L836, 1996

5.3.4 Inelastic X-ray scattering studies of phonons in $La_{1.85}Sr_{0.15}CuO_4$

Tatsuo FUKUDA, Jun'ichiro MIZUKI, Kazuhiko IKEUCHI[a], Kazuyoshi YAMADA[a], Yasuo ENDOH[b], Alfred Q.R. BARON[c], Yoshikazu TANAKA[d], Satoshi TUTUI[c]
a) Inst. Chem., Kyoto Univ. b) Inst. Mat. Res., Tohoku Univ. c) JASRI, SPring-8 d) RIKEN, SPring-8

1. Introduction

The coupling between electrons and phonons is known to play an important role to form Cooper-pairs in conventional superconductors. On the other hand, its role in the high-T_c superconductors (HTcS) is not fully known and it is one of the central research subjects of these materials. Moreover, some recent studies have pointed out that the distribution of electronic charge and spin seems not to be homogeneous, rather form stripes in which spin and charge separate into different regions in HTcS materials, and that the stripes may play a crucial role in the transport and superconducting properties. In order to study phonons, or dynamical charge fluctuations, we did inelastic x-ray scattering (IXS) measurements on a single crystal of $La_{0.85}Sr_{0.15}CuO_4$. For many years, inelastic neutron scattering (INS) experiments have been done to study dynamical fluctuations of wide (Q, ω) space. However, recent progresses of IXS measurement technique makes it possible to investigate with samples smaller than INS experiments. Furthermore, IXS is superior to INS for studying dynamical charge structure because x-rays can directly interact with electrons, but neutrons cannot.

2. Experiments

The sample we studied is a crystal of $La_{0.85}Sr_{0.15}CuO_4$, which was grown at Kyoto University using the traveling-solvent floating-zone (TSFZ) method with radiation heating without crucible. The experiments were performed at the high-energy-resolution IXS beam line 35XU of SPring-8. The incident x-rays from an undulator source were monochromated using a Si(111) double-crystal monochromator, followed by a Si(888) high-energy-resolution backscattering monochromator, operating at 15.816keV. The x-ray beam was led by two mirrors to the sample position, and the scattered photons were energy analyzed by 4 spherical silicon crystal analyzers, which were settled at 10 m apart from the sample. The total momentum and energy resolutions were about 0.15 $Å^{-1}$ and 6.6meV. The measurements were done mainly with a reflection mode (Bragg geometry) at the room temperature.

3. Results

We mainly measured the spectrum at the scattering vector $Q=(H, 0, 0)$ $[H=2\sim4]$ with an energy-loss mode. Clear peaks at around 10, 20 and 80meV were observed which have clear dispersion and are possibly originated from phonon branches. Fig. 1 shows the dispersion relation and the Q dependence of peak intensity of a highest optical phonon branch around 80 meV along <100> direction. It has maximum at zone boundary in intensity. Recently, this bond-stretching phonon also attracts an attention, because it shows similar softening in many materials with the perovskite structure including HTcS.

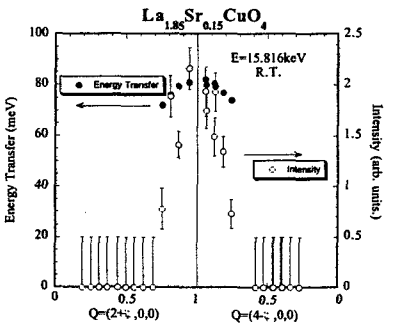

Fig. 1 the Q dependences of peak position (energy transfer) and intensity of a highest optical phonon branch along <100>

5.3.5 Electrochemical synthesis of superconducting boride MgB_2

Kenji YOSHII, Hideki ABE [a] and Jun'ichiro MIZUKI
a) National Institute for Materials Science (NIMS), Tsukuba, Ibaraki 305-0047, Japan

A recent discovery of superconductivity in MgB_2 at a transition temperature (T_C) as high as 39 K [1] has shown the possibility of manufacturing of low-cost and high-performance electrical devices and magnets based on superconducting materials. From the viewpoint of industrial applications, wires, tapes, thin films as well as bulk samples were fabricated by means of direct reactions between elemental Mg and B. We recently found that this compound is electrochemically synthesized from the mixtures of molten salts [2,3]. Black deposits containing MgB_2 were obtained by means of electrolysis on a fused mixture of $MgCl_2$, KCl, NaCl and MgB_2O_4 in an Ar flow at 600°C. The low-cost starting materials and the simple apparatus used in this method are favorable for practical application.

Figure 1 shows the magnetic susceptibility plotted against temperature for the sample prepared from the mixtures of $MgCl_2$, KCl and MgB_2O_4 with a molar ration of 5:5:1 [1]. It is seen that the FC (field-cooled) and ZFC (zero-field-cooled) susceptibilities deviate from each other below T_C~37 K. Taking into account the constituent elements in the starting materials, this behavior is attributed to the superconducting transition of MgB_2. The existence of MgB_2 in this sample was confirmed by X-ray diffraction measurements. Both susceptibilities shown in Fig. 1 commonly exhibit a negative polarity below ~33 K, which is understood in terms of the Meissner effect of the superconductivity. Electrical transport properties of this sample could not be measured accurately due to large contact resistance.

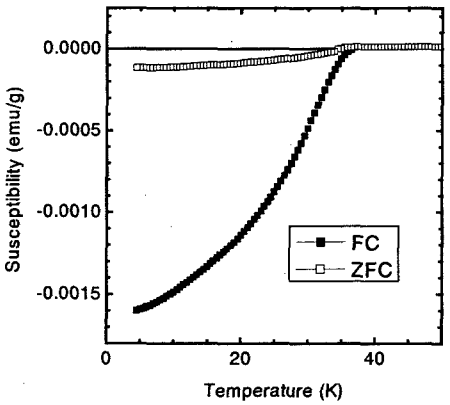

Fig. 1 Magnetic susceptibility plotted against temperature measured with an applied field of 20 Oe

It was found that the contact resistance is drastically decreased by the substitution of NaCl for KCl, which allows reliable electrical transport measurements [3]. Figure 2 shows the electrical resistivity plotted as a function of temperature for the sample prepared from the mixture of $MgCl_2$, NaCl, KCl and MgB_2O_4 with a molar ration of 10:7:3:2 [3]. The onset of a superconducting transition is observed at T_C~37 K, which is almost the same temperature as that shown in Fig. 1. The resistivity is lowered to zero below ~32 K. This result indicates that the present synthesis method can be adopted to fabricate realistic superconducting magnets and devices. From the applied-field dependence of resistivity, the upper critical field and the coherence length at 0 K were calculated to be 9.7 T and 5.9 nm, respectively, both of which are close to those for bulk samples reported so far [3].

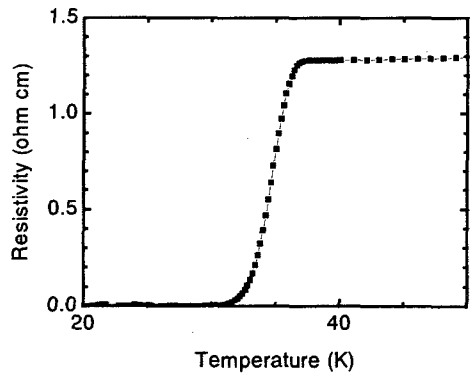

Fig. 2 Electrical resistivity plotted against temperature in the absence of applied magnetic field

References

1) J. Nagamatsu et al, Nature, **410**, 63-64, 2001
2) H. Abe and K. Yoshii, J. J. Appl. Phys., **41**, L685-L687, 2001
3) K. Yoshii and H. Abe, Supercond. Sci. Technol.2001, in press

5.3.6 Intermediate structure in crystallization process of amorphous $Bi_4Ti_3O_{12}$

Yasuhiro YONEDA, Ken'ichirou YAGI[a], Hikaru TERAUCHI[b] and Masaaki TAKASHIGE[c]
a) Tokyo Inst. of Tech., b) Kwansei-Gakuin univ., c) Iwaki-Meisei univ.

1. Introduction

Ferroelectric thin films have attracted considerable attention because of their use in non-volatile memory applications [ferroelectric random-access memories (FeRAM)]. Ferroelectric oxides with $SrBi_2Ta_2O_9$ (SBT) and $Bi_4Ti_3O_{12}$ (BiT) Bi-layered structures are promising materials for these films and have been extensively studied.[1)]

Recently, the crystallization process of amorphous BiT had been investigated and an intermediate structure of $Bi_2Ti_2O_7$ appeared in the temperature range around 700°C.[2)] By adjusting the heat-treatment temperature and the length of time above crystallization temperature (T_{crys}), polycrystalline materials with desired constant and electro-optic coefficient are strongly affected by the size of crystal grains. Thus, from the material science viewpoint, this can be one of the useful methods to optimize physical properties of polycrystalline ferroelectrics.

2. Sample preparation

To prepare amorphous samples, the twin-roller quenching system was adopted. The BiT was melted in a quarts tube at about 1100°C. The melt was sprayed onto the twin-roller and rapidly quenched into an amorphous thick ribbon of 20-40 μm thickness and 1-3 cm length.

From differential thermal analysis, two crystallization temperatures were determined (T_{crys1} = 611°C and T_{crys2} = 830°C). It is concerned that the intermediate structure was appeared in the temperature range from 611°C to 830°C. Then, the amorphous BiT was annealed at 700°C for X-ray powder diffraction.

3. Results

The X-ray powder diffraction was performed at BL02B2, SPring-8 (E = 25 keV). The crystal structure was refined by the Rietveld technique.

The resulting X-ray diffraction pattern and Rietveld refinement were obtained as shown in Fig. 1. From the Rietveld analysis, the intermediate structure consisted of two phases, one was well-known $Bi_2Ti_2O_7$ pyrochlore structure and the other was Bi_2WO_6-like structure. The Bi_2WO_6-like structure is new structure of Bi-layered materials.

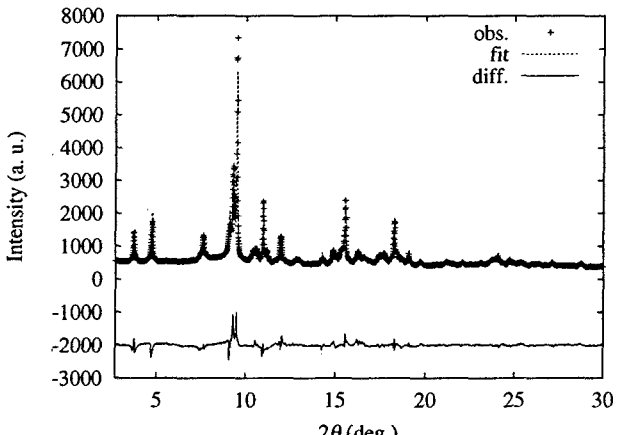

Fig. 1 X-ray diffraction pattern of 700°C-annealed BiT and the Rietveld refinement profile

References

1) Y. Shimakawa, Y. Kubo, Y. Tauchi, H.Asano, T. Kamiyama, F. Izumi and Z. Hiroi, Appl. Phys. Lett. **79**, 2791, 2001
2) M. Takashige, S. Hamazaki, Y. Takahashi, F. Shimizu, T. Yamaguchi, M. S. Jang and S. Kojima, Jpn. J. Appl. Phys. **39**, 5716, 2000

5.4 Surface Chemistry Research

5.4.1 Photon Stimulated Desorption from DNA Components induced by Oxygen K-excitation

Kentaro FUJII, Ken AKAMATSU[a)] and Akinari YOKOYA
[a)] Japan Society for the Promotion Science

1. Introduction

Photon stimulated desorption from DNA components, 2-deoxy-*D*-ribose as well as thymine and guanine, were observed by using a residual gas analyzer installed in a synchrotron soft X-ray beamline to reveal the mechanism of DNA damage through direct ionization/excitation of DNA. Radiation damage to DNA, which induces serious biogenetic effects such as mutation, can be classified as (1) structural damage leading to a single- or double-strand break, (2) a release of nucleobases from DNA, and (3) chemical modification of the nucleobases. Some of the damages of (2) and (3) are known to be processed by base excision repair enzymes. However, there are few reports for the direct measurement of the released nucleobases or molecular fragment from the damaged DNA. Core level excitation induced by monochromatized synchrotron soft X-rays is one of important probes to investigate the photon stimulated desorption of the nucleobases or smaller fragments as the consequence of photochemical reaction at the specific site in DNA. Recently, we measured XANES spectra of DNA nucleobases around oxygen and nitrogen K-edges[1)]. In order to obtain the evidence of the base lesions as well as strand breaks by the site selective photoreaction, we have developed an apparatus for direct observation of molecular fragments from DNA or released nucleobases in the photon energy range (400 ~ 560 eV)[2)].

2. Experimental

Desorbed ions by ultrasoft X-rays irradiation were detected by a quadrupole mass spectrometer (RC501PIC; Hiden Analytical Ltd.). The analyzer was positioned at ~ 30 mm from the sample. By attracting positive ions to the analyzer, the sample was floated at + 60 V during the measurement. The photon stimulated desorption measurement was carried out at the JAERI soft X-ray beamline (BL23SU) at the SPring-8. All the measurements were performed at room temperature.

3. Results and discussion

Figure 1 shows the mass spectra for (a) 2-deoxy-*D*-ribose, (b) thymine and (c) guanine thin films obtained by 540 eV photo excitation. In the spectrum for D-ribose, H^+, CH_2^+, $C_2H_2^+$, CHO^+, $C_3H_3^+$ and C_2HO^+ were mainly observed. On the other hand, only H^+ was detected as a main desorbed ion from the thymine and guanine thin films. It is shown that the core excitation more drastically degraded the 2-deoxy-*D*-ribose molecule into small fragments than was in the case with the nucleobases. The sugar moiety in DNA would be one of the molecular fragile sites conducive to a single-strand DNA break as well as the base release.

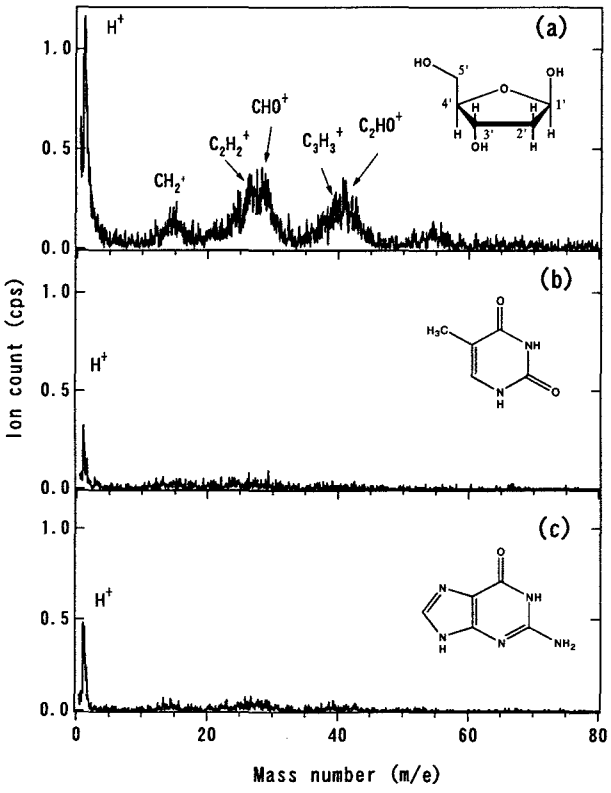

Fig. 1 PSD mass spectra of positive ions from (a) 2-deoxy-*D*-ribose, (b) thymine and (c) guanine thin films following oxygen core excitation (540 eV). Ion counts were normalized with photon-flux and irradiation time.

References

1) K. Fujii, K. Akamatsu, Y. Muramatsu and A. Yokoya, *Nucl. Instr. Meth. B., in press*
2) K. Fujii, K. Akamatsu and A. Yokoya, *Surf. Sci., in press*

5.4.2 Core level Spectroscopy study for cluster-like Si deposited on graphite and insulating sapphire

Krishna G. NATH, Iwao SHIMOYAMA, Tetsuhiro SEKIGUCHI and Yuji BABA

1. Introduction

In the coming nanotechnology age, Si-assembled nanostructures will be the key components for fabrication of many nanodevices. Due to technological and research importance, study of Si-epitaxy on inert substrates, such as semi-metallic graphite[1] and insulating sapphire[2] has attracted much attention in recent years. For example, scanning tunneling microscopy measurement was performed to observe the Si nanowires on graphit[1]. However, electronic structures of Si nanowires and Si-clusters on HOPG are not known.

2. Experimental

The core level photoemission and photoabsorption experiments were carried out for different Si thin films deposited on Highly Oriented Pyrolitic Graphite (HOPG) and insulating Sapphire (Al_2O_3). The in-situ measurements were performed at the BL27A, Photon Factory. Si was deposited on the substrates at room temperature by using electron deposition method. After Si deposition, the sample was transferred to the analysis chamber, and Si 1s photoemission spectra and photoabsorption spectra at Si 1s near edge were measured.

3. Results and Discussion

In Figs. 1(a), 1(b) and 1(c), several Si 1s photoemission spectra are shown. The excitation energy was hν=2.2 keV. Figures 1(a) and 1 (b) show spectra for Si films on HOPG. The thicknesses of Si films are 0.3 Å and 5.5 Å, respectively. In Fig. 1(b), there is only one component, "A". However, in the case of thinner film, i.e., 0.3 Å film in Fig. 1(a), there are more three components along with component "A". The relative binding energies for four components (A, B, C and D) are 0, 1.45, 2.85 and 4.25 eV, respectively.

The presence of several components in the photoemission spectra confirms the existence of a range of Si morphologies consisting of clusters and nanowires. Compared with other films, such as 0.4 Å, 2.3 Å and 4.5 Å, we identified two relatively stable Si phases corresponding to components "A" and "C". The binding energy difference between A and C is about 2.85 eV. Comparing with a previous result[3], we describe the component "C" originates from a cluster forming with an average of 10 Si atoms. According to Ref. 1, we predict that the 10-atom Si-clusters are polymerized, and become Si nanowires. With further deposition, the bulk-like component (A) starts to dominate, and finally becomes thicker films. Similar with thin Si on HOPG, thin Si on Sapphire in Fig. 1(c) also shows four different components, and their relative binding energy positions are also the same as Si/HOPG. However, component C is more intense than others. From this photoemission measurement, it is understood that the morphology of Si corresponding to component "C" is a stable when Si is very thin grown on both HOPG and Sapphire.

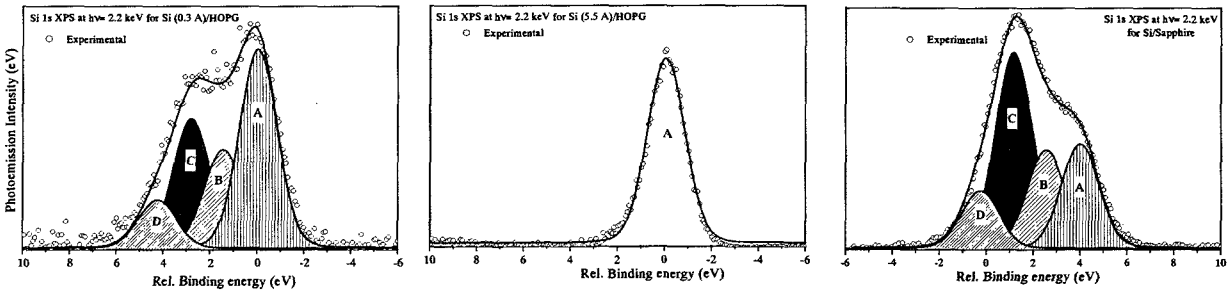

Fig. 1 (a) Si1s photoemission spectra for a thin Si on HOPG
Four peaks are fitted to the experimental spectrum.

(b) Si1s photoemission spectrum for thicker Si film on HOPG
Only a single component is observed.

(c) Si1s photoemission spectra for a thin Si on Sapphire
Similar with thin Si on HOPG, four components are found.

References

1) B. Marsen and K. Sattler, Phys. Rev. B 60, 11593 (1999).
2) S. Cristoloveanu, Solid-State Electronics 45, 1403 (2001).
3) K. Fuke, et al., J. Chem. Phys. 99, 7807 (1993).

5.4.3 Different oxidation mechanisms for clean and H_2O-chemisorbed Si(001) surface

Yuden TERAOKA and Akitaka YOSHIGOE

1. Introduction

Potential energy barriers for O_2 chemisorption have been found in the oxidation of Si(001) surface passivated by H_2O molecules. They are close to the prediction of first-principle calculation for the clean Si(001) oxidation.[1] In order to experimentally verify the theoretical prediction, the saturated oxygen amount and chemical bonding states have been studied [2,3] by O-1s and Si-2p photoemission spectroscopy as a function of incident energy (E_t) of O_2 molecules and compared with those of the H_2O-chemisorbed surface oxidation. No potential energy barriers have been observed in the case of clean surface oxidation. The reason for such a different performance has been discussed on the basis of the high-energy-resolution photoemission spectroscopy and the incident energy control of O_2 molecules.

2. Experimental

All experiments have been performed at the surface chemistry experimental station (SUREAC2000) installed at the JAERI soft x-ray beamline, BL23SU, in the SPring-8. In order to obtain the clean Si(001) surface, the base pressure of the analysis chamber has been improved to be less than $5x10^{-9}$ Pa using a shroud and a manipulator cooled by liquid N_2. The clean surface was irradiated by supersonic O_2 molecular beams (SSMB) perpendicularly until the surface was saturated by oxygen. The upper limit of O_2 incident energy was 3 eV. The ultra-thin oxide-layers were analyzed using the high-energy-resolution photoemission spectroscopy with synchrotron radiation in the surface sensitive conditions.

3. Results

No theoretically-predicted two potential energy barriers (0.8 eV and 2.4 eV) were found by O-1s photoemission measurements for oxygen saturated surfaces in contrast to the H_2O-chemisorbed surface case. In order to clarify the different oxidation mechanisms between the clean and H_2O-chemisorbed Si(001) surface, high-energy-resolution Si-2p photoemission spectra were measured as a function of O_2 incident energy for the oxygen saturated surfaces. The representative spectra are shown in Fig. 1. Since U (up atoms of Si dimers) and D (down atoms) components were apparent as shown in Fig. 1(a), the topmost Si dimers were not terminated as Si-H and Si-OH. After the O_2 irradiation with the incident energy of 0.6 eV, the spectra changed dramatically as shown in Fig. 1(b). The increase of Si^{3+} and Si^{4+} components were attributed to the oxidation of the topmost Si dimer backbond sites. Consequently, Si dimer backbonds are oxidized by O_2 molecules with the incident energy less than 0.8 eV, while they are not oxidized in the H_2O-chemisorbed surface unless the incident energy exceeds the first potential energy barrier. The theory pointed out the possibility of barrier-less oxidation of Si dimer backbonds, that is, a chemisorption path from bridge sites of dimers to backbonds through dangling bonds. Dangling bonds termination by H atoms and OH radicals due to the H_2O chemisorption must prevent taking place of the predicted chemisorption path in the oxidation of the H_2O-chemisorbed surface.

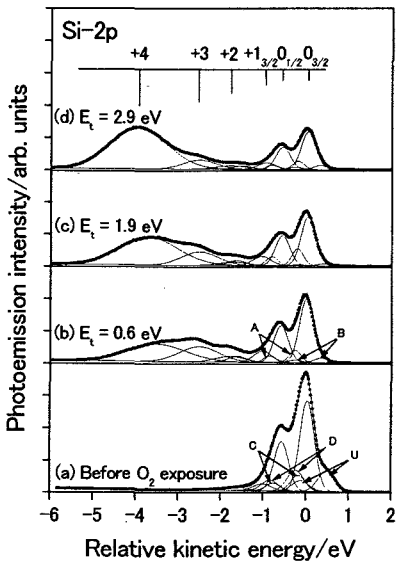

Fig. 1 Si-2p photoemission spectra for (a) clean Si(001) surface, (b) oxygen saturated surface by O_2 SSMB irradiation with E_t=0.6 eV, (c) with E_t=1.9 eV and (d) with E_t=2.9 eV

References

1) K. Kato and T. Uda, Phys. Rev. B **62**, 15978, 2000
2) Y. Teraoka and A. Yoshigoe, Surf. Sci. **507-510**, 797, 2002
3) A. Yoshigoe and Y. Teraoka, Appl. Surf. Sci. **190**, 60, 2002

5.4.4 Electroparamagnetic Resonance in DNA bases Induced by Core Level Resonance Photoexcitation of Oxygen

Akinari YOKOYA, Ken AKAMATSU[a)] and Kentaro FUJII
[a)] Japan Society for the Promotion Science

1. Introduction

Studies employing soft X-rays under a few keV as probes to investigate genetic changes have highlighted the high efficiency of the biological effects, such as mutations, related with the molecular process on DNA damages. To understand the physicochemical mechanism of the DNA damages induced by K-photoabsorption in the energy region, we have developed an X-band EPR system combined with a synchrotron soft X-ray beamline[1)]. Short-lived radical process following the *K*-absorption of oxygen in DNA bases has been revealed by *in-situ* EPR signal detection[2)]. In this study, we further examined the radical yield of guanine around the oxygen *K*-edge.

2. Experimental

EPR signal of DNA bases, guanine and thymine, was measured using a newly developed X-band electron paramagnetic resonance device (SLEEPRS: Synchrotron Light Excited Electron Paramagnetic Resonance Spectrometer) [1)] installed in a JAERI soft X-ray beamline (BL23SU) in SPring-8. The sample pellet was irradiated with soft X-ray photons at a microwave cavity in a vacuum chamber ($<10^{-6}$ Pa). A closed-cycle cryogenic system was used to control the sample temperature from 77 K to room temperature. Relatively low microwave power ranging 0.1 to 7 mW was used to avoid power saturation of EPR signals. Based on a XANES spectrum of guanine film reported in our previous paper[3)], several photon energies were chosen for irradiation. Resolution power, E/ΔE ~ 1,000 at the O K-edge (0.5 keV) region, and a photon flux of the order of 10^{11} (photons/sec/100 mA ring current/0.02 % band width) were realized at the sample position.

3. Results and discussion

Figure 1 shows the EPR spectra of the short-lived guanine radicals obtained around *K*-exciation energy (540 eV) of oxygen (O6 of guanine). Two components were observed in the spectra as described by ***a*** and ***b*** in the Fig.1. The component ***b*** was insignificant by irradiation below and above the *K*-edge (524 and 548 eV). These are thought to be respective radicals because of different power saturation response. The signal intensity of both components immediately disappeared by beam-off. Figure 2 shows a photon energy dependency of the signal intensity of the component ***a***. A characteristic large peak was found in the spectrum. At the peak (536 eV), the signal intensity was about 5 and 2 times larger than those obtained at 524 eV and 548 eV. It is inferred that the short-lived species is radical cations as the result of the core level excitation of a 1*s* electron of O6 to an anti-bonding orbital (σ*) of O-C and following resonant Auger decay process in the molecule. These radicals would be instantly transformed to be a stable radical previously reported. These results clearly demonstrate that the *in situ* measurement of EPR combined with a brilliant soft X-ray source will provide a possibility for pursuing physicochemical process for induction of DNA base damage such as 8-oxo-guanine, which efficiently induce a point mutation on DNA in a living cell.

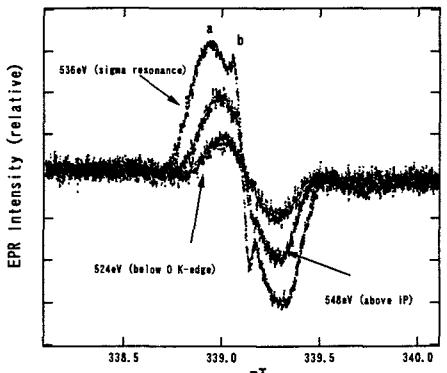

Fig. 1 EPR spectra of guanine pelletirradiated at oxygen K-resonance (536 eV), below (524 eV) and above (548 eV) at 77 K.

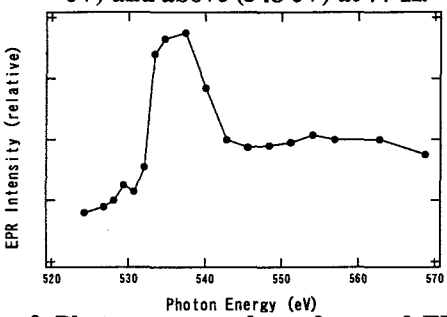

Fig. 2 Photon energy dependence of EPR signal intensity around oxygen K-dege
The intensity of the component *a* is normalized with photon flux and the EPR gain.

References

1) A. Yokoya and K. Akamatsu, Nucl. Instr. Meth A.**467-468**, 1333-1337, 2001
2) A. Yokoya, K. Akamatsu and K. Fujii, Nucl. Instr. Meth B, in press.
3) K. Fujii, K. Akamatsu and A. Yokoya, Nucl. Instr. Meth B, in press.

5.5 Heavy Atom Science

5.5.1 Resonant inelastic x-ray scattering study on $La_{1-x}Sr_xMnO_3$ (x = 0.2, 0.4)

Kenji ISHII, Toshiya INAMI, Kenji OHWADA, Kaori KUZUSHITA,
Youichi MURAKAMI, Jun'ichiro MIZUKI, Yasuo ENDOH [a], Sumio ISHIHARA [b],
Hiroshi KONDO [a], Sadamichi MAEKAWA [a], Kazuma HIROTA [b] and Yutaka MORITOMO [c]
a) IMR, Tohoku Univ., b) Dept. of Physics, Tohoku Univ., c) CIRCE, Nagoya Univ.

1. Introduction

Strongly correlated electron systems, such as high-T_C superconducting cuprates and colossal magnetoresistive (CMR) manganites, attract much attention in condensed matter physics. Particularly, the electronic structure and electronic excitation spectrum are important to understand the electronic properties of these materials. Inelastic scattering in the hard x-ray regime can be a powerful technique to investigate the electron dynamics with momentum resolution. Resonant inelastic x-ray scattering (RIXS), which occurs when the incident x-ray energy is tuned near the absorption edge of an element, has advantages of resonant enhancement of the scattering intensity and element selectivity. Up to now, we have constructed a spectrometer for RIXS study at BL11XU of SPring-8[1], and investigated the electronic excitation spectra of $LaMnO_3$ which is a parent compound of CMR manganites. Hole-doping to the antiferromagnetic Mott insulator changes the electronic properties dramatically, as seen in high-T_C superconductor in cuprates and phase transition to ferromagnetic metal with CMR effect in manganites. Here we report on the RIXS study of the hole-doping effect to $LaMnO_3$. We chose two hole concentrations. One is $La_{0.6}Sr_{0.4}MnO_3$, corresponding to 0.4 holes per Mn atom. $LaMnO_3$ is a Mott insulator, while $La_{0.6}Sr_{0.4}MnO_3$ has enough holes to make the compound metallic. We compared the RIXS spectra of insulating and metallic phase. The other is $La_{0.8}Sr_{0.2}MnO_3$, which shows an electronic phase transition from a paramagnetic insulator to a ferromagnetic metal. We measured RIXS spectra across the transition temperature.

2. Experimental

The RIXS spectra of $La_{1-x}Sr_xMnO_3$ were measured by the spectrometer mentioned above. Single crystals of $La_{1-x}Sr_xMnO_3$ of typical size of several millimeters were used. The energy of incident x-rays was tuned near the Mn-*K* absorption edge by diamond (111) double crystal monochrometer and that of scattered x-rays are analyzed by Ge (531) crystal. The energy resolution is 0.5 eV. Helium-closed-cycle refrigerator equipped to the spectrometer was used for the measurement of temperature dependence.

3. Results and Discussion

Figure 1 shows the RIXS spectra of $LaMnO_3$ and $La_{0.6}Sr_{0.4}MnO_3$ at **Q** = (3.3,0,0) in *Pbnm* orthorhombic setting. Resonantly enhanced peaks at 8 eV and 11.5 eV were observed at the incident x-ray energy of 6.556 keV, as was in the case of $LaMnO_3$. The peaks at 8 eV and 11 eV are attributed to the charge transfer (CT) excitation from O 2*p* orbitals to the Mn 3*d* and 4*s*/4*p* orbitals, respectively. Moreover we successfully found a clear difference at low energy excitations; there is a peak at 2.5 eV in $LaMnO_3$, which corresponds to the excitation across the Mott gap, while the low energy excitations of $La_{0.6}Sr_{0.4}MnO_3$ form a shoulder of elastic peak, and the gap disappears completely. Another difference in the spectra is an energy shift of the peak at 11 eV. This may be understood by chemical shift of Mn 4*s*/4*p* orbitals due to the difference of valence states. In the momentum transfer dependence, these excitations show flat dispersion in this energy resolution. In the RIXS spectra of $La_{0.8}Sr_{0.2}MnO_3$, the scattering intensities increase gradually with decreasing temperature, though no drastic change observed at the metal-insulator transition temperature (T_C = 309 K). This feature suggests a definite change of electronic structure with temperature.

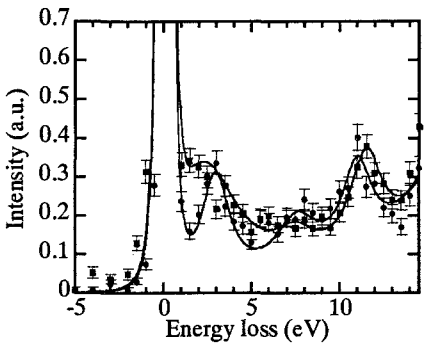

Fig. 1 RIXS spectra of $LaMnO_3$ (circles) and $La_{0.6}Sr_{0.4}MnO_3$ (squares)
The energy of incident x-ray is 6.556 keV, and the scattering vector Q is (3.3,0,0).

Reference

1) T. Inami et al., Nucl. Instr. and Meth. A **467-468**, 1081, 2001.

5.5.2 Symmetry Breaking in the Metal-to-Insulator Transition of $BaVS_3$

Toshiya INAMI, Kenji. OHWADA, Hiroyuki KIMURA[a)], Yukio NODA[a)], Hiroyuki NAKAMURA[b)], Tomoaki YAMASAKI[b)], Masayuki SHIGA[b)], Naoshi IKEDA[c)], Youichi MURAKAMI[d)]

a) IMRAM, Tohoku University, b) Department of Materials Science and Engineering, Kyoto University, c) Japan Synchrotron Radiation Research Institute, d) Department of Physics, Tohoku University

It has been believed for a long time that the metal-to-insulator (MI) transition of $BaVS_3$ is not accompanied by any spatial order of spin and lattice.[1,2] Hence, the order parameter of the transition has been vague, and it is even suggested that the transition is a realization of the pure Mott transition.[1] In this study, we have performed single-crystal x-ray diffraction measurements in order to find the hidden order parameter of the MI transition in $BaVS_3$.

The x-ray diffraction measurements were carried out using a two-axis diffractometer at IMRAM, Tohoku University. A single crystal (ϕ0.2mm×3mm) was mounted on the cold finger of a closed-cycle He refrigerator. We also performed synchrotron x-ray diffraction measurements at beamline BL02B1 of SPring-8. The x-ray energy was 30 keV. A small single crystal ($100 \times 100 \times 150\mu$ m^3) was mounted on the cold finger of a closed-cycle He refrigerator on a four-circle diffractometer.

We first took oscillation photographs at 100 K ($> T_{MI} = 70$ K) and at 25 K ($< T_{MI}$). Below T_{MI}, weak superlattice reflections are clearly observed just midway between the fundamental Bragg peaks, indicating a structural phase transition which doubles the c axis. We then measured Weissenberg photographs at 25 K. In the $(h,k,\frac{1}{2})$ plane, superlattice reflections were observed only at $h+k=2n+1$. Since the lattice type above T_{MI} is C-lattice, the superlattice is I-lattice (body centered lattice). In the $(h,k,\frac{1}{2})$ plane, superlattice reflections are intense around the b^* axis, while no peak is found around the a^* axis. The intensity of a superlattice reflection was also measured as a function of temperature. The integrated intensity at $(0,11,\frac{1}{2})$ decreases smoothly with increasing temperature, and vanishes just at T_{MI} (Fig. 1). The result definitely illustrates that the structural distortion is the primary order parameter of the MI transition.

Synchrotron radiation experiments were carried out for an estimation of the space group below T_{MI}. We first confirmed the reflection condition. We observed weak superlattice reflections at $(h,0,\frac{1}{2})$ at 30 K. Total reflection condition was thus as follows; for the superlattice ($c'=2c$), $hkl: h+k+l=2n, hk0: h+k=2n, h0l: h+l=2n, 0kl: k+l=2n, h00: h=2n, 0k0: k=2n, 00l: l=2n$. Therefore the superlattice is an I lattice without any glide plane. We then measured four superlattice reflections $(0,\pm7,\pm0.5)$, and found that the diffracted intensities are not all the same to each other. Inequality in the diffracted intensities indicates that the crystal structure below T_{MI} is a monoclinic lattice of the unique a axis. From above results, possible space groups are $I211, Im11$ and $I2/m11$. Since the MI transition is of second order, the space group below T_{MI} is a subgroup of the space group above T_{MI} ($Cmcm$). Under this restriction, two group-subgroup chains are possible; (i) $Cmcm \rightarrow C2/m11 \rightarrow I2/c11 \rightarrow I211$, (ii) $Cmcm \rightarrow Cm2m \rightarrow Im2m \rightarrow Im11$.

It is likely that the overall pattern of superlattice reflections in a monoclinic lattice should be reminiscent of that in its supergroup. In this sense, the space group $I211$ is not plausible. The space group $I2/c11$ (the supergroup of $I211$) has a reflection condition $k,l=2n$ for $0kl$. This is inconsistent with the intense superlattice reflections observed at $(0,k,\frac{1}{2})$. On the other hand, the reflection conditions of $Im2m$ are the same as the observed ones. Accordingly, the best candidate for the space group below T_{MI} is $Im11$. We also think that the space group $Im2m$ (the supergroup of $Im11$) already contains major features of the transition, because superlattice reflections appear at this space group. From an argument of the symmetry, we can infer the origin of the MI transition. A notable difference between the space groups $Cmcm$ and $Im2m$ is the number of the vanadium sites. All vanadium ions are equivalent in $Cmcm$, whereas in $Im2m$ the vanadium ions are divided into two crystallographically independent sites. It is therefore likely that a charge disproportionation of the vanadium ions is the major driving force of the MI transition in $BaVS_3$.

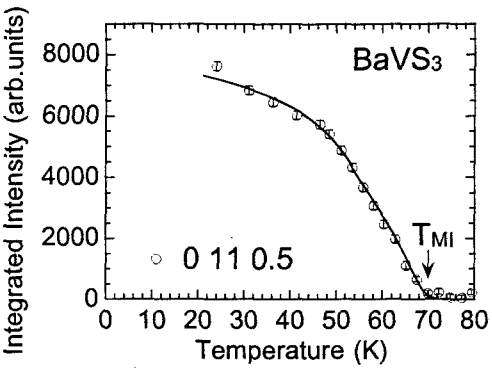

Fig. 1: Integrated intensity of a superlattice reflection as a function of temperature

References

1) G. Mihály *et al.*, Phys. Rev. B, **61**, R7831, 2000
2) M. Ghedira *et al.*, J. Phys. C: Solid State Phys., **19**, 6489, 1986

5.5.3 Resonant x-ray scattering study on the filled skutterudite $PrFe_4P_{12}$

Kenji ISHII, Toshiya INAMI, Youichi MURAKAMI, Lijie HAO [a], Kazuaki IWASA [a], Masahumi KOHGI [a], Yuji AOKI [a], Hitoshi SUGAWARA [a], Hideyuki SATO [a], Shin IMADA [b], Hironori NAKAO [c], Yusuke WAKABAYASHI [d], Hiroshi SAWA [d]

a) Department of Physics, Tokyo Metropolitan University, b) Department of Material Physics, Osaka University
c) Department of Physics, Tohoku University, d) Photon Factory, Institute of Materials Structure Science

1. Introduction

The filled skutterudites RT_4X_{12} (R = rare earth, T = Fe, Ru, and Os, X = P, As, and Sb), which crystallize in a *bcc* structure, exhibit a wide variety of electronic properties, such as superconductivity, magnetic order, and metal-insulator transition. Among them, our interest in $PrFe_4P_{12}$ stems from the anomalous ordered state at low temperatures. The phase transition at T_A = 6.5 K is confirmed by the specific heat measurement[1], but no magnetic reflection was observed in neutron powder diffraction[2]. On the other hand, the lattice distortion characterized by the modulation wave vector of **q** = [1,0,0] was observed below T_A in recent x-ray diffraction study[3]. A magnetic field induced antiferromagnetic moment with the same characteristic wave vector **q** as above was also observed at temperatures below T_A by a neutron diffraction experiment[4]. These facts strongly suggest that the phase transition at T_A is accompanied by an antiferroquadrupolar ordering. This ordered state is suppressed by magnetic field, and a heavy-fermion-like behavior appears, which is evidenced by large electronic specific heat coefficient and large cyclotron effective mass. Here we report the resonant x-ray scattering (RXS) experiments at the Pr-L_{III} absorption edge to investigate the ordered state of $PrFe_4P_{12}$. RXS is a combined technique of diffraction and spectroscopy, and can elucidate a spatially ordered electronic state, such as charge, magnetic, and orbital order.

2. Experimental

Single crystals of $PrFe_4P_{12}$ were grown by a tin-flux method. X-ray scattering experiments were carried out at beamline 4C and 16A2 at Photon Factory, KEK. We measured three reflections, (300), (111), and (210) which are forbidden in the *bcc* structure above T_A and become allowed below T_A due to the lattice distortion.

3. Result and Discussion

Figure 1 shows fluorescence and scattering intensity of (111) reflection near the Pr-L_{III} absorption edge. Two resonant features were observed around 5.965 eV and 6.000 eV. We also observed the resonance in (300) and (210) reflections. The scattering amplitude of the superlattice reflections at the absorption edge of Pr consists of two components, the lattice distortion and the resonant scattering of Pr. If both components are finite, interference term appears in the intensity. The assumption that Pr atoms do not change the position at the phase transition is reasonable in the structural model proposed experimentally[3] and theoretically[5]. Based on this assumption, resonant scattering term for the odd number of *h+k+l* corresponds to the difference of anomalous scattering factor between two Pr atoms in the *bcc* unit cell. Anomalous scattering factor is closely related to the electronic states of resonating atom. Therefore our result suggests a spatial ordering of two different electronic states of Pr atom, which is probably an antiferroquadrupolar ordering, appears below T_A

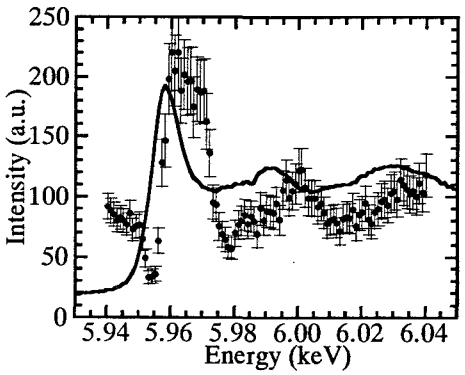

Fig. 1 X-ray energy dependence of fluorescence yield (solid line) and (111) reflection (filled circles)

References

1) T. D. Matsuda *et al.*, Physica B **281-282**, 220, 2000.
2) L. Keller *et al.*, J. Alloys Compd. **323-324**, 516, 2001.
3) K. Iwasa *et al.*, Physica B **312-313**, 834, 2002.
4) L. Hao *et al.*, to be published.
5) S. H. Curnoe *et al.*, Physica B **312-313**, 837, 2002.

5.6 Electronic Material Science

5.6.1 Study of beam fluctuation of high speed variably-polarizing undulator APPLE-2 at BL23SU at SPring-8 using the wavelet transformation

Akane AGUI, Tomohiro MATSUSHITA [a)], Takeshi NAKATANI, Akitaka YOSHIGOE, Hitoshi TANAKA [a)], Masaru TAKAO[a)] , Hideki AOYAGI [a)] and Masao TAKEUCHI [a)]
a) Japan Synchrotron Radiation Research Institute

1. Introduction

Circular dichroism (CD) experiments require good polarization quality and fast switching of photon helicity. To promote high-sensitivity studies and to improve the signal-and-noise ratio, the monochromator control system was synchronized to the movement of the magnetic row (phase shift) of an APPLE-2 type variably-polarizing undulator (ID23).[1,2] The magnetic field error of an undulator might cause electron-beam fluctuations in the storage ring. We have introduced the wavelet transformation for the analysis of the e-beam position in the SPring-8 storage ring. Using the result a new correlation table of steering magnets for ID23.[3]

2. Experimental system

Figure 1 shows the ID23 phase motion (a) and the raw data of the e-beam position (b) in the storage ring. The ID23 phase motion maight cause the position shift of the e- beam may but this signal is hidden by the white noise and the low frequency background. We applied the wavelet transformation to analyze of the noise elements in the raw data (b) and got the wavelet intensity for-1~-4th octave elements. The e-beam fluctuation caused by ID23 phase motion was successfully extracted after the wavelet filtering (e).

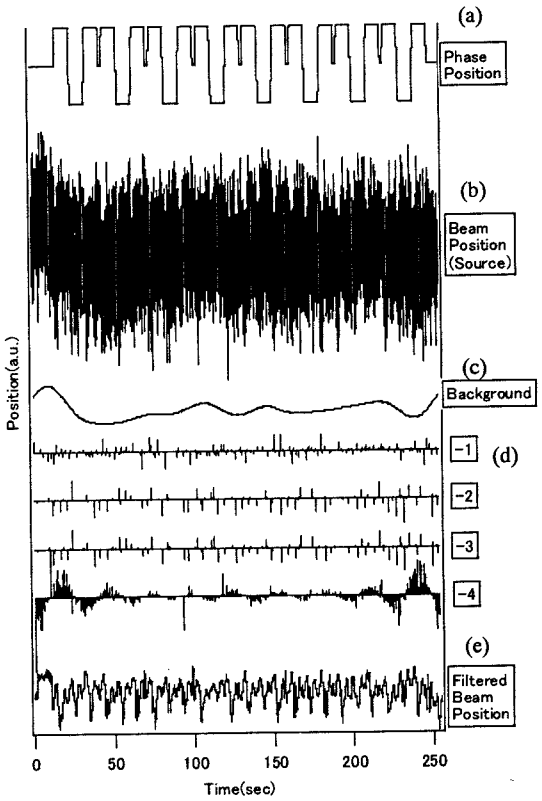

Fig. 1 The wavelet transformation of the electron orbital signal
Background (c) is calculated by WT. The captions –1, • • , –4 (d) are the octave of the wavelets.

3. Result

By using the wavelet transformation analysis, we have improved the correlation table of the steering magnets for ID23. Figure 2 shows the e-beam position for the static phase position at gap distance 60 mm as an example of the improvement. The static e-beam fluctuation is repressed below ±5 μm.

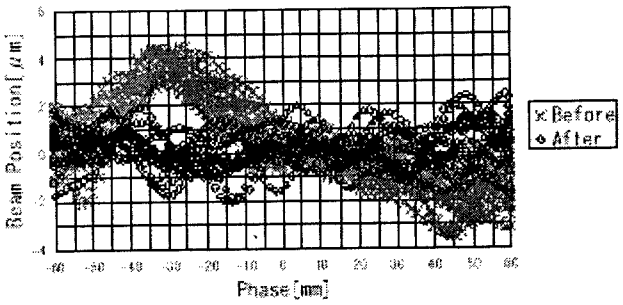

Fig. 2 Beam fluctuation at gap distance 60 mm × before and ○ after

References

1) A. Agui *et al.,* Rev. Sci. Inst, 72, 3191, 2001
2) A. Yokoya, *at al.*, J. Synchrotron Rad. 5, 10,1998
3) A. Agui *et al.* JAERI-Tech 2002-064, 2002

5.6.2 Photoemission spectroscopy of $YbCu_{5-x}Ag_x$

Tetsuo OKANE, Sin-ichi FUJIMORI, Kazutoshi MAMIYA, Jun OKAMOTO, Yasuji MURAMATSU, Atsushi. FUJIMORI[a], Naoto TSUJII[b] and Kazuyoshi YOSHIMURA[c]
a) University of Tokyo, b) National Institute for Materials Science, c) Kyoto University

1. Introduction

$YbCu_4Ag$ shows a typical dense Kondo behavior and has a moderately large electronic specific heat coefficient of γ 245 mJ/mol K^2. Its solid solution system $YbCu_{5-x}Ag_x$ crystallizes in the cubic $AuBe_5$-type structure in the range of 0.125 x 1 and belongs to a series of dense Kondo compounds[1]. It was experimentally confirmed that, in going from x =1.0 to 0.25, the Kondo temperature decreases and the specific heat coefficient γ increases from 210 to 440 mJ/ mol K^2.[1] In this study, we have performed the high-resolution photoemission spectroscopy (PES) experiments for the alloy system $YbCu_{5-x}Ag_x$ (x = 1.0, 0.7, 0.5, 0.25) to elucidate their electronic structure variation depending on the Ag concentration x.

2. Experiments

The PES spectra were measured with two excitation energies: He I radiation ($h\nu$ = 21.2 eV) produced by a He discharge lamp and synchrotron radiation ($h\nu$ = 700 eV) produced at the beamline BL23SU of SPring-8. The energy resolution for the He I and synchrotron radiation measurements were 5 meV and 200 meV, respectively.

3. Results

Figure 1 shows the valence band spectra of $YbCu_{5-x}Ag_x$ for $h\nu$ =700 eV. The two peaks at binding energies E_B of about 0.1 and 1.4 eV are the spin-orbit-doublet of the Yb^{2+} $4f^{13}{}_{7/2}$ and $4f^{13}{}_{5/2}$ final states. The complicated peak structures in the range from 5 to 11 eV are the Yb^{3+} $4f^{12}$ multiplet. Small humps around 1.0 and 2.3 eV are the surface component of the spin-orbit-doublet of the Yb^{2+} $4f$ signal. As x decreases, the intensity of the Yb^{2+} signal decreases and the intensity of the Yb^{3+} signal increases. Thus, the intensity ratio Yb^{3+}/Yb^{2+} increases with decreasing x, meanimg an increase in the Yb $4f$ hole number and thus an increase in the Yb valence. This tendency is consistent with the increase in the γ value with decreasing x. One can also notice that the peak positions of the Yb^{3+} $4f$ multiplet structure shift towards E_F as x decreases. This indicates a rise of the $4f$ energy level with decreasing x, which leads to the stabilization of the Yb^{3+} configuration compared to Yb^{2+}. The near-E_F region measured with a high energy resolution is shown in Fig. 2. The observed peak structure in each spectrum is regarded as the Kondo peak whose energy position, intensity, and width can be related to the Kondo temperature of the compounds[2]. As x decreases, the intensity of the Kondo peak decreases and its energy position shifts from 20 meV to 14 meV in going from x =1.0 to 0.25. The behavior can be interpreted as reflecting the drop of the Kondo temperature with decreasing x, based on the Kondo scaling scenario of the single impurity Anderson model using non-crossing approximation[2].

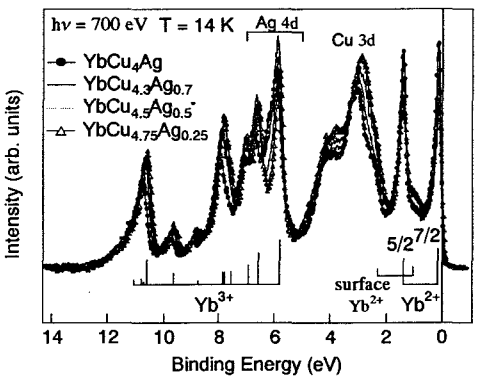

Fig. 1 Valence band SRPES spectra of $YbCu_{5-x}Ag_x$

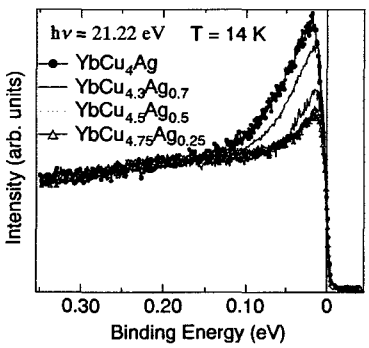

Fig. 2 Temperature dependence of near-E_F region

References

1) N.Tsujii, J.He, N.Hamdaoui, A. Herr, and A.Meyer., Phys. Rev. B **55**, 1032, 1997.
2) N.E. Bickers, D.L. Cox, and J.W. Wilkins, Phys. Rev. B **36**, 2036, 1987.

5.6.3 Photoemission study of Ce*M*In$_5$ (*M*=Rh, Ir): nearly localized nature of *f* elecrons

Shin-ichi FUJIMORI, Tetsuo OKANE, Jun OKAMOTO, Kazutoshi MAMIYA Yasuji MURAMATSU, Atsushi FUJIMORI[a)], Hisatomo HARIMA[b)], Dai AOKI[c)], Shugo IKEDA[c)], Hiroaki SHISHIDO[c)], Yoshifumi TOKIWA[c)], Yoshinori HAGA[d)] and Yoshichika ÔNUKI[c,d)]

a) University of Tokyo, b) ISIR-SANKEN, c) Graduate School of Science, Osaka University, d) Advanced Science Research Center, Japan Atomic Energy Research Institue

1. Introduction

Recently, a new class of heavy-fermion Ce-based compounds Ce*M*In$_5$ (*M*=Rh and Ir) has been discovered. They attract much attention in recent years, since they are considered to be located near a quantum critical point of the Doniach phase diagram. CeRhIn$_5$ displays antiferromagnetism with T_N=3.8K in ambient pressure, but it undergoes superconducting state under high pressure. On the other hand, CeIrIn$_5$ is a superconductor with T_C=0.4 K in ambient pressure. In the present study, the electronic structures of these two compounds are investigated by the resonant photoelectron spectroscopy.

2. Results

The experiments are performed at BL23SU at SPring-8. Figure 1 (a) shows Ce $3d_{5/2}$ XAS spectrum of Ce*M*In$_5$. We have constructed the Ce 4*f* derived spectra by subtracting the off-resonance spectra (*h*ν=870 eV) from on-resonance spectra (*h*ν=881.2 eV). Figure 1 (b) shows the Ce 4*f* partial spectra. The spectra consist of the f^1 final-state peak located just below the Fermi level and the f^0 final-state peak at about 2 eV. These spectral features have been observed in other Ce-based compounds, and understood within the framework of the single impurity Anderson model (SIAM). According to SIAM, the stronger the *f* electrons hybridize with conduction electrons, the stronger the f^1 peak becomes. Here, the intensity of f^0 final state peak, located at 2 eV, is very strong compared with other HF Ce-based compounds measured so far, such as $CeRu_2Si_2$, where the f^0 final state peak intensity was extremely weak. In addition, the peak intensity of $3d^9 4f^1$ final state in the XAS spectrum of CeIrIn$_5$, which originated from $4f^0$ state in the ground state, is almost invisible, suggesting that the number of Ce 4*f* electrons in the initial state is very close to the unity. This strongly argues that the Ce 4*f* electrons in these compounds are in the nearly localized regime. We also note that although both spectra are very similar, the f^1 to f^0 intensity ratio is somewhat large in CeIrIn$_5$ compared with that of CeRhIn$_5$. This indicates that the hybridization between the conduction electrons and the Ce 4*f* electrons in CeIrIn$_5$ is slightly larger than that in CeRhIn5. This suggests that although the Ce 4*f* sates in these compounds are very similar, the hybridization is a little stronger in CeIrIn$_5$ than in CeRhIn$_5$. This is consistent with the fact that CeIrIn$_5$ corresponds to CeRhIn$_5$ under pressure.

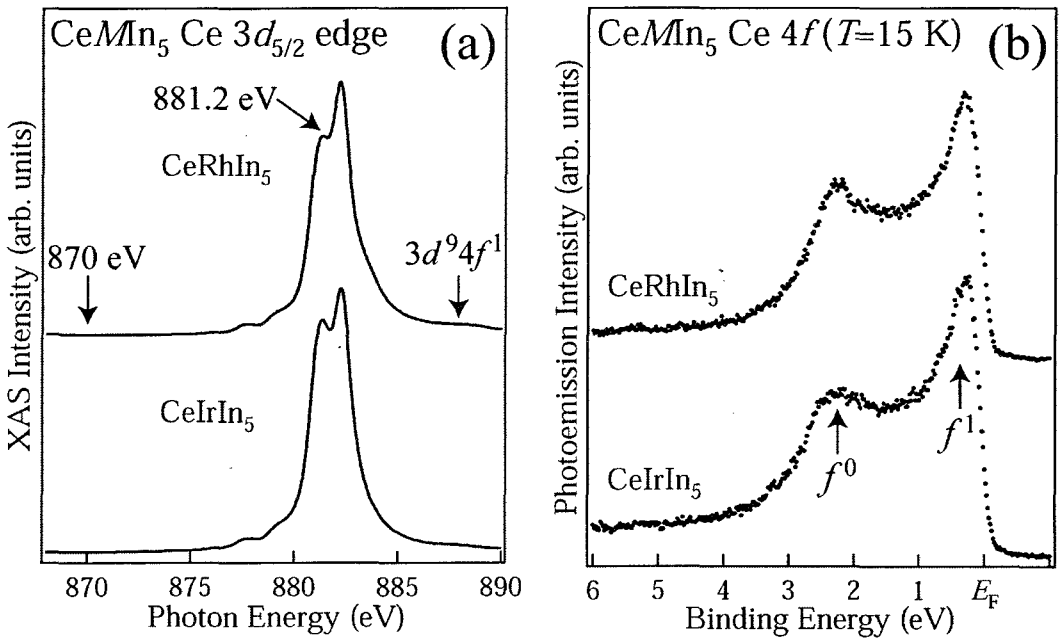

Fig. 1 (a)Ce $3d_{5/2}$ XAS spectra of Ce*M*In$_5$ (b)Ce $3d$-$4f$ RPES spectra of Ce*M*In$_5$.

5.6.4 Electronic structure of the pyrochlore-type Ru oxides through the metal-insulator transition

Jun OKAMOTO, Shin-ichi FUJIMORI, Tetsuo OKANE, Atsushi FUJIMORI[a)], Miguel ABBATE[b)], Shunsuke YOSHII[c)] and Masatoshi SATO[d)]
a) University of Tokyo, b) Universidade Federal de Parana, c) KYOKUGEN , d) Nagoya University

1. Introduction

It has been reported that pyrochlore-type Ru oxides $A_2Ru_2O_7$ show a wide range of electrical properties for different *A*-site ions[1)] and is expected that the effect of electron correlation plays important roles in their electronic structure and physical properties. $Sm_{2-x}Bi_xRu_2O_7$ ($0 < x < 2$) exhibits the Mott insulator to metal transition with increasing Bi concentration, in other words, changing the Ru *4d* t_{2g} band width.[1),2)] $Sm_{2-x}Ca_xRu_2O_7$ ($0 < x < 0.6$) also shows metal-semiconductor transition with increasing Ca concentration, in other words, doping holes in the Ru *4d* t_{2g} band.[3)] Those electronic structures have been measured systematically through metal-insulator transition by ultraviolet photoemission spectroscopy (UPS).

2.Result

As for the spectral changes near the Fermi level, as shown in the insets of Figs. 1 and 2, in both systems spectral intensity near the Fermi level increases monotonically through the metal-insulator transition, which well corresponds to the doping dependence of the transport properties. Spectral changes in the entire Ru *4d* t_{2g} band, however, are different from each other as shown in Figs 1 and 2. In the Fig. 1, with increasing Ca concentration, the O *2p* band edge around 2.5 eV shifts closer to the Fermi level without large changes in the shape of the Ru *4d* t_{2g} band. In the Fig. 2, with increasing Bi concentration, the spectral weight near the Fermi level of the Ru *4d* t_{2g} band which has close relationship with the metallic conductivity is transferred from the higher energy region. It is concluded that this difference has close relationship with the different routes of the metal-insulator transition in those systems, hole-doping or band-width control.

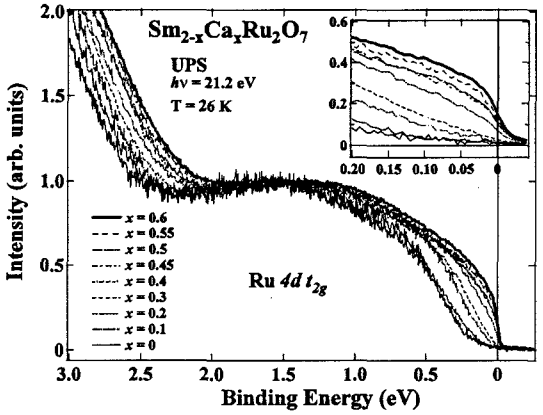

Fig. 1 UPS spectra of $Sm_{2-x}Ca_xRu_2O_7$ ($0 < x < 0.6$) through the metal-insulator transition
Inset shows spectral changes near the Fermi level.

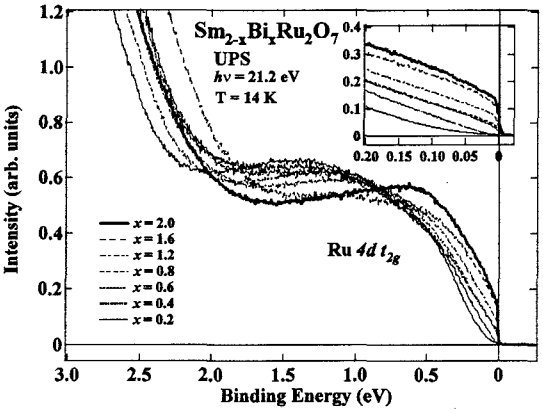

Fig. 2 UPS spectra of $m_{2-x}Bi_xRu_2O_7$ ($0.2 < x < 2$) through the metal-insulator transition
Inset shows spectral changes near the Fermi level.

References

1) J. B. Goodenough *et al.*, *Localization and Metal-Insulator Transition*, p.161 1985
2) T. Yamamoto *et al.*, J. of Solid State Chem. **109**, 372, 1994
3) S. Yoshii,*et al.*, J. of Phys. Soc. Jpn. **69**, 17, 2000.

5.6.5 Study of magnetic circular x-ray dichroism measuring system at BL23SU

Jun OKAMOTO, Kazutoshi MAMIYA, Shin-ichi FUJIMORI, Tetsuo OKANE, Yuji SAITOH, Yasuji MURAMATSU and Atsushi FUJIMORI[a)]
a) University of Tokyo

1. Introduction

Magnetic circular x-ray dichroism (MCXD) in the core-level soft x-ray absorption is a powerful method to obtain information about the magnetic states at each atomic site. With use of the magneto-optical sum rules, it gives the orbital[1)] and spin[2)] magnetic moments on each atom that composes the measured magnetic compound.

2. Experimental system

MCXD measuring system at BL23SU mainly consists of a superconducting magnet and a sample chamber. The base pressure of the chamber is 4×10^{-7} Pa at RT. Sample can be cooled down to 10 K with use of a *Liq.* He flow cryostat. The sample surface is cleaned by *in situ* scraping before each measurement. The superconducting magnet generates magnetic field up to 10 T parallel and anti-parallel to the propagation vector of the incident circularly polarized light.

3. Result

Figure 1 shows the Co *2p* MCXD spectra of $La_{1-x}Sr_xCoO_3$ (x = 0.1, 0.4, 0.8). $La_{1-x}Sr_xCoO_3$ becomes metallic and ferromagnetic as increasing Sr doping: semiconducting spin-glass state at x = 0.1 and itinerant ferromagnetic state at x = 0.4 and x = 0.8.[3)] The intensity of the MCXD structure is proportional to the amount of the total magnetic moment of the $La_{1-x}Sr_xCoO_3$ and the spectral change around the Co $2p_{3/2}$ peak corresponds to the itinerant property of the $La_{1-x}Sr_xCoO_3$ as previously reported.[3)] Figure 2 shows the Fe *2p* MCXD measurement of $SrFeO_3$ at 150 K. $SrFeO_3$ shows a spiral anti-ferromagnetic transition at 134 K[4)] and is expected to have strong ferromagnetic correlation between nearest neighbor Fe ions. MCXD structure of 6 % have been observed around Fe $2p_{3/2}$ peak under magnetic field of 8 T even in the paramagnetic state. It is shown that MCXD structure can be observed even at paramagnetic phase where strong ferromagnetic correlation exists by using the superconducting magnet.

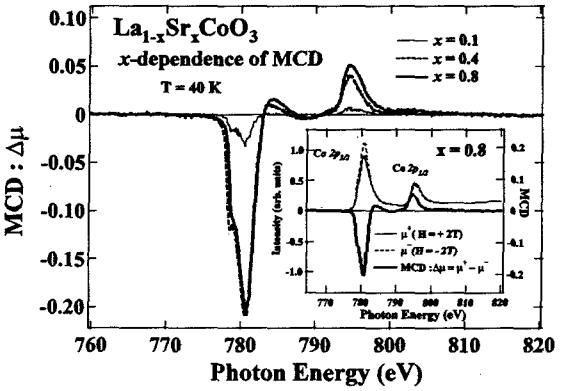

Fig. 1 Co *2p* MCXD spectra of $La_{1-x}Sr_xCoO_3$ (x = 0.1, 0.4, and 0.8) Inset shows the Co *2p* XAS and MCXD spectra of $La_{0.2}Sr_{0.8}CoO_3$.

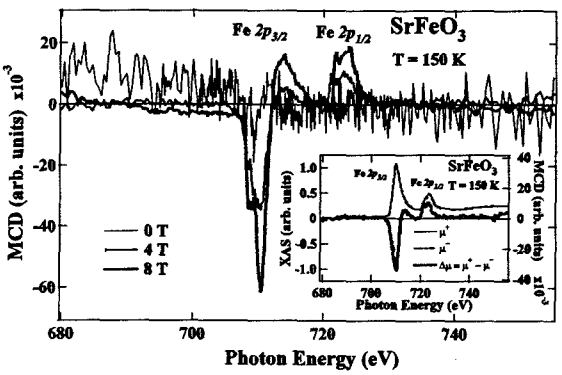

Fig. 2 Fe *2p* MCXD spectra of $SrFeO_3$ at paramagnetic phase (at 150 K) Inset shows the Fe *2p* XAS and MCXD spectra of $SrFeO_3$ under magntic field of ± 4 T.

References

1) B. T. Thole *et al.*, Phys. Rev. Lett. **68**, 1943 (1992).
2) P. Carra *et al.*, Phys. Rev. Lett., **70**, 152 (1995).
3) J. Okamoto *et al.*, Phys. Rev. B **62**, 4455 (2000).
4) Y. M. Zhao *et al.*, Phys. Rev. B **64**, 024414 (2001).

5.6.6 Soft x-ray spectroscopic studies of Fe_xNbS_2

Yuji SAITOH, Keisuke KOBAYASHI[a)], Atsushi FUJIMORI[b)],
Yasuhisa YAMAMURA[c)], Toshihide TSUJI[c)], Mikio KOYANO[c)] and Shin-ichi KATAYAMA[c)]
a) Japan Synchrotron Radiation Research Institute, b) University of Tokyo, c) Japan Advanced Institute of Science and Technology

1. Introduction

There has been much interest in the properties of layered structure transition-metal dichalcogenides, TX_2. They exhibit charge density wave distortions and also can be intercalated by a wide variety materials ranging from organic amines to alkali metals and transition metals. The intercalation reaction of interest in this work is usually accompanied by charge transfer from the intercalant to the host layer, leading to fine-tune the electronic properties of the host material in a controllable way.

Among the intercalation compounds we have selected in this work is Fe_xNbS_2. The intercalation of Fe atoms into the octahedral sites between the van der Waals gaps of the $2H$-NbS_2 layers yields a new magnetic system of Fe_xNbS_2. It is known that $2a \times 2a$ and $\sqrt{3}\,a \times \sqrt{3}\,a$ nano-size superstructures of Fe atoms for x=1/4 and 1/3, respectively, exhibit antiferromagnetic ordering at low temperatures[1)]. Recent study has revealed that the sample with x~1/3 shows three anomalies in both heat capacity and magnetic susceptibility in the temperature range of 40-50K.It is, therefore, important to understand how the magnetic properties of Fe layers affect the host NbS_2 layers.

On the experimental side, on the other hand, the characterization of interfaces is a challenging problem in material science. It becomes increasingly more important not only for fundamental understanding but also for device applications. Experimental techniques capable of providing element specific information about local structure, electronic structure and magnetic structure are essential for the studies of layered magnetic systems such as Fe_xNbS_2. In this study, we applied high-resolution soft x-ray photoemission spectroscopy to Fe_xNbS_2 (x=0.239 and 0.325) in order to check the feasibility as a tool for extracting the interfacial information.

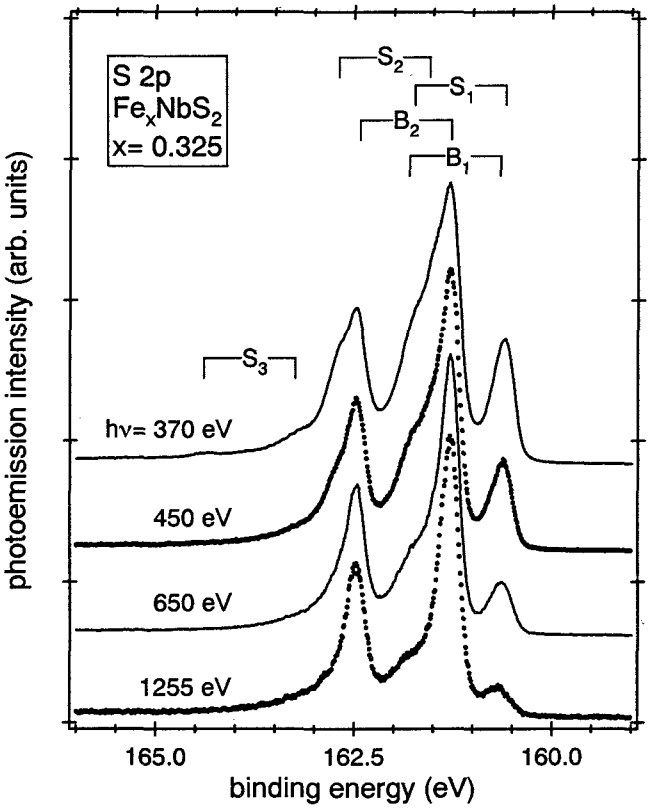

Fig. 1 S 2p photoemission spectra of $Fe_{0.325}NbS_2$

2. Experimental results

Figure 1 shows the S 2p photoemission spectra of $Fe_{0.325}NbS_2$ measured at various photon energies ($h\nu$). Many components observed in the figure are due to core level shifts arising from different chemical and structural environments. The photon energy dependence reveals that the surface region is different from bulk (interface) in electronic structure. We found that the high-resolution core-level photoemission spectroscopy has the capability of isolating the interfacial electronic structure.

In addition, we have measured Fe 2p and Nb 3d core-level spectra and observed x dependence of the spectral line shapes.

Reference

1) F. Hulliger and E. Pobitschka, J. Solid State Chem., 1, 117, 1970.

5.6.7 Total-electron-yield x-ray standing-wave measurements of multilayer x-ray mirrors for interface structure evaluation

Yasuji MURAMATSU, Hisataka TAKENAKA[a], Eric M. GULLIKSON[b]
and Rupert C. C. PERERA[b]
a) NTT Advanced Technology Corporation,
b) Center for X-Ray Optics, Lawrence Berkeley National Laboratory

1. Introduction

Functional multilayer x-ray mirrors are needed for the high-flux x-ray optical systems used with highly brilliant synchrotron/laser-plasma x-rays. In the development of such multilayer x-ray mirrors, optical evaluations of reflectivity and layer/interface structure are necessary for improving their optical quality. Reflectivity and layer structure information have typically been obtained from Bragg reflection measurements, while details of the interface structure are usually evaluated by transmission electron spectroscopy (TEM) which is regarded as a *destructive* method. For evaluation of the interface structure of multilayer x-ray mirrors, x-ray standing-wave measurements in the soft x-ray region have recently proved to be a powerful tool for *nondestructive* evaluation of interface roughness and layer density.

In this study, total-electron-yield (TEY) x-ray standing-wave measurements of multilayer x-ray mirrors have been performed, by monitoring sample photocurrents to obtain information on their layer/interface structure. Specifically, we have measured mapping spectra of x-ray standing-wave signals in a Mo/Si multilayer at normal incidence, which visibly illustrates the spatial distribution of layer structure in the sample plane [1,2].

2. Experiments

The Mo/Si multilayer x-ray mirror, deposited on a 4-inch silicon wafer, consists of 50 periods of 19.6-Å Mo and 45.2-Å Si layers. In this multilayer, Bragg reflection condition will be satisfied around the 90 eV region for near normal incidence. Optical measurements were carried out in beamline BL-6.3.2 at the Advanced Light Source (ALS). The multilayer x-ray mirror sample is mounted on a sample holder in the reflectmeter and a wire is connected to monitor the sample photocurrent. In total electron yield (TEY) x-ray absorption spectral measurements, x-ray standing-wave structure is observed when the photon-energy/wavelength of incident x-rays and the incident angle satisfy the Bragg reflection condition of the multilayer sample. Energy resolution (E/ E) of incident x-rays in these measurements is estimated to be about 10^4 in the region around 90 eV with a 20-μm exit slit and a 600-line/mm grating of the beamline monochromator.

3. Results and Discussion

Figure 1 shows the TEY x-ray standing-wave spectra of a Mo/Si multilayer mirror measured along the 4-inch-wafer-size sample plane at the center (denoted by A in the Figure), middle (Bx, By) and periphery (Cx, Cy) positions. In the center position spectrum, standing-wave structures are observed near 96 eV and the standing-wave peak is observed at 97.68 eV. In the spectra of the middle and periphery positions, standing-wave structures are clearly shifted to higher-energy regions. Figure 2 shows the mapping spectrum of TEY x-ray standing-wave signals over the quarter of the 4-inch-wafer-size Mo/Si multilayer mirror measured with an incident angle of 90°. The photon energy of incident x-rays is fixed at 97.68 eV, identical to the peak energy of the center position x-ray standing-wave. The spot size of incident x-rays on samples is estimated to be less than 0.5 mm$^{\phi}$, and spectra are obtained using a 1-mm step scan along the x- and y-axes. This figure depicts periodic-length-changes of Mo/Si layers in the sample plane; the Mo/Si layers gradually become shorter from the center toward the periphery. The contour line also reveals a distribution of layer structure that is slightly wider along the y-axis than along the x-axis. This implies the sputtering source gas used in the deposition process of the multilayers is distributed slightly offset from the y-axis. These results indicate that TEY x-ray standing-wave measurements are useful for evaluating the layer/interface structure of multilayer x-ray mirrors.

This work is supported by the Hyogo Science and Technology Association and the US Department of Energy under contract No. DE-AC03-76SF00098.

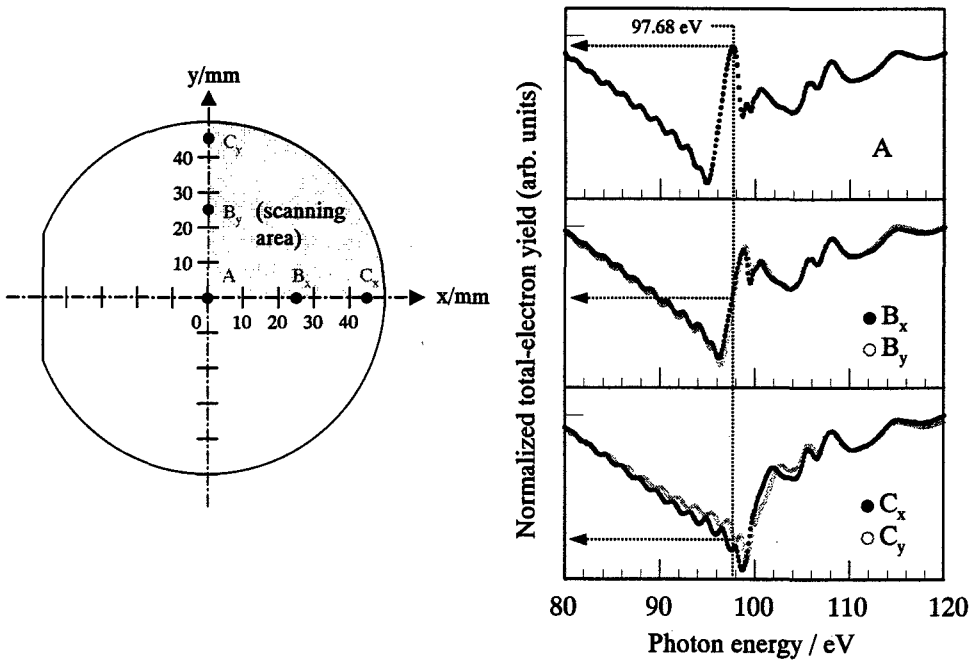

Fig. 1 TEY x-ray standing-wave spectra of the Mo/Si multilayer measured at the center (denoted by A), middle (Bx, By), and edge (Cx, Cy) positions along the 4-inch sample plane

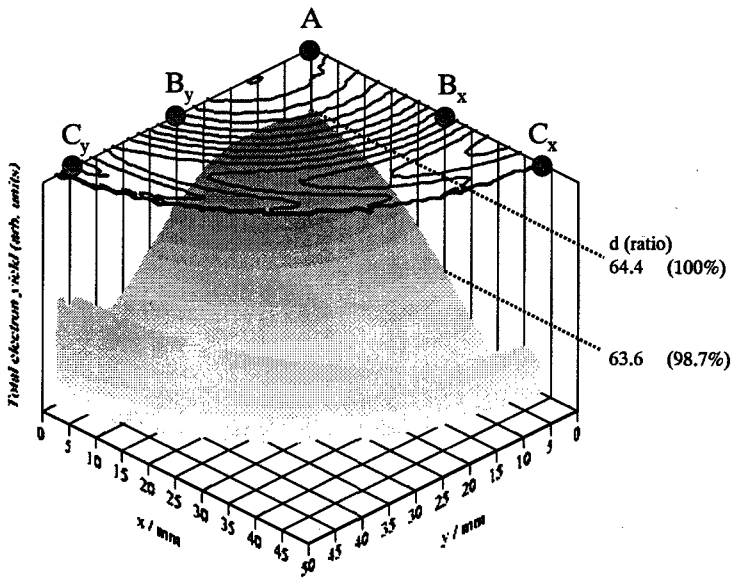

Fig. 2 Mapping spectrum of the TEY x-ray standing-wave signals in the quarter of the 4-inch-wafer-size Mo/Si multilayer measured with an incident angle of 90°
The photon energy of incident x-rays is fixed at 97.68 eV.

References

1) Y. Muramatsu, H. Takenaka, E. M. Gullikson, and R. C. C. Perera, Jpn. J. Appl. Phys., **41**, 4250, 2002.
2) Y. Muramatsu, H. Takenaka, E. M. Gullikson, and R. C. C. Perera, Advances in X-Ray Chemical Analysis, Japan, **33**, 145, 2002.

5.6.8 Theoretically predicted soft x-ray emission and absorption spectra of graphitic-structured BC_2N

Yasuji MURAMATSU

1. Introduction

In the search for advanced materials with novel physical and chemical properties, boron/carbon/nitrogen materials are attractive targets. A new and particularly exciting area for such BCN materials is the synthesis and characterization of graphitic-structured BC_2N. In the synthesis of graphitic-structured BC_2N materials, structural characterization is important because various structural isomers are possible and the properties of each exhibit strong structural dependence. For the characterization of composite materials consisting solely of light elements, high-resolution soft x-ray emission and absorption spectroscopy using synchrotron radiation is a powerful tool that reveals detailed information regarding the electronic and chemical structure. Spectroscopic analysis of these x-ray spectra can best be achieved using discrete variational (DV) Xα molecular orbital (MO) calculations, which approximately reproduce the x-ray spectral features from the calculated density-of-states (DOS) spectra. Characterizing graphitic-structured BC_2N materials using soft x-ray emission and absorption spectroscopy requires theoretically calculated x-ray spectra in order to identify the x-ray spectral features of the various structural isomers. Here, the author reports theoretically predicted x-ray emission and absorption spectra calculated for the possible structural isomers of BC_2N using DV-Xα MO calculations[1].

2. DV-Xα MO Calculations

Three possible structures of BC_2N were predicted by Liu et al. as shown in Figure 1. Carbon atoms in model (a) form poly-acetylene-like structures. Each carbon atom in model (b) is bound to carbon, boron, and nitrogen atoms. There are two kinds of carbon atoms in model (c): one carbon atom is bound to one carbon atom and two boron atoms, while the other is bound to one carbon atom and two nitrogen atoms. Based on these structures, DV-Xα MO calculations were performed for the three cluster models of $B_{24}C_{48}N_{24}H_{24}$ and reference models of graphite ($C_{96}H_{24}$) and *h*-BN ($B_{48}N_{48}H_{24}$). The geometries of these model structures were initially optimized by the MM2 method. DV-Xα MO calculations of these cluster models were performed on the electronic ground states with a basis set of 1s, 2s, and 2p orbitals for B, C, and N atoms.

3. Results and Discussion

Figure 2 shows the occupied and unoccupied DOS spectra of 2s- and 2p-orbitals in B, C, and N atoms of the three BC_2N cluster models. DOS spectra for B and N atoms in *h*-BN and for C in graphite are also shown as references. The occupied DOS spectra of B atoms for all three BC_2N models exhibit a low-energy tail feature in B2p-DOS. However, the low-energy peak observed in *h*-BN is not observed in the BC_2N. This low-energy peak feature therefore represents an index for distinguishing BC_2N from *h*-BN. The high-energy features differ among the three BC_2N models. These differences in high-energy features will provide useful indices for identifying BC_2N structures in B *K* x-ray emission spectra. In the occupied DOS spectra of N atoms, the N2p-DOS spectrum of *h*-BN is the main peak feature with a high-energy peak and a low-energy step-like shoulder. However, such fine structure is not observed in the BC_2N models. This difference in N2p-DOS spectra between BC_2N and *h*-BN is another clear index for distinguishing BC_2N from *h*-BN. However, there is little significant difference in the N2p-DOS spectra among the three BC_2N models. It therefore appears difficult to distinguish between the three BC_2N structures based solely on N *K* x-ray emission spectra. In the occupied DOS spectra of C atoms, there are clear differences in C2p-DOS spectral features of the main peak and high-energy shoulder/peak between the BC_2N models and graphite. In the BC_2N models, there are clear differences among the three models. Spectral features of the main peak and high-energy peak in C *K* x-ray emission can also be used as indices for identifying BC_2N structures. In the unoccupied DOS spectra, there are distinctive differences in B2p-, N2p-, and C2p-DOS among the three BC_2N models and the reference *h*-BN and graphite in the fine threshold structures. This demonstrates that BC_2N structures can be identified from high-resolution x-ray absorption spectra at the B *K*, C *K*, and N *K* thresholds, in addition to identification using the above-mentioned x-ray emission spectra.

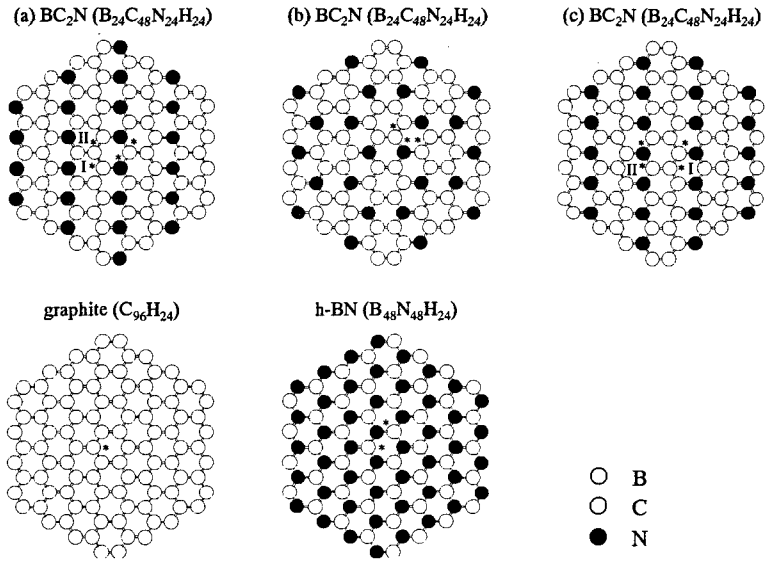

Fig. 1 Cluster models of three possible structural isomers of graphitic-structured BC_2N ($B_{24}C_{48}N_{24}H_{24}$) with references *h*-BN ($B_{48}N_{48}H_{24}$) and graphite ($C_{96}H_{24}$)
Hydrogen atoms terminating the edge atoms in the cluster models are not shown in the figure.

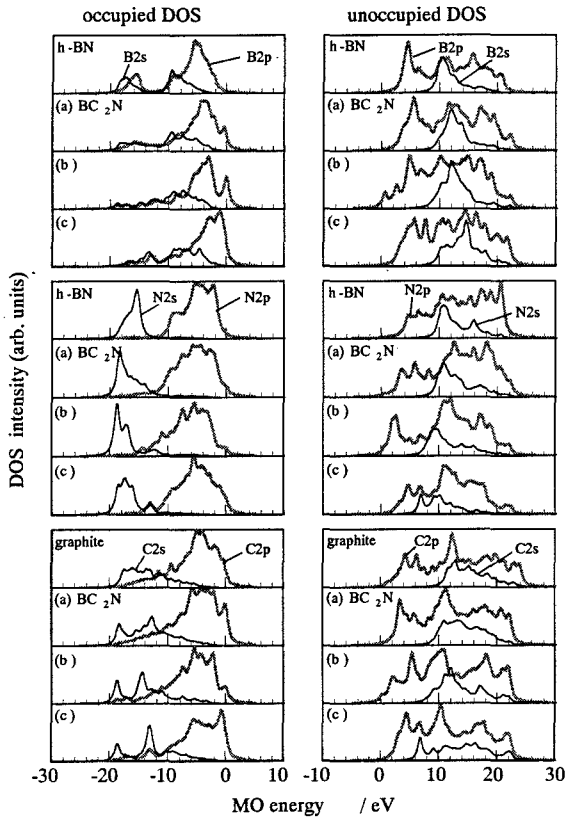

Fig. 2 Occupied and unoccupied DOS spectra of 2s- and 2p-orbitals in B, C and N atoms of the three BC_2N cluster models
Molecular structures of the BC_2N models (a – c) are shown in Fig. 1.

Reference

1) Y. Muramatsu, Advances in Quantum Chemistry (in press).

5.7 Synchrotron Radiation Simulation Research

5.7.1 Theory of Order and Excitations in Antiferro-quadrupolar Phase of CeB_6

Hiroyuki SHIBA[a) b)], Ryousuke SHIINA[c)], Atsushi TAKAHASHI[d)] and Peter THALMEIER[e)]

a) Department of Physics, Kobe Univ., Kobe 657-8501, Japan
b) JAERI, Hyogo 679-5198, Japan
c) Department of Physics, Tokyo Metropolitan Univ., Hachoji 192-0397, Japan
d) Department of Physics, Tokyo Institute of Technology, Tokyo 152-8501, Japan
e) Max-Planck-Institute for Chemical Physics of Solids, 01187 Dresden, Germany

1. Introduction

CeB_6 is a typical dense Kondo system, which exhibits at 3.3K a phase transition associated with antiferro-quadrupole order of 4f electrons of Ce ions. The nature of this phase transition was a mystery for some time, since the antiferro-quadrupole order cannot be observed by ordinary methods. Therefore it is a challenging problem for synchrotron radiation facilities. Nakao et al.[1)] have recently succeeded in detecting resonant X-ray scattering due to a staggered quadrupolar ordering. Prior to this experiment we proposed that the order parameter at zero magnetic field is a staggered order of Γ_5 quadrupoles with (1/2, 1/2, 1/2) and that the uniform magnetic field induces fairly large staggered octupoles of T_{xyz} with (1/2, 1/2, 1/2). Although the staggered order with (1/2, 1/2, 1/2) was detected, a unique identification of the order parameter is still needed. We believe it possibe by using the X-ray from sychrotron radiation facilities, although difficult. Another interesting problem, which has not been explored fully, is the excitations from the quadrupole ordered phase. Experimentally Bouvet[3)] carried out inelastic neutron scattering experiments by applying magnetic fields. However, no theoretical analysis was made so far except for our previous study[4)]. The purpose of our study is to clarify the nature of excitations in CeB_6.

2. Results

Since the crystal-field ground state of CeB_6 is Γ_8 quartet, there are 4 states. To describe all the transitions within the Γ_8 quartet and check the reliability of the results, we have used two independent methods: the equation-of-motion method and the Holstein-Primakoff method generalized for Γ_8 quartet[5)]. We have studied the excitations in finite magnetic fields. There are 6 branches for each wave vector, since there are 3 transitions from the ground state within the quartet and 2 sublattices are present. They are mixed multipolar modes, which contribute to various experiments in a different way. To compare with Bouvet's experiments, we have calculated the neutron scattering intensity, which picks up fluctuations of magnetic dipoles. Our results for a suitable set of parameters and 7T show that 2 branches have reasonably large intensities in neutron scattering: a strong peak around 1.5meV and a weak peak around 2.5meV. This result is in a good agreement with Bouvet's results. In this connection we have done some preliminary analyses on nonlinear couplings of the modes also, which might be important for some experiments.

3. Summary

We have studied theoretically the excitations in antiferro-quadrupole-ordered CeB_6. The neutron scattering intensitites have been calculated and compared with Bouvet's expeiments, which had been left out without any analyses. Thereby the present calculation could give an assignment of the modes observed by the neutron scattering.

References

1) H. Nakao *et al.*, J. Phys. Soc. Jpn. **70**, 18575, 2001
2) R. Shiina *et al.*, J. Phys. Soc. Jpn. **66**, 1741, 1997; ibid. **67**, 941, 1998
3) A. Bouvet, Ph. D. Thesis (Grenoble, 1993)
4) P. Thalmeier *et al.*, J. Phys. Soc. Jpn. **67**, 2363, 1998
5) R. Shiina, P. Thalmeier, A. Takahashi and H. Shiba., in preparation

6. List of Publications

6.1 List of publications on Advanced Photon Research Center

High peak power laser development (Laser System Development Group)

1. Journals

1) Second - harmonic generation of ultra-high intensity femtosecond pulses with a KDP crystal
M. Aoyama, T. Harimoto, J. Ma, Y. Akahane and K. Yamakawa
Opt. Exp. Vol.9, pp. 579-585 (2001)
2) Noncollinear SHG with compensation of phase mismatch by controlling frequency chirp and tilted pulse fronts of femtosecond laser pulses
M. Aoyama, T.Harimoto, F, Nakano, Y. Akahane and K. Yamakawa
Proceedings of CLEO / Pacific Rim 2001 , Chiba , Japan , July 2001
3) In-situ" Focused, peak intensity measurement by optical field ionization of Argon
Y. Akahane, S. Sagisaka, M. Aoyama, F, Nakano and K. Yamakawa
Proceedings of CLEO / Pacific Rim 2001 , Chiba , Japan , July 2001
4) Ultrafast, ultrahigh-peak power Ti: sapphire laser system
K. Yamakawa,M.Aoyama,S.Matsuoka, Y. Akahane,T. Kase, F. Nakano and S.Sagisaka
JAERI-RESEARCH 2000-051(2001)
5) Ultrahigh peak power lasers
K. Yamakawa
KOGAKU, "50 years aniversaly issue", vol. 31, p.287、2002 (in Japanese)
6) Status and Future Developments of Ultrahigh Intensity Lasers at JAERI
K. Yamakawa
AIP Conference Proceedings on Super Strong Fields in Plasmas, vol. 611, pp. 385-396, 2002
7) Suppression of cubic nonlinearity in second-harmonic generation of ultrahigh intensity laser pulses by initial frequency chirp
T. Harimoto, M. Aoyama, K. Yamakawa and M. Yonemura
Jpn. J. Appl. Phys., Vol. 41, pp.139-144, 2002
8) Compensation for third-order nonlinearity with initial phase mismatch in second-harmonic generation of ultrahigh intensity laser pulses
T. Harimoto, M. Aoyama, K. Yamakawa and M. Yonemura
Jpn. J. Appl. Phys., Vol. 41, pp.6859-6861, 2002
9) High power Nd:YAG laser with a ring-type phase conjugation mirror
K. Tei, F. Matsuoka and T. Arisawa
Rev. Laser Engineering, Vol.30, pp.182-185 2002 (in Japanese)
10) High-efficiency frequency doubling of a Nd:YAG laser in a two-pass quadrature frequency-conversion scheme using $CsLiB_6O_{10}$ crystals
Hiromitsu Kiriyama, Fumihiko Nakano and Koichi Yamakawa
Journal of the Optical Society of America B, Vol. 19, pp. 1857-1864 (2002)
11) Demonstration of high-efficiency, high-average-power second-harmonic generation in multi-pass quadrature arrangement using $CsLiB_6O_{10}$ crystals
Hiromitsu Kiriyama, Fumihiko Nakano and Koichi Yamakawa
Technical Digest 2001 Conference on Lasers and Electro-Optics (CLEO/QELS 2001), CtuM16, p.164(2001)
12) Multi-pass quadrature arrangement using $CsLiB_6O_{10}$ crystals for highly efficient second-harmonic generation of high-power Nd:YAG laser
Hiromitsu Kiriyama, Fumihiko Nakano and Koichi Yamakawa
Technical Digest 2001 Conference on Lasers and Electro-Optics/Pacific Rim (CLEO/Pacific Rim 2001), P1-46, p.II-150(2001)
13) Demonstration of quadrature arrangement using $CsLiB_6O_{10}$ crystals
Hiromitsu Kiriyama, Shinichi Matsuoka, Fumihiko Nakano and Koichi Yamakawa
JAERI-Research 2001-019(2001)
14) High efficiency second-harmonic generation in multi-pass quadrature arrangement
Hiromitsu Kiriyama, Fumihiko Nakano and Koichi Yamakawa

JAERI-Research 2001-030(2001)
15) Four-pass quadrature arrangement or highly efficient second-harmonic generation
Hiromitsu Kiriyama, Shinichi Matsuoka and Takashi Arisawa
JAERI-Research 2001-031(2001)
16) Laser Peak Intensity Measurements by Optical Field Ionizaton of Argon in a Relativistic Regime
Y. Akahane, A. Sagisaka, M. Aoyama, and K. Yamakawa
Technical Digest, Applications of High Field and Short Wavelength Sources IX (HFSW 2001) MB4 (2001)
17) 134 nm vacuum ultraviolet emission using an Ar/Kr gas mixture excited by a quasi-continuous-wave gas jet discharge
J. Kawanaka, S. Kubodera, and W. Sasaki
Appl. Phys. B, vol. 72, pp. 179-182 (2001)
18) 1.5 kW high-peak-power vacuum ultraviolet flash lamp using a pulsed silent discharge of krypton gas
J. Kawanaka, T. Shirai, S. Kubodera, and W. Sasaki
Appl. Phys. Lett. 79, pp. 3752-3754 (2001)
19) Observation of vacuum ultraviolet Kr_2* laser oscillation pumped by a compact discharge device
W. Sasaki, T. Shirai, S. Kubodera, J. Kawanaka and T. Igarashi
Optics. Lett., vol. 26, pp. 503-505 (2001)
20) Tunable continuous-wave Yb:YLF laser operation with a diode-pumped chirped-pulse amplification system
J. Kawanaka, H. Nishioka, N. Inoue, and K. Ueda
Appl. Opt. 40, pp. 3542-3546 (2001)
21) Improved high-field laser characteristics of a diode-pumped Yb:$LiYF_4$ crystal at low temperature
J. Kawanaka, K. Yamakawa, H. Nishioka, and K. Ueda
Opt. Exp. 10, pp. 455-460 (2002)
22) Broadened gain bandwidth in diode-pumped Yb-doped materials at low temperature
J. Kawanaka, H. Nishioka, A. Yasuhara, K. Yamakawa and K. Ueda
Technical Digest of Conference on Lasers and Electro-Optics / Pacific Rim (CLEO/Pac) 2001 (OSA) I, pp. 84-85 (2001)
23) Observation of vacuum ultraviolet Kr_2* laser oscillation pumped by a compact discharge device
S. Kubodera, T. Shirai, W. Sasaki, J. Kawanaka and T. Igarashi
Technical Digest of Conference on Lasers and Electro-Optics (CLEO) 2001 (OSA), pp. 461 (2001)
24) Efficient femto-second laser operation with LD-pumped Yb-doped materials at low temperature
J. Kawanaka, H. Nishioka, K. Yamakawa, and K. Ueda
2001 International Laser, Lightwave and Microwave Conference
Proceedings(NNSFC/OSA/LSJ/STCSM/IEEE), pp. 24-27 (2001)
25) Laser oscillation with cooled Yb:YLF
J. Kawanaka, K. Yamakawa, H. Nishioka and K. Ueda
JAERI-Review 2001-003 Annual Report of KANSAI Research Establishment 1999, pp. 21 (2001)
26) An efficient laser oscillator with a wide tuning range using Yb-doped materials at low temperature
J. Kawanaka, K. Yamakawa, H. Nishioka and K. Ueda
Proceedings of the second symposium on advanced photon research (JAERI-Conf 2001-011), pp. 82-83 (2001)
27) Diode-pumped Q-switched Yb:$LiYF_4$ laser at low temperature for chirped pulse regenerative amplification
J. Kawanaka, K. Yamakawa, H. Nishioka, and K. Ueda
Advanced Solid-State Lasers (Seventeenth Topical Meeting and Tabletop Exhibit, OSA and IEEE), WB7 (2002)
28) Recent progress of advanced vacuum ultraviolet light sources and applications
S. Kuobodera, W. Sasaki, M. Kaku, T. Shirai and J. Kawanaka
Recent Res. Devel. Applied Phys. 4, Transworld Research Network, India, pp. 1-10 (2001)
29) New Research Trend from Laser Isotope Separation to Advanced Photon Research in JAERI
Nishimura
Trends in Vacuum Science & Technology, 4,55, (2001)

30) Silicon Plate Penetration with a High Energy Laser Pulse
Nishimura, T. Usami, K. Deki, Y. Shimobeppu, N. Hayasaka, T. Arisawa
Conference on Laser and Electro-Optics Pacific Rim, 2001, P2-26, 280-281 (2001)
31) Measurement for titanium density distribution on Ti:sapphire rods for high intensity pump source
T. Usami, A. Nishimura and A. Sugiyama
JAERI-Conf, 2001-001, 221-224 (2001)
32) Temporal Change of Thermal Lens Effects on Highly Pumped Ytterbium Glass by Wavefront Measurement
A. Nishimura, K. Akaoka, A. Ohzu, T. Usami
J. Nucl. Sci. Technol., 38, 1043, (2001)
33) Reduction in thermal lens effects by index-matching fluid on the hybrid material of Yb:glass and sapphire
A. Nishimura, T. Usami, A. Sugiyama, K. Ohara and A. Nagashima
JAERI-Conf, 2001-001, 84-88 (2001) (in Japanese)
34) High-peak power diode-pumped Nd:YAG laser with a Brillouin phase-conjugation-pulse compression mirror
A.Shilov, G.A.Pasmanik, O.V.Kulagin, and K.Deki
Optics Letters vol.26, No.20 (2001)p.1565-1567
35) Short Pulse Solid-State Raman Laser and its Application to Laser Machining
K.Deki, T.Arisawa, A.Nishimura, T.Usami, Y.Shimobeppu, N.Hayasaka, I.Kubo, A.Shilov
Technical Digest CLEO/Pacific Rim 2001 P2-30, vol. II (2001) p. II -288

X-ray laser development (X-ray Laser Research Group)

1. Journals

1) X-ray laser development at Advanced Photon Research Center
Y. Kato, A. Nagashima, K. Nagashima, M. Kado, T. Kawachi, M. Tanaka, N. Hasegawa, G. Sukegawa, S. Nanba, P. Lu, A. Sasaki
J. Phys. IV France, 11, Pr2-3 (2001)
2) Recombination plasma X-ray laser assisted by charge exchange recombination
T. Kawachi, M. Kado, M. Tanaka, N. Hasegawa, A. Nagashima and Y. Kato
J. Phys. IV France, 11, Pr2-255 (2001)
3) Gain profile of transient collisional excitation x-ray laser
M. Tanaka, T. Kawachi, M. Kado, N. Hasegawa, K. Sukegawa, A. Nagashima, Y. Kato, H. Takenaka
J. Phys. IV France, 11, Pr2-55 (2001)
4) Transient collisional excitation x-ray laser generation with picoseconds laser pulses
M. Kado, T. Kawachi, N. Hasegawa, M. Tanaka, K. Sukegawa, K. Nagashima, Y. Kato
J. Phys. IV France, 11, Pr2-39 (2001)
5) Numerical study of laser wake field generated by two colliding laser beams
K. Nagashima, J. Koga, M. Kando
Phys. Rev. E 64, 66403 (2001)
6) Basic aspect of X-ray lasers
T. Kawachi
Journal of plasma and fusion science, vol.77, No.2, 140-145 (2001)
7) Introduction on X-ray Lasers: Question and Answers
Y. Kato
Journal of plasma and fusion science, vol.77, No.2, 138-139 (2001)
8) Q&A related to experimental x-ray laser research
K. Midorikawa, T. Hara, T. Tomie, T. Kawachi, M. Kado
Journal of plasma and fusion science, vol.77, No.4, 372-379 (2001)
9) New Research Field Developed by T3 lasers
Y. Kato
O plus E, vol.23, No.1, 59-61 (2001)
10) Challenge to Ultra Short Time Phenomena using T3 Lasers
Y. Kato

Monthly Journal ENERGY, vol.34, No.3, 50-53 (2001)

11) Prospects of High Field Science
Y. Kato
Journal of Laser Engineering, vol.29, No.4, (2001)

2. Proceedings

1) Soft X-ray emission of cluster target irradiated with ultrashort high-intensity pulse laser
S. Namba, T. Kawachi, M. Kado, N. Hasegawa, M. Tanaka, K. Sukegawa, K. Nagashima, Y. Kato
The 10th International Symposium on Applied Electromagnetics and Mechanics, (2001)

2) X-ray laser research in JAERI-Kansai
T. Kawachi, M. Kado, N. Hasegawa, T. Tanaka, K. Sukegawa, K. Takahashi, S. Namba, P. Lu, H. Tang, K. Nagashima, A. Sasaki, A. Nagashima, M. Koike, H. Daido and Y. Kato
CLEO Pacific Rim2001, Technical Digest of CLEO/Pacific Rim2001, pp64

3) Near field imaging of transient collisional excitation x-ray laser
M. Tanaka, T. Kawachi, M. Kado, N. Hasegawa, K. Sukegawa, P. Lu, H. Takenaka, K. Nagashima, Y. Kato
CLEO Pacific Rim2001, Technical Digest of CLEO/Pacific Rim2001, pp66

4) Production of Highly-Charged Ions by Clusters Irradiated with UltraShort High-Intense Pulse Laser
S. Namba, T. Kawachi, N. Hasegawa, K. Nagashima, K. Sukegawa, M. Tanaka, Y. Kato, H. Daido
CLEO Pacific Rim2001, Technical Digest of CLEO/Pacific Rim2001, pp16-19

5) Near field imaging of transient collisional excitation Ni-like Ag x-ray laser
Momoko Tanaka, Tetsuya Kawachi, Masataka Kado, Noboru Hasegawa, Kouta Sukegawa, Peixiang Lu, Keisuke Nagashima, Yoshiaki Kato and Hisataka Takenaka
The Thirteenth International Conference on Vacuum Ultraviolet Radiation Physics (2001)

6) X-ray laser research at Advanced Photon Research Center of JAERI/Kansai
M. Kado, T. Kawachi, M. Tanaka, N. Hasegawa, K. Takahashi, S. Namba, K. Sukegawa, A. Sasaki, P. Lu, H. Tang, K. Nagashima, H. Daido, A. V. Kilpio, Y. Kato
Proc. SPIE vol.4505, 54 (2001)

7) Higher harmonics generation for the high coherent x-ray laser
N. Hasegawa, A. V. Kilpio, K. Nagashima, T. Kawachi, M. Kado, M. Tanak1, S. Namba, K. Takahashi, K. Sukegawa, P. Lu, T. Huajing, M. Kishimoto, T. Renzhong, H. Daido, Y. Kato
Proc. SPIE vol.4505, 204-210 (2001)

8) Gain saturation regime at 11.9nm using a traveling wave pumping
T. Kawachi, M. Tanaka, N. Hasegawa, A. Kilpio, K. Sukegawa, P. Lu, S. Namba, K. Takahashi, H. Tang, R. Tai, K. Nagashima, H. Daido and Y. Kato
The 2nd International Conference on Inertial Fusion Sciences and Applications (IFSA2001)

9) X-ray Laser research in JAERI-Kansai
T. Kawachi, M. Tanaka, N. Hasegawa, A. Kilpio, K. Sukegawa, P. Lu, S. Namba, K. Takahashi, H. Tang, R. Tai, K. Nagashima, H. Daido and Y. Kato
2001 IEEE/LEOS Annual Meeting Conference Proceedings, IEEE, pp.457 (2001)

Free-electron laser development (Free Electron Laser Research Group)

1. Journals

1) Decomposition Study of Dioxins by IR laser Irradiation
T. Yamauchi
Society of Environmental Science,14(6), p.567-575 (2001)

2) JAERI design options for realizing a compact and stand-alone superconducting rf linac-based high power free-electron laser
E. Minehara, T. Yamauchi, M. Sugimoto, M. Sawamura, R. Hajima, R. Nagai, N. Kikuzawa, N. Nishimori, T. Shizuma
Nuclear Instrument and Methods in Plysical Research, A475, p.II47-II48 (2001)

3) Analyses of superradiance and spiking-mode lading observed at JAERI-FEL

R. Hajima, N. Nishimori, R. Nagai, E. Minehara
Nuclear Instrument and Methods in Plysical Research, A475, p.270-275 (2001)
4) 3rd-Harmonic Lasing at JAERI-FEL
R. Hajima, R. Nagai, N. Nishimori, N. Kikuzawa, E. Minehara
Nuclear Instrument and Methods in Plysical Research, A475, p.43-46 (2001)
5) An Optical Resonator with Scraper Output Coupler for the JAERI Far-Infrared Free-Electron Laser
R. Nagai, M. Sawamura, R. Hajima, N. Kikuzawa, N. Nishimori, T. Shizuma, E. Minehara
Nuclear Instruments and Methods in Physics Research, A475, p.519-523 (2001)
6) Simulated performance of energy-recovery transport system for the JAERI-FEL
T. Shizuma, R. Hajima, E. Minehara
Nuclear Instrument and Methods in Plysics Research, A 475, p.569-573 (2001)
7) High extraction efficiency observed at JAERI Free Electron Laser
N. Nishimori, R. Hajima, R. Nagai, E. Minehara
Nuclear Instrument and Methods in Plysics Research, A 475, p.266-269 (2001)
8) Sustained saturation in a free-electron laser oscillator at pergect synchronism of an optical cavity
N. Nishimori, R. Hajima, R. Nagai, E. Minehara
Physical Review Letters, vol86, No.25, p.5707-5710 (2001)
9) The JAERI Free-Electron Laser driven by a Superconducting rf Linac Towards Ultra-short pulse, Highly-Efficient, High Power, and Tunable Coherent Light Sourees
E. Minehara
Journal of the Japanese Society for Synchrotron Radiation Research, 14(3), p.20-27 (2001)
10) Multi-quasiparticle states and K-forbidden transitions in 183Os
T. Shizuma, M. Matsuura, Y. Tou, T. Hayakawa, M. Oshima, Y. Hatsukawa, M. Matsuda, K. Yoshino, Y. Sasaki, T. Komatsubara, Y. Shimizu
Nuclear Physics, A696, p.337-370 (2001)
11) Technology of the ultra-fast pulse and high-power FELs driven by a superconducting rf linac
E. Minehara, R. Hajima, M. Sawamura, R. Nagai, N. Nishimori, N. Kikuzawa, M. Sugimoto, T. Yamauchi, T. Hayakawa, T. Shizuma
OYO BUTURI, 71(2), p.214-216 (2002)
12) Status and Perspectives of the Next Generation Light Sources – XFEL and ERL
R. Hajima
Journal of the Japanese Society for Synchrotron Radiation Research, 14(5), p.323-330 (2001)
13) An Intense Ultrashort Pulse Generation in the JAERI Far-Infrared Free-Electron Laser
R. Nagai, R. Hajima, N. Nishimori, N. Kikuzawa, M. Sawamura, E. Minehara
Nuclear Instruments and Methods in Physics Research, A483, p.129-133 (2002)
14) Systematic measurement of maximum efficiencies and detuning lengths at JAERI Free Electron Laser
N. Nishimori, R. Hajima, R. Nagai, E. Minehara
Nuclear Instruments and Methods in Physics Research, A483, p.134-137 (2002)
15) High-efficiency ultrashort pulse generation in a high-gain FEL oscillator near the perfect synchronism
R. Hajima, N. Nishimori, R. Nagai, E. Minehara
Nuclear Instruments and Methods in Physics Research, A483, p.113-118 (2002)
16) Highly-Efficient and High-Power Industrial FELs driven by a Compact, Stand-alone and Zero-Boil-Off Superconducting rf Linac
E. Minehara
Nuclear Instruments and Method for Physical Research, A483, p.8-13 (2002)

2. Proceedings

1) The JAERI Superconducting free-Electron Laser : Recent Progress and Future Plans
R. Hajima, N. Nishimori, R. Nagai, T. Shizuma, M. Sawamura, N. Kikuzawa, E. Minehara
International Journal of Applied Electromagnetics and Mechanics
2) Second Harmonic Generation in CdTe Crystal and Te by Free Electron Laser
T. Yamauchi, N. Kikuzawa, E. Minehara, R. Nagai
CLEO/Pacific Rim 2001, I, p.426-427 (2001)
3) Decomposition Experiment of Dioxins by IR Laser Irradiation
T. Yamauchi, S. Ito, E. Minehara
CLEO/Pacific Rim 2001, I, p.148-149 (2001)

4) Plasma Behavior Confined in High-Tc Superconducting Tube
T. Yamauchi, H. Matsuzawa, K.Mikami, J. Ishikawa
Proceedings of International Conference on Phenomena in Ionized Gases, 19(3), p.295-296 (2001)
5) Correction of a Quadrupole Magnet by the Pole Length Tapering Method
R. Nagai, R. Hajima, N. Nishimori, N. Kikuzawa, M. Sawamura, E. Minehara
Proceedings of the 26th Linear Accelerator Meeting in Japan, p.317-319 (2001)
6) Characteristics of the Intense Ultrashort Pulse Generation in the JAERI Far-Infrared Free-Electron Laser
R. Nagai, R. Hajima, N. Nishimori, N. Kikuzawa, M. Sawamura, E. Minehara
Proceedings of the 26th Linear Accelerator Meeting in Japan, p.240-242 (2001)
7) Measurement of absolute detuning length of efficiency detuning curve at JAERI-FEL
N. Nishimori, R. Hajima, R. Nagai, E. Minehara
Proceedings of the 26th Linear Accelerator Meeting in Japan, p.58-60 (2001)
8) Design and Construction of an energy-recovery system at JAERI-FEL
R. Hajima, T. Shizuma, M. Sawamura, R. Nagai, N. Nishimori, N. Kikuzawa, E. Minehara
Proceedings of the 26th Linear Accelerator Meeting in Japan, p61-63 (2001)
9) Demonstration of a high-power FEL oscillator with high extraction-efficiency
R. Hajima, N. Nishimori, R. Nagai, M. Sawamura, N. Kikuzawa, T. Shizuma, E. Minehara
Proceedings of 2001 Particle Accelerator Conference
10) The JAERI energy-recovery linac : construction and testing status
R. Hajima, T. Shizuma, M. Sawamura, R. Nagai, N. Nishimori, N. Kikuzawa, E. Minehara
Proceedings of the 23rd International FEL Conference
11) Energy-recovery option for a future X-ray Free-Electron Laser
R. Hajima, E. Minehara
Proceedings of 2001 Particle Accelerator Conference
12) Pulse width measurement of the JAERI-FEL
R. Nagai, R. Hajima, N. Nishimori, N. Kikuzawa, T. Shizuma, M. Sawamura, E. Minehara
Proceedings of Atomic Energy Society of Japan 2001
13) K-forbiddenness in 183Os and its neighbors
T. Shizuma, Y. Tou, T. Hayakawa, M. Oshima, K. Furuno, Y. Sasaki, T. Komatsubara, Y. Shimizu
Proceedings of International Nuclear Physics Conference in USA
14) Bright electron multi-bunch production for the high power JAERI-FEL oscillator
N. Nishimori, R. Hajima, R. Nagai, T. Shizuma, M. Sawamura, N. Kikuzawa, E. Minehara
Proceedings of the 13th Symposium on Accelerator Science and Technology, p458-460 (2001)
15) The JAERI Superconducting rf Linac-based FELs and their Cryogenics
E. Minehara
Proceedings of The 10th Workshop on RF Superconductivity
16) Demonstration of the highly-efficient and high-power FELs driven by a superconducting rf linac
E. Minehara, R. Hajima, M. Sawamura, R. Nagai, N. Nishimori, N. Kikuzawa, M. Sugimoto, T. Yamauchi, T. Hayakawa, T. Shizuma
The 13th Symposium on Accelerator Science and Technology (2001)
Proceedings of the 13th Symposium on Accelerator Science and Technology, p150-154 (2001)
17) Energy Recovery Options for the JAERI High Power FELs driven by a superconducting rf linac
E. Minehara
Proceedings of the 2nd International Conference on Inertial Fusion Sciences and Applications (IFSA2001)
18) Intense FEL light pulses with a length of three optical cycles produced at zero detuning of an optical cavity
N. Nishimori, R. Nagai
Proceedings of the 13th Symposium on Accelerator Science and Technology, p95-99 (2001)
19) Generation of a few-cycle optical pulse in an FEL oscillator
R. Hajima, R. Nagai, N. Nishimori, E. Minehara
Proceedings of International Symposium on Infrared Free Electron Laser and Its Application
20) Study of bulk chemical reaction by FEL

T. Yamauchi, E. Minehara, T. Hayakawa, T. Shizuma, S. Ito
Proceedings of International Symposium on Infrared Free Electron Laser and Its Application

21) A thermionic electron gun for energy-recovery system at JAERI-FEL
N. Nishimori, R. Nagai, R. Hajima, M. Sawamura, N. Kikuzawa, E. Minehara
Proceedings of International Symposium on Infrared Free Electron Laser and Its Application

22) Industrial Free-Electron Lasers driven by a Super-conducting rf Linac
E. Minehara, M. Sawamura, R. Hajima, R. Nagai, N. Kikuzawa, N. Nishimori, M. Sugimoto, T. Yamauchi, T. Hayakawa, T. Shizuma
Proceedings of International Symposium on Infrared Free Electron Laser and Its Application

Optics research and development (Novel Optics Research Group)

1. Journals

1) Growth of neodymium doped Y3Al5O12 single crystals by double crucible method
M..Katurayama, Y. Anzai, Akira Sugiyama, Masato Koike, Yoshiaki Kato
J of Crystal Growth, 229,193-198, 2001

2) Geometric theory for the design of multielement optical systems
T. Namioka, M. Koike and S. Masui
Optics and Precision Engineering (China), 9, 458-466, 2001

3) Grazing-incidence Monk-Gillieson monochromator based on surface normal rotation of a varied-line-spacing grating
M. Koike and T. Namioka
Appl. Opt., 41, 245-257, 2002

4) New evaluation beamline for soft X-ray optical elements
M. Koike, K. Sano, O. Yoda, Y. Harada, M. Ishino, N. Moriya, H. Sasai, H. Takenaka, E. Gullikson, S. Mrowka, M. Jinno, Y. Ueno, J. H. Underwood, T. Namioka
Rev. Sci. Instrum. 73, 1641-1644 (2002)

5) Boundary structure of Mo/Si multilayers for soft X-ray mirrors
M. Ishino, O. Yoda, Y. Haishi, F. Arimoto, M. Takeda, S. Watanabe, S. Ohnuki
Jpn. J. Appl. Phys. 41, 3052-3056,2002

2. Proceedings

1) Evaluations of bonded region in a direct bonded Ti:sapphire laser crystal
A. Sugiyama, H. Fukuyama, Y. Kataoka, Y. Okada
Technical Digest on 4th Pacific Rim Conference on Lasers and Electro-Optics (CLEO/Pacific Rim 2001), WH-3, p.II-460, 2001

3. Patents

1) Conical diffraction grazing incidence monochromators and its grating
M. Koike, K, Sano, Y. Harada
Japanese Patent Application number 2001-246318, Aug. 8, 2001

Research on laser particle acceleration (Laser Acceleration Research Group)

1. Journals

1) Direct measurement of coherent ultrahigh wakefields excited by intense ultrashort laser pulses in a gas-jet plasma
H. Kotaki, M. Kando, T. Oketa, S. Masuda, J. K. Koga, S. Kondo,S. Kanazawa, T. Yokoyama, T. Matoba and K. Nakajima
Phys. Plasmas, vol.9, 1392 (2002)

2. Proceedings

1) High Energy Laser Wakefield Acceleration
H. Kotaki, M. Kando, T. Hosokai, S. Kondo, S. Masuda, S. Kanazawa, T. Yokoyama, T. Matoba and K. Nakajima
Proceedings of The 10th International Symposium on Applied Electromagnetics and Mechanics, May 13-16, 2001, Toshi Center Hotel, Tokyo, Japan

(Accepted in the International Journal Applied Electromagnetics and Mechanics)

2) A Compact Ultrashort High Brightness X-ray and Gamma-ray Sources by Laser-Electron Beam Interactions
K. Nakajima
21st ICFA Beam Dynamics Workshop on Laser-Beam Interactions, Long Island, NY USA, June 11-15, (2001)

3) Laser-Plasma Accelerator Developments in Japan
K. Nakajima
APS Snowmass 2001, Workshop (T8) on Advanced Accelerator Technology, Snowmass Village, CO USA, July 6, (2001)

4) Super-High Energy Super-Intense Particle Physics by Super-Strong Laser-Matter Interactions
K. Nakajima
2nd International Conference on SUPERSTRONG FIELDS IN PLASMAS, Villa Monastero, Varenna, Italy, Aug. 27-Sep. 1, (2001)

5) Extremely high energy particle acceleration and interactions by super strong laser pulses
K. Nakajima
Workshop on Laboratory Astrophysics Using High Intensity Particle And Photon Beams, Stanford Linear Accelerator Center, Oct. 11-13, (2001)

6) Nonlinear interaction of intense ultrashort laser pulses in plasmas
H. Kotaki, M. Kando, T. Oketa, S. Masuda, J. K. Koga, S. Kondo,S. Kanazawa, T. Yokoyama, T. Matoba and K. Nakajima
Science of Super-Strong Field Interactions, March 13-16, 2002, The Graduate University for Advanced Studies, HAYAMA, Japan

7) Laser Acceleration research project at JAERI Kansai
M. Kando, H. Kotaki, S. Masuda, T. Yokoyama, S. Kondo, S. Kanazawa, I. V. Smetanin, T. Matoba and K. Nakajima
Science of Super-Strong Field Interactions, March 13-16, 2002, The Graduate University for Advanced Studies, HAYAMA, Japan

8) Generation of Relativistic Electrons via Interaction between Intense
Ultra-short Laser Pulse and Supersonic Gas Jet
T. Hosokai, K. Kinoshita, W. Ghaly, Y. Kanegae, T. Ohkubo, K. Yoshii, T. Ueda, T, Watanabe, A. Zhidokov, M. Uesaka, K. Nakajima, H. Kotaki and M. Kando
Science of Super-Strong Field Interactions, March 13-16, 2002, The Graduate University for Advanced Studies, HAYAMA, Japan

9) Review of relativistic self-focusing with application to proton acceleration
J. K. Koga, K. Nakajima, K. Nakagawa, M. Yamagiwa and A. Zhidkov
Science of Super-Strong Field Interactions, The Graduate University for Advanced Studies, HAYAMA, Japan, March 13-16, (2002)

10) Particle Acceleration and Radiation with Super-Strong Field Interactions
V. Smetanin and K. Nakajima
Science of Super-Strong Field Interactions, The Graduate University for Advanced Studies, HAYAMA, Japan, March 13-16, (2002)

11) 1D PIC Simulation of Laser Ponderomotive Acceleration in Plasmas
S. Masuda, I. V. Sm,etanin and K. Nakajima
Science of Super-Strong Field Interactions, The Graduate University for Advanced Studies, HAYAMA, Japan, March 13-16, (2002)

12) HIGH ENERGY ELECTRON ACCELERATION BY HIGH PEAK POWER LASER
H. Kotaki, M. Kando, S. Kondo, S. Masuda, . Kanazawa,T. Yokoyama, T. Matoba and K. Nakajima
Proceedings of the 13th Symposium on Accelerator Science and Technology, October 29-31, 2001, Osaka University, Osaka, Japan

Advanced photon simulation research (Simulation Group for Advanced Photon Science)

1. Journals

1) Multiple-scattering analysis of triply differential cross sections for electron emission in energetic

ion-atom collisions
L. Gulyas, P.D. Fainstein, T. Shirai
J. Phys. B: At. Mol. Opt. Phys., Vol. 34, No. 8, pp. 1473-1483 (2001)
2) The Constrained interpolation profile method for multiphase analysis
T. Yabe, F. Xiao, T. Utsumi
Journal of Computational Physics, Vol. 169, No. 2, pp. 556-593 (2001)
3) Molecular dynamics analysis of laser shock phenomena due to Gaussian beam irradiation
I. Fukumoto, E. Ohmura
Journal of the Society for Precision Engineering, Vol. 67, No. 6, pp. 916-921 (2001)
4) Short-laser-pulse-driven emission of energetic ions into a solid target from a surface layer spalled by a laser prepulse
A.G. Zhidkov, L.V. Zhigilei, A. Sasaki, T. Tajima
Appl. Phys. A, Vol. 73, pp. 741-747 (2001)
5) Pulse duration effect on the distribution of energetic particles produced by intense femtosecond laser pulses irradiating solids
A.G. Zhidkov, A. Sasaki, I. Fukumoto, T. Tajima, T. Auguste, P. D'Oliveira, S. Hulin, P. Monot, A.Ya. Faenov, T.A. Pikuz, I.Yu. Skobelev
Phys. Plasmas, Vol. 8, No. 8, pp. 3718-3723 (2001)
6) Pressure formulae for liquid metals and plasmas based on the density-functional theory
J. Chihara, I. Fukumoto, M. Yamagiwa, H. Totsuji
J. Phys.: Condens. Matter, Vol. 13, No. 33, pp. 7183-7198 (2001)
7) Z-dependence of photo-emission spectra for highly charged neonlike ions
D. Kato, N. Nakamura, S. Ohtani, A. Sasaki
Physica Scripta, Vol. T92, pp. 126-129 (2001)
8) Productions of hollow atoms from solids irradiated by high intensity laser
K. Moribayashi, A. Sasaki, A. Zhidkov
Physica Scripta, Vol. T92, pp. 185-187 (2001)
9) Polarization, hosing and long time evolution of relativistic laser pulses
N.M. Naumova, J. Koga, K. Nakajima, T. Tajima, T.Zh. Esirkepov, S.V. Bulanov, F. Pegoraro
Phys. Plasmas, Vol. 8, No. 9, pp. 4149-4155 (2001)
10) Theoretical study on dielectronic recombination of O^6+ ions in metastable states
Li-Bo Zhao, T. Shirai
Phys. Rev. A, Vol. 64, pp. 052704-1 - 6 (2001)
11) One-dimensional electromagnetic solitons in a hot electron-positron plasma
M. Lontano, S.V. Bulanov, J. Koga
Phys. Plasmas, Vol. 8, No. 12, pp. 5113-5120 (2001)
12) The gain distribution of the transient collisional excited x-ray lasers
A. Sasaki, T. Utsumi, K. Moribayashi, M. Kado, M. Tanaka, N. Hasegawa, T. Kawachi, H. Daido
J. Quant. Spectrosc. Radiat. Transf. Vol. 71, No. 2-6, pp. 665-674 (2001)
13) Observation of MeV multicharged ions and hot electrons accelerated by a 65-fs laser pulse
T. Auguste, A.Y. Faenov, I. Fukumoto, S. Hulin, A.I. Magunov, P. Monot, P. D'Olivera, T.A. Pikuz, A. Sasaki, B.Y. Sharkov, I.Y. Skoblev, T. Tajima, A.G. Zhidkov
J. Quant. Spectrosc. Radiat. Transf. Vol. 71, No. 2-6, pp. 147-156 (2001)
14) X-ray emission from hollow atoms produced by collisions of multiply charged ions with a solid
K. Moribayashi, K. Suto, A. Zhidkov, A. Sasaki, T. Kagawa
Laser and Particle Beams, Vol. 19, pp. 643-646 (2001)

2. Proceedings

1) Numerical simulation for plasma electron acceleration by 12TW 50fs laser pulse
N. Hafz, J. Koga, R. Hemker, M. Uesaka
Advanced Accelerator Concepts, AIP Conference Proceedings, Vol. 569, pp. 122-126 (2001)
2) Analyses of the short pulse laser pumped transient collsional excited x-ray lasers
A. Sasaki, T. Utsumi, K. Moribayashi, A. Zhidkov, M. Kado, M. Tanaka, N. Hasegawa, T. Kawachi
Proceedings of 7th International Conference on X-ray Laser (ICXRL 2000)
Journal de Physique, IV, Vol. 11 (Pr2), pp. Pr2_75-Pr2_78 (2001)

3) Large-scale simulation and advanced photon research
Y. Ueshima, Y. Kishimoto
Lecture Notes in Computer Science 1940, pp. 524-534 (2001)
4) Let's talk about multi-dimensional information
Y. Ueshima
Proceeding of the 4th Visual Data Mining, pp. 51-58 (2002)

3. Reports

1) Visualization program development using Java
A. Sasaki, K. Suto, H. Yokota
JAERI-Data/Code 2002-003, 54p, 2002
2) Visualization system in large scale simulation
Y. Ueshima
FNS Today, Vol. 8, pp. 2-3 (2001)
3) Inner-shell ionization in high density hot plasma produced by high intensity laser irradiation
K. Moribayashi, A. Zhidkov, A. Sasaki, K. Suto, S. Suzuki
Atomic collision research in Japan (Progress Report, The Society for Atomic Collision Research), No. 27, pp. 1-3 (2001)

High Power Laser Applications (Applied Photon Research Group)

1. Journals

1) Review of Collisional Excitation Neon-like and Nickel-like Soft X-Ray Lasers Pumped by Multiple Infrared Laser Pulses (Invited Paper)
H. Daido, H. Tang, Y. Kato, K. Murai, Compte Rendus
Special Issue on X-Ray Lasers, Serie IV, No.8, pp.999-1018, 2000.
2) Review of soft x-ray laser development (Invited review paper)
H. Daido
Rep. Prog. Phys. 65 1513-1576(2002)
3) Charge-Separation Process of the $C_2H_4 + Cl_2$ Reaction in Water: Ab Initio Molecular Orbital Study Using a Cluster Model
Y. Kurosaki J. Phys. Chem. A 105, 11080-11087 (2001).
4) Ab initio molecular orbital study of the O(1D) insertion into the C-C bond in cyclopropane and ethane
Y. Kurosaki and T. Takayanagi
Chem. Phys. Lett. 355, 424-430 (2002)
5) Femtosecond time-resolved fluorescence spectra of a coumarine dye in glycerol
H. Murakami,
Journal of Molecular Liquids 89 33-45 (2000)
6) Centrally Peaked X-Ray Supernova Remnants in the Small Magellanic Cloud Studied with ASCA and ROSAT
J. Yokogawa, K. Imanishi, K.Koyama, M.Nishiuchi and N.Mizuno
Publ. Astron. Soc. Japan, Volume 54, pp53--59 (2002)
7) Detection of pulsating soft X-ray excess in the Magellanic Cloud pulsars with ASCA
B. Paul, F.Nagase, T.Dotani, J, Yokogawa and M. Nishiuchi
Advanced in Space Research, Volume 28, pp399--403 (2002)

2.Proceedings

1) Solve the spectral discrepancy between the X-ray astronomical observations and the existing ionization codes (~1 keV Fe L-shell lines)
M. Nishiuchi, K. Yasuike, T. Kawachi, H. Daido and K. Koyama
accepted to the IFSA proceedings

6.2 List of publications on Synchrotron Radiation Research Center

Experimental facilities development (Experimental Facilities Development Group)

Journals

1) Transport channels of X-ray beamlines at SPring-8
S.Gotoh, H.Ohashi, K.Takeshita, M.Yabashi, M.Yamagata, Y.Asano, T.Ishikawa
Nucl.Inst&Meth.Physics Research A, 467-468,813-815, 2001
2) Construction and commissioning of a 215-m-long beamlines at SPring-8
S.Gotoh, K.Takeshita, Y.Suzuki, H.Ohashi, Y.Asano, H.Kimura, T.Matsushita, N.Yagi, Y.Isshiki, H.Yamasaki, Y.Yoneda, K.Umetani, T.Ishikawa
Nucl.Inst.&Meth. Physics Research A, 467-468, 682-685, 2001
3) Demagnetization of undulator magnets irradiated with electron beam
T.Bizen, R.Tanaka, Y.Asano, D.E.Kim, J.S.Bak, H.S.Lee, H.Kitamura
Nucl.Inst.&Meth. Physics Research A, 467-468, 185-189, 2001
4) Structural Analysis of Corrosion Product of Fe-Cr Alloy Film Using Synchrotron Radiation
M.Yamashita, H.Konishi, M.Takahashi, J.Mizuki, H.Uchida
Mater. Sci. Res. Int., Special Technical Publication 1, 398-401, 2001
5) X-ray absorption study of molten yttrium trihalides
Y. Okamoto, M. Akabori, H. Motohashi, H. Shiwaku and T. Ogawa
J. Synchrotron Rad., 8, 1191-1199, 2001
6) Development of Phase Contrast Radiography for Bone Imaging Using Synchrotron Radiation
Koishi MORI, Hitoshi SATO, Norio SEKINE, Naoto SHIKANO, Masaru SATO, Daisuke SHIMAO, Takashi IGARASHI, Hideaki SHIWAKU and Kazuyuki HYODO
Analytical Sciences, Vol.17 Supplement, i1427-i1430, 2001

Proceedings

1) International Workshop on Radiation Safety at Synchrotron Radiation Sources
Y.Asano
Proceedings of 1st International Workshop on Radiation Safety at Synchrotron Radiation Sources (Argonne USA) 7,2001

High pressure science (High Pressure Science Group)

1. Journals

1) A liquid-liquid phase transition in phosphorus
Y. Katayama
Solid State Physics, 36, 217-222, 2001, in Japanese
2) In-situ observation of a pressure-induced first-order phase transition in liquid phosphorus
Y. Katayama
Jpn. Soc. Synchrotron Rad. Res., 14, 116-120, 2001, in Japanese
3) Pressure Dependence of Effective Pair Potentials in AgBr Determined by Extended X-ray Absorptio Fine Structure
A. Yoshiasa, K. Murai, T. Nagai, Y. Katayama
Jpn. J. Appl. Phys., 40, 2395-2398, 2001
4) The effect of temperature, pressure, and sulfur content on viscosity of the Fe-FeS melt
H. Terasaki, T. Kato, S. Urakawa, K. Funakoshi, A. Suzuki, T. Okada, M.. Maeda, J. Sato, T. Kubo and S. Kasai
Earth and Planetary Science Letters,190, 93-101, 2001
5) X-ray diffraction technique in energy-dispersive mode at SPring-8 for fluids at high temperatures and high pressures
K. Tamura, M. Inui, K. Funakoshi, and W. Utsumi
Nuclear Instruments and Methods in Physics Research A 467-468, 1065-1068, 2001
6) High-pressure x-ray diffraction of icosahedral Zr-Al-Ni-Cu-Ag quasicrystal
J. Z. Jiang, K. Saksl, H. Rasmussen, T. Watanuki, N. Ishimatsu, and O. Shimomura
Appl. Phys, Lett. 79 1112-1114, 2001

7) Imaging of Electron Density Distributions by MEM
T. Ikeda, M. Sakata, M. Takata, E. Nishibori, and S. Yamaura
The Journal of Structural Biology Sakabe Project 7, 28-38,2001 in Japanese
8) Phase relations and EOS of ZrO_2 and HfO_2 under high-temperature and high-pressure
O. Ohtaka, H. Fukui, K. Funakoshi, W. Utsumi, T. Irifune, and T. Kikegawa
High Pressure Research 22, 221-226, 2002
9) High-pressure phase relationships for FeS
S. Urakawa, M. Hasegawa, J. Yamakawa, K. Funakoshi, W. Utsumi
High Pressure Research 22, 491-494, 2002
10) Anharmonicity of gold under high-pressure and high-temperature
M. Okube、A. Yoshiasa, O. Ohtaka, H. Fukui, Y. Katayama, W. Utsumi
Solid State Commun. 121, 235-239, 2002
11) Mechanisms and kinetics of the post-spinel transformation in Mg_2SiO_4
T. Kubo, E. Ohtani, T. Kato, S. Urakawa, A. Suzuki, Y. Kanbe, K. Funakoshi, W. Utsumi, T. Kikegawa and K. Fujino
Phys. Earth Planet. Inter. 129, 153-171, 2002

2. Proceedings

1) Synthesis of Crystalline Carbon Nitride Thin Films by Electron Cycrlotron Resonance Sputtering Method
E. Kamijo, Y. Aoi, M. Hisa, K. Tamaoka, W. Utsumi, T. Watanuki, K. Yamaguchi
Proceedings of 2000 Powder Metallurgy World Congress 1320-1323, 2001

Structural physics research (Structural Physics Research Group)

1. Journals

1) Fixed-height exit bender of synchrotron X-rays above 40 keV,
Y. Yoneda, N. Matsumoto, Y. Furukawa and T. Ishikawa,
J. Synchrotron Rad. 8, 18-21 (2001)
2) High-energy X-ray focusing with fixed exit bender
Y. Yoneda, N. Matsumoto, Y. Furukawa and T. Ishikawa,
Nucl. Instrum. Methods A 467-468, 370-372 (2001)
3) 31P NMR Study of Magnesium Phosphate Glasses
F. Fayon, D. Massiot, K. Suzuya and D.L. Price,
Journal of Non-Crystalline Solids 283 (2001) 88-94
4) A horizontal two-axis diffractometer for high-Energy X-ray diffraction using synchrotron radiation on bending magnet beamline BL04B2 at SPring-8
S. Kohara, K. Suzuya, Y. Kashihara, N. Matsumoto, N. Umesaki, and I. Sakai
Nuclear Instruments and Methods in Physics Research A 467-468 (2001) 1031-1034
5) Neutron Inelastic Scattering of Densified GeO_2 Glass
K. Suzuya, K. Shibata, N. Umesaki, N. Kitamura and S. Kohara
Journal of the Physical Society of Japan 70 (2001) Supplement A, 256-258
6) A Highly Conductive RTMS; Alkylimidazolium Fluorohydrogenates Proceedings of 6th International Conference of Molten Salt Chemistry and
R. Hagiwara, K. Matsumoto, T. Tsuda, Y. Ito, S. Kohara and K. Suzuya
Technology, China, Shanghai, (2001) P. 136 - 139
7) High-Energy X-ray Diffraction Studies of Non-Crystalline Materials"
H. Ohno, S. Kohara, N. Umesaki and K. Suzuya,
Journal of Non-Crystalline Solids 293-295 (2001) 125-135
8) Short-Range Structure of Vitreous P2O5 by MD Simulation
Y. Suzuki, K. Takase, I. Akiyama, K. Suzuya, N. Umesaki and N. Ohtori
Materials Transactions 42 (2001) 2242-2246
9) Evidence for the Diffusion of Au Atoms into the Te upd layer Formed on a Au(111) Substrate.
H. Kawamura, M. Takahasi, N. Hojo, M. Miyake, K. Murase, k. Tamura, K. Uosaki, Y. Awakura, J. Mizuki and E. Matsubara
J. Electrochem. Soc. 149 (2002) C83-88.

10) EXAFS spectra above Pb and Pt K edges observed at low temperature
Y. Nishihata, J. Mizuki, S. Emura, T. Uruga
J. Synchrotron Rad. 8 (2001) 294-296.
11) Structural changes of quartz-type crystalline and vitreous GeO2 under pressure
O. Ohtaka, A. Yoshiasa, H. Fukui, K. Murai, M. Okube, Y. Katayama, W. Utsumi, Y. Nishihata
J. Synchrotron Rad. 8 (2001) 791-793.
12) An intelligent catalyst
H. Tanaka, M. Uenishi, I. Tan, M. Kimura, J. Mizuki, Y. Nishihata
SAE Paper 2001-01-1301 (2001).
13) Diamond double-crystal monochromator in Bragg geometry installed on BL-11XU at SPring-8
M. Marushita, T. Mitsui, T. Fukuda, M. Takahasi, T. Inami, Y. Katayama, H. Shiwaku and J. Mizuki
Nucl. Insstr. and Meth. A 467-468 (2001) 392-395.
14) An inelastic X-ray scattering spectrometer for materials science on BL-11XU at SPring-8
T. Imani, T. Fukuda, J. Mizuki, H. Nakao, T. Matsumura, Y. Murakami, K. Hirota and Y. Endoh
Nucl. Insstr. and Meth. A 467-468 (2001) 1081-1083.
15) Structural Analysis of Corrosion Product of Fe-Cr Alloy Film Using Synchrotron Radiation
M. Yamashita, H. Konishi, M. Takahasi, J. Mizuki and H. Uchida,
Materials Science Res. Int. , Special Technical Publication – 1, (2001) 398-401.
16) Magnetic and transport studies of $LaFe_{1-x}Ni_xTiO$,
K. Yoshii, H. Abe, N. M. Masaki and A. Nakamura,
Ferrites: Proceedings of the eighth international conference on ferrites, 2000 (ICF8), (2001) 278-280.
17) Magnetism and transport of $Ln_{0.5}Sr_{0.5}Fe_{0.5}Co_{0.5}O_3$ (*Ln*=La and Pr)
K. Yoshii and H. Abe,
Transactions of the Materials Research Society of Japan, 26[1] (2001) 75-78.
18) Magnetic properties of $LnTi_{0.5}V_{0.5}O_3$ (*Ln*=Ce and Pr),
K. Yoshii and H. Abe,
J. Solid State Chem., 156 (2001) 452-457.
19) Magnetism and transport of $Ln_{0.5}Sr_{0.5}CoO_3$ (*Ln*=Pr, Nd, Sm and Eu)
K. Yoshii, H. Abe and A. Nakamura
Mater. Res. Bull., 36 (2001) 1447-1454.
20) Magnetic properties of perovskite $GdCrO_3$
K. Yoshii,
J. Solid State Chem., 159 (2001) 204-208.
21) XAS and MCD studies in $Eu_{0.6}Sr_{0.4}MnO_3$.
M. Mizumaki, Y. Saitoh, A. Agui, K. Yoshii, A. Fujimori and S. Nakamura
J. Synchrotron Rad., 8 (2001) 440-442.
22) Structure, magnetism and transport of $Ln_{1-x}TiO_3$ (Ln=Ce and Pr)
K. Yoshii, H. Abe, S. Tsutsui and A. Nakamura
J. Magn. Magn. Mater., 226-230 (2001) 900-901.
23) Magnetic and structural properties of $Pr_{1-x}A_xCoO_3$ (A=Sr and Ba)
K. Yoshii, S. Tsutsui and A. Nakamura
J. Magn. Magn. Mater., 226-230 (2001) 829-830.
24) Antiferromagnetic-ferromagnetic crossover in UO_2-TiO_x multi-phase systems
Nakamura, S. Tsutsui and K. Yoshii,
J. Magn. Magn. Mater., 226-230 (2001) 876-878.
25) Ferromagnetism in $ErTi_2Ga_4$
H. Abe, K. Yoshii and H. Kitazawa
J. Phys. Soc. Jpn., 70, 3042-3045 (2001).
26) Magnetic properties of $La_{1-x}Pr_xCrO_3$
K. Yoshii, A. Nakamura, Y. Ishii and Y. Morii
J. Solid State Chem. 162, 84-89 (2001).
27) Magnetic properties of $CaRuO_3$
K.Yoshii and H. Abe
Physica B 312-313, 791-792 (2002).

28) Complex magnetic phase diagram of $CeRh_2Ge_2$
H. Abe, K. Yoshii and H. Kitazawa
Physica B 312-313, 253-255 (2002).
29) Magnetism and transport of $Ln_{0.5}Sr_{0.5}CoO_3$ (*Ln*=Pr, Nd, Sm, Eu and Gd)
K. Yoshii, H. Abe and A. Nakamura, M. Mizumaki and T. Muro
J. Magn. Magn. Mater. 239, 85-87 (2002).
30) Magnetic properties of $(Mn_{1-x}V_X)Sb_2O_4$ with one-dimensional magnetic arrays
H. Abe, K. Yoshii and H. Kitazawa
Phys. Stat. Sol. (a) 189, 429-432 (2002).
31) Magnetic behavior of $CeTi_{1-x}V_xO_3$
K. Yoshii and H. Abe
J. Alloys Compd. 343, 199-203 (2002).
32) Magnetic properties of $LnMnO_3$ (*Ln*=Ho, Er, Tm, Yb and Lu)
K. Yoshii and H. Abe
J. Solid State Chem. 165, 131-135 (2002).
33) Structure and electrical transport property of a silicopnictide ZrCuSiP
H. Abe and K. Yoshii
J. Solid State Chem.165, 372-374 (2002).
34) Single crystal growth of silver-lead oxide $Ag_5Pb_2O_6$ from fused nitrates
H. Abe, J. Ye, M. Imai, K. Yoshii, A. Matsushita and H. Kitazawa
J. Crystal Growth 241, 347-351 (2002).
35) Electrochemical synthesis of superconductive boride MgB_2 from molten salts
H. Abe and K. Yoshii
Jpn. J. Appl. Phys. (Part 2) 41, L685-L687 (2002).
36) MCD studies in 2p and 3d XAS of $La_{1-x}Sr_xCoO_3$
M. Mizumaki, K. Yoshii, N. Kawamura and M Nakazawa
Surf. Rev. Lett. 9, 855-859 (2002).

Surface chemistry research (Surface Chemistry Research Group)

1. Journals

1) Initial oxidation states on Si(001) surface induced by translational kinetic energy of O_2 at room temperature studied by Si-2p core-level spectroscopy using synchrotron radiation
A. Yoshigoe, Y. Teraoka
Surf. Sci. 482-485, 189-195, 2001
2) In-situ Si-2p core-level spectroscopy using synchrotron radiation for initial oxidation on Si(001) surfaces induced by translational kinetic energy of O_2 molecules
A. Yoshigoe, Y. Teraoka
Transactions of the Materials Research Society of Japan, 26, 755-758, 2001
3) First results from the Actinide Science beamline BL23SU at SPring-8
Y. Saitoh, T. Nakatani, T. Matsushita, A. Agui, A. Yoshigoe, Y. Teraoka, A. Yokoya
Nulc. Instrum. Methods Phys. Res. A, 474, 253-258, 2001
4) First operation of circular dichroism measurements with periodic photon-helicity switching by a variably-polarizing undulator at BL23SU at SPring-8
A. Agui, A. Yoshigoe, T. Nakatani, T. Matsushita, Y. Saitoh, A. Yokoya, H. Tanaka, Y. Miyahara, T. Shimada, M. K. Takeuchi, T. Bizen, S. Sasaki, M. Takao, H. Aoyagi, T. P. Kubo, K. Satoh, S. Wu, Y. Hiramatsu, H. Ohkuma
Rev. Sci. Instrum. 72, 3191-3197, 2001
5) High-resolution photoemission spectroscopic analysis of initial oxidation processes on Si(001) surfaces induced by kinetic energy of O_2 molecules (Review)
Y. Teraoka, A. Yoshigoe
J. Jpn. Soc. Synchrotron Radiation Research, 15, 27-35, 2002, in Japanese
6) In situ photoemission spectroscopy using synchrotron radiation for O_2 translational kinetic energy induced oxidation processes of partially-oxidized Si(001) surfaces
Y. Teraoka, A. Yoshigoe
J. Surf. Sci. Soc. Jpn. 22, 530-536, 2001, in Japanese

7) Real time observation of oxygen chemisorption states on Si(001) during supersonic oxygen molecular beam irradiation
A. Yoshigoe, Y. Teraoka
Appl. Surf. Sci. 190, 60-65, 2002
8) Si 2p and O 1s photoemission from oxidized Si(001) surfaces depending on translational kinetic energy of incident O2 molecules
Y. Teraoka, A. Yoshigoe
Appl. Surf. Sci. 190, 75-79, 2002
9) Photoemission spectroscopic study on influence of O_2 translational kinetic energy for Si(001) initial oxidation
Y. Teraoka, A. Yoshigoe
Surf. Sci. 507-510, 797-802, 2002
10) In situ analysis of Si(001) initial oxidation by supersonic O_2 molecular beams using synchrotron radiation photoemission spectroscopy
A. Yoshigoe, Y. Teraoka
Surface and Interface 34, 432-436, 2002
11) Precise control of Si(001) initial oxidation by translational kinetic energy of O_2 molecules
Y. Teraoka, A. Yoshigoe
Jpn. J. Appl. Phys. 41, 4253-4260, 2002
12) Photon-stimulated ion desorption from mono- and multilayered silicon alkoxide on silicon by core-level excitation
Y. Baba, G. Wu, T. Sekiguchi, I. Shimoyama
J. Vac. Sci. Technol. A 19, 1485-1489, 2001
13) Fragment-ion desorption from sulfur-containing amino acids by localized core-level excitation
Y. Baba, T. Sekiguchi, I. Shimoyama
Surf. Rev. Lett. 9, 77-83, 2002
14) Local electronic and geometric structures of silicon atoms implanted in graphite
Y. Baba, T. Sekiguchi, I. Shimoyama
Nucl. Instrum. Meth. Phys. Res. B 194, 41-46, 2002
15) Uniaxial and biaxial field dependence of the thermal oxidation rate of silicon
H. Noma, H. Takahashi, H. Fujioka, M. Oshima, Y. Baba, K. Hirose, M. Niwa, K. Usuda, N. Hirashita
J. Appl. Phys. 90, 5434-5437, 2001
16) Local structure of the silicon implanted in a graphite single crystal
Y. Baba, I. Shimoyama, T. Sekiguchi
J. Surf. Sci. Soc. Jpn. 23, 417-422, 2002, in Japanese
17) Electroparamagnetic Resonance in biomolecules induced by core level resonance photoexcitation
A. Yokoya, K. Akamatsu, K. Fujii
Nucl. Instr. Meth. Phys. Res. B, in press
18) Infrared spectral changes in 2-deoxy-D-ribose by irradiation with monochromatic photons around oxygen K-edge
K. Akamatsu, K. Fujii, A. Yokoya
Nucl. Instr. Meth. Phys. Res. B, in press
19) X-ray absorption near edge structure of DNA bases around oxygen and nitrogen K-edge
K. Fujii, K. Akamatsu, A. Yokoya
Nucl. Instr. Meth. Phys. Res. B, in press
20) Repairbility of Lethal Lesions Produced by Phosphorus Photoabsorption in Yeast Cells
N. Usami, A. Yokoya, S. Ishizaka, K. Kobayashi,
J. Radiat. Res. 42, 317-331, 2001
21) Oxygen K-edge X-ray absorption near edge structures (XANES) of sublimated films of amino acids
M. Tanaka, T. Koketsu, K. Nakagawa, A. Agui, A. Yokoya
J. Synchrotron Radiat. 8, 1009-1011, 2001
22) Local Structure Analysis of Carbon Nitride Films by Utilizing NEXAFS Spectroscopy
I. Shimoyama
Jounal of the Japanese Society for Synchrotron Radiation Research, 15, 12-19, 2002, in Japanese
23) Fragmentation and Charge-Neutralization Pathways Depending on Molecular Orientation at Surfaces

T. Sekiguchi, H. Ikeura-Sekiguchi, M. Imamura, N. Matsubayashi, H. Shimada, Y. Baba
Surface Science, 482-485, 279-284, 2001

2. Proceedings

1) Precise control of Si(001) initial oxidation by translational kinetic energy of O_2 molecules (Invited)
Y. Teraoka, A. Yoshigoe
Digest of Papers, 2001 International Microprocess and Nanotechnology Conference, 108-109, 2001
2) Initial reaction dynamics in O_2/Si(001) system (Invited)
Y. Teraoka, A. Yoshigoe
Digest of Papers, The Vacuum Society of Japan 3rd Kansai Brunch Regular Meeting in 2001, 1-8, 2001, in Japanese
3) Initial oxidation processes of Si(001) surfaces induced by supersonic O_2 molecular beams (Invited)
Y. Teraoka, A. Yoshigoe
Proceedings of the 12th Symposium on Beam Engineering of Advanced Material Syntheses, 159-165, 2001, in Japanese
4) The effect of hydration on the radiation induction of DNA base lesions produced by base excision repair enzymes
A. Yokoya, S.M.T Cunniffe, P. O'Neill
Proceedings of the Workshop: Recognition of DNA damage as onset of successful repair: Computational and experimental approachs, JAERI-Conf 2002-005, 24-42, 2001
5) Characterization of radiation damages in DNA components by energy deposition from monochromatic synchrotron ultrasoft X-rays
K. Akamatsu, K. Fujii, A. Yokoya
Proceedings of the Workshop: Recognition of DNA damage as onset of successful repair: Computational and experimental approachs, JAERI-Conf 2002-005, 157, 2001
6) X-ray absorption near edge structure of DNA bases
K. Fujii, K. Akamatsu, A. Yokoya
Proceedings of the Workshop: Recognition of DNA damage as onset of successful repair: Computational and experimental approachs, JAERI-Conf 2002-005, 155, 2001
7) Surface Chemical Reaction Induced by Beams with Non-Thermal Energies
T.Sekiguchi, I.Shimoyama, Y.Baba
KEK Proceedings Vol.13(June-2001-M), 61-62, 2001
8) Influence of O_2 Incident Energy for Initial Sticking Probability and Product SiO Desorption Rate on Si(001) Surfaces
Y. Teraoka, A. Yoshigoe
Proceedings of 3rd International Symposium on Atomic Level Characterizations for New Materials and Devices 01, (2001) 341-344
9) Oxidation of HF-treated Si(001) Surfaces Induced by O_2 Translational Energy
A. Yoshigoe, Y. Teraoka
Proceedings of 3rd International Symposium on Atomic Level Characterizations for New Materials and Devices 01, (2001) 345-348

3. Report

1) Soft x-ray beamline -BL23SU- at SPring-8
A. Agui, A. Yoshigoe, Y. Saitoh, Y. Teraoka, A. Yokoya
JAERI-Review, 2001-003, 87, 2001
2) Photoemission spectroscopy on initial oxidation of Si(001) induced by O_2 translational energy using synchrotron radiation
Y. Teraoka, A. Yoshigoe
Atomic Collision Research in Japan, 27, 77-79, 2001
3) Real-time observation of oxidation states on Si(001)-2x1 during supersonic O_2 molecular beam irradiation
A. Yoshigoe, Y. Teraoka
Atomic Collision Research in Japan, 27, 80-82, 2001
4) Atomic level solid surface reactions and their analysis promoted by quantum beams

T. Urisu, M. Kitajima, Y. Teraoka
OYOBUTURI, 71, 114-115, 2002

5) Photoemission spectroscopic study on initial oxidation of Si(001) surfaces induced by supersonic O_2 molecular beams
Y. Teraoka, A. Yoshigoe
JAERI-Review 2001-046, 87, 2002

6) First results from the actinide beamline BL23SU at SPring-8
Y. Saitoh, T. Nakatani, T. Matsushita, A. Agui, A. Yoshigoe, Y. Teraoka, A. Yokoya
JAERI-Review 2001-046, 93, 2002

7) A soft x-ray beamline BL23SU
A. Agui, A. Yoshigoe, T. Nakatani, Y. Miyahara
JAERI-Review 2001-046, 70, 2002

8) Circular dichroism measurements with periodic photon-helicity switching by a variably-polarizing undulator at BL23SU at SPring-8
A. Agui, A. Yoshigoe, T. Nakatani, T. Matsushita, Y. Saitoh, A. Yokoya, H. Tanaka, Y. Miyahara, T. Shimada, M. Takeuchi, T. Bizn, S. Sasaki, H. Aoyagi, T. Kudo, K. Sato, S. Wu, Y. Hiramatsu, M. Mizumaki, H. Ohkuma
JAERI-Review 2001-046, 92, 2002

9) Highlights of SPring-8 BL23SU in 2000
A. Agui, A. Yoshigoe, T. Nakatani, Y. Saitoh, Y. Teraoka, A. Yokoya
JAERI-Tech 2001-043, 2001

10) Initial reaction dynamics in O_2/Si(001) system
Y. Teraoka, A. Yoshigoe
J. Vac. Soc. Jpn. 45, 36, 2002, in Japanese

11) Evidence for the Existence of a Nitrogen-Substituted Graphite Structure by the Polarization Dependence of NEXAFS
I. Shimoyama, G. Wu, T. Sekiguchi, Y. Baba
Photon Factory Activity Report 2000, Part A pp23-24, 2000.

Heavy atom science (Heavy Atom Science Research Group)

Journals

1) Orbital and Charge Ordering in $La_{1-x}Sr_{1+x}MnO_4$ ($0.4<x<0.5$)
Y. Wakabayashi, Y. Murakami, Y. Moritomo, I. Koyama, H. Nakao, T. Kiyama, T. Kimura, Y. Tokura, and N. Wakabayashi,
J. Phys. Soc. Jpn. 70, 1194-1197, 2001

2) Resonant X-ray-scattering study of Octahedral Tilt Ordering in $LaMnO_3$ and $Pr_{1-x}Ca_xMnO_3$
M. v. Zimmermann, C. S. Nelson, Y.-J. Kim, J. P. Hill, Doon Gibbs, H. Nakao, Y. Wakabayashi, Y. Murakami, Y. Tokura, Y. Tomioka, T. Arima, C.-C. Kao, D. Casa,C. Venkataraman, Th. Gog
Phys. Rev. B 64, 064411:1-9, 2001

3) Antiferro-Quadrupole Ordering of CeB_6 Studied by Resonant X-Ray Scattering
Hironori Nakao, Ko-ichi Magishi, Yusuke Wakabayashi, Youichi Murakami, Kuniyuki Koyama, Kazuma Hirota, Yasuo Endoh and Satoru Kunii
J. Phys. Soc. Jpn. 70, 1857-1860, 2001

4) X-ray Resonant Scattering Studies of Charge and Orbital Ordering in $Pr_{1-x}Ca_xMnO_3$
M. v. Zimmermann, C. S. Nelson, J. P. Hill, Doon Gibbs, M. Blume, D. Casa, B. Keimer, Y. Murakami, C.-C. Kao, C. Venkataraman, T. Gog, Y. Tomioka and Y. Tokura
J. Magn. Magn. Mater. 233, 31-37, 2001

5) Study of the eg Orbitals in the Bilayer Manganite $La_{2-2x}Sr_{1+2x}Mn_2O_7$ by Using Magnetic Compton-Profile Measurement
Akihisa Koizumi, Satoru Miyaki, Yukinobu Kakurani, Hiroyasu Koizumi, Nozomu Hiraoka, Kenji Makoshi, Nobuhiko Sakai, Kazuma Hirota and Youichi Murakami
Phys. Rev. Lett. 86, 5589-5592, 2001

6) "Devil's Staircase" -Type Phase Transition in NaV_2O_5 under High Pressure
K. Ohwada, Y. Fujii, N. Takesue, M. Isobe, Y. Ueda, H. Nakao, Y. Wakabayashi, Y. Murakami, K. Ito, Y. Amemiya, H. Fujihisa, K. Aoki, T. Shobu, Y, Noda and N. Ikeda

Phys. Rev. Lett. 87, 086402:1-4, 2001
7) X-ray resonant scattering studies of orbital and charge ordering in $Pr_{1-x}Ca_xMnO_3$
M. v. Zimmermann, C. S. Nelson, J. P. Hill, Doon Gibbs, M. Blume, D. Casa , B. Keimer, Y. Murakami , C.-C. Kao, C. Venkataraman, T. Gog, , Y. Tomioka and Y. Tokura
Phys. Rev. B 64, 195133:1-17, 2001
8) Orbital correlations in doped manganites
J. P. Hill, C. S. Nelson, M. v. Zimmermann, Y. －J. Kim, D. Gibbs, D. Casa, B. Keimer, Y. Murakami, C. Venkataraman, T. Gog, Y. Tomioka, Y. Tokura, V. Kiryukhin, T. Y. Koo, S.－W. Cheong
Appl. Phys. A 73, 723-730, 2001
9) Vibrational Dynamics of some Amorphous and Quasicrystalline Alloys
Gupta, P. Shah, N. P. Lalla, B. A. Dasannacharya, T. Harami, Y. Yoda, M. Seto, M. Yabashi and S. Kikuta
Materials Science and Engineering A304-306, 731-734, 2001
10) Transport channels of X-ray beamlines at SPring-8
S.Gotoh, H.Ohashi, K.Takeshita, M.Yabashi, M.Yamagata, Y.Asano, T.Ishikawa
Nucl.Inst&Meth.Physics Research A, 467-468,813-815, 2001
11) Construction and commissioning of a 215-m-long beamlines at SPring-8
S.Gotoh, K.Takeshita, Y.Suzuki, H.Ohashi, Y.Asano, H.Kimura, T.Matsushita, N.Yagi, Y.Isshiki, H.Yamasaki, Y.Yoneda, K.Umetani, T.Ishikawa
Nucl.Inst.&Meth. Physics Research A, 467-468, 682-685, 2001
12) Demagnetization of undulator magnets irradiated with electron beam
T.Bizen, R.Tanaka, Y.Asano, D.E.Kim, J.S.Bak, H.S.Lee, H.Kitamura
Nucl.Inst.&Meth. Physics Research A, 467-468, 185-189, 2001
13) Structural Analysis of Corrosion Product of Fe-Cr Alloy Film Using Synchrotron Radiation
M.Yamashita, H.Konishi, M.Takahashi, J.Mizuki, H.Uchida
Mater. Sci. Res. Int., Special Technical Publication 1, 398-401, 2001
14) X-ray absorption study of molten yttrium trihalides
Y. Okamoto, M. Akabori, H. Motohashi, H. Shiwaku and T. Ogawa
J. Synchrotron Rad., 8, 1191-1199, 2001
15) Development of Phase Contrast Radiography for Bone Imaging Using Synchrotron Radiation"
Koishi MORI, Hitoshi SATO, Norio SEKINE, Naoto SHIKANO, Masaru SATO, Daisuke SHIMAO, Takashi IGARASHI, Hideaki SHIWAKU and Kazuyuki HYODO
Analytical Sciences, Vol.17 Supplement, i1427-i1430, 2001

Proceedings

1) "Devil's staircase" type phase transition of NaV_2O_5 under high pressure
K. Ohwada
Bulletin of APS March Meeting, Vol.47, No.1, 483, 2002
2) International Workshop on Radiation Safety at Synchrotron Radiation Sources
Y.Asano
Proceedings of 1st International Workshop on Radiation Safety at Synchrotron Radiation Sources (Argonne USA) 7,2001

Reports

1) Study of Condensed Matter by Using Nuclear Resonant Scattering
M. Seto
Journal of the Crystallographic Society of Japan 43, 405-412, 2001 (in Japanese)

Electric material science (Electronic Material Science Group)

1. Journals

1) Photoemission Study of Quasi-One-Dimensional Halogen-Bridged Compound $[Ni(chxn)_2Br]Br_2$
S.-i. Fujimori, A. Ino, T. Okane, A. Fujimori, K. Okada, T. Manabe, M. Yamashita, H. Kishida, H. Okamoto
Surf. Rev. Lett., 9, 1065, 2002.

2) Angle-resolved photoemission study of the quasi-two-dimensional heavy-fermion compounds $CeRhIn_5$ and $CeIrIn_5$
S.-i. Fujimori, A. Ino, T. Okane, A. Fujimori, H. Harima, D. Aoki, S. Ikeda, H. Shishido, Y. Haga, Y. Tokiwa, Y. Onuki
Physica, B312-313, 132, 2002.
3) Soft x-ray absorption spectra in the O K region of microporous carbon and some reference aromatic compounds
Y. Muramatsu, K. Kuramoto, E. M. Gullikson, R. C. C. Perera,
Surf. Rev. Lett., 9, 267-270, 2002.
4) Total-electron-yield x-ray standing-wave measurements of multilayer x-ray mirrors for the interface structure evaluation
Y. Muramatsu, H. Takenaka, E. M. Gullikson, R. C. C. Perera.,
Jpn. J. Appl. Phys., 41, 4250-4252, 2002.
5) Evaluation methods of interlayer-structure distribution in multilayers by total-electron-yield x-ray standing wave measurements
Y. Muramatsu, H. Takenaka, E. M. Gullikson, R. C. C. Perera,
Advances in X-Ray Chemical Analysis, Japan 33, 145 - 154, 2002.
6) High-resolution photoemission spectroscopy of $Yb_2Co_3X_9$ (X = Ga and Al)
T. Okane, S.-i. Fujimori, A. Ino, A. Fujimori, S. K. Dhar, C. Mitra, P. Manfrinetti, A. Palenzona
Physica, B312-313, 349, 2002.
7) Photoemission study of $Yb_2Co_3X_9$ (X = Ga, Al): Variation of the electronic structure from a mixed-valent to Kondo-lattice system
T. Okane, S.-i. Fujimori, A. Ino, A. Fujimori, S. K. Dhar, C. Mitra, P. Manfrinetti, A. Palenzona, O. Sakai
Physical Review, B65, 125102, 2002.
8) First results from the actinide science beamline BL23SU at SPring-8
Y. Saioh, T. Nakatani, T. Matsushita, A. Agui, A. Yoshigoe, Y. Teraoka, A. Yokoya
Nucl. Instrum. Meth. Phys. Res., A474, 253-258, 2001
9) High resolution soft x-ray absorption spectroscopy of solids
Y. Saitoh, T. Muro, M. Kotsugi, T. Iwasaki, A. Sekiyama, S. Imada and S. Suga
J. Synchrotron Rad., 8, 339-341, 2001.
10) Soft x-ray beamline for spectroscopy of solids at SPring-8
Y. Saitoh, H. Kimura, Y. Suzuki, T. Nakatani, T. Matsushita, T. Muro, T. Miyahara, M. Fujisawa, K. Soda, S. Ueda, A. Sekiyama, S. Imada and S. Suga
Nucl. Instrum. Meth. Phys. Res., A467-468, 553-556, 2001.
11) Electronic-structure investigation of CeB_6 by means of soft-x-ray scattering
M. Magnuson, S. M. Butorin, J.-H. Guo, A. Agui, J. Nordgren, H. Ogasawara, A. Kotani, T. Takahashi, S. Kunii
Phys. Rev., B63, 75101, 2001.
12) Performance of soft x-ray emission spectrometer employing charge-coupled device detector
T. A. Sasaki, N. Chugan, Y. Muramatsu
Nucl. Instrum. Meth. Phys. Res., A467-468, 1489-1492, 2001.
13) Soft x-ray reflectivity and structure evaluation of CoCr/C multilayer x-ray mirrors for spectral region around 6 nm
H. Takenaka, K. Nagai, H. Ito, Y. Muramatsu, T. Kawamura, E. M. Gullikson, R. C. C. Perera
Nucl. Instrum. Meth. Phys. Res., A467-468, 337-340, 2001.
14) Soft x-ray reflectivity and structure evaluation of Ni/C/Ti/C multilayer x-ray mirrors for water-window region
H. Takenaka, H. Ito, K. Nagai, Y. Muramatsu, E. M. Gullikson, R. C. C. Perera
Nucl. Instrum. Meth. Phys. Res., A 467-468, 341-344, 2001.
15) Magnetic Circular Dichroism of X-Ray Emission for Gadolinium in *4d-4f* Excitation Region
Y. Takayama, M. Shinoda, K. Obu, C. Lee, H. Shiozawa, M. Hirose, H. Ishii, T. Miyahara, J. Okamoto
J. Phys. Soc. Jpn., 71, 340, 2002.
16) X-ray Absorption of the Negative Charge-Transfer Material $SrFe_{1-x}Co_xO_3$
M. Abbate, G. Zampieri, J. Okamoto, A. Fujimori, S. Kawasaki, M. Takano

Phys. Rev. B 65, 165120, 2002.
17) Magnetic Circular Dichroism at Transition Metal $L_{2,3}$ Edges in $D0_3$-type $(Fe_{1-x}Mn_x)_3Al$ Alloys
K. Soda, O. Yoshimoto, H. Nozaki, T. Takeuchi, U. Mizutani, H. Kato, M. Kato, Y. Nishino, S. Imada, S. Suga, T. Matsushita, Y. Saitoh
J. Synchrotron Rad., 8, 455-456, 2001.
18) Magnetic Circular Dichroism at Transition Metal $L_{2,3}$ Edges in $D0_3$-type $(Fe_{1-x}V_x)_3Al$ Alloys
O. Yoshimoto, M. Kato, K. Soda, H. Nozaki, T. Takeuchi, U. Mizutani, M. Kato, Y. Nishino, S. Imada, S. Suga, T. Matsushita, Y. Saitoh
J. Synchrotron Rad., 8, 457-459, 2001.
19) X-MCD at twin-helical undulator beamline BL25SU of SPring-8
S. Suga, S. Imada, A. Yamasaki, S. Ueda, T. Muro, Y. Saitoh
J. Magn. Magn. Mater., 233, 60-64, 2001.
20) Construction of two-dimensional photoelectron spectrometer at SPring-8
M. Kotsugi, Y. Miyatake, K. Enomoto, K. Fukumoto, A. Kobayashi, T. Nakatani, Y. Saitoh, T. Matsushita, S. Imada, T. Furuhata, S. Suga, K. Soda, M. Jinno, T. Hirano, K. Hattori, H. Daimon
Nucl. Instrum. Meth., A 467-468, 1493-1496, 2001.
21) Bulk-sensitive high-resolution Ce 3d-4f resonance photoemission study of CeNiSn and CePdSn
A. Sekiyama, S. Suga, T. Iwasaki, S. Ueda, S. Imada, Y. Saitoh, T. Yoshino, T. Adroja, T. Takabatake
J. Electron Spectrosc. Relat. Phenom., 114-116, 699-703, 2001.
22) Magnetic circular dichroism in Mn 2p core absorption of $Ga_{1-x}Mn_xAs$
S. Ueda, S. Imada, T. Muro, Y. Saitoh, S. Suga, F. Matsukura, H. Ohno,
Physica , E10, 210-214, 2001.
23) Magnetic circular dichroism in the soft X-ray absorption spectra of intercalation compounds Fe_xTiS_2
A.Yasaki, S. Imada, H. Utsunomiya, T. Muro, Y. Saitoh, H. Negishi, M. Sasaki, M. Inoue, S. Suga,
Physica, E10, 387-390, 2001.

3. Reports

1) Operation of circular dichroism measurements with periodic photon-helicity switching by an APPLE-2 type undulator at BL23SU in SPring-8
A. Agui, A. Yoshigoe, T. Nakatana, T. Matsushita, Y. Saitoh, M. Mizumaki, A. Yokoya, H. Tanaka, Y. Miyahara, T. Shimada, M. Takeuchi, M. Takao, S. Sasaki, H. Aoyagi, T. Kudo, K. Sato, S. Wu, H. Ohkuma
Journal of the Japanese Society for Synchrotron Radiation Research, 14, 17-26, 2001.

Synchrotron radiation simulation research (Simulation Group for Materials Science)

1) Theory of Field-Induced Gap Formation in Charge-Ordered Yb_4As_3
H. Shiba, K. Ueda, O. Sakai and S. -J. Qin
Physica B312-313, 309, 2002.
2) Structure, Effective Hamiltonian and Magnetic Excitation Spectrum in Charge-Ordered Yb_4As_3
H. Shiba, K. Ueda, O. Sakai and S. -J. Qin
Proceeding of French-Japanese Symposium on Quantum Properties of Low-Dimensional Antiferromagnets, p.183, 2002

Appendix A Activities of the Research Committee

A research committee was organized in FY1996 to promote activities on advanced photon and synchrotron radiation research in Kansai Research Establishment, JAERI. There are three technical subcommittees for Laser System, Laser Utilization and Synchrotron Radiation Utilization, under the committee.

Committee for Advanced Photon and Synchrotron Radiation Research

First meeting	March 21	1997	Tokyo
Second meeting	February 3	1998	Tokyo
Third meeting	March 9	1999	Tokyo
Fourth meeting	February 10	2000	Tokyo
Fifth meeting	March 2	2001	Kashiwa
Sixth meeting	March 11	2002	Kizu

Technical Subcommittee for Laser System

First meeting	December 8	1997	Tokyo
Second meeting	July 30	1998	Tokyo
Third meeting	December 13	1999	Tokyo
Fourth meeting	February 1	2001	Tokyo
Joint meeting	February 12	2002	Kashiwa

Technical Subcommittee for Laser Utilization

First meeting	December 10	1997	Tokyo
Second meeting	December 3	1998	Tokyo
Third meeting	December 24	1999	Tokyo
Fourth meeting	February 15	2001	Kizu
Joint meeting	February 12	2002	Kashiwa

Technical Subcommittee for Synchrotron Radiation Utilization

First meeting	December 9	1997	Tokyo
Second meeting	November 27	1998	Harima (SPring-8)
Third meeting	February 8	2000	Harima (SPring-8)
Fourth meeting	February 28	2001	Harima (SPring-8)
Fifth meeting	February 25	2002	Harima (SPring-8)

Members of Committee

Committee for Advanced Photon and Synchrotron Radiation Research (FY2001)

Chair	Chiyoe	YAMANAKA	Director General, Institute for Laser Technology
Vice-Chair	Susumu	NAMBA	Professor, Technical Research Center, Nagasaki Institute of Applied Science
	Shuntaro	WATANABE	Professor, Institute for Solid State Physics, The University of Tokyo
	Seishi	KIKUTA	Executive Director, Deputy Director General, Japan Synchrotron Radiation Research Institute
	Katsunobu	AOYAGI	Professor, Interdisciplinary Graduate School of Science and Engineering, Tokyo Institute of Technology
	Fumio	INABA	Professor Emeritus, Tohoku University
	Nobutsugu	IMANISHI	Professor, Graduate School of Engineering, Kyoto University
	Naoki	SATO	Professor, Institute for Chemical Research, Kyoto University
	Yoshitaka	KIMURA	Director, Institute of Materials Structure Science, High Energy Accelerator Research Organization
	Hiroshi	TAKADA	Director, Harima Research Laboratory, Sumitomo Electric Industries, Ltd.
	Takeshi	NAMIOKA	Professor Emeritus, Tohoku University
	Kazuyoshi	YAMADA	Professor, Institute for Chemical Research, Kyoto University
	Tatsuhiko	YAMANAKA	Director, Institute of Laser Engineering, Osaka University
	Mamoru	FUJIWARA	Assistant Professor, Research Center for Nuclear Physics, Osaka University Invited Researcher, Advanced Science Research Center, JAERI
	Kenji	NODA	Director, Office of Planning, JAERI
	Yoshiaki	KATO	Director General, Kansai Research Establishment, JAERI
Subcommittee	Takashi	ARISAWA	Director, Advanced Photon Research Center, JAERI
	Osamu	SHIMOMURA	Director, Synchrotron Radiation Research Center, JAERI
Secretary	Toyoaki	KIMURA	Senior Staff, Office of Planning, JAERI
	Tohru	MATOBA	General Manager, Advanced Photon Research Center, JAERI
	Junichiro	MIZUKI	Deputy Director, Synchrotron Radiation Research Center, JAERI
	Noboru	TSUCHIDA	Deputy General Manager, Advanced Photon Research Center, JAERI
	Hironobu	OGAWA	Deputy General Manager, Synchrotron Radiation Research Center, JAERI

Technical Subcommittee for Laser System (FY2001)

Chief	Shuntaro	WATANABE	Professor, Institute for Solid State Physics, The University of Tokyo
	Shinichiro	AOSHIMA	Central Research Laboratory, Mahatmas Photonics K.K.
	Ichita	ENDO	Professor, Graduate School of Advanced Sciences of Matter, Hiroshima University
	Hiroo	KINOSHITA	Professor, Laboratory of Advanced Science and Technology for Industry, Himeji Institute of Technology
	Takatomo	SASAKI	Professor, Faculty of Engineering, Osaka University
	Toshihisa	TOMIE	Principal Scientist, Electro technical Laboratory
	Masahiro	NAKATSUKA	Professor, Institute of Laser Engineering, Osaka University
	Takashi	FUJIMOTO	Professor, Graduate School of Engineering, Kyoto University
	Tetsuo	YAMAZAKI	Professor, Institute of Advanced Energy Laboratory, Kyoto University
	Kuniyoshi	YOKOO	Professor, Research Institute of Electrical Communication, Tohoku University
	Kenzo	MIYAZAKI	Invited Researcher, Advanced Photon Research Center, JAERI Professor, Institute of Advanced Energy Laboratory, Kyoto University
	Takashi	ARISAWA	Director, Advanced Photon Research Center, JAERI
Secretary	Noboru	TSUCHIDA	Deputy General Manager, Advanced Photon Research Center, JAERI
	Akihiko	NISHIMURA	Senior Scientist, Advanced Photon Research Center, JAERI

Technical Subcommittee for Applied Photon Research (FY2001)

Chief	Susumu	NAMBA	Professor, Technical Research Center, Nagasaki Institute of Applied Science
	Akira	IWATA	Deputy Director, Kanto Technical Institute, Kawasaki Heavy Industries, Ltd.
	Atsushi	OGATA	Professor, Graduate School of Advanced Sciences of Matter, Hiroshima University
	Ichiro	KATAYAMA	Professor, Institute of Particle and Nuclear Studies, High Energy Accelerator Research Organization
	Yoneyoshi	KITAKAWA	Assistant Professor, Institute of Laser Engineering, Osaka University
	Takayoshi	KOBAYASHI	Professor, Faculty of Science, The University of Tokyo
	Seiichi	TAGAWA	Professor, Institute of Scientific and Industrial Research, Osaka University
	Akira	NODA	Professor, Institute for Chemical Research, Kyoto University
	Takayasu	MOCHIDUKI	Professor, Laboratory of Advanced Science and Technology for Industry, Himeji Institute of Technology
	Kazuhisa	NAKAJIMA	Invited Researcher, Advanced Photon Research Center, JAERI Assistant Professor, Accelerator Laboratory, High Energy Accelerator Research Organization
	Hiroyuki	DAIDO	Group Leader, Advanced Photon Research Center, JAERI
Secretary	Tohru	MATOBA	General Manager, Advanced Photon Research Center, JAERI
	Yuzuru	KUROSAKI	Senior Scientist, Advanced Photon Research Center, JAERI

Technical Subcommittee for Synchrotron Radiation (FY2001)

Chief	Seishi	KIKUTA	Executive Director, Deputy Director General, Japan Synchrotron Radiation Research Institute
	Tatsuo	UEKI	Director, Japan Synchrotron Radiation Research Institute
	Shik	SHIN	Professor, Institute for Solid State Physics, The University of Tokyo
	Toshio	TAKAHASHI	Assistant Professor, Institute for Solid State Physics, The University of Tokyo
	Kenichiro	TANAKA	Professor, Faculty of Science, Hiroshima University
	Kazuhiko	TSUJI	Professor, Faculty of Science and Technology, Keio University
	Saburo	NASU	Professor, Faculty of Engineering Science
	Kotaro	HIEDA	Professor, Faculty of Science, Rikkyo University
	Yoshichika	OHNUKI	Invited Researcher, Advanced Science Research Center, JAERI Professor, Faculty of Science, Osaka University
	Yoichi	MURAKAMI	Invited Researcher, Synchrotron Radiation Research Center, JAERI Assistant Professor, Institute of Materials Structure Science, High Energy Accelerator Research Organization
	Osamu	SHIMOMURA	Director, Synchrotron Radiation Research Center, JAERI
Secretary	Junichiro	MIZUKI	Deputy Director, Synchrotron Radiation Research Center, JAERI
	Hironobu	OGAWA	Deputy General Manager, Synchrotron Radiation Research Center, JAERI

Appendix B Organization of Kansai Research Establishment

(April 1, 2001～March 31, 2002)

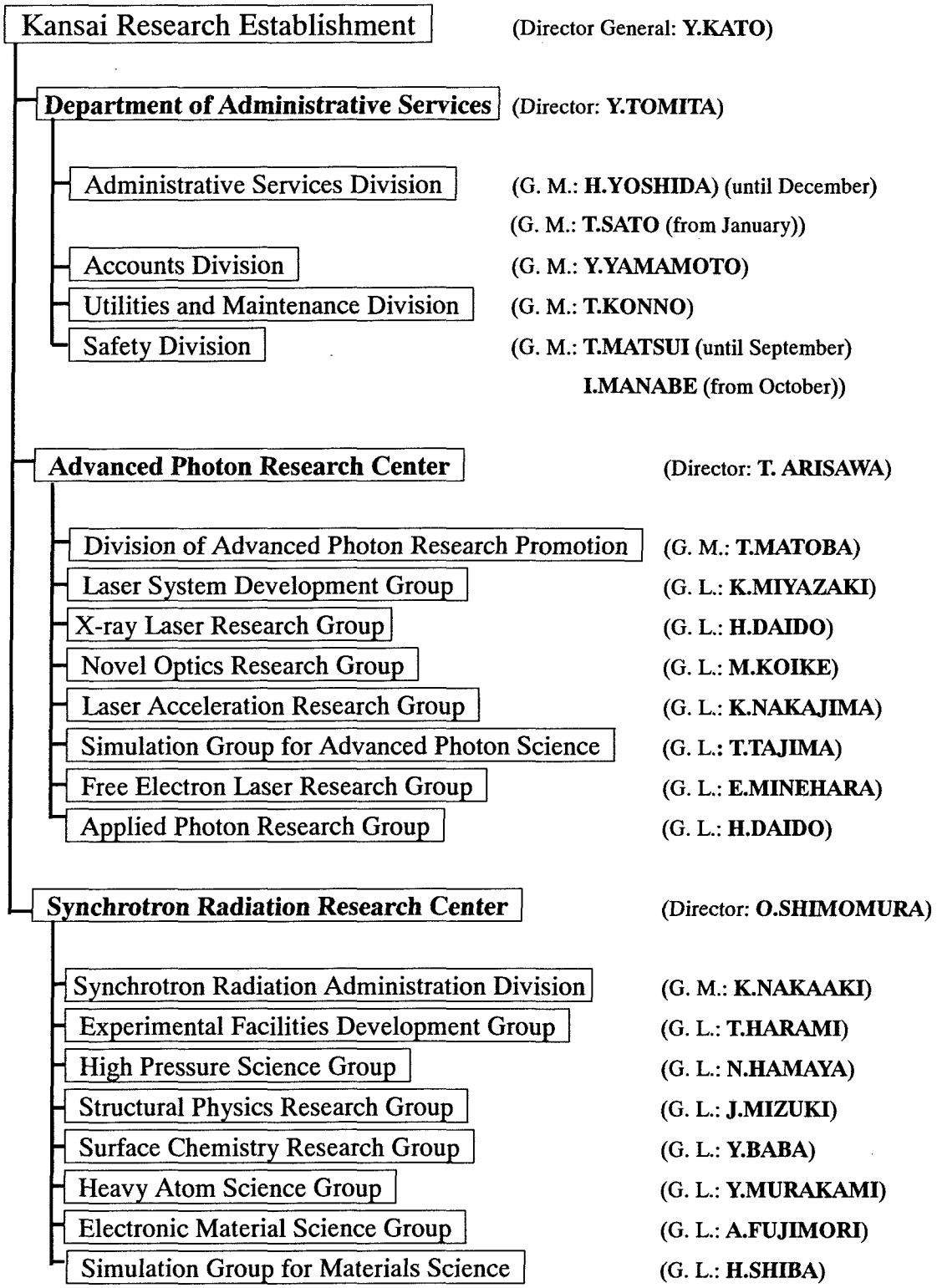

G. M.: General Manager G. L.: Group Leader

Appendix C Personnel

(April 1, 2001～March 31, 2002)

Personnel at Advanced Photon Research Center

Takashi ARISAWA
Norio OGIWARA
Osamu YAMASHITA
Tsutomu WATANABE(until September)
Shigeru MORI(from October)
Kazunori KIKUCHI
Naohiko KAYORA
Jun NAKAJIMA
Kiyomi ENDOH
Masako SHIGENARI

Division of Advanced Photon Research Promotion
Tohru MATOBA
Noboru TSUCHIDA
Sayaka HARAYAMA
Shuichi FUJITA
Noriko UEHARA

Laser System Development Group
Kenzo MIYAZAKI
Koichi YAMAKAWA
Akihiko NISHIMURA
Akira OZU
Junji KAWANAKA
Hiromitsu KIRIYAMA
Yutaka AKAHANE
Keiichi YOKOYAMA
Kyoichi DEKI
Fumiaki MATSUOKA
Tsutomu USAMI
Norihiro INOUE
Makoto AOYAMA
Yuji FUKUDA
Akio YASUHARA
Kenichi YAGI
Koichi WADA
Jinglong MA

X-ray Laser Research Group
Hiroyuki DAIDO
Keisuke NAGASHIMA
Yoji SUZUKI
Masataka KADO
Maki KISHIMOTO
Tetsuya KAWACHI
Noboru HASEGAWA
Momoko TANAKA
Kouta SUKEGAWA
Kenjiro TAKAHASHI
Shinichi NANBA
Renzhong TAI
Peixiang LU
huajing TANG

Novel Optics Research Group
Masato KOIKE
Osamu YODA
Akira SUGIYAMA
Masahiko ISHINO
Hiroyasu FUKUYAMA
Kazuo SANO

Laser Acceleration Research Group
Kazuhisa NAKAJIMA
Shuhei KANAZAWA
Hideyuki KOTAKI
Shuji KONDO
Masaki KANDO
Takashi YOKOYAMA
Shinichi MASUDA
Igor V. SNETANIN

Simulation Group for Advanced Photon Science
Toshiki TAJIMA
Mitsuru YAMAGIWA
Toshizo SHIRAI
Akira SASAKI
James KOGA
Kengo MORIBAYASHI
Yutaka UESHIMA
Takayuki UTSUMI
Takuya ARAKAWA
Ichirou FUKUMOTO
Keiko SUTO
Hiroo TOTSUJI
Shingo SUZUKI
Sergei V. BULANOV(from March)

Free Electron Laser Research Group
Eisuke MINEHARA
Toshihiko YAMAUCHI
Masaru SAWAMURA
Ryoichi HAJIMA
Ryoji NAGAI
Nobuhiro KIKUZAWA
Takehito HAYAKAWA
Nobuyuki NISHIMORI
Toshiyuki SHIZUMA

Applied Photon Research Group
Hiroyuki DAIDO
Yuichi SHIMIZU
Yuzuru KUROSAKI
Koichi OGURA
Hiroshi MURAKAMI
Akito SAGISAKA
Satoshi ORIMO
Mamiko NISHIUCHI
Yukio HAYASHI
Junkei KOU
Kazuhito YASUIKE
Masayuki SUZUKI
Takatsugu OKETA
Hiroki BABA
Etsuya YANASE(from June)
Koji MATSUKADO(from September)

(April 1, 2001～March 31, 2002)

Personnel at Synchrotron Radiation Research Center

Osamu SHIMOMURA
Jun-ichiro MIZUKI
Nobuo NIIMURA
Hironobu OGAWA
Teikichi SASAKI
Hiroko NISHIZAKI
Akiko SHIMAMURA

Experimental Facilities Development Group
Taikan HARAMI
Hiroyuki KONISHI
Yoshihiro ASANO
Hideaki SHIWAKU
Yukio HAYASHI
Haruhiko MOTOHASHI
Kazukiyo TOZAWA
Takahisa SHOBU

High Pressure Science Group
Nozomu HAMAYA
Makoto SAKATA
Wataru UTSUMI
Yoshinori KATAYAMA
Tetsu WATANUKI
Hiroshi KANEKO
Naoki ISHIMATSU
Taku OKADA
Yasuhiro INAMURA
Tomohiro IKEDA
Kazutaka NAKANO

Structural Physics Research Group
Junichiro MIZUKI
Yasuo NISHIHATA
Kentaro SUZUYA
Norimasa MATSUMOTO
Kenji YOSHII
Masamitu TAKAHASI
Yasuhiro YONEDA
Tatsuo FUKUDA
Hiroyuki KAWAMURA
Yusuke AZUMA
Yusuke HIRAMITSU
Naomasa YAMAMOTO
Hiroki WATANABE

Surface Chemistry Research Group
Yuji BABA
Akinari YOKOYA
Yuden TERAOKA
Tetsuhiro SEKIGUCHI
Akinari YOKOYA
Akitaka YOSHIGOE
Iwao SHIMOYAMA
Kentaro FUJII
Krishna G. NATH
Ken AKAMATSU

Heavy Atom Science Group
Yoichi MURAKAMI
Makoto SETO
Toshiya INAMI
Takaya MITSUI
Kenji ISHII
Kenji OHWADA

Electronic Material Science Group
Atsushi FUJIMORI
Yasuji MURAMATSU
Tetsuo OKANE
Yuji SAITOH
Akane AGUI
Shin-ichi FUJIMORI
Jun OKAMOTO
Kazutoshi MAMIYA
Nobuhiko NAKAGISHI
Kentoro KURAMOTO

Electronic Material Science Group
Hiroyuki SHIBA

Synchrotron Radiation Administration Division
Katsuhiko NAKAAKI
Hironobu OGAWA
Masahiko MATSUMOTO
Kensin DOI
Sachiko MITSUDERA

(April 1, 2001～March 31, 2002)

Personnel at Kansai Research Establishment

Yoshiaki KATO
Siro NAGAI(until September)

Personnel at Department of Administrative Services

Yusuke TOMITA
Tetsuo KANAZAWA(until December)
Hiroshi YOSHIDA(from January)

Administrative Services Division

Hiroshi YOSHIDA
Hisayoshi KUROHA(until September)
Hiroshi YOSHIDA(from October)
Yoshimi KURATA
Ken SASAKI
Fumiyuki SAIZEN
Yuko HASEGAWA
Shinji KOMATA
Michiyo YABUTA

Accounts Division

Yoshio YAMAMOTO
Saburo YAMAGISHI
Hiroyuki YAMANO
Tatsuki SUKEGAWA
Taiki IKEJIMA
Kazumi TAKEDA
Susumu KAWAKAMI
Shinobu KOIZUMI

Utilities and Maintenance Division

Toshio KONNO
Tadashi HANAWA
Jun MATSUMOTO
Tetsuya YAMAMOTO
Tsutomu TOMIYA
Kotomi WAKI

Safety Division

Tomoaki MATSUI(until September)
Iwao MANABE(from October)
Yaichi FUKUSHIMA
Masayuki UENO
Masayuki KABUTOU
Izumi TAMURA

Appendix D Symposia

(1) The first JAERI-Kansai International Workshop on Ultrashort-pulse Ultrahigh-power Lasers and Simulation for Laser-plasma Interactions (held as "Joint ICFA/JAERI-Kansai International Workshop '97", organized by International Committee for Future Accelerators, hosted by Japan Atomic Energy Research Institute and High Energy Accelerator Research Organization)
July 14-18, **1997**, Kyoto, Japan
JAERI-Conf 98-004, "Proceedings of The first JAERI-Kansai International Workshop on Ultrashort-pulse Ultrahigh-power Lasers and Simulation for Laser-plasma Interactions, July 14-18, 1997, Kyoto Research Park, Kyoto, Japan", March 1998.

(2) The 6th International Conference on Synchrotron Radiation Instrumentation (cosponsored by Japan Atomic Energy Research Institute, Japanese Society for Synchrotron Radiation Research, RIKEN and Japan Synchrotron Radiation Research Institute)
August 4－8, **1997**, Himeji, Japan
J. Synchrotron Radiation, 5 part 3, "SRI'97 Proceedings", May 1998.

(3) 6th International Conference on X-Ray Lasers (cosponsored by Japan Atomic Energy Research Institute and Osaka University)
August 31-September 4, **1998**, Kyoto, Japan
Institute of Physics Conference Series Number 159, "Proceedings of the 6th International Conference on X-Ray Lasers held in Kyoto, Japan, August 31-September 4, 1998"

(4) The Second International Conference on Synchrotron Radiation in Materials Science (cosponsored by Japan Atomic Energy Research Institute, RIKEN and Japan Synchrotron Radiation Research Institute)
October 31－November 3, **1998**, Kobe, Japan
Jpn. J. Appl. Phys. Suppl., 38-1, "Proceedings of the SRMS－2", June 1999.

(5) The First Symposium on Advanced Photon Research
November 8-9, **1999**, Kyoto, Japan
JAERI-Conf 2000-006, "Proceedings of The First Symposium on Advanced Photon Research, November 8-9, 1999, Keihanna Plaza/Advanced Photon Research Center, Kyoto, Japan", March 2000.

(6) Workshop on Surface and Interface Using Synchrotron Radiation
March 16-17, **2000**, SPring-8, Japan

(7) The Second Symposium on Advanced Photon Research
November 9-10, **2000**, Kyoto, Japan
JAERI-Conf 2001-011, "Proceedings of The Second Symposium on Advanced Photon Research, November 9-10, 2000, Advanced Photon Research Center, Kyoto, Japan", July 2001.

(8) 2nd UK-Japan International Seminar of Application Radiation to Studies of Nano-structured Materials
(cosponsored by institute of Molecular Science, Japan Atomic Energy research Institute, RIKEN and JASRI)
July 9-10, **2000**, SPring-8, Japan

(9) International Workshop on "Crystallography at High Pressure and High Temperature using X-ray and Neutrons"
(cosponsored by Synchrotron Radiation Research Center of JAERI, JASRI and International Union of Crystallography Commission on High Pressure)
September 30-October 3, **2000**, SPring-8, Japan

(10) OECD Global Science Forum "Workshop on Compact High-Intensity Short-Pulse Lasers: Future Directions and Applications"
(cosponsored by OECD Global Science Forum and JAERI)
May 28-30, **2001**, Kansai Research Establishment, Kyoto, Japan
OECD Global Science Forum, "Final Report from the Workshop"

(11) The Third Symposium on Advanced Photon Research
December 13-14, **2001**, Kyoto, Japan
JAERI-Conf 2002-008, "Proceedings of The Third Symposium on Advanced Photon Research, December 13-14, 2001, Advanced Photon Research Center, Kyoto, Japan", July 2002.

(12) Korean-Japanese International workshop on Strongly Correlated Electron Systems
September 3-4, **2001**, SPring-8, Japan

This is a blank page.

国際単位系 (SI) と換算表

表 1　SI 基本単位および補助単位

量	名称	記号
長さ	メートル	m
質量	キログラム	kg
時間	秒	s
電流	アンペア	A
熱力学温度	ケルビン	K
物質量	モル	mol
光度	カンデラ	cd
平面角	ラジアン	rad
立体角	ステラジアン	sr

表 2　SI と併用される単位

名称	記号
分，時，日	min，h，d
度，分，秒	°，′，″
リットル	l，L
トン	t
電子ボルト	eV
原子質量単位	u

1 eV = 1.60218 × 10^{-19} J

1 u = 1.66054 × 10^{-27} kg

表 5　SI 接頭語

倍数	接頭語	記号
10^{18}	エクサ	E
10^{15}	ペタ	P
10^{12}	テラ	T
10^{9}	ギガ	G
10^{6}	メガ	M
10^{3}	キロ	k
10^{2}	ヘクト	h
10^{1}	デカ	da
10^{-1}	デシ	d
10^{-2}	センチ	c
10^{-3}	ミリ	m
10^{-6}	マイクロ	μ
10^{-9}	ナノ	n
10^{-12}	ピコ	p
10^{-15}	フェムト	f
10^{-18}	アト	a

表 3　固有の名称をもつ SI 組立単位

量	名称	記号	他の SI 単位による表現
周波数	ヘルツ	Hz	s^{-1}
力	ニュートン	N	m·kg/s^2
圧力，応力	パスカル	Pa	N/m^2
エネルギー，仕事，熱量	ジュール	J	N·m
工率，放射束	ワット	W	J/s
電気量，電荷	クーロン	C	A·s
電位，電圧，起電力	ボルト	V	W/A
静電容量	ファラド	F	C/V
電気抵抗	オーム	Ω	V/A
コンダクタンス	ジーメンス	S	A/V
磁束	ウェーバ	Wb	V·s
磁束密度	テスラ	T	Wb/m^2
インダクタンス	ヘンリー	H	Wb/A
セルシウス温度	セルシウス度	℃	
光束	ルーメン	lm	cd·sr
照度	ルクス	lx	lm/m^2
放射能	ベクレル	Bq	s^{-1}
吸収線量	グレイ	Gy	J/kg
線量当量	シーベルト	Sv	J/kg

表 4　SI と共に暫定的に維持される単位

名称	記号
オングストローム	Å
バーン	b
バール	bar
ガル	Gal
キュリー	Ci
レントゲン	R
ラド	rad
レム	rem

1 Å = 0.1 nm = 10^{-10} m

1 b = 100 fm^2 = 10^{-28} m^2

1 bar = 0.1 MPa = 10^5 Pa

1 Gal = 1 cm/s^2 = 10^{-2} m/s^2

1 Ci = 3.7 × 10^{10} Bq

1 R = 2.58 × 10^{-4} C/kg

1 rad = 1 cGy = 10^{-2} Gy

1 rem = 1 cSv = 10^{-2} Sv

（注）

1. 表 1 − 5 は「国際単位系」第 5 版，国際度量衡局 1985 年刊行による。ただし，1 eV および 1 u の値は CODATA の 1986 年推奨値によった。
2. 表 4 には海里，ノット，アール，ヘクタールも含まれているが日常の単位なのでここでは省略した。
3. bar は，JIS では流体の圧力を表わす場合に限り表 2 のカテゴリーに分類されている。
4. EC 閣僚理事会指令では bar，barn および「血圧の単位」mmHg を表 2 のカテゴリーに入れている。

換　算　表

力	N(=10^5 dyn)	kgf	lbf
	1	0.101972	0.224809
	9.80665	1	2.20462
	4.44822	0.453592	1

粘度　1 Pa·s(N·s/m^2) = 10 P(ポアズ)(g/(cm·s))

動粘度　1 m^2/s = 10^4 St(ストークス)(cm^2/s)

圧力	MPa(=10 bar)	kgf/cm^2	atm	mmHg(Torr)	lbf/in^2(psi)
	1	10.1972	9.86923	7.50062 × 10^3	145.038
	0.0980665	1	0.967841	735.559	14.2233
	0.101325	1.03323	1	760	14.6959
	1.33322 × 10^{-4}	1.35951 × 10^{-3}	1.31579 × 10^{-3}	1	1.93368 × 10^{-2}
	6.89476 × 10^{-3}	7.03070 × 10^{-2}	6.80460 × 10^{-2}	51.7149	1

エネルギー・仕事・熱量	J(=10^7 erg)	kgf·m	kW·h	cal(計量法)	Btu	ft·lbf	eV
	1	0.101972	2.77778 × 10^{-7}	0.238889	9.47813 × 10^{-4}	0.737562	6.24150 × 10^{18}
	9.80665	1	2.72407 × 10^{-6}	2.34270	9.29487 × 10^{-3}	7.23301	6.12082 × 10^{19}
	3.6 × 10^6	3.67098 × 10^5	1	8.59999 × 10^5	3412.13	2.65522 × 10^6	2.24694 × 10^{25}
	4.18605	0.426858	1.16279 × 10^{-6}	1	3.96759 × 10^{-3}	3.08747	2.61272 × 10^{19}
	1055.06	107.586	2.93072 × 10^{-4}	252.042	1	778.172	6.58515 × 10^{21}
	1.35582	0.138255	3.76616 × 10^{-7}	0.323890	1.28506 × 10^{-3}	1	8.46233 × 10^{18}
	1.60218 × 10^{-19}	1.63377 × 10^{-20}	4.45050 × 10^{-26}	3.82743 × 10^{-20}	1.51857 × 10^{-22}	1.18171 × 10^{-19}	1

1 cal = 4.18605 J（計量法）

= 4.184 J　（熱化学）

= 4.1855 J　（15 °C）

= 4.1868 J（国際蒸気表）

仕事率　1 PS（仏馬力）

= 75 kgf·m/s

= 735.499 W

放射能	Bq	Ci
	1	2.70270 × 10^{-11}
	3.7 × 10^{10}	1

吸収線量	Gy	rad
	1	100
	0.01	1

照射線量	C/kg	R
	1	3876
	2.58 × 10^{-4}	1

線量当量	Sv	rem
	1	100
	0.01	1

（86 年 12 月 26 日現在）

Annual Report of Kansai Research Establishment 2001 April 1, 2001 — March 31, 2002

R100
古紙配合率100%
白色度70%再生紙を使用しています